

Some pages of this thesis may have been removed for copyright restrictions.

If you have discovered material in Aston Research Explorer which is unlawful e.g. breaches copyright, (either yours or that of a third party) or any other law, including but not limited to those relating to patent, trademark, confidentiality, data protection, obscenity, defamation, libel, then please read our [Takedown policy](#) and contact the service immediately (openaccess@aston.ac.uk)

Nanotechnology and Microfluidics:
Formulation Design and on-chip Manufacture of Nanoparticles

Elisabeth Kastner
Doctor of Philosophy

ASTON UNIVERSITY
October 2015

©Elisabeth Kastner, 2015

Elisabeth Kastner asserts her moral right to be identified as the author of this thesis

This copy of the thesis has been supplied in condition that anyone who consults it is understood to recognise that its copyright rests with its author and that no quotation from the thesis and no information derived from it may be published without appropriate permission or acknowledgement.

Aston University
Nanotechnology and Microfluidics:
Formulation Design and on-chip Manufacture of Nanoparticles

Elisabeth Kastner
Doctor of Philosophy
2015

Summary

Nanoparticles offer an ideal platform for the delivery of small molecule drugs, subunit vaccines and genetic constructs. Besides the necessity of a homogenous size distribution, defined loading efficiencies and reasonable production and development costs, one of the major bottlenecks in translating nanoparticles into clinical application is the need for rapid, robust and reproducible development techniques. Within this thesis, microfluidic methods were investigated for the manufacturing, drug or protein loading and purification of pharmaceutically relevant nanoparticles.

Initially, methods to prepare small liposomes were evaluated and compared to a microfluidics-directed nanoprecipitation method. To support the implementation of statistical process control, design of experiment models aided the process robustness and validation for the methods investigated and gave an initial overview of the size ranges obtainable in each method whilst evaluating advantages and disadvantages of each method. The lab-on-a-chip system resulted in a high-throughput vesicle manufacturing, enabling a rapid process and a high degree of process control.

To further investigate this method, cationic low transition temperature lipids, cationic bola-amphiphiles with delocalized charge centers, neutral lipids and polymers were used in the microfluidics-directed nanoprecipitation method to formulate vesicles. Whereas the total flow rate (TFR) and the ratio of solvent to aqueous stream (flow rate ratio, FRR) was shown to be influential for controlling the vesicle size in high transition temperature lipids, the factor FRR was found the most influential factor controlling the size of vesicles consisting of low transition temperature lipids and polymer-based nanoparticles. The biological activity of the resulting constructs was confirmed by an *in-vitro* transfection of pDNA constructs using cationic nanoprecipitated vesicles. Design of experiments and multivariate data analysis revealed the mathematical relationship and significance of the factors TFR and FRR in the microfluidics process to the liposome size, polydispersity and transfection efficiency. Multivariate tools were used to cluster and predict specific *in-vivo* immune responses dependent on key liposome adjuvant characteristics upon delivery a tuberculosis antigen in a vaccine candidate. The addition of a low solubility model drug (propofol) in the nanoprecipitation method resulted in a significantly higher solubilisation of the drug within the liposomal bilayer, compared to the control method. The microfluidics method underwent scale-up work by increasing the channel diameter and parallelisation of the mixers in a planar way, resulting in an overall 40-fold increase in throughput. Furthermore, microfluidic tools were developed based on a microfluidics-directed tangential flow filtration, which allowed for a continuous manufacturing, purification and concentration of liposomal drug products.

Keywords: Nanoparticles, liposomes, microfluidics, process control

Acknowledgement

First, I want to thank my family and friends back home in Germany, who kept on motivating and driving me through this work, especially thanks to Philipp, Robert and Martin.

At Aston University, I first want to thank my research group and people within lab MB328. Many thanks go to the technician team, Jit, Christine and Tom, for helping out with materials and equipment. Especially thanks to Tom, who had to deal with the “Panicking Liz Syndrome” quite a few times. Many thanks to my hard-working MPharm students, Varun and Nicola, for the great work. Furthermore, thanks to Andrew Devitt and Vinod, for recent in-vitro work and exciting discussions. John, I own you lots, not only for the many discussions, ideas, methods, motivation and your open ear for whatever bothered me, but further for many enjoyable trips to conferences and the casual pints after work (scampi?). Thu, many thanks for being my rock in the lab (and for making me love Vietnamese food), your positive nature and spirit made me enjoy our long days in the lab (and long walks along the canal).

I want to thank Nicolas Szita for giving me the chance to work within his lab at UCL where I was exposed to the exciting world of microfluidics. I want to thank Brian, Mat, Marco, Nelson and Ya-Yu for letting me be part of their research group; you guys were so much fun. I own lots of thanks to Nikolay, who patiently helped me with my work and introduced many exciting ideas and concepts. Furthermore, I own big thanks to the team of Precision NanoSystems, especially to Euan, who arranged my stay in Vancouver where I could work within the Precision NanoSystems team. Also thanks to Pieter Cullis, who allowed me to work within his lab during my stay in Vancouver. Furthermore, special thanks go to Kevin, for his ideas and input regarding the scalability work and the whole Precision team, especially James, Colin and Tim for always taking the time to help with my work, giving feedback and input regarding my research.

Finally, I own most to Yvonne. Yvonne was an excellent supervisor, inspiring and supportive throughout the whole 3 years, always having an open ear. Working with Yvonne was so much fun, equally inside and outside the lab. Thanks for giving me the opportunity to take part in all those exciting conferences, the fantastic trips and research collaborations, which allowed me to broaden my horizon and to meet so many great and inspiring scientists.

Die Endlosigkeit des wissenschaftlichen Ringens sorgt unablässig dafür, dass dem forschenden Menschegeist seine beiden edelsten Antriebe erhalten bleiben und immer wieder von neuem angefacht werden: Die Begeisterung und die Ehrfurcht.

Max Planck
23.04.1858 - 04.10.1947

Own Publications

Kastner E., Ramsay E., Kaur R., Ingham A.J. and Perrie Y. (2013). Controlled and scalable synthesis of liposomes using microfluidic mixing. CRS Newsletter Spotlight Article. Vol 30 (2).

Perrie Y., Kastner E., Kaur R., Wilkinson A. and Ingham A. (2013). A case-study investigating physico-chemical characteristics that control the function of a liposomal adjuvant. Vaccines & Immunotherapeutics. Vol 9 (6).

Kastner E., Kaur R., Lowry D., Moghaddam B., Wilkinson A. and Perrie Y. (2014). High-throughput manufacturing of liposomes by a new microfluidics method using enhanced statistical tools for characterization. International Journal of Pharmaceutics. 477.1, 361-368.

Kastner E., Hussain M. J., Bramwell V. W., Christensen D. and Perrie Y. (2015). Correlating liposomal adjuvant characteristics to in-vivo cell-mediated immunity using a novel Mycobacterium tuberculosis fusion protein: a multivariate analysis study. Journal of Pharmacy and Pharmacology. 67(3), 450-463.

Kastner E., Schmidt S. T., Wilkinson A., Christensen D. and Perrie Y. (2015). The Application of Liposomes as Vaccine Adjuvants. In Foged C., Rades T., Perrie Y., Hook, S. Eds *Subunit Vaccine Delivery* Springer New York. pp. 77-94.

Kastner E., Verma V., Lowry D. and Perrie Y. (2015). Microfluidic-controlled synthesis of liposomes for the solubilisation of a poorly water soluble drug. International Journal of Pharmaceutics. 485(1-2):122-30.

Perrie Y., Crofts F., Devitt A., Griffiths H., Kastner E. and Nadella V. (2015). Designing liposomal adjuvants for the next generation of vaccines. Advanced Drug Delivery Reviews (accepted).

Kastner E. and Perrie Y., (2015). Particle size analysis for micro- and nanoparticles in Analytical Methods in Pharmaceutical Sciences (submitted).

Kastner E., Dimov N., Ingham A., Perrie Y. and Szita N. (2015). Formation and purification of tailored nanoparticles for drug delivery using continuous microfluidics (submitted).

Conference Abstracts

Kastner E., Semple N., Ingham A., Perrie Y. (2015). A microfluidics-based platform for high-throughput manufacturing of lipid- and polymer-based nanoparticles with enhanced drug encapsulation properties. *UK PharmSci, Nottingham UK*, 7-9th September 2015.

Kastner E., Semple N., Ingham A., Perrie Y. (2015). Microfluidics-controlled manufacturing of drug-loaded nanoparticles in a scalable and high-throughput setup. *CRS Annual Meeting, Edinburgh UK*, 26-29th July 2015.

Kastner E., Ingham A., Perrie Y. (2015). High Throughout manufacturing of drug-loaded nanoparticles. *Aston Research Day, Aston University UK*, 26th June 2015.

Kastner E., Ingham A., Perrie Y. (2015). High Throughout manufacturing of drug-loaded nanoparticles. *UKICRS Symposium, Nottingham UK*, 17th April 2015.

Kastner E., Verma V., Ingham A., Perrie Y. (2014). Exploring microfluidics as a new method for high-throughput solubilisation of low solubility drugs into liposomes. *Royal Society of chemistry, Innovations in Encapsulation, London UK*, 12th December 2014.

Kastner E., Verma V., Ingham A., Perrie Y. (2014). Microfluidics-controlled manufacturing of liposomes for drug delivery and gene transfer. *1st International Congress: From Drug discovery to Drug delivery, Athens Greece*, 13-15th November 2015.

Kastner E., Verma V., Ingham A., Perrie Y. (2014). Encapsulation of low solubility drugs into liposomes by microfluidics. *UK PharmSci, Hardfort UK*, 6-9th September 2014.

Kastner E., Ingham A., Perrie Y. (2014). Applying statistical process control in process development – Liposome manufacturing by sonication, high shear mixing and microfluidics. *CRS Annual Meeting, Chicago IL USA*, 13-16th July 2014.

Kastner E., Ingham A., Perrie Y. (2014). Manufacturing of liposomes with desired particle characteristics by factorial design. *Aston Research Day, Aston University Birmingham UK*, 02nd July 2014.

Kastner E., Ingham A., Perrie Y. (2014). Manufacturing of liposomes with desired particle characteristics by factorial design. *UKICRS Symposium, Cork Ireland*, 11th April 2014.

Kastner E., Ingham A., Perrie Y. (2013). Microfluidics – A Promising new Method for Controlled Liposome Manufacture. *International Liposome Society, London UK*, 14-17th December 2013.

Kastner E., Ingham A., Perrie Y. (2013). A QbD-based process development for robust production of liposomal subunit vaccines. *UK PharmSci, Edinburgh UK*, 4th September 2013.

Kastner E., Ingham A., Perrie Y. (2013). Controlled Synthesis of limit size cationic liposomes by microfluidic mixing. *CRS Annual Meeting, Hawaii USA*, 21-24th July 2013.

Kastner E., Ingham A., Perrie Y. (2013). Controlled Synthesis of limit size cationic liposomes by microfluidic mixing. *Aston Research Day, Aston University Birmingham UK*, 26th June 2013.

Kastner E., Kaur R., Ingham A., Perrie Y. (2013). Controlled Synthesis of limit size cationic liposomes by microfluidic mixing. *UKICRS Symposium, Reading UK*, 16th April 2013.

Contents

Title	1
Summary	2
Acknowledgement	3
Own Publications	5
Conference Abstracts	6
Table of Contents	8
List of Tables	15
List of Figures	18
Abbreviations	29

Chapter 1

1 General Introduction	32
1.1 Liposomes	33
1.1.1 The importance of liposome size	34
1.1.2 Liposomes as immunological adjuvants	34
1.1.3 Liposomes as transfection agents	37
1.1.4 Liposomes for the solubilisation	38
1.1.5 Traditional liposome manufacturing methods	39
1.2 Microfluidics	42
1.2.1 Background	42
1.2.2 Microflow physics	42
1.2.2.1 Dimensionless numbers	42
1.2.2.2 Micromixer characterisation	44
1.2.3 Classification active passive micromixers	45
1.2.3.1 Staggered herringbone micromixer	46
1.2.4 Microfluidics for liposome manufacturing	48
1.3 Statistical tools for reproducible manufacturing	50
1.4 Aim and Objectives	52

Chapter 2

2 Materials and Methods	53
2.1 Materials	54
2.2 Methods in liposome manufacturing	58
2.2.1 Lipid film hydration	58
2.2.2 Sonication	58

2.2.3	High shear mixing	58
2.2.4	Microfluidics	58
2.2.4.1	Setup.....	58
2.2.4.2	Nanoprecipitation	59
2.3	Methods for quantification	60
2.3.1	Solvent quantification by gas chromatography	60
2.3.2	Lipid and drug quantification by liquid chromatography and evaporative light scattering	60
2.4	Liposome purification	62
2.4.1	Dialysis	62
2.4.2	Spin columns	62
2.5	Liposome characterisation	62
2.5.1	Dynamic light scattering.....	62
2.5.2	Nanoparticle tracking analysis.....	62
2.5.3	Zeta potential	63
2.5.4	Recovery of lipids and drug.....	63
2.6	Liposome Imaging	63
2.6.1	Transmission electron microscopy	63
2.6.2	Freeze fracturing electron microscopy	64
2.6.3	Fluorescent imaging of liposomes.....	64
2.7	Loading of protein	64
2.7.1	Adsorption of protein.....	64
2.7.2	Gel electrophoresis for qualitative protein detection	64
2.8	Loading of a low solubility drug	65
2.8.1	Solubilisation of low solubility drug	65
2.8.2	Determination of drug loading into liposomes.....	65
2.8.3	Drug release study.....	65
2.9	Stability Studies.....	65
2.10	Solvent evaporation of polymer-based nanoparticles	66
2.11	<i>In-vitro</i> studies	66
2.11.1	Culture and maintenance of continuous cell lines.....	66
2.11.2	Determination of cell number.....	66
2.11.3	Cryopreservation.....	67
2.11.4	Transfection of COS-7 Cells.....	67
2.11.5	Luciferase Assay.....	67
2.11.6	Detection of fluorescent protein expression.....	68
2.11.7	Cytotoxicity study	68

2.11.8	<i>In-vitro</i> association assay	68
2.11.9	<i>In-vitro</i> migration assay	69
2.12	<i>In-vivo</i> studies immunisation study	69
2.12.1	Vaccination of mice	69
2.12.2	Sera collection.....	69
2.12.3	Mice termination and in vitro spleen cell culture	70
2.12.4	Assessment of H56 specific antibody isotype titres	70
2.12.5	Quantification of cytokine production by the sandwich ELISA.....	71
2.13	Scalability assessment of the nanoprecipitation method	71
2.13.1	Scale-up by increase of channel diameter	71
2.13.2	Scale-out by mixer parallelisation	71
2.14	Tangential flow filtration for liposome purification	72
2.14.1	Filtration unit manufacturing	72
2.14.2	Filtration device	73
2.14.3	Backpressure regulation.....	73
2.14.4	Membrane fouling	73
2.14.5	Integrity testing.....	74
2.14.6	Liposome formulations for spiking the filtration system.....	74
2.14.7	Filtration	74
2.14.8	Micromixer for liposome formation in combination with TFF purification	75
2.15	Statistical analysis.....	76
2.16	Design of experiments.....	76
2.16.1	Model evaluation	77
2.16.2	Normal probability and replicate plot	78
2.16.3	Coefficient plot	78
2.16.4	ANOVA	78
2.17	Multivariate Analysis	79
2.17.1	Principal component analysis	79
2.17.2	Partial least square analysis.....	79
2.17.3	Validation	80

Chapter 3

3	Method development and evaluation: Quantification, particle sizing and microfluidics.....	81
3.1	Introduction.....	82

3.2	Aim and Objectives.....	88
3.3	Results and Discussion.....	88
3.3.1	Development and validation of quantification methods based on HPLC and ELSD	88
3.3.1.1	Linearity	89
3.3.1.2	Precision	90
3.3.1.3	Accuracy	91
3.3.1.4	Robustness	91
3.3.1.5	Level of detection and level of quantification.....	92
3.3.1.6	Summary of validation criteria for lipids used	93
3.3.1.7	Bimodal populations measurement by DLS	93
3.3.1.8	Direct comparison DLS and NTA measurement of liposomes	95
3.3.2	Methods for liposome manufacturing: sonication, high shear mixing and microfluidics.....	97
3.3.2.1	Design of experiments for method investigation and validation	100
3.3.2.2	Lipid quantification for process recovery	109
3.4	Conclusion	110

Chapter 4

4	Manufacturing of cationic liposomes by microfluidics for <i>in-vitro</i> transfection and assessment of statistical tools for process development	111
4.1	Introduction.....	112
4.2	Aim and Objectives.....	113
4.3	Results and Discussion.....	113
4.3.1	In-process control of vesicle size using microfluidics-directed nanoprecipitation	113
4.3.2	Evaluating the microfluidics-based manufacturing for process recovery - Lipid quantification by ELSD	117
4.3.3	<i>In-vitro</i> transfection efficiency and the effect of vesicle size.....	118
4.3.4	Statistical impact of the factors flow rate and flow ratio in a design of experiments study	119
4.3.5	Statistical impact of the factors flow rate and flow ratio in a multivariate study	131
4.4	Conclusion	139

Chapter 5

5	Microfluidics-directed manufacturing of a gene delivery system made from dequalinium™	141
5.1	Introduction	142
5.2	Aim and Objectives	144
5.3	Results and Discussion	144
5.3.1	A feasibility study of DQAsome manufacturing by microfluidics	144
5.3.2	The effect of flow rate ratio and total flow rate on vesicle characteristics	146
5.3.3	The effect of CM2 concentration in the microfluidics-directed DQAsome formation	148
5.3.4	DQAsome stability and integrity upon manufacturing by microfluidics	150
5.3.5	DQAsome purification and recovery upon manufacturing by microfluidics	152
5.3.6	<i>In-vitro</i> transfection efficiency of DQAsomes	154
5.4	Conclusion	157

Chapter 6

6	Microfluidics-controlled solubilisation of a low-solubility drug and scale-up considerations	159
6.1	Introduction	160
6.2	Aim and Objectives	160
6.3	Results and Discussion	161
6.3.1	Influence of the flow rate ratio of the aqueous and solvent streams on particle characteristics	161
6.3.2	Influence of flow rate on throughput and particle characteristics	163
6.3.3	Drug loading studies: The effect of drug encapsulation by the liposome manufacturing method	165
6.3.4	Microscopy images for vesicle verification	168
6.3.5	The effect of manufacturing method to drug release	172
6.3.6	The effect of manufacturing methods on liposome stability and drug encapsulation over 6 months	173
6.3.7	The effect of drug, drug loading and manufacturing method to the biological toxicity	177
6.3.8	Assessment of the scalability of the microfluidics-directed nanoprecipitation method	178
6.4	Conclusion	191

Chapter 7

7	Development of continuous microfluidic systems for manufacture and purification of liposomes.....	193
7.1	Introduction.....	194
7.2	Aim and Objectives.....	195
7.3	Results and Discussion.....	196
7.3.1	Backpressure regulation	196
7.3.2	Membrane fouling	198
7.3.3	Batch -type purification of liposomes – pressure testing	200
7.3.4	Membrane integrity testing	203
7.3.5	The effect of filtration on particle characteristics for cationic and anionic liposomes	204
7.3.6	Purification of non-incorporated moieties from liposome formulations	206
7.3.7	Purification of cationic liposomes with spiked model protein.....	207
7.3.8	Continuous setup	210
7.3.8.1	Continuous manufacture and purification of liposomal solubilisation agents	211
7.3.8.2	Continuous manufacture and purification of cationic liposomes with adsorbed protein	212
7.4	Conclusion	213

Chapter 8

8	A multivariate analysis study to correlate liposomal adjuvant characteristics	214
8.1	Introduction.....	215
8.2	Aim and Objectives.....	216
8.3	Results and Discussion.....	217
8.3.1	Summary of <i>in-vivo</i> responses	217
8.3.2	Multivariate analysis for clustering Th1 and Th2 type immune responses to adjuvant characteristics	220
8.3.2.1	Principal component analysis and partial least square regression.....	220
8.3.2.2	Model validation	226
8.4	Conclusion	228

Chapter 9

9 Protein association with adjuvants and polymer nanoparticles manufactured by microfluidics.....	229
9.1 Introduction.....	230
9.2 Aim and Objectives.....	230
9.3 Results and Discussion.....	231
9.3.1 Manufacturing of lipid-based vaccine adjuvants by microfluidics	231
9.3.2 <i>In-vitro</i> activity of adjuvants manufactured via microfluidics.....	236
9.3.3 Manufacturing of polymer-based nanoparticles	240
9.4 Conclusion	245

Chapter 10

10 Overall Discussion and Conclusion.....	247
10.1 Development of microfluidics-directed nanoparticle manufacturing...248	
10.2 The role of quantification and recovery studies	249
10.3 Biological activity of vesicles manufactured by microfluidics-directed nanoprecipitation	249
10.4 Drug loading with nanoprecipitation	250
10.5 The role of continuous manufacturing.....	251
10.6 The importance of scale up and scalability	252
10.7 The role of process control and modelling	253
10.8 Overall Conclusion	255

Chapter 11

11 Reference List.....	256
-------------------------------	------------

List of Tables

Chapter 1

Table 1.1: Overview of traditional methods of liposome manufacturing, adapted from (Kastner et al., 2015).....	41
Table 1.2: Selection of common passive micromixers	46

Chapter 2

Table 2.1: Lipids and polymers used throughout this thesis. IPA = Isopropanol, n/a = not applicable.	59
Table 2.2: Detailed HPLC methods for compounds used in this study, mobile phase comprised A (0.1%TFA in water) and B (100% methanol) in all runs.....	61

Chapter 3

Table 3.1: Direct comparison of DLS and NTA.	87
Table 3.2: Evaluation of %RSD and recovery during the validation of the assay accuracy.....	91
Table 3.3: Overview over the validation of lipids, drug (propofol) and protein (ovalbumin).	93
Table 3.4: Particle size and polydispersities measured from various liposome mixtures to assess the impact of bimodal size distributions on the measurement outcome.	94
Table 3.5: ANOVA for the response size in the sonication, HSM and microfluidics method. The p-statistics were analysed as well as the Lack-of-fit (LOF), together with fit power (R^2) and predictive power (Q^2).	105
Table 3.6: Determined significant coefficients and respective regression model in each method, predicting the liposome size. Amp = amplitude	106

Chapter 4

Table 4.1: The chemical structure and key characteristics of lipids used to formulate liposomes in this study.	113
Table 4.2: Coefficient list for the responses size, PDI and transfection efficiency. Coefficients were determined as statistically significant ($p < 0.05$).	125
Table 4.3: ANOVA for the responses size, PDI and transfection efficiency. The p-statistics were analysed as well as the Lack-of-fit (LOF), together with fit power (R^2) and predictive power (Q^2).	125
Table 4.4: Coefficient list with coefficients (scales and centred), standard error, p-values and confidence intervals for three responses.	126

Table 4.5: Validation of the regression models built during the DoE analysis. Predicted values are compared to experimentally obtained results for two process settings; 1 mL/min, 1:1 and 2 mL/min 1:3 (TFR, FRR).....	130
---	-----

Chapter 6

Table 6.1: Determined Re and Pe numbers in the chip design with a channel diameter of 200 μm ranging at TFR between 1 to 3 mL/min.....	179
---	-----

Table 6.2: Corresponding flow rates in the 200 μm and 300 μm design considering a constant pressure drop throughout scale up.....	182
---	-----

Chapter 7

Table 7.1: Comparison of theoretical and actual backpressures in the TFF setup at increasing flow rates from 0.01 to 0.1 mL/min. Deviation in actual backpressure was extrapolated from fluctuations in the pressure recordings and expressed as \pm compared to the average pressure recording (5 cm capillary I.D. 50 μm).	197
--	-----

Table 7.2: Continuous purification of PC-Chol liposomes loaded with propofol. Here, propofol and lipids were included in the solvent stream and liposome formation and drug encapsulation was performed in a SHM, run at 2 mL/min and a 1:3 solvent:aqueous ratio. na= not applicable.....	212
--	-----

Table 7.3: Continuous purification of DOPE-DOTAP liposomes loaded with protein (ovalbumin). Here, lipids were included in the ethanol stream and liposome formation was performed in a SHM, run at 2 mL/min and a 1:3 solvent:aqueous ratio. Protein was added post-liposome synthesis. OVA = ovalbumin, na= not applicable.	213
---	-----

Chapter 8

Table 8.1: Incorporation of DSPC into DDA-TDB formulations at 25, 50 and 75 mol%. Values of weight or μmoles in the various liposome formulations where DDA-TDB was locked at a 5:1 wt ratio/8:1 molar ratio and increasingly replaced with DSPC in a 50 μL dose.	216
--	-----

Table 8.2: DDA-TDB and its substitution with 25-75 mol% DSPC with effect to particle characteristics prior to and post H56 antigen adsorption. Results denote mean \pm SD for three independent experiments. Mean serum H56 specific antibody isotype titres stimulated by DDA-TDB and DSPC substitution (n=5, +/- standard error). Values display the positive reciprocal end point dilution (log10). Spleen cell proliferation stimulated by H56 vaccine antigen and spleen cell cytokine production in response to re-stimulation with H56 antigen. Results represent mean average of five spleens per vaccination group \pm standard error. Experiment performed by M. Jubair Hussain.	219
---	-----

Chapter 9

Table 9.1: Vesicle characteristics of DDA-TDB adjuvants manufactured.	236
--	-----

List of Figures

Chapter 1

Figure 1.1: A) Schematic representation of a liposome, comprised of a bilayered lipid membrane. B) Schematic representation of liposome structures.	34
Figure 1.2: Flow profile around a cylinder for increasing Re numbers.....	43
Figure 1.3: A) Schematic zoom into the microfluidic chip of a SHM. B) Schematic of six grooves per half cycle of a SHM. C) Schematic streamlines in the cross section of the channel with the angle $\Delta\phi_m$ as the angular displacement of the fluid volume along the wide arms of the herringbones. h = height of chamber, w = width of chamber, d_g = depth of grooves, w_g = width of grooves, p = asymmetric factor, c = centre of rotation, θ = angle of grooves, p_w = asymmetry factor over the width of the long herringbone arms.	47
Figure 1.4: Schematic depiction of the nanoprecipitation method by A) dialysis method and B) dropping method.	48
Figure 1.5: Overview of the chaotic advection SHM method and the flow focusing method.	49
Figure 1.6 Schematic depiction of screening of two factors; left: screening one factor at a time resulting in 5 experiments. Right: Designed experiment with only one experiment.	50
Figure 1.7: Overview over a MVA process with A) data scattered in a multidimensional space, B) two PCs are fitted and C) projection of the data and the PCs onto a plane.	51

Chapter 2

Figure 2.1: A) Chip in PDMS for size comparison next to a penny. B) Detailed flow path including two full cycles of herringbones.....	59
Figure 2.2: Schematic of the scale-out layout for A) 2x syringe driven, B) 4x syringe driven, C) 1x continuous flow and D) 4x continuous flow.	72
Figure 2.3: Filtration mode with a syringe pump driving the sample through the TFF. Retentate and permeate were collected manually.	74
Figure 2.4: A) Schematic overview over the continuous manufacturing setup with B) loading of the low solubility drug and C) loading of the protein.	76

Chapter 3

Figure 3.1: Schematic overview over the range of vesicle manufacturing methods investigated in this study.	82
---	----

Figure 3.2: Schematic of a correlation function as obtained from a DLS measurement with indicated qualitative properties of suspended particles. Adapted from (Kastner and Perrie, 2015).	84
Figure 3.3: Stepwise procedure during NTA analysis. Adapted from (Kastner and Perrie, 2015).	86
Figure 3.4: Elution peak for cholesterol detected by ELSD with the elution protocol. The flow rate was 1 mL/min throughout. Mobile phase A was 0.1%TFA water, B was methanol.	89
Figure 3.5: Linearity assessment of cholesterol (0.025 to 1 mg/mL) used to determine the calibration curve to assess the cholesterol concentration.	90
Figure 3.6: Cholesterol quantification - assessment of A) intraday and B) interday variability with linear regression coefficients and %RSD.....	91
Figure 3.7: Resulting intensity and volume based size distribution plots for the A) 80 nm sized and B) 500 nm sized population, C) increasing the ratio of the larger 500 nm population and D) increasing the ratio of the smaller 80 nm sized population. Adapted from (Kastner and Perrie, 2015).	95
Figure 3.8: Direct comparison of a monomodal liposome size determination as measured by A) DLS and B) NTA with particle imaging by light scattering. Adapted from (Kastner and Perrie, 2015).	96
Figure 3.9: Overlay plot showing the difference in liposome population in size and PDI produced by high shear mixing (HSM), sonication (sonic.) and microfluidics (MF) compared to liposomes produced by lipid hydration (LFH) method.	97
Figure 3.10: CryoTEM pictures obtained of A) MLV produced by lipid hydration B) SUV microfluidic mixing C) high shear mixing D) sonication. Bar represents A) 200 nm, B-D) 100 nm.	98
Figure 3.11: Design of Experiments predicting the liposome size in the sonication process dependent on the factors sonication time (1-2 minutes) and amplitude (1-10). Model type was a screening design (full factorial) with 3 centre points. Depicted is A) Summary plot ($R^2=0.91$, $Q^2=0.85$, Validity=0.97, Reproducibility=0.73), B) Observed vs. predicted, C) Replicates plot and D) Contour Plot.	102
Figure 3.12: Design of Experiments predicting the liposome size in the HSM process dependent on the factors mixing time (1-10 minutes), rotational speed (1 000-25 000 rpm). Model type was a screening design (full factorial) with 3 centre points. Depicted is A) Summary plot ($R^2=0.81$, $Q^2=0.25$, Validity=0.5, Reproducibility=0.93, B) Observed vs. predicted, C) Replicates plot and D) Contour Plot.....	103
Figure 3.13: Design of Experiments predicting the liposome size in the microfluidics process dependent on the factors flow rate ratio (1:2 to 1:5) and total flow rate (1.2 to	

2.5 mL/min). Model type was a response surface model (full factorial, CCC) with 3 centre points. Depicted is A) Summary plot ($R^2=0.92$, $Q^2=0.39$, Validity=0.85, Reproducibility=0.80, B) Observed vs. predicted, C) Replicates plot and D) Contour Plot.....	104
Figure 3.14: Validation of the DoE models generated by direct comparison of experimentally obtained vesicle sizes against predicted vesicle sizes at different set points.	107
Figure 3.15: Recovery of DDA (%) and TDB (%) within the lipid film hydration (LFH), sonication, HSM and microfluidics (MF) process. Lipids were quantified using HPLC and expressed as % relative to the initial amount of lipids dissolved in the stock solution.....	110

Chapter 4

Figure 4.1: Liposome characteristics. A) Vesicle size, B) polydispersity and C) zeta potential of DOPE-DOTAP formulations manufactured by microfluidic mixing. Results denote the mean of triplicate formulations \pm SD.	114
Figure 4.2: Quantification of total lipid content (DOPE + DOTAP) by HPLC, shown as A) recovery (%) and B) ratio of both lipids, DOTAP/DOPE. Results are the mean of triplicate formulations \pm SD.....	118
Figure 4.3: A) Comparison of transfection efficiency of cationic nanoparticles. Liposomes were complexed with gWiz plasmid DNA expressing firefly luciferase. B) Relative cell viability of nanoparticles formulated. Results are the mean of triplicate formulations \pm SD.....	119
Figure 4.4: Design space in a two factorial design including 2 Factors (TFR and FRR) with a total 15 experimental points, triplicate centre point (N11, 12, 13) and replicate experimental point (N1, N2) were added.	120
Figure 4.5: Summary plots to evaluate the model fit (R^2), prediction (Q^2), validity and reproducibility for the responses liposome size, polydispersity and transfection efficiency. For an excellent model, all values are approaching 1.	121
Figure 4.6: Results from the analysis of the DoE study for the prediction of the liposome size, PDI and transfection efficiency with A) Coefficient Plot B) Observed vs. Predicted C) Residuals vs. Normal Probability, D) Replicate plots.....	124
Figure 4.7: Response surface predictions for A) liposome size, B) polydispersity and C) transfection efficiency as a function of TFR (0.5 – 2 mL/min) and FRR (1:1 to 1:3 in the microfluidics-directed manufacturing of DOPE-DOTAP liposomes.	128

Figure 4.8: Sweet spot analysis for the desired criteria 1, size (80-150 nm); criteria 2, PDI (0.125-0.3) and criteria 3, transfection efficiency (150-280%). Dark blue = criterion 1 met, light blue = criterion 2 met, green = sweet spot.....	129
Figure 4.9: Summary plot with two principal components added, showing the model fit (R^2) and predictive power (Q^2).....	132
Figure 4.10: Score scatter plot as identified during the PCA. Colour coding simplifies the cluster analysis and trending in the data set with A) coloured according to FRR, B) coloured according to PDI, C) coloured according to TFR and D) coloured according to liposome size. The numbers represent observations as obtained from the DoE study.	134
Figure 4.11 Results from the PLS regression analysis coloured according to model term. A) Coefficient plot including 95% confidence interval for the two principal components. B) The loading scatter plot indicating significance of the factors (X) and responses (Y) to each other.	136
Figure 4.12: Permutations plot for A) size, B) PDI and C) transfection efficiency. Model validity was assessed for 40 permutations. The correlation between permuted Y-vector to the original X-vector is depicted by the horizontal correlation axis. The criterion for model validity was selected as the intercept of the Q^2 regression line at or below zero.	138

Chapter 5

Figure 5.1: A) 1,1-Decamethylene bis (4-aminoquinadiniumchloride) and its derivate B) 1,1'-(decane-1,10-diyl)bis(9-amino-1,2,3,4- tetrahydroacridinium) diiodide (CM2). Adopted from (Weissig, 2015).	142
Figure 5.2: Assembly of a liposome-like vesicle comprising U-shaped and stretched-confirmation of bola-form amphiphiles. Adapted from (Gregoriadis, 2007).	143
Figure 5.3: Reproducibility (intra-day variability) and inter-day variability of DQAsomes manufactured by microfluidics (TFR 2 mL/min, FRR 1:3) and sonication (30 min, amplitude 5) showing the particle size, polydispersity and zeta potential. Results denote mean \pm SD of 3 separate batches.	145
Figure 5.4: A) Intensity-based, B) volume-based size distribution and C) correlogram of particles manufactured via microfluidics-based nanoprecipitation. D) Intensity-based, E) volume-based size distribution and F) correlogram of particles manufactured via lipid film hydration followed by sonication. Plots show the average out of three batches and the inter-day variability for the microfluidics-manufactured vesicles.....	146
Figure 5.5: Effect of increase in A) FRR at constant TFR of 2 mL/min and B) TFR at constant FRR of 1:3 to DQAsome characteristics. Change is represented in % relative	

to the start size of 250 nm, PDI 0.3. Where shown, significance between data is against results at a FRR 1:1 (**p<0.01, ***p<0.001). Results denote mean ± SD of 3 separate batches.	147
Figure 5.6: Effect of increase in CM2 concentration to A) quantification, B) recovery (%), C) DQAsome size, D) PDI and E) zeta potential. The heating block was used for formulations ≥ 3 mg/mL to maintain solubility. Where shown, significance between data is against results at a concentration of 0.6 mg/mL (*p<0.05, **p<0.01). Results denote mean ± SD of 3 separate batches.	149
Figure 5.7: Effect of storage temperature to DQAsome size and PDI over A) 5 hours, B) 8 days and respective effect to C) zeta potential. D) Effect of storage temperature on stability of the CM2 compound over 8 days. RT = room temperature. Results denote mean ± SD of 3 separate batches.	151
Figure 5.8: A) Effect of a spin column process on vesicle characteristics. B) Effect of membrane cutoff to recovery of the CM2 compound. Results denote mean ± SD of 3 separate batches and purification cycles. Correlogram of the filtrate C) in comparison to the concentrate side of the spin column membrane D).....	153
Figure 5.9: Two plasmids used in the in-vitro study evaluating the transfection potential of the microfluidics-manufactured DQAsomes. Structures obtained from www.aldevron.com	154
Figure 5.10: Transfection efficiency (RLU, relative light units) as obtained by microfluidics-manufactured DQAsomes (FRR 1:3, TFR 2 mL/min), sonicated DQAsomes (30 min, amplitude 5) as compared to cationic liposome transfection efficiency (DOPE-DOTAP, FRR 1:5, TFR 1.5 mL/min). Significance between data is against the transfection efficiency achieved by vesicles manufactured in the sonication method (*p<0.05). Results denote mean ± SD of 3 separate transfections.....	155
Figure 5.11: A, B) Confocal microscopy images showing the <i>in-vitro</i> expression of the fluorescent protein in transfected COS-7 cells.....	156

Chapter 6

Figure 6.1: Schematic depiction of the proposed drug encapsulation methodology by incorporation of a low solubility drug into the solvent stream during the microfluidics-directed nanoprecipitation reaction of liposome formation.	161
Figure 6.2: Particle size, polydispersity and zeta potential of empty liposomes. The effect of increasing flow rate ratio (FRR) in the microfluidics method on A) particle size and zeta potential and B) polydispersity. Where shown, significance between data is against results of the FRR 1:1 (*p<0.05). The effect of increase in sonication time on C) particle size and zeta potential and D) polydispersity. Where shown, significance	

between data is against the control (**** $p < 0.0001$). ns, not significant; CTR, control. Results denote mean \pm SD of at least 3 separate batches.	162
Figure 6.3: The effect of increasing n total flow rate (TFR) on vesicle size, polydispersity and zeta potential. Results were not significant compared to the vesicle characteristics obtained at 2 mL/min. Results denote mean \pm SD of 3 separate batches.	163
Figure 6.4: The effect of increased lipid concentration on A) vesicle size and B) polydispersity for the standard lipid concentration and increased lipid concentrations. The lipid concentration is shown in the table below the graph, which was tailored to the FRR. Where shown, significance between data is against results of standard lipid concentration (* $p < 0.05$). Results denote mean \pm SD of 3 separate batches.	164
Figure 6.5: The effect of incorporating a low solubility model drug (propofol) at 0.5, 1 and 3 mg/mL in the solvent stream on A) particle size, B) polydispersity, at different FRR and C) total loading (mg) in 3 mL formulation and encapsulation (mol%). D) Direct comparison of the loading (mol%) at different FRR to the loading in the sonication method, achieved with a propofol concentration of 1 mg/mL in the solvent phase for both methods. Significance between data is against results of loading achieved in the sonication method (**** $p < 0.0001$). E) Recovery of propofol in the formulations at different FRR and in comparison to the recovery obtained in the sonication method. F) Recovery of lipids and propofol at different FRR employed (TFR 2 mL/min, 1 mg/mL propofol in solvent stream). Significance between data is against the recovery achieved in at the FRR of 1:1 (* $p < 0.05$, ** $p < 0.01$). Results denote mean \pm SD of 3 separate batches.	166
Figure 6.6: Freeze fracturing electron microscopy images (A-D) obtained of PC-Chol liposomes manufactured by microfluidics (TFR 2 mL/min, FRR 1:3).	169
Figure 6.7: Freeze fracturing electron microscopy images (A-D) obtained of PC-Chol liposomes loaded with propofol manufactured by microfluidics (TFR 2 mL/min, FRR 1:3, 1 mg/mL propofol in solvent stream).....	170
Figure 6.8: Images obtained by confocal microscopy showing liposomes manufactured by (A, B) lipid film hydration/ sonication, encapsulating the aqueous marker (carboxyfluorescein). Note that fluorescence spot size does not correspond to actual vesicle size as liposomes in this sample were below the optical resolution.	171
Figure 6.9: Images obtained by confocal microscopy showing liposomes manufactured by (A, B) microfluidics (TFR 2 mL/min, FRR 1:3), encapsulating the aqueous marker (carboxyfluorescein). Note that fluorescence spot size does not correspond to actual vesicle size as liposomes in this sample were below the optical resolution.	171

Figure 6.10: <i>In-vitro</i> drug release profile for propofol-loaded liposomes manufactured by microfluidics and sonication. Release profiles show A) the cumulative drug release and B) the release of the drug in mol% over 16 hours. Results denote mean \pm SD of 3 separate batches.....	173
Figure 6.11: Results depicting the effect of long term storage conditions to A) vesicle size B), polydispersity, C) drug encapsulation, D) drug recovery and E) stability at 4-fold lipid and drug concentration. Results denote mean \pm SD of 3 separate batches.	175
Figure 6.12: Images taken throughout the stability study duration, showing vials of microfluidics-manufactured vesicles stored at 4°C, 25°C and 40°C and sonication-vesicles (25°C), from left to right at respective time points.....	176
Figure 6.13: Viability (%) as determined by a MTT study. Significance between data is against the viability of the control (untreated cells) (* $p < 0.05$, *** $p < 0.001$). Results denote mean \pm SD of 3 separate measurements in 3 independent cell passage numbers (n=9).....	177
Figure 6.14: Overview over micromixers identifying the operating ranges for passive micromixers at low (< 1) and high (> 100) Re numbers. Adopted from (Nguyen and Wu, 2005).....	180
Figure 6.15: Depiction of rectangular cross section and equivalent diameter in a pipe.	181
Figure 6.16: Evaluation of the scale-up design with a channel diameter of 300 μ m for effect of increase in A) FRR at constant TFR of 10 mL/min and B) TFR at constant FRR of 1:3 on vesicle size, PDI and zeta potential. Significance between data is against the FRR of 1:1 (* $p < 0.05$). C) Effect of increase in TFR at constant FRR (1:3) on drug loading and vesicle characteristics. Results denote mean \pm SD of 3 separate batches.	183
Figure 6.17: Evaluation of the scale-up design with a channel diameter of 300 μ m for A) increase in lipid concentration to counter dilution of liposomes tailored to the FRR at constant TFR of 10 mL/min. B) Particle characteristics and loading achieved with a higher concentrated lipid/drug concentration compared to the 200 μ m design, at constant FRR of 1:3. Results denote mean \pm SD of 3 separate batches.	184
Figure 6.18: Scale-out platform from A) side and B) top view, fluid manifolds as set for a C) 4x and D) 2x flow, E) syringe driven and F) continuous flow pump system.	185
Figure 6.19: Effect of scale-out by a syringe-driven 2x and 4x setup to A) particle characteristics of empty and drug loaded liposomes and B) recovery of lipid and drug as well as overall drug encapsulation. All runs were performed at a FRR 1:3 and a TFR of 10 mL/min per chip. SUV, small unilamellar vesicles. Results denote mean \pm SD of 3 separate batches.....	186

Figure 6.20: Effect of scale-out by a continuous flow setup to particle characteristics in a A) 1x and B) 4x setup as well as on drug loaded liposomes in a C) 1x and D) 4x setup. All runs were performed at a FRR 1:3 and a TFR of 10 mL/min per chip, 5 mL were collected as waste in the 1x setup, 10 mL in the 4x setup. SUV, small unilamellar vesicles. Results denote mean \pm SD of 3 separate batches.	187
Figure 6.21: Effect of scale-out by a continuous flow 1x and 4x setup to the recovery of lipid and drug as well as overall drug encapsulation. All runs were performed at a FRR 1:3 and a TFR of 10 mL/min per chip. Significance between data is against the results obtained in the batch system (* $p < 0.05$, ** $p < 0.01$). Results denote mean \pm SD of 3 separate batches as the average out of the cumulative batches collected in the continuous flow setup.....	187
Figure 6.22: Overall comparison between the different scale-up platforms tested on A) size, B) PDI, C) ZP, D) encapsulation and E) recovery of lipids and drug. Significance between data is against the results obtained in the batch system (* $p < 0.05$, ** $p < 0.01$, *** $p < 0.001$, **** $p < 0.0001$). Results denote mean \pm SD of 3 separate batches and the average out of the cumulative batches collected in the continuous flow setup.....	188
Figure 6.23: Effect of tubing material (PEEK vs. FEP) and pressure to the recovery of the lipids and drug. Significance between data is against the results obtained in the lowest flow rate and pressure (* $p < 0.05$). Results denote mean \pm SD of 3 separate batches.	190

Chapter 7

Figure 7.1: A) 3D image of the TFF system with two PMMA plates used as in a clamping system to hold the membrane in place. B) Dimensions of the assembled TFF device. Adopted from (O'Sullivan et al., 2012).	195
Figure 7.2: Overview over the continuous flow microfluidics-based liposome manufacturing and purification setup.....	196
Figure 7.3: Determined theoretical backpressures at different flow rates from 0.01 to 3 mL/min at various capillary lengths and I.D. of A) 800 μm , B) 50 μm , C) 63 μm , D) 100 μm	197
Figure 7.4: Determination of membrane fouling at flow rates of 0.01 mL/min, 0.02 mL/min and 0.05 mL/min for liposomes (SUV) and water (NWP). Smaller picture represents a zoom of NWP and SUV cumulative permeate volumes at the lowest flow rate of 0.01 mL/min, with initial indication of membrane fouling. All experiments were performed at a particle concentration of 5×10^{10} P/mL.	199
Figure 7.5: Particle size and polydispersity as a function of increasing backpressures in the TFF system. A) Samples collected and analysed on the retentate side including	

images obtained from NTA analysis and particle characteristics obtained via DLS. B) Backpressures were controlled with differently sizes capillaries, varying in inner diameter (I.D.) and length allowing different flow rates to be used in the system. C) Samples collected and analysed on the permeate side including images obtained from NTA analysis and particle characteristics obtained via DLS. n/a = not applicable. All runs are presented as average of three independent runs \pm SD.....	201
Figure 7.6: DLS measurement of A) intensity and B) volume based size distribution profiles comparing the retentate (red) and permeate (green) at 80 psi backpressure, confirming presence of particulates in the permeate.....	202
Figure 7.7: SDS-PAGE of ovalbumin filtered in the TFF system at 1 mg/mL (red) and 0.5 mg/mL (green) at backpressures of 15 and 80 psi.....	204
Figure 7.8: Vesicle size, polydispersity, zeta potential (zp) and particle concentration (P/mL) for cationic (DDA-TDB) and anionic (DPPC-Chol-DPPG) liposomes before and after the TFF purification. Images from NTA show vesicles present on the retentate side only.....	205
Figure 7.9: A) Vesicle size, polydispersity, zeta potential (zp) and particle concentration (P/mL) for anionic liposomes (DPPG-DPPC-Chol) prior and post ova-addition (ovalbumin, 100 μ g/mL), and particle characteristics after the TFF purification. B) Protein (ovalbumin) and ethanol removal in three diafiltration cycles for anionic liposomes (DPPG-DPPC-Chol), expressed as % to the initial amount of contaminants present. C) Ovalbumin and ethanol removal in three diafiltration cycles with no liposomes present D) Propofol and ethanol removal in three diafiltration cycles for anionic liposomes (DPPG-DPPC-Chol), expressed as % to the initial amount of contaminants present. All runs are presented as average of three independent runs \pm SD.....	207
Figure 7.10: A) Vesicle size, polydispersity and zeta potential (zp) for cationic (DDA-TDB) liposomes prior and post ova-addition (ovalbumin, 100 μ g/mL) and particle characteristics after the TFF purification. B) Protein (ovalbumin) and ethanol removal in three diafiltration cycles for cationic liposomes (DDA-TDB), expressed as % to the initial amount of contaminants present. C) NTA analysis for liposomes before (left) and after (right) loading with model protein (ovalbumin, 100 μ g/mL). All runs are presented as average of three independent runs \pm SD.	209
Figure 7.11: A) Schematic overview of the continuous on-chip liposome manufacturing. Liposomes were manufactured with a SHM mixer upstream and lead through the TFF system for consecutive on-chip purification. B) Schematic overview of the formation of liposomes loaded with a low-solubility model drug. Vesicle assembly and drug loading are performed with a SHM, non-entrapped (free) drug to be removed by consecutive	

TFF. C) Schematic overview of the formation of liposomes loaded with a protein model. Vesicle assembly is performed with a SHM, with protein addition post assembly, non-entrapped (free) protein to be removed by consecutive TFF.	210
Figure 7.12: Lipid recovery in the continuous process setup for A) lipid recovery after four diafiltration cycles. B) Lipid concentration in four concentration cycles, related to the initial amount of lipids present prior to the concentration cycles. All runs are presented as average of three independent runs \pm SD.....	211

Chapter 8

Figure 8.1: X/Y overview plot indicating the cumulated R^2 and Q^2 values for each response for A) DDA and size and B) DDA, size and zeta potential. Well modelled responses show a R^2 and Q^2 value above 0.5 poor model fit was indicated by negative Q^2 (statistical insignificance).....	221
Figure 8.2: PCA cluster analysis with colour coding according to A) ZP, B) DDA concentration, C) vesicle size D) IgG, E) INF- γ , F) IL-2, G) spleen proliferation and H) IL-6.....	222
Figure 8.3: PLS analysis results with coefficient overview, displaying the coefficients for all responses to interpret how the X-variables affect the Y-variables for A) DDA and size and B) DDA, size and zeta potential. Loading scatter plot, where the relation between X and Y- variables are displayed for C) DDA and size and D) DDA, size and zeta potential.....	223
Figure 8.4: VIP plot (variable importance for projection) summarizing the importance of the variables liposome size and zeta potential. The VIP plot is sorted from high to low and indicates the value of the variable DDA and zeta potential as the most important X-variables in the PLS model for A) DDA and size and B) DDA, size and zeta potential.	225
Figure 8.5: Permutations plot for A) zeta potential, B) IgG, C) spleen proliferation, D) IFNg, E) IL-2, F) IL-6. Model validity was assessed for 40 permutations. The correlation between permuted Y-vector to the original X-vector is depicted by the horizontal correlation axis. The criteria for model validity have been selected as the intercept of the Q^2 regression line at or below zero.....	227

Chapter 9

Figure 9.1: The effect of alterations in A) TFR and FRR at a constant solvent flow rate of 0.5 mL/min and B) FRR at constant TFR of 1 mL/min to the physicochemical vesicle characteristics in the 200 μ m chip design. Results denote mean \pm SD of 3 separate batches.	231
--	-----

Figure 9.2: Freeze-fractured liposome samples manufactured with the microfluidics-method. Bar represents A) 1 μ m, B) 200 nm, C) 100 nm and D) 200 nm.....	232
Figure 9.3: Schematic depiction over the setups for antigen incorporation for A) consecutive liposome mixing, B) consecutive mixing of liposomes and antigen and C) direct mixing of lipids and antigen.....	233
Figure 9.4: The effect of increasing A) total flow rate and B) flow rate ratio (TRIS buffer only) to liposome vesicle characteristics. C) The effect of increase in flow rate to liposome vesicle characteristics at consecutive protein addition in the microfluidic mixing process and addition of the protein to vesicles without microfluidic mixing. Start formulation was manufactured at 2 mL/min, 1:3. Where shown, significance between data is against the start formulation characteristics (* $p < 0.05$). Results denote mean \pm SD of 3 separate batches.	235
Figure 9.5: Time dependent migration assay for A) immature dendritic cells (iDC) and B) macrophages (MO) over 12h.	237
Figure 9.6: Association assay for dendritic cells (DC) expressed as A) MFI, B) %+ve cells over 2h and for macrophages expressed as C) MFI, D) %+ve cells over 2h.....	239
Figure 9.7: A) Effect of alteration in flow rate ratio to particle characteristics. The total flow rate has been maintained constant at 4 mL/min. B) Effect of dialysis for solvent removal to particle characteristics. C) Effect of method of polymer nanoparticle manufacturing to particle characteristics. Nanoparticles were prepared by solvent evaporation (Rescignano et al., 2013) and microfluidics (TFR 4 mL/min, FRR 1:4). The setting in the microfluidics have been maintained at FRR 1:4, TFR 4 mL/min. Results denote mean \pm SD of 3 separate batches. Solvent = Acetonitrile, 200 μ m chip design.	241
Figure 9.8: A) Effect of polymer choice to particle characteristics. The setting in the microfluidics have been maintained at FRR 1:4, TFR 4 mL/min. B) Stability of PLGA nanoparticles manufactured by microfluidics over a storage period of 7 days at 4°C. Results denote mean \pm SD of 3 separate batches in each method.....	242
Figure 9.9: Effect of protein loading to A) size, B) zeta potential and C) polydispersity. The setting in the microfluidics have been maintained at FRR 1:4, TFR 4 mL/min, protein has been added post particle manufacturing and particle characteristics were assessed after 45 min incubation time at room temperature. Results denote mean \pm SD of 3 separate batches.....	243

Abbreviations

ANOVA	Analysis of variance
APC	Antigen presenting cell
CF	Carboxyfluorescein
Chol	Cholesterol
CM2	1,1'-(decane-1,10-diyl)bis(9-amino-1,2,3,4-tetrahydroacridinium) diiodide
CoC	Cyclic olefin copolymer
COS-7	African green monkey kidney cells
DDA	Dimethyldioctadecylammonium bromide
DLS	Dynamic light scattering
DMEM	Delbecco's modified eagles medium
DoE	Design of experiments
DOPE	1,2-dioleoyl-sn-glycero-3-phosphoethanolamine
DOTAP	1,2-dioleoyl-3-trimethylammonium-propane
DOTMA	N-[1-(2,3-dioleoyloxy)propyl]-N,N,N-trimethylammonium chloride
DQA	Dequalinium
DSPC	1,2-distearoyl-sn-glycero-3-phosphocholine
ELISA	Enzyme-linked immunosorbent assay
ELSD	Evaporative light scattering detector
EPR	Enhanced permeability and retention effect
FBS	Foetal bovine serum
FRR	Flow rate ratio
GC	Gas chromatography
HeLa	Human cervical carcinoma cells
HPLC	High performance liquid chromatography
HRP	Horseradish peroxidase
HSM	High shear mixing
i.m.	Intramuscularly
iDC	Immature dendritic cell
IPA	Isopropanol
LOD	Limit of detection
LOF	Lack of fit
LOQ	Limit of quantification
LUV	Large unilamellar vesicles
MLV	Multilamellar vesicles
MTB	Mycobacterium tuberculosis

mtDNA	Mitochondrial DNA
MTT	Thiazolyl blue tetrazolium bromide
MVA	Multivariate analysis
MVV	Multivesicular vesicles
NTA	Nanoparticle tracking analysis
NWP	Normalized water permeability
OFAT	One factor at a time
PAMP	Pathogen associated molecular pattern
PBS	Phosphate buffer saline tablets
PC	Phosphatidylcholine
PCA	Principal component analysis
PCS	Photon correlation spectroscopy
PDI	Polydispersity index
PDMS	Poly(dimethylsiloxane)
Pe	Peclet number
PLA	Poly(lactic acid)
PLGA	Poly(lactide-co glycolide)
PLS	Partial least square
PMMA	Poly(methylmethacrylate)
PRR	Pattern recognition receptor
PSG	Penicillin-streptomycin-58 glutamine
PTFE	Polytetrafluoroethylene
QbD	Quality by design
QELS	Quasielastic light scattering
Re	Reynolds number
RES	Reticuloendothelial system
RP	Reverse phase
RSD	Relative standard deviation
SDS-PAGE	Sodium dodecyl sulfate polyacrylamide gel electrophoresis
SHM	Staggered herringbone micromixer
siRNA	Small interfering RNA
SUV	Small unilammelar vesicles
TDB	Trehalose 6,6-dibehenate
TDM	Trehalose 6,6 -dimycolate
TEM	Transmission electron microscopy
TFA	Trifluoroacetic acid
TFF	Tangential flow filtration

TFR	Total flow rate
TMP	Transmembrane pressure
VIP	Variable importance for the projection

Chapter 1

General Introduction

Papers relating to this chapter:

Kastner E., Schmidt S. T., Wilkinson A., Christensen D. and Perrie Y. (2015). The Application of Liposomes as Vaccine Adjuvants. In Foged C., Rades T., Perrie Y., Hook S. Eds *Subunit Vaccine Delivery* Springer New York. pp. 77-94.

1.1 Liposomes

Liposomes were discovered by Bangham in 1965, initially being used as a model of cell walls to investigate receptors (Bangham et al., 1965). In 1974, Gregoriadis first described liposomes as a delivery vehicle for drugs and suggested their effectiveness as vaccine delivery systems (Allison and Gregoriadis, 1974). To date, liposome-based research and developed technologies have led to several candidates on the market and in clinical trials.

By definition, liposomes are vesicles comprised of lipids. The amphiphilic structure of lipids combines a polar head groups and a hydrophobic carbon tail, leading to spontaneous formation of lipid bilayers when suspended in an aqueous medium (Lasic, 1998). The orientation of the lipids triggers the assembly into vesicles with a closed-off aqueous core (Figure 1A). As the core component of the liposomes, lipids strongly influence the physicochemical parameters of the resulting liposomes, including surface charge and membrane rigidity (Watson et al., 2012), whereas the resulting size of the vesicles is not only dominated by the lipid composition but also dictated by the manufacturing method (Perrie et al., 2013).

Liposomes are categorized by their vesicle size (diameter) and numbers of lipid bilayers usually ranging within 25 nm to 2.5 μm in size (Figure 1B) (Taylor et al., 2005).

- i) Small unilamellar vesicles (SUV); size $\leq 0.1 \mu\text{m}$; single bilayer membrane.
- ii) Large unilamellar vesicles (LUV); size $> 0.1 \mu\text{m}$; single bilayer membrane.
- iii) Multilamellar vesicles (MLV); size $> 0.1 \mu\text{m}$; multi-bilayer membrane.
- iv) Multivesicular vesicles (MVV); size $> 0.1 \mu\text{m}$; multi-bilayer membrane, incorporation of several vesicles into a singly bilayer.

The bilayer vesicle structure of liposomes allows for the entrapment of hydrophilic components in the core of the vesicles as well incorporation of hydrophobic components incorporated within the lipid bilayer. Furthermore, components can be attached to the surface of the vesicles, based on electrostatic interaction or covalent bonding to lipophilic anchors incorporated into the lipid bilayer (Watson et al., 2012). The flexibility in different lamellarity structure and sizes of the vesicles, along with a range of lipid choices influencing the surface potential of the vesicles, liposomes comprise a flexible drug delivery method.

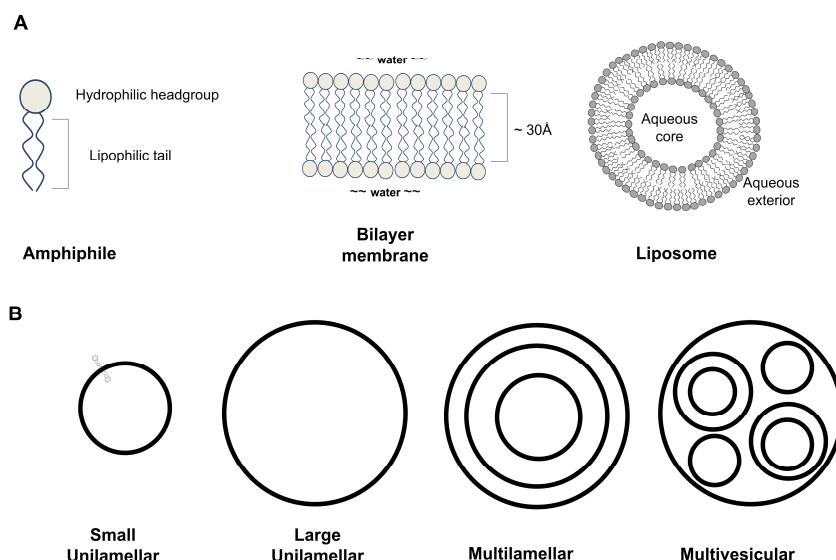


Figure 1.1: A) Schematic representation of a liposome, comprised of a bilayered lipid membrane. B) Schematic representation of liposome structures.

1.1.1 The importance of liposome size

The size of the liposomal vesicles dictates clearance and targeting *in-vivo*. A liposome with a diameter greater than 400 nm is quickly captured by the reticuloendothelial system (RES), whereas smaller vesicles (< 200 nm) are circulating longer after systemic administration (Liu et al., 1992; Maruyama et al., 1992). Due to greater capillary permeability in tumours, small liposomes accumulate and retain in well-vascularized tumours, as described by the enhanced permeability and retention effect (EPR) (Maeda, 1992). In the design of liposomal adjuvants, the vesicle size is well known to affect the immune responses towards a Th1 or Th2 cytokine profile via a range of routes (Brewer et al., 2004; Brewer et al., 1998b; Carstens et al., 2011; Mann et al., 2009; Manolova et al., 2008). Where smaller particles promoted enhanced Th2 responses, larger vesicles promoted typical Th1 responses (Brewer et al., 1998a; Mann et al., 2009), linked to differences in particle trafficking to local lymph nodes and uptake by antigen presenting cells (APCs).

1.1.2 Liposomes as immunological adjuvants

It was Gregoriadis in 1974 who first described liposomes to act as immunological adjuvants, despite little being known about the immune system (Allison and Gregoriadis, 1974). Since then, liposomes have been extensively developed and investigated for the delivery of a wide range of disease antigens (Christensen et al., 2007b; Gregoriadis et al., 1987). The effectiveness of liposomes acting as immunological adjuvants is linked to their flexibility in delivering an antigen, which may be incorporated (Perrie and Gregoriadis, 2000) or associated into the bilayer (May et

al., 2000; McNeil et al., 2010). The ability to act as adjuvants for protein-based vaccines is further strengthened by the flexibility in formulation, the particulate nature and the versatility, all promoting a range of immune responses (May et al., 2000; McNeil et al., 2010).

A successful subunit vaccine requires the delivery of the non-immunogenic antigen along with an immunostimulatory compound. In subunit vaccines, antigens are often highly purified proteins or peptides derived from pathogens, which lack an immunostimulation if delivered alone, and additional immunostimulatory compounds like lipids, proteins, peptides, DNA or RNA are required. As mentioned, liposomes allow for a range of designs, sizes, surface charges, and the incorporation of these immunostimulatory compounds in the interior, the bilayer, or the particle surface comprises a powerful delivery system of these components to APCs. Such immunostimulatory or –potentiating compounds are often (synthetic) pathogen associated molecular patterns (PAMPs), which are ligands for the pattern recognition receptors (PRRs). These are often specific to natural ligands from specific pathogens (Hafner et al., 2013).

Cationic lipids interact with negatively charged molecules like nucleic acids (Karmali and Chaudhuri, 2007), proteins and peptides (Christensen et al., 2009). In comparison to encapsulation methods, the charged-based interaction between liposomes and target molecules is less time and cost consuming. Compared to neutral or negatively charged liposomes, cationic liposomes account for an enriched protection of anionic antigens as well as promoting the formation of a depot at the injection-site (Kaur et al., 2012b). Furthermore, the positive charge enhances antigen uptake by dendritic cells and macrophages and antigen presentation (Lonez et al., 2008).

It was Gall and colleagues who first described the immunological properties of cationic lipids in 1966 (Gall, 1966). The quaternary ammonium compound dimethyldioctadecylammonium bromide (DDA) is a synthetically derived amphiphilic molecule that consists of a hydrophilic positively charged dimethylammonium head-group and a tail of two hydrophobic 18-carbon alkyl chains. DDA spontaneously form bilayer vesicles once exposed to an aqueous environment. The adjuvant effect was first described by Gall in the 1960s (Gall, 1966) and has to date been used as a liposomal subunit vaccine to trigger immune responses. DDA itself was shown to trigger a weak Th1 type immune response (Olsen et al., 2001). DDA-liposomes deliver the antigen to the cell surface and trigger efficient antigen uptake and presentation

(Smith Korsholm et al., 2007). Liposomes based solely on DDA were shown to efficiently induce humoral and cell mediated immune responses; however, physical instabilities has limited its use in adjuvants (Davidsen et al., 2005). For example, salt addition leads to aggregation observed in aqueous environment over time (Davidsen et al., 2005). In order to address considerations, a range of additional lipids have been investigated and evaluated to both improve stability and enhance efficacy of DDA liposomes. In particular, trehalose 6,6-dibehenate (TDB) has been used as an immunostimulatory compound in DDA-liposomes to enhance the immune response and vaccine efficiency (Smith Korsholm et al., 2007). TDB glycolipid consists of a 6,6' - diester of α - α' trehalose with two 22-carbon acyl chains (behenic acids). TDB is a synthetic analogue of trehalose 6,6 -dimycolate (TDM); often referred to as cord factor; a component in the mycobacterial cell wall. TDM has a strong immunostimulating effect; the shorter fatty acid chains of TDB are associated with its lower toxicity (Davidsen et al., 2005). Without the addition of TDB, the liposomes were found not able to induce an immune response, while its incorporation induced strong immune responses (Nordly et al., 2011; Rosenkrands et al., 2005).

Cationic DDA-TDB liposomes were shown to stimulate cell mediated immune response as well as an antibody response and TDB serves as a stabilizing agent for the DDA vesicles (Davidsen et al., 2005). The size of DDA-TDB vesicles was shown to influence the cell-mediated immune response (Henriksen-Lacey et al., 2011a). The cationic head group of DDA allows to target the negatively-charged cell membrane of APCs, stimulating the uptake of an associated protein antigen (Smith Korsholm et al., 2007). The incorporation of TDB furthermore enhances the immune response against a range of subunit vaccine antigens (Ishikawa et al., 2009; Werninghaus et al., 2009).

The induction of the immune response strongly depends on the association between the adjuvant and the antigen. Studies have shown that DDA-TDB together with a negatively-charged tuberculosis antigen, Ag85B-ESAT-6 (H1 antigen) significantly increased the immune response once compared to the same antigen not associated to the adjuvant (Andersen and Doherty, 2005; Kamath et al., 2012). Furthermore, the combination of the cationic delivery system together with the negatively charged H1 antigen remained localized at the site of injection, whereas an antigen, not able to electrostatically associate with the delivery system, was found in the draining lymph nodes (Henriksen-Lacey et al., 2010b). For the delivery of peptides similar results were observed. Peptides encapsulated in a vesicle or associated on the surface induced a Th1 immune response, whereas free peptide did not raise any immune response

(Guan et al., 1998). The adsorption onto the surface of the liposome further induced humoral immune response, opposed to peptide encapsulated within the vesicles (Guan et al., 1998). The combination of DDA-TDB liposomes with the H1 antigens is a promising candidate for a new TB vaccine currently in clinical trials (NCT 00922363); accompanied by strong protective immune responses (Andersen and Doherty, 2005; Henriksen-Lacey et al., 2011b).

1.1.3 Liposomes as transfection agents

Other than the delivery of proteins and peptides, liposomes have been extensively investigated as particulate systems for non-viral gene delivery (Allison and Gregoriadis, 1974). Felgner showed in 1987 that cationic liposomes promote gene expression *in-vitro* (Felgner et al., 1987). The incorporation of DNA into cationic liposomes resulted in high levels of gene expression (Karmali and Chaudhuri, 2007). The fusion of a cationic liposome with a negatively charged nucleic acid is referred to as lipoplex. Cationic lipids are the core of these gene delivery systems, which led to many cationic liposome mediated transfection studies (Fumoto et al., 2004; Majeti et al., 2004; Perrie et al., 2002). Lipoplexes typically range within 80-400 nm, which strongly depends upon cationic lipid/DNA ratio, type of lipids used and method of preparation.

The delivery strategy is based on the intracellular liposome mediated gene transfer, where DNA or other polynucleotides are translated to a protein or peptide. The cationic surface charge of lipoplexes mediates electrostatic interaction with the negatively charged cell wall. The incubation of lipoplexes with cultured cells triggers the release of the DNA into the cytoplasm after the uptake based on a vesicular pathway based on clathrin-mediated endocytosis, caveolae-mediated endocytosis or macropinocytosis (Uyechi-O'Brien and Szoka, 2003; Wasungu and Hoekstra, 2006). DNA trafficked into the nucleus is transcribed and translated into the protein encoded by the DNA. The size of the DNA and the time of transfection was shown to influence the transfection outcome (McNeil and Perrie, 2006). Furthermore the charge and lipid/DNA ration have previously been shown to effect transfection efficiency (Aljaberi et al., 2007; Caracciolo et al., 2007). The commercially available LipofectinTM has been extensively used to transfect a wide variety of cells (Fortunati et al., 1996; Malone et al., 1989); made of 1,2-dioleoyl-sn-glycero-3-phosphoethanolamine (DOPE) and N-[1-(2,3-dioleoyloxy)propyl]-N,N,N-trimethylammonium chloride (DOTMA) (Felgner et al., 1987).

1.1.4 Liposomes for the solubilisation

Besides the use of liposomes for the delivery of nucleic acids and aqueous soluble moieties, they are also well placed to act as solubilisation agents for drugs with low aqueous solubility. With currently more than 40% (Williams et al., 2012) of all new chemical entities in discovery having low solubility, this is of considerable interest. Drugs with low aqueous solubility effects bioavailability and efficacy (Savjani et al., 2012; Williams et al., 2012). The therapeutic application of a drug with low aqueous solubility is associated with poor absorption, potentially leading to aggregates formed upon intravenous administration of the low solubility drug, leading to embolisation of blood vessels and potential failure of the respiratory system (Lukyanov and Torchilin, 2004). Aggregation may further lead to local toxicity and lowered systemic bioavailability (Lukyanov and Torchilin, 2004). Poor aqueous solubility has been listed as one of the main challenges in the formulation industry (Muller and Keck, 2004). Therefore, solubilisation strategies are urgently required. Approaches to enhance the solubility include the adjustment of the pH of ionisable drugs, a function of the aqueous media conditions. Nevertheless, drugs without any ionisable moiety cannot be ionized by altering the pH. Co-solvents have been used to aid the solubility of drugs (Seedher and Bhatia, 2003) and polyethylene glycol has been described to enhance the solubility of sparingly soluble drugs (Nandi et al., 2003). Furthermore, solid dispersions maybe used to improve the oral bioavailability of poorly water soluble drugs using melting or evaporation methods (Vasconcelos et al., 2007). Solubilizing a low solubility drug in the bilayer of liposomes allows the solubilisation in aqueous media, protection from degradation and control of the drug distribution profile along with aiding the therapeutic efficacy. The advantage of using liposomes as solubilisation vesicles is linked to their particulate nature, the ability for targeted delivery and the flexibility in range of lipids incorporated. Research on using liposomes as solubilizing agents has shown that drug incorporation and release rates were strongly linked to the properties of the drug as well as the lipid concentration and the choice of lipids (Ali et al., 2010; Ali et al., 2013; Mohammed et al., 2004). The molecular weight of the drug, as well as the log P, were important factors influencing the effective loading of liposomes (Ali et al., 2013). Furthermore, the lipophilic volume was shown to enhance the loading of a low solubility drug into liposomes by using longer alkyl chain lipids (Mohammed et al., 2004; Ali et al., 2013). Other than the chain length, the charge of the lipids was shown to impact the loading efficiency, as like-charged lipids result in electrostatic repulsion of drugs (Mohammed et al., 2004). Given cholesterol being well known to enhance the stability of vesicles, it was further shown to reduce bilayer drug loading, giving its space-filling action in the bilayer membrane (Ali et al., 2010). Furthermore, the incorporation of

cholesterol into the lipid bilayer shifted the drug release profile from a zero-order (when no cholesterol was present) to first order (when 11 to 33 mol% of cholesterol was incorporated). Following, the membrane could be associated more porous without the incorporation of cholesterol, whereas the incorporation of cholesterol rendered the membrane into a more condensed and less-permeable bilayer (Ali et al., 2010).

1.1.5 Traditional liposome manufacturing methods

The method of vesicle manufacturing can be a dominating factor influencing the resulting particle size (Table 1.1). All methods rely on the assembly of the vesicles based on the exposure of the amphiphilic lipid molecules to an aqueous buffer system (Taylor et al., 2005). Generally, traditional manufacturing methods rely on a “top-down” method, comprising the manufacturing of initially large vesicles, which are sequentially reduced in size and lamellarity by mechanical methods.

For example, the lipid film hydration method (first described in 1961 by Alec Bangham (Bangham, 1961; Bangham et al., 1965)) involves a mixture of lipids being dissolved in a solvent, often chloroform or a mixture of chloroform and methanol. Solvent removal via rotary evaporation results in the formation of a dried lipid film on the wall of the round bottom flask. Nitrogen is further used to remove any residual solvent left prior to addition of the aqueous phase. This hydration step is key in forming the vesicles, aided by mechanical agitation and performed above the transition temperature of the lipids (Bangham et al., 1965; Szoka Jr and Papahadjopoulos, 1980). Mechanical stresses, such as vortexing result in the rearrangement of the lipids and budding into MLV by swelling lamella from the flask bottom. The resulting vesicles are generally quite polydisperse and relatively large, ranging up to several microns in size. The resulting size is primarily dictated by the choice of lipids, the aqueous hydration buffer and the temperatures adopted during vesicle formation (Bangham et al., 1965; Gregoriadis et al., 2002). A molecule of interest may be added into the aqueous hydration buffer or in the solvent phase, leading to encapsulation in the aqueous core or into the lipid bilayer respectively. Nevertheless, reported encapsulation efficiencies are usually low (Riaz, 1996) and the hydration time was found as a contributing factor controlling the encapsulation efficiency time (Bangham et al., 1965). Other methods used that result in the formation of large vesicle structures include reverse-phase evaporation and depending on the size range required, injection methods may also produce a range of liposome sizes as required (Table 1.1). To reduce vesicle sizes, subsequent mechanical methods are used. These methods often rely on shear or pressure forces, including a microfluidisation, high-pressure homogenisation or other shear force-

induced homogeniser (Szoka Jr and Papahadjopoulos, 1980; Wagner and Vorauer-Uhl, 2010). Those methods introduce a high and controlled pressure, disrupting the MLV and leading to the formation of SUV in a continuous and scalable process setup (Wagner and Vorauer-Uhl, 2010). Pressures are as high as 20 000 psi, where forcing MLV thorough a small gap and collision with a stainless steel wall results in smaller vesicles generated (Barnadas-Rodríguez and Sabés, 2001; Bergstrand et al., 2003). Often, several cycles are required to yield a homogenous and final size distribution; the option of continuous processing accomplishes this. During an extrusion method, MLV are lead through a membrane, filter or mesh with desired pore size. The pressure can be adjusted to yield the final size distribution, which is often dictated by the pore size and the number of recirculation runs (Riaz, 1996). The sonication method is another frequently applied method, mainly used in research and development processes. A probe or a bath sonicator breaks up larger vesicles into smaller ones, and the process runs at temperatures above the transition temperature of the lipids (Wagner and Vorauer-Uhl, 2010). The main disadvantages of these methods is the lack of scalability and relatively low encapsulation efficiencies and drug loading (Riaz, 1996). Furthermore, lipids subjected to the sonication power might degrade and the direct contact with the probe tip results in a contamination with metal residues. The high-energy input is required for breaking up larger vesicles into smaller ones. Heat developing during the process might be a further problem for heat sensitive material. A bath sonication process circumvents the contamination by metal residues, maintaining the sterility in the formulation (Kataria et al., 2011). In contrast to the mechanical top down method, methods around fluidic control can be summarized as bottom-up methods (Table 1.1). The ethanol injection method was the first one reported in the 1970s by Batzri and Korn (Batzri and Korn, 1973). Lipids are initially dissolved in a solvent, followed by rapid injection of the solvent into an aqueous buffer stream. The precipitation of the lipids leads to the formation of vesicles. The method itself is relatively simple; however, results are dictated by the solubility of the lipids in the water-miscible solvent, which strongly influences resulting homogeneity. Furthermore, solvent residues remain. These are removed by heating in the similar ether-injection method. Using this type of method, encapsulation efficiencies within liposomes may be relatively high for hydrophobic drugs, where the encapsulation of a hydrophilic drug is generally relatively low due to the high volumes of aqueous phase and resulting dilution (Jaafar-Maalej et al., 2010). However, this type of methods can generally be considered scalable, simple and highly applicable for a large-scale process. Indeed, the control of lipid sizes has been reported in an adaptive method, called inkjet method (Hauschild et al., 2005).

Table 1.1: Overview of traditional methods of liposome manufacturing, adapted from (Kastner et al., 2015).

Method		Advantages	Disadvantages	Vesicles	Sizes reported	Ref.
Mechanical methods	Rotary evaporation	Easy Simple	Organic solvent residue No control over vesicle size Additional method for size reduction required Heterogeneity Low encapsulation	MLV	Up to several microns	(Bangham, 1961)
	“Top-down” methods	Homogenization, extrusion, high shear mixing	Easy Simple design Bulk production Continuous	SUV	Dependent on no of cycles and pressure	(Bally et al., 1991)
		Sonication	Easy Relatively quick	SUV	> 90 nm	(Wagner and Vorauer-Uhl, 2010)
	Reverse phase evaporation	High encapsulation efficiencies	Contact with organic phase Time intensive Limited scalability	LUV	Intermediate nm to um	(Meure et al., 2008)
Fluid control “bottom up” methods	Injection	Ethanol injection	Rapid, easy No special equipment required High encapsulation of hydrophobic drugs	SUV	Dependent on needle diameter pressure and concentration < 100 nm	(Batzri and Korn, 1973) (Jaafar-Maalej et al., 2010)
		Ether injection	Size controlled SUV Higher encapsulation efficiencies	SUV	100-300 nm	(Deamer and Bangham, 1976) (Deamer, 1978)
		Inkjet	Small unilamellar SUV Loading in combination with liposome formation High reproducibility	SUV	50 – 200 nm	(Hauschild et al., 2005)
		Supercritical fluid	Very small particles reported	SUV	>25 nm	(Frederiksen et al., 1997) (Karn et al., 2013)
			High costs High pressures Encapsulation lower than with conventional methods			

1.2 Microfluidics

1.2.1 Background

Despite all the advances in the application of liposomes they are limited by their manufacturing methods and new systems for reproducibly vesicle manufacturing are needed.

Microfluidic devices comprise fluid handling in a constrained volume, achieving millisecond mixing at the nanoliter scale (Demello, 2006; Song et al., 2008). The area of microfluidics and its associated development of novel lab-on-a-chip based devices considerably gained attention over the past decades (Nguyen and Wu, 2005). Microfluidics is a complex area; besides the fundamentals of physics and chemistry, mass transport, heat and mass transfer, fluid flow, thermodynamics, elasticity, electrostatics are important areas incorporated (Squires and Quake, 2005). Characterisation of the fluid flow in micromixing is essential for understanding its impact to the mixing performance. It is important to understand that a micromixer is not just a copy of a mixer at larger size. The design has to leverage physical characteristics as far as possible (Capretto et al., 2011). With an increasing number of liposomal products in clinical trials and development (Chang and Yeh, 2012) the demand for rapid process development tools rises, emphasised by several microfluidic-based methodologies in drug development (Dittrich and Manz, 2006; Hood et al., 2014a; Weigl et al., 2003; Whitesides, 2006). Microfluidic-based technologies offer an enhanced control over processing conditions, thus yielding a set-up for reproducible and robust manufacturing, which is required to achieve uniform liposome size distributions; at the same time, the miniaturisation makes efficient use of materials. Whilst reducing volumes during development processes, costs can be diminished whereas throughput is increased (Jensen, 2001; van Swaay, 2013; Weibel and Whitesides, 2006).

1.2.2 Microflow physics

1.2.2.1 Dimensionless numbers

Dimensionless numbers describe fluid flow patterns and physical phenomena for flow characterisation. The Reynolds Number (Re) is one the most frequently used dimensionless numbers in fluid flow. Describing the ratio of inertia to viscous forces it is used to determine whether fluid flow is categorised as laminar or turbulent (Figure 1.2). Determination of the Re number includes the assessment of the characteristic length

L_0 , which differs according to system studied; for mixing in a channel or pipe, the characteristic length is described by the channel diameter (Equation 1.1).

$$Re = \frac{\rho u L_0}{\mu} = \frac{\rho u D_h}{\mu} = \frac{u D_h}{\nu} \quad \text{Equation 1.1}$$

With

L_0	Characteristic length
u	Fluid velocity
D_h	Hydraulic channel diameter
ν	Kinematic viscosity
μ	Dynamic viscosity
ρ	Fluid density

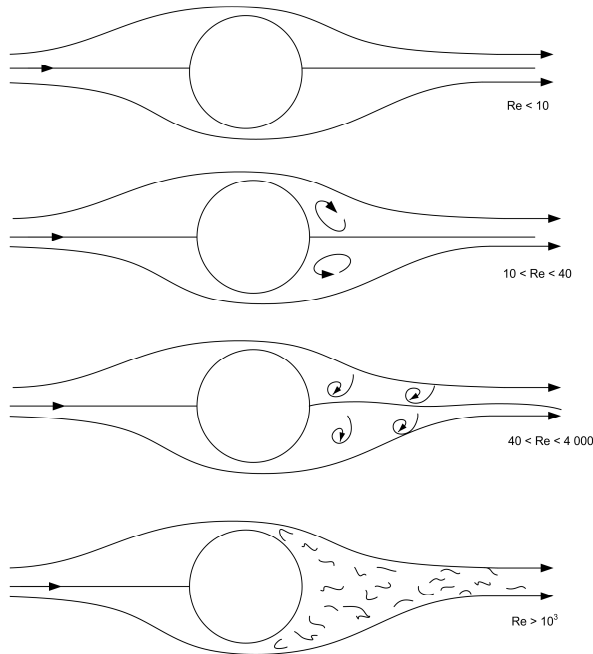


Figure 1.2: Flow profile around a cylinder for increasing Re numbers.

Due to small characteristic length in micromixing devices, Re numbers are usually small (< 100) and generally fall into laminar flow regime (Capretto et al., 2011). At such low Re numbers, mixing is dominated by diffusion, considerably taking a long time. Besides diffusion, advection dominates mixing performance in microchannels (Das and Chakraborty, 2009) indicated the difference transition number from laminar to turbulent applicable for microfluidic mixing. The Peclet number (Pe) expresses ratio of convection to diffusion and is used to characterize the nature and strength of diffusion. The Pe number is used to calculate the approximate number of channel widths in length that is required for achieving diffusive mixing. At high Pe numbers, advection is dominant in a fluid (Equation 1.2). The characteristic mixing length grows linearly with Pe (Stroock et al., 2002).

$$Pe = \frac{uL_0}{D} = \frac{uw}{D} \quad \text{Equation 1.2}$$

With

L_0	Characteristic length
u	Fluid velocity
w	Channel diameter
D	Diffusion coefficient

1.2.2.2 Micromixer characterisation

Both Re and Pe numbers are strongly influenced by the channel diameter; which underlies its significance in microfluidic mixing and mixer characterisation. The channel geometries significantly affect diffusion and are hence a key point of interest for the design of a microfluidic channel. The aim is to decrease the mixing path and increase the contact surface area (Capretto et al., 2011). As described above, the Re numbers in microfluidic channels are generally laminar and typically smaller than 100. Hence, mixing in microchannels is mainly dominated by passive molecular diffusion and advection. Diffusion describes a transport phenomena based on the Brownian motion of molecules; molecules spread from higher to lower concentrations and within a certain time achieve equilibrium. Diffusion hence results in gradual mixing of molecules and can be described by Fick's Law (Equation 1.3) (Capretto et al., 2011).

$$j = -D \frac{d\varphi}{dx} \quad \text{Equation 1.3}$$

With

φ	Molecule concentration
x	Molecule position
D	Diffusion coefficient

For the assumption of simple spherical particles, Einstein-Stokes equation is used to derive the diffusion coefficient (Equation 1.4).

$$D = \frac{kT}{6\mu R} \quad \text{Equation 1.4}$$

With

μ	Viscosity of the medium
k	Boltzmann constant
T	Absolute temperature
R	Radius of the particles

A molecule requires a certain time to diffuse, whereas the diffusion process itself is a nonlinear which is modelled into Equation 1.5 (Capretto et al., 2011).

$$x^2 = 2Dt \quad \text{Equation 1.5}$$

With

t Average time for a molecule to diffuse over the distance x

x Stream width in channel

Equation 1.5 indicates the importance of the channel width in microfluidic mixers. As the stream width varies with squares power, an increase in channel width drastically affects the diffusion process and hence leads to an increase in time till mixing can be sufficiently achieved. Hence, diffusion actually becomes a variable in microfluidic mixing (Capretto et al., 2011).

1.2.3 Classification active passive micromixers

In order achieve complete diffusive mixing, devices have been developed to decrease mixing length. Developed micromixers can be classified into active and passive micromixers (Capretto et al., 2011). Active micromixers require an input from an external energy source; this can be pressure-driven, temperature-induced or ultrasonic-driven. Active micromixers are categorized by their energy input or disturbance, meaning pressure, electrokinetics, dielectrophoretic, electrowetting, magneto-hydrodynamic or ultrasound (Nguyen and Wu, 2005). Despite high mixing efficiencies in active micromixers, their engineering setup can be quite complex. The incorporation of the external power source into the microfluidic mixing chamber or device is cost and time intensive, with resulting restricted application in industry. Besides, high temperatures or ultrasonic applications might lead to damage of biological materials (Capretto et al., 2011).

So called passive mixers (Table 1.2) do not require an additional external energy source to achieve mixing, but use the fluid flow and specially designed micro-structures that enhance diffusion and advection processes (Nguyen and Wu, 2005). In order to maximize diffusion by decreasing the diffusion path and increasing the surface area between different fluids, passive micromixers often undergo extensive channel engineering to modify the flow pattern. Engineering activities, including the splitting of fluid flow streams, introduction of bubbles or gas, alterations in channel design, width and shape by introduction of grooves, lead to a number to extensively altered micromixing chambers. Their integration to lab-on-a-chip based devices is easier; as no external power source has to be incorporated (Capretto et al., 2011).

Table 1.2: Selection of common passive micromixers

Passive Micromixer	Mixing principle	Type	References
T- and Y-shaped	To stream are guided in one flow path; mixing solely by diffusion and hence generally slow		(Gobby et al., 2001)
Parallel lamination	Split of inlet stream into a number of sub-streams and their rejoin. Enhanced mixing by increased surface area and decreased diffusion length	Bifurcation-type feeds, Interdigital-type feeds, Chessboard micromixer, Circular micromixer	(Erbacher et al., 1999)
Sequential lamination	Sequential splitting and recombination and rearrangement of fluid streams	Split-and-recombine micromixer, crossing manifold micromixer	(Lee et al., 2003)
Flow focusing	Hydrodynamic focusing of the middle inlet stream by two outer fluids, leading to decreased lamination width of the inner stream	Horizontal and vertical flow focusing devices	(Wu and Nguyen, 2005)
Chaotic advection	Increase in interfacial area by altering channel shapes (split, stretch, fold, break) to alter flow direction and induce whirls and chaotic flow, grooved pattern in channel design	Slanted groove micromixer, staggered herringbone micromixer, connected-groove micromixer, circulation disturbance micromixer, 3D serpentine micromixers, zig-zag micromixer	(Stroock et al., 2002)
Droplet	Microdroplet generation by electric fields, micro-injectors or needles or multiphase flows, droplets lead to reduction in diffusion length and generation of recirculating flow in the droplet	T-junction droplet generator, planar serpentine micromixer	(Quevedo et al., 2005)

1.2.3.1 Staggered herringbone micromixer

The low Re numbers, as described earlier, have been the basis for engineering of novel micromixers. Stroock et al described a method for introducing chaotic flow even at low Re numbers ($0 < Re < 100$). The staggered herringbone micromixer (SHM) is a micromixer based on patterns of grooves in the channel floor (Figure 1.3A). The design introduces a chaotic flow in a microchannel by subjecting the fluid to repetitive series of a rotational flow profile, which is achieved by alteration of the grooves as a function of the axial position in the channel. Characterisation work by Stroock et al. (2002) determined the orientation of grooves in the floor changing after a half cycle in the design. This “centre of rotation” is hence changed along with the local extensional flow in the transverse flow (Stroock et al., 2002).

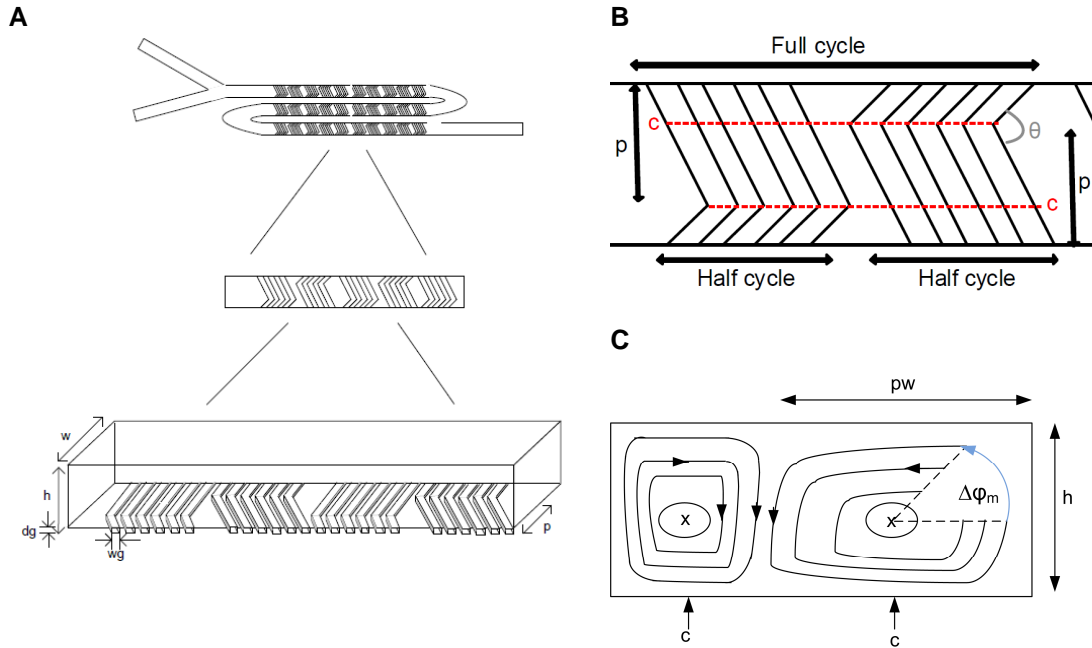


Figure 1.3: A) Schematic zoom into the microfluidic chip of a SHM. B) Schematic of six grooves per half cycle of a SHM. C) Schematic streamlines in the cross section of the channel with the angle $\Delta\phi_m$ as the angular displacement of the fluid volume along the wide arms of the herringbones. h = height of chamber, w = width of chamber, dg = depth of grooves, wg = width of grooves, p = asymmetric factor, c = centre of rotation, θ = angle of grooves, pw = asymmetry factor over the width of the long herringbone arms.

The mixing efficiency is characterised and controlled by the asymmetry of the herringbones as well as the rotational amplitude (Figure 1.3 B and C). The asymmetry of the herringbones is determined as p . p approaches one-half for symmetric herringbones, which results in a non-chaotic flow. Ideally, p approaches 2/3, which involves the majority of the cross sectional area in the chaotic flow. The rotation amplitude of the fluid at half a cycle is determined as $\Delta\phi_m$ (Figure 1.3C). This angular displacement is controlled by the design and number of the grooves per half cycle. A non-chaotic flow results for $\Delta\phi_m$ approaching zero. Ideally, $\Delta\phi_m = 60^\circ$; involving the majority of the cross sectional area in the chaotic flow (Stroock et al., 2002).

The flow in the SHM design was found independent of Re for $Re < 100$ (Stroock et al., 2002). When mixing two streams, the design allows for a rapid increase in the number of filaments, and the respective decrease in the filament thickness as a function of mixing cycles. Confocal micrographs showed the distribution of fluorescent molecules in the cross sectional area of the channel; the increase in number of filaments as well as the decrease of the thickness of fluid layers correlates with increases in mixing cycles. With increase in cycles the fluid layers are folded on top of each other, aiding mixing (Stroock et al., 2002). The design from Stroock et al. showed that even at high Pe numbers (9×10^5) mixing occurs.

1.2.4 Microfluidics for liposome manufacturing

The application of microfluidic tools for liposome manufacturing is based on the theory of a nanoprecipitation reaction. Nanoprecipitation produces nanoparticles in a one-step process (Bally 2012). The process has been described as the formation of particles sub-micron size at right polymer concentration and high enough ratio between aqueous to solvent flow (Stainmesse et al., 1995). This work was taken further, defining the nanoprecipitation process relying on a nucleation process, based on chemical instability (Mora-Huertas et al., 2011). The solvent needs to be miscible with the non-solvent phase, which is usually a buffer. Due to the mixing process of the two streams, molecules dissolved in the solvent phase are diluted, and this drastic dilution in the aqueous phase leads to the formation of precipitated molecules (Zook and Vreeland, 2010). With less solvent available for solubilisation of the hydrophobic chains, the closure time for the vesicle decreases, triggering the precipitation process and the formation of nanoparticles. With more solvent remaining present during the mixing process, hydrophobic components remain stabilised for a prolonged time. A dialysis tubing can be used to drive the nanoprecipitation method (Figure 1.4A) (RemziáBecer, 2009). The method was used in a larger-scale format (volumes of 20 mL per batch) where solvent phase was added dropped into an aqueous phase, stirred magnetically, after which evaporation of the solvent was conducted (Govender et al., 1999) (Figure 1.4B). Opposed to the top-down methods, no further disruption of the resulting nanoparticles is required and the method is categorized as a bottom-up method.

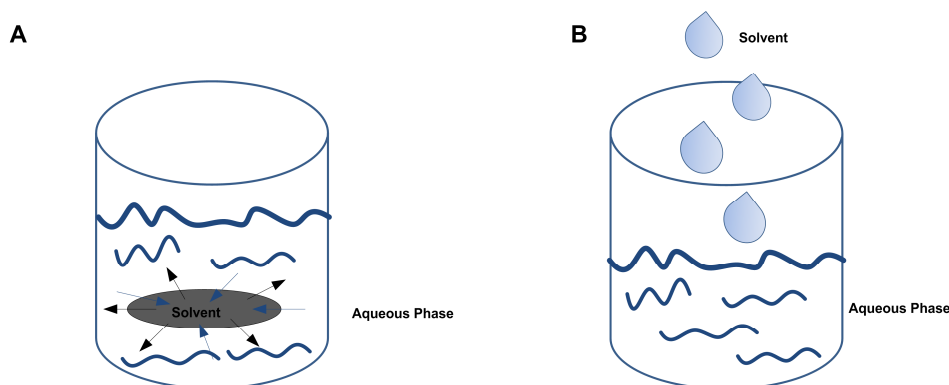


Figure 1.4: Schematic depiction of the nanoprecipitation method by A) dialysis method and B) dropping method.

Recently, the method has been transferred onto microfluidic platforms taking advantage of the high-throughput systems. Opposed to the initial larger scale methods, microfluidics allows for a controlled input of fluid streams in micro-sized flow channels. Given the theory of nanoprecipitation, an aqueous volume is required in order to trigger the precipitation of the amphiphilic molecules. Microfluidic mixing allows for a controlled mixing of solvent and aqueous phase in a rapid process. The alteration of the flow

channel, e.g. by aiding the diffusion process in a chaotic advection micromixer further enhances this mixing process. Using a microfluidic-sized flow channel allows for a tight control of flow rates, and opposed to the ethanol injection method (Batzri and Korn, 1973), gives a controlled precipitation method on a small footprint, well suited for a high-throughput screening. Compared with process optimisation on a larger scale, process development with microfluidic devices allows for a better control of mixing efficiencies, which at this scale is predominantly based on molecular diffusion. The increased surface-to-volume ratios generate fast mixing times by minimizing dimensions and diffusion lengths (Lee et al., 2011; Mengeaud et al., 2002) accompanied with a reduced time for sample handling (Weigl, 2003).

Staggered Herringbone Micromixer - Chaotic Advection

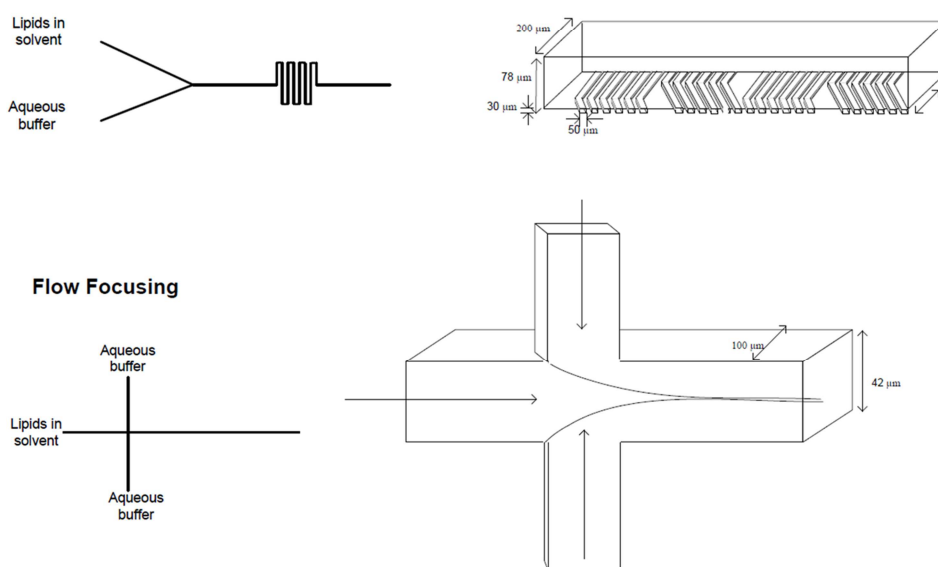


Figure 1.5: Overview of the chaotic advection SHM method and the flow focusing method.

Early work focused on the use of a flow-focusing technique on a microfluidic platform. This platform resulted in successful formation of liposomes in size ranges from 35 – 180 nm (Jahn et al., 2007; Valencia et al., 2010). Here, the lipid-solvent stream was centred between two streams of aqueous buffer, where mixing occurs at the interfaces primarily dominated by diffusion (Figure 1.5). The nanoprecipitation method was adapted into a multilamination micromixer for the production of polymer nanoparticles (Bally et al., 2012). A chaotic advection micromixer has been initially described for the nanoprecipitation of liposomes, now commercialized by Precision Nanosystems Inc. A SHM mixer resulted in limit-size synthesis of lipid based nanoparticles. Variations in flow rate and flow rate ratios led to the engineering of liposomes in the range of 20-80 nm for small interfering RNA (siRNA) delivery (Belliveau et al., 2012; Zhigaltsev et al., 2012).

1.3 Statistical tools for reproducible manufacturing

In addition to new methods for vesicle manufacturing, systems can be more effectively developed using statistical tools. In the traditional one-factor-at-a-time (OFAT) method only one factor is optimised while all other factors remain constant (Figure 1.6), overall a very time intensive method, which might lead to overlooking the optimum process or factor-interactions (Montgomery et al., 1997). Design of experiments (DoE) is a statistical optimisation method applied in pharmaceutical and biopharmaceutical process development and optimisation (Lawrence, 2008; Singh et al., 2011; Vandervoort and Ludwig, 2002). The difference to the OFAT method lies in a systematic approach of creating structured experiments, where the effect of changes in a factor is related to a response (Figure 1.6). Here, a minimum number of experiments performed leads to enhanced process understanding and overall aiding the process robustness and product quality. Factors and responses are the basis of a DoE, defining the variables in the process and the outcome that is measured qualitatively or quantitatively. The selected factors manipulate the system and effect the responses. In a DoE, the variation in a factor is mathematically linked to the resulting responses. Besides assessing the statistical significant factors (main effects), a possible interaction between the factors is identified (Eriksson, 2008; Mandenius and Brundin, 2008).

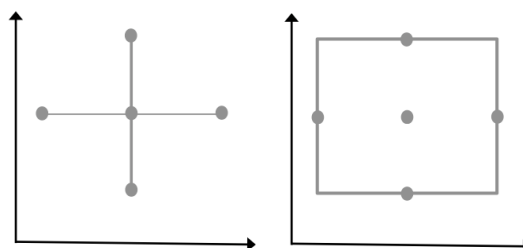


Figure 1.6 Schematic depiction of screening of two factors; left: screening one factor at a time resulting in 5 experiments. Right: Designed experiment with only one experiment.

Multivariate analysis (MVA) is a tool used to analyse more than one statistical variable at a time. The dimensionality in a data set is reduced, allowing for identifying patterns and relationships between several variables (Wold et al., 2001a; Wold et al., 2001b). MVA is frequently used for data analysis, mining, classification (e.g. cluster analysis or outlier detection), regression analysis and predictive modelling and allows to link the effect of alteration in one variable to other variables (Eriksson, 2006; Pasqualoto et al., 2007; Rathore et al., 2011).

The accumulation of large data sets is linked to advances in analytical high-throughput methodologies being developed. The challenge lies in the extraction of valuable information from such large data quantities in a reasonable timeframe. Besides

analysing only one variable at a time, MVA allows to incorporate the analysis of several variables simultaneously, representing a flexible and multipurpose data analysis method. The analysis allows generating an overview in a data set and classifies and compares groups of data by regression modelling. Similar to DoE, variables (X) and responses (Y) are defined. MVA handles several variables simultaneously, extrapolate from limited data sets and is robust to noise in the responses or variables (Eriksson, 2006). The analysis commences with fitting a principal component (PC) through the multidimensional space in order to approximate the best data fit (Figure 1.7 A and B). Usually at least two PCs are computed orthogonal to each other. A principal component analysis (PCA) allows for grouping of the data, generating an overview and identifying trends, groups and outliers (Jackson, 2005; Wold et al., 1984). The PCA results in a correlation between the observations and identifies sudden shifts or trends in the data set and the relationship between the X-variables is identified (Figure 1.7 C). The addition of the Y-variables in a partial least square (PLS) analysis includes the responses in a system or measurement, aiming to predict Y from X. PLS links the influence of the factor variation to the responses and identifies the controlling or most influential factors that are desired to achieve a certain response (Wold et al., 1984; Wold et al., 2001a; Wold et al., 2001b).

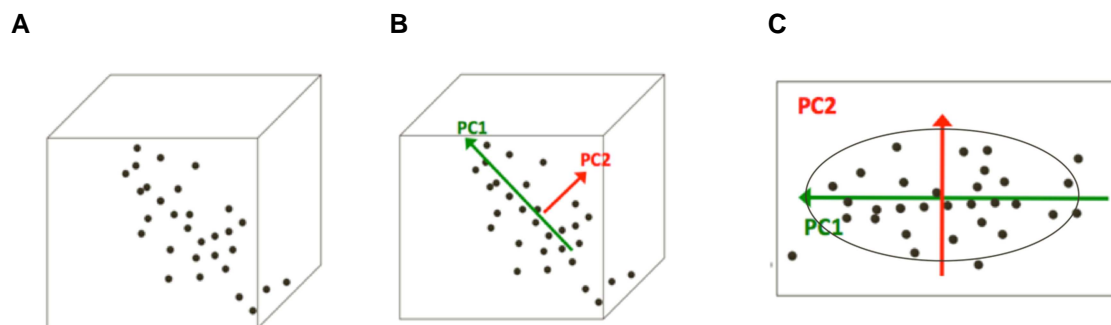


Figure 1.7: Overview over a MVA process with A) data scattered in a multidimensional space, B) two PCs are fitted and C) projection of the data and the PCs onto a plane.

The combination of such theoretical models with experimentally obtained data provides extra information and overall leading to an enhanced confidence level. Both statistical-based tools, DoE and MVA, allow building knowledge around a specific research application, aiming to enhance the robustness of a process with generally fewer experiments required for identifying the local optima. Identified factor interactions can be used for process simulation and predictions in an overall cost-effective method (Singh et al., 2005). Generally, the combined application of multivariate methods with experimental design allows identifying process optima by accelerating the developing process.

1.4 Aim and Objectives

Given the need to support the translation of liposomal products into the clinical application in a cost-effective manner, the overall aim of this thesis was to explore methods for manufacturing SUV and investigate the potential of microfluidics for the manufacturing and purification of liposomes and nanoparticles. Microfluidics was assessed as a bottom-up method in drug and protein delivery to better understand the link between manufacturing method and formulation outcome.

To achieve this aim, the main objectives of this thesis were to:

1. Compare and evaluate three different methods for manufacturing SUV (sonication, high shear mixing and microfluidics) and assess the resulting physicochemical particle characteristics using statistical process modelling by DoE.
2. Investigate the microfluidics-based nanoprecipitation method for the manufacturing of liposomes comprised of low transition temperature lipids for gene transfer and *in-vitro* transfection efficiencies.
3. Investigate the microfluidics-based nanoprecipitation method for the manufacturing of DQAsomes comprised of cationic bola-amphiphiles (dequalinium) for gene transfer and *in-vitro* transfection efficiencies.
4. Investigate the microfluidics-based nanoprecipitation method for the manufacturing of polymer-based nanoparticles for the delivery of protein.
5. Investigate the microfluidics-based nanoprecipitation method for the manufacturing of liposomes comprised of low transition temperature lipids for the solubilisation of a drug with low aqueous solubility.
6. Investigate the scalability of the microfluidics-based nanoprecipitation method by alteration of the channel geometries and mixer parallelisation in a continuous flow setup.
7. Investigate the microfluidics-based nanoprecipitation method for the manufacturing of liposomes comprised of high transition temperature lipids DDA and TDB in an adjuvant formulation.
8. Investigate and implement MVA to statistically relate the physicochemical adjuvant characteristics of DDA-TDB liposomes to *in-vivo* derived immune responses upon delivery of a tuberculosis antigen.
9. Design and implement a microfluidics-based purification method based on tangential flow filtration and combination into a continuous manufacturing setup.

Chapter 2

Materials and Methods

2.1 Materials

Material / Chemicals

Supplier

1,1'-(decane-1,10-diyl)bis(9-amino-1,2,3,4-tetrahydroacridinium) diiodide (CM2)	Procarta Biosystems Ltd., Norwich, UK
1,2-dioleoyl-3-trimethylammonium-propane (DOTAP)	Avanti Polar Lipids, Alabaster, AL, USA
1,1'-dioctadecyl-3,3,3',3'-tetramethylindocarbocyanine perchlorate (DiIC)	Sigma-Aldrich, Poole, Dorset, UK
1,2-dioleoyl-sn-glycero-3-phosphoethanolamine (DOPE)	Avanti Polar Lipids, Alabaster, AL, USA
1,2-distearoyl-sn-glycero-3-phosphocholine (DSPC)	Avanti Polar Lipids, Alabaster, AL, USA
12 % Tris-glycine gels	Invitrogen, CA, USA
12-well plates	Greiner Bio-One Ltd, Gloucestershire, UK
2,2'-azino-bis(3-ethylbenzthiazoline-6-sulfonic acid)	Sigma-Aldrich, Poole, Dorset, UK
2,6-Bis(isopropyl)phenol (Propofol)	Sigma-Aldrich, Poole, Dorset, UK
3-(4,5-dimethylthiazol-2-yl)-5-(3-carboxymethoxyphenyl)-2-(4-sulfophenyl)-2H tetrazolium (MTS)	Sigma-Aldrich, Poole, Dorset, UK
96-well plates	Greiner Bio-One Ltd, Gloucestershire, UK
Acetonitrile	Fisher Scientific, Leicestershire, UK
African green monkey kidney cells (COS-7)	European collection of cell cultures (ECACC), Salisbury, UK
BALB/C mice	Charles River, Margrate, UK
Capillary I.D. 100 µm	Postnova Analytics GmbH, Lech, Germany
Capillary I.D. 50 µm	VICI AG International, Schenk, CH
Capillary I.D. 63 µm	IDEX Health & Science, WA, USA
cell harvester	Titertek Instruments, Alabama, USA
Cell IQ	CM Technologies OY, Finland
CellTiter 96® AQueous One Solution Cell	Promega, Madison, WI, USA

Proliferation Assay

Centrifuge Universal 32	Hettich Lab Technology, Tuttlingen, Germany
Centrifuge MSE Mistral 3000i	DJB Labcare Ltd., Buckinghamshire UK
Chloroform	Fisher Scientific, Leicestershire, UK
Cholesterol	Sigma-Aldrich, Poole, Dorset, UK
CO ₂ laser	Synrad Inc., Mukilteo, WA, USA
Colouring agent 2,2'-azino-bis (3-ethylbenzthiazoline-6-sulfonic acid)	ABTS; Sigma, Dorset, UK
Column Jupiter 300 C18(2)	Phenomenex, Cheshire ,UK
Column Luna C18(2)	Phenomenex, Cheshire ,UK
Concanavalin A	Sigma-Aldrich, Poole, Dorset, UK
Continuous Flow pumps Flash 100	Scientific System Inc (SSI), PA, USA
Cytometer FC500	Beckman-Coulter, High Wycombe, UK
Delbecco's Modified Eagles Medium (DMEM)	Biosera, Leicestershire, UK
Dialysis tubing	Medicell, London, UK
Dihydroxyvitamin D3	Enzo Life Sciences, Exeter UK
Dimethyldioctadecylammoniumbromide (DDA)	Avanti Polar Lipids, Alabaster, AL, USA
DuoSet ELISA development kit	R&D Systems, Oxfordshire, UK
Ethanol	Fisher Scientific, Leicestershire, UK
Evaporative light scattering detector (ELSD)	Sedere, Alfortville, France
Foetal bovine serum (FBS)	Biosera, Leicestershire, UK
Fusion protein Ag85B-ESAT-6-Rv2660c (H56 antigen)	Statens Serum Institut, Copenhagen, Denmark
Gas Chromatography (GC) CSi 200	Cambridge Scientific Instruments Ltd, Witchford, UK
Gasket TFF Sylgard 184	Dow Corning, Midland, USA
GC column TRACE, 15 m x 0.25 mm x 0.25 µm	Fisher Scientific UK Ltd , Loughborough, UK
GeneFlash gel photoimager	Syngene bioimaging, Cambridge, UK
Goat anti-mouse IgG, IgG1, IgG2b	AbD Serotec, Oxford, UK
gWiz™ Luciferase	Aldveron Freiburg GmbH, Freiburg, Germany

High shear mixing apparatus, SilentCrusher M	Heidolph instruments, Schwabach, Germany
HPLC	YoungLin Instruments, Korea
Human cervical carcinoma cells (HeLa)	European collection of cell cultures (ECACC), Salisbury, UK
Hydrogen Peroxide	Sigma-Aldrich, Poole, Dorset, UK
IL4 & GM-CSF	Enzo Life Sciences, Exeter UK
Illuminometer Spectra Max Gemini XPS	Molecular Devices, CA, USA
L-glutamine/Penicillin-Streptomycin	Biosera, Leicestershire, UK
Lipofectin™ reagent	Invitrogen Life Technologies, UK
Loading buffer	Promega, Madison, WI, USA
Luciferase assay system	Promega, Madison, WI, USA
Malvern Nano ZS	Malvern Instruments, Worcestershire, UK
Marvel milk	Premier Int. Foods Ltd, Lincs, UK
MES buffer	Sigma-Aldrich, Poole, Dorset, UK
Methanol	Fisher Scientific, Leicestershire, UK
Microfluidic fittings	P-221, Upchurch Scientific, Oak Harbor, WA, USA
MilliGAT pump	VICI Valco, Valco Instruments Co., Schenkon, CH
Milling machine	Folken IND, Glendale, USA
Modulyo bench top freeze dryer	Edwards, West Sussex, UK
Mouse DuoSet capture ELISA	R & D Systems, Abingdon, UK
NanoAssemblr™	Precision Nanosystems Inc., Vancouver, Canada
Nanosight LM20	NanoSight, Amesbury, UK
Ovalbumin	Sigma-Aldrich, Poole, Dorset, UK
Phosphate buffer saline tablets (PBS)	Sigma-Aldrich, Poole, Dorset, UK
Phosphatidylcholine (PC)	Avanti Polar Lipids, Alabaster, AL, USA
Plastic syringes (1mL, 2mL, 5mL, 10mL, 20mL)	Becton, Dickinson and Company, New Jersey, USA
Plate reader	ThermoFisher Scientific Inc., MA, USA
Plate washer	MTX Lab Systems, INC., Virginia, USA
Poly(lactide-co glycolide) (PLGA)	Sigma-Aldrich, Poole, Dorset, UK
Polylactic acid (PLA) MW 1,600-2,400	Polysciences Inc., PA, USA

Pressure sensor	40PC100, Honeywell, NJ, USA
Probe sonicator Soniprep150plus	MSE Ltd., London, UK
Propan-1-ol	Fisher Scientific, Leicestershire, UK
Propan-2-ol	Fisher Scientific, Leicestershire, UK
Quartz filter mats	Skatron/Molecular Devices, Berkshire, UK
Rotary evaporation rotavapor-R	Buchi Labortechnik GmbH, Essen, GE
RPMI 1640	Biosera, Leicestershire, UK
Scintillation vials	Sarstedt, Leciester, UK
SDS PAGE Apparatus	Bio-Rad Laboratories Inc., CA, USA
Serum free and antibiotic free medium (Opti-MEM)	Gibco, Invitrogen, Paisley, UK
Spin columns	Sartorius AG, Goettingen, Germany
Sscintillation cocktail	Ultima Gold, PerkinElmer, Cambridgeshire, UK
Stop solution	R & D Systems, Abingdon, UK
Syringe pump	Harvard Apparatus, MA, USA
Syringe pump	Nemesys, Cetoni GmbH, Germany
Syringe pump KDS 200 CE	Cole-Parmer-Instruments Co. Ltd., London, UK
Thiazolyl Blue Tetrazolium Bromide (MTT)	Sigma-Aldrich, Poole, Dorset, UK
Trehalose 6,6'-dibehenate (TDB)	Avanti Polar Lipids, Alabaster, AL, USA
Trifluoroacetic acid (TFA)	Sigma-Aldrich, Poole, Dorset, UK
TRIS buffer	ICN Biomedicals Inc, US
Ultrafiltration membrane PBMK06210, 100kDa	Merck Millipore, Darmstadt, Germany
Ultrafiltration membrane U3630, 10kDa	Sigma-Aldrich, Poole, Dorset, UK

Software	Version	Supplier
GraphPad Prism	6.0	GraphPad Software, Inc., USA
MODDE	10	Umetrics, Sweden
SIMCA	13.0	Umetrics, Sweden
Clarity	2.4.1.91	DataApex, Czech Republic
Clarity	4.0.3.876	DataApex, Czech Republic
NanoAssemblr™	3.0	Presicion NanoSystems Inc., Canada
Labview		National Instruments, TX, USA

2.2 Methods in liposome manufacturing

2.2.1 Lipid film hydration

MLV were prepared using the lipid film hydration method (Bangham et al., 1965). Weighted amounts of lipids were dissolved in chloroform:methanol (9:1, v/v). The organic solvents were subsequently removed by rotary evaporation under vacuum, followed by flushing of the dried lipid film with N₂ for removal of solvent residues. The thin lipid film on the bottom of a round bottom flask was rehydrated with the aqueous phase at 20°C above the transition temperature of the lipids. Each formulation was vortexed every 5 minutes for a total time of 20 minutes, incubating the suspension between vortexing in a water bath, which heated above the transition temperature of the lipids. The suspension was left to cool for 15 minutes before further work was conducted.

2.2.2 Sonication

A probe sonicator was used for subsequent size reduction of MLV produced by the lipid film hydration method. Sonication time varied from 1 to 2 min at an amplitude ranging of 1 to 10. A titanium probe was emerged into the required volume of MLV formulations. Temperature during the process was maintained above the transition temperature of the lipids. A change from a milky MLV suspension to a clear suspension was observed throughout the sonication process. The suspension was left to cool for 15 minutes before further work was conducted. To remove metal residues from the probe tip, the suspension was centrifuged for 10 minutes at 500 x g.

2.2.3 High shear mixing

A high shear mixing (HSM) apparatus was used subsequent size reduction of MLV produced by the lipid film hydration method. High shear mixing time was varied from 1 to 10 min at a rotational speed from 1000 to 25000rpm. The mixer tip was immersed into the required volume of MLV formulations. Temperature during the process was maintained above the transition temperature of the lipids. The suspension was left to cool for 15 minutes before further work was conducted.

2.2.4 Microfluidics

2.2.4.1 Setup

The micromixer was obtained from Precision NanoSystems Inc., Vancouver, Canada. The mixer was a staggered herringbone micromixer (SHM) with moulded channels in poly(dimethylsiloxane) (PDMS) (Figure 2.1A), which were 200 µm x 79 µm (width x

height) with herringbone features of $50 \times 31 \mu\text{m}$ (Figure 2.1B). Disposable syringes (1mL, Luer Lock) were used to connect to the inlet streams by fluid connectors. Formulations were performed on a NanoAssemblr™ bench top instrument (Precision NanoSystems Inc., Vancouver, Canada).

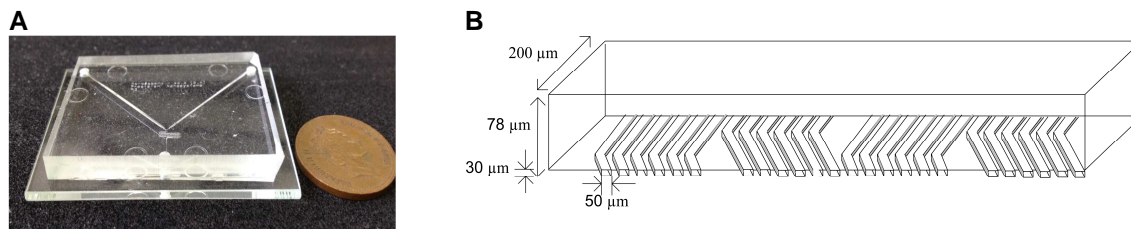


Figure 2.1: A) Chip in PDMS for size comparison next to a penny. B) Detailed flow path including two full cycles of herringbones.

2.2.4.2 Nanoprecipitation

Lipids in solvent and aqueous buffer (Table 2.1) were injected in 1 mL disposable syringes into separate chamber inlets. Syringe pumps were used to drive the fluids into the chamber. The total flow rate (TFR) as well as the flow rate ratio (FRR, rate of solvent to aqueous stream) was set in the user interface. The heating block was used to maintain the lipid solubility above the transition temperature of the lipids, if required (Table 2.1). The system was primed with the respective solvent and aqueous phase prior to making the formulation. The first droplets (30% of the total sample volume) were collected as the waste and the remaining 70% of the formulation was collected as the core of the sample (steady state). After each run, the system was flushed with ethanol for cleaning.

Table 2.1: Lipids and polymers used throughout this thesis. IPA = Isopropanol, n/a = not applicable.

Compound*	Solvent	Aqueous Phase	Concentration	Heating block
DDA	IPA	TRIS, 10 mM, pH7.2	1.25 mg/mL	60°C
TDB	IPA	TRIS, 10 mM, pH7.2	0.25 mg/mL	60°C
DOPE	Ethanol	TRIS, 10 mM, pH7.2	5.9 mg/mL	n/a
DOTAP	Ethanol	TRIS, 10 mM, pH7.2	5.5 mg/mL	n/a
PC	Ethanol	TRIS, 10 mM, pH7.2	6.06 – 36.48 mg/mL	n/a
Chol	Ethanol	TRIS, 10 mM, pH7.2	0.77 – 4.62 mg/mL	n/a
CM2	Methanol	MES, 100mM, pH 5.5	0.6 – 5 mg/mL	60°C ≥ 3 mg/mL
PLA	Acetonitrile	TRIS, 10 mM, pH7.2	10 mg/mL	n/a
PLGA	Acetonitrile	TRIS, 10 mM, pH7.2	10 mg/mL	n/a

* DDA = Dimethyldioctadecylammoniumbromide, TDB = Trehalose 6,6'-dibehenate, DOPE = 1,2-dioleoyl-sn-glycero-3-phosphoethanolamine, DOTAP = 1,2-dioleoyl-3-trimethylammonium-propane, PC = Phosphatidylcholine, Chol = Cholesterol, CM2 = 1,1'-(decane-1,10-diyl)bis(9-amino-1,2,3,4-tetrahydroacridinium) diiodide, PLA = Polylactic acid, PLGA = Poly(lactide-co glycolide).

2.3 Methods for quantification

2.3.1 Solvent quantification by gas chromatography

Solvent concentration was quantified by gas chromatography (GC) using a flame ionization detector with detector temperature 230°C, injector temperature 200°C and an injection volume of 1 µL. Carrier gas was helium at 15 psi inlet pressure. An internal reference standard (propan-1-ol) was chosen in order to account for variations in injection volumes. A calibration curve (6 standards ranging from 0.5-50% v/v) was established and used for quantification using an internal reference standard (propan-1-ol). All analysis was made in Clarity DataApex version 2.4

2.3.2 Lipid and drug quantification by liquid chromatography and evaporative light scattering

Quantification was performed by reverse phase high performance liquid chromatography (HPLC) using a C18 column (Luna 5µ for lipids and drug, Jupiter 5µ for protein) with a UV detector set at wavelength described in Table 2.2. Lipids were quantified using an evaporative light scattering detector (ELSD), which required separation of lipids by reverse phase (RP) high performance liquid chromatography (RP-HPLC). UV wavelength, flow rate, analysis time, gradient flow, gain value was adjusted and optimised for each method (Table 2.2). Lipids injected were dissolved in chloroform:methanol (9:1 v/v). Loop volume was 100 µL, tubing volume 15 µL and, injection volume was 30 µL in partial loopfill injection mode. Flush volume as 10 µL with a wash between vials (wash solution 50:50 IPA:water). Auto sampler analysis time was adjusted dependent on each method (Table 2.2). Column temperature was controlled at 35°C. Carrier gas in the ELSD was nitrogen at 3.5 bar inlet pressure. All analysis was made in Clarity, DataApex version 4.0.3.876. Each method was validated by assessing the linearity, reproducibility, robustness, accuracy and level of detection and level of quantification. For quantification, established calibration curves were used.

Table 2.2: Detailed HPLC methods for compounds used in this study, mobile phase comprised A (0.1%TFA in water) and B (100% methanol) in all runs.

Compound	Detector	Elution time (min)	Flow rate (mL/min)	Method		
Chol	ELSD Gain 6	12.2	1	t (min)	A%	B%
				0	15	85
				4	0	100
				13	0	100
				13.1	15	85
PC	ELSD Gain 8	15.2	1	15	15	85
				t (min)	A%	B%
				0	15	85
				6	0	100
				25	0	100
DOPE	ELSD Gain 8	13.5	1	26	15	85
				35	15	85
				t (min)	A%	B%
				0	15	85
				6	0	100
DOTAP	ELSD Gain 8	8.9	1	25	0	100
				26	15	85
				35	15	85
				t (min)	A%	B%
				0	15	85
DDA	ELSD Gain 8	7.1	1.5	6	0	100
				25	0	100
				26	15	85
				35	15	85
				t (min)	A%	B%
TDB	ELSD Gain 8	19.5	1.5	0	15	85
				6	0	100
				25	0	100
				26	15	85
				35	15	85
Propofol	UV 268 nm	6.4	1	t (min)	A%	B%
				0	95	5
				3	0	100
				8	0	100
				8.1	95	5
Ovalbumin	ELSD Gain 10	11.5	1	10	95	5
				t (min)	A%	B%
				0	100	0
				10	0	100
				15	0	100
CM2	UV 254 nm	5.3	1	15.1	10	0
				20	10	0
				t (min)	A%	B%
				0	95	5
				3	0	100
				6	0	100
				6.1	95	5
				9	95	5

2.4 Liposome purification

2.4.1 Dialysis

Liposome samples were dialysed (3500Da membrane) over night against buffer at room temperature to remove residual solvent (nanoprecipitation method) and untrapped drug (nanoprecipitation method and sonication method). The dialysis tubing was cut into the desired length and soaked under running water for at least 2 hours to remove contaminants. The buffer volume was exchanged every hour to optimize the dialysis protocol to a total dialysis time of 4 hours.

2.4.2 Spin columns

Disposable spin columns (Hydrosart® membrane 30kDa, 50kDa, 100kDa) were used for liposome purification. The membrane was wetted with 1 mL of distilled water through the membrane (2000 x g, 2 minutes). The required volume of liposome sample was placed on the concentrate side, followed by centrifugation at 2000 x g for 5 minutes in a swing bucket rotor. For washing steps, the filtrate was weighted after and respective volume of fresh buffer was added to the concentrate side. For washing the liposomes, three centrifugation cycles were performed. For concentration, no buffer was added to the concentrate side and only the filtrate was removed.

2.5 Liposome characterisation

2.5.1 Dynamic light scattering

Characterisation of the vesicles was performed by dynamic light scattering (DLS) (Malvern Zetasizer Nano-ZS). If not stated otherwise, the z-average (intensity based mean particle diameter) was reported for monomodal size distributions. For multimodal distributions, average diameter reported was based on intensity- and volume-based distribution. Recording time was automatically determined by the system and three runs were performed for each measurement. Vesicles were diluted in distilled water to obtain the best attenuator (6-9) and measurements took place at 25°C. Polydispersity measurements (Malvern Zetasizer Nano-ZS) were assessed based on the width of the particle distribution.

2.5.2 Nanoparticle tracking analysis

Nanoparticle tracking analysis (NTA) was performed with a Nanosight LM20, connected to a 20x magnification microscope. Liposomes were diluted 1:10 to 1:100 in distilled water, to achieve an optimal particle concentration of $10^7 - 10^9$ particles/mL during measurement. NTA analysis was used for determination of the particle size

concentration (particles/mL) and as a visual confirmation of particles. Recording time was 60 seconds and camera settings (shutter and gain) were adjusted manually to obtain the best resolution.

2.5.3 Zeta potential

Characterisation of the liposomes included zeta potential measurements using particle electrophoresis (Malvern Zetasizer Nano-ZS) with vesicles diluted 1:100 in distilled water.

2.5.4 Recovery of lipids and drug

Recovery in the microfluidics process was expressed as in Equation 2.1, relating the determined concentration in the steady state of the process to the concentration in the stock prior to the manufacturing by microfluidics, incorporating the dilution by the FRR. Recovery in the lipid film hydration, sonication and HSM process was expressed as in Equation 2.2. If the formulation contained more than one compound, the individual recovery was assessed as in Equation 2.1 or Equation 2.2 and the overall recovery assessed according to Equation 2.3. All concentrations were assessed by HPLC-ELSD as described in Section 2.3.2.

$$\text{Recovery (\%)} = \frac{\text{Conc.steady state } (\frac{\text{mg}}{\text{mL}})}{\text{Conc.stock } (\frac{\text{mg}}{\text{mL}})} * \text{FRR} * 100 \quad \text{Equation 2.1}$$

$$\text{Recovery (\%)} = \frac{\text{Conc. final formulation } (\frac{\text{mg}}{\text{mL}})}{\text{Conc.stock } (\frac{\text{mg}}{\text{mL}})} * 100 \quad \text{Equation 2.2}$$

$$\text{Recovery}_{\text{overall}} (\%) = \frac{(\text{Recovery}_{\text{compound 1}} (\%) + \text{Recovery}_{\text{compound 2}} (\%) + \dots + \text{Recovery}_{\text{compound n}} (\%))}{n} \quad \text{Equation 2.3}$$

2.6 Liposome Imaging

2.6.1 Transmission electron microscopy

Images were taken on a Jeol 2011 with a 200kv beam using minimal dose protocol; scanned at low magnification and jumped to high magnification without exposing the sample to the beam first. Camera used was a Gatan ultrascan (2k by 2k pixels). Grids were lacey carbon, 200 mesh and were prepared by adding 8 μL of sample to a glow discharged grid, blotting from both sides for approximately 5 seconds then plunging into nitrogen cooled ethane propane mix (70% ethane). CryoTEM pictures were taken at Warwick University, UK with the help of Mr. Hands-Portman.

2.6.2 Freeze fracturing electron microscopy

The liposome suspension (2 μ L) were placed in a ridged gold specimen support, frozen rapidly by plunging into a briskly stirred mixture of propane:isopentane (4:1) and cooled in a liquid nitrogen bath. Fracturing was performed with a cold knife, and replication used a Balzers BAF 400D apparatus (Forge et al., 1978; Forge et al., 1989). Prior to mounting the replicas on grids for electron microscopy, replicas were floated off on water, cleaned in domestic bleach, diluted 1:1 in distilled water and then washed several times in distilled water. Replicas were viewed in a transmission electron microscope (JEOL 1200EXII), which operated at 80 kV and digital images collected with a Gatan camera. Images of the freeze-fractured samples were presented in reverse contrast, where the shadows appear black. Imaging was performed with help of Prof. Andrew Forge at UCL Ear Institute, London, UK.

2.6.3 Fluorescent imaging of liposomes

Vesicles were manufactured as described in Section 2.2.2 and 2.2.4 with 1 mM carboxyfluorescein (CF) included in the aqueous buffer (Tris, 10 mM, pH 7.2). Vesicles were subjected to dialysis over night against 1 L fresh TRIS buffer, pH 7.2 to remove untrapped CF, prior to imaging under a confocal microscope SP5 TCS II MP, Leica Microsystems, Leica TCSSP5 II, 63 x objective (HCX PLAPO 63 x/1.4-0.6 oil CS).

2.7 Loading of protein

2.7.1 Adsorption of protein

Vesicles were performed as described in Section 2.2.2, 2.2.4, and were mixed with various concentrations of protein / antigen (ovalbumin, lysozyme, H56). Adsorption of the protein onto the particle surface was performed by adding the required amount of protein to the particles. Frequent mixing of the eppendorf tube over a period of 45 minutes was performed. Protein adsorption took place at room temperature.

2.7.2 Gel electrophoresis for qualitative protein detection

Semi-qualitative protein detection was performed by sodium dodecyl sulfate polyacrylamide gel electrophoresis (SDS-PAGE) with 12% Tris-glycine gels. Tris/ Glycine/ SDS running buffer was made by the mixing of Tris (15 g), glycine (72g) and SDS (5g) made up to 1 L with deionised H₂O. All samples were heated at 90°C for 3 minutes to denature the protein present in the sample. The samples containing the proteins of interest were separated on a 12 % Tris-glycine gel in the running buffer using Novex Mini Cell gel apparatus. 10 μ L each sample was loaded into the gel, with

a total run time of 90 min at constant 30 mA per gel. All samples were compared against 10 μ L of a protein marker. The gel was subsequently stained overnight using Coomassie Blue, followed by destaining for several hours (4-5 hours). The gels were imaged using a photoimager.

2.8 Loading of a low solubility drug

2.8.1 Solubilisation of low solubility drug

The low solubility drug (propofol) was dissolved with the lipids in the solvent phase at concentrations ranging from 0.5 – 3 mg/mL. Liposome formation and encapsulation of the drug was performed simultaneously using the lipid film hydration method (Section 2.2.1 followed by sonication Section 2.2.2) or the nanoprecipitation method (Section 2.2.4).

2.8.2 Determination of drug loading into liposomes

The drug loading was quantified after removal of non-entrapped drug by dialysis (sink conditions) against 1 L of Tris buffer, 10 mM pH 7.2 (Section 2.4.1) after which quantification was performed by HPLC as described in Section 2.3.2. Validation assessed the rate of propofol removal by dialysis.

2.8.3 Drug release study

Drug-loaded liposomes were incubated at 37°C in a shaking water bath (150 shakes/min) in 1 L Tris buffer (10 mM, pH 7.2) after removal of the non-incorporated drug. Drug-loaded liposomes were manufactured by the nanoprecipitation method (Section 2.2.4) and lipid film hydration followed by sonication (Section 2.2.2). 3 mL per formulation were incubated and samples of 200 μ L were withdrawn at time intervals of 0.5 h, 1 h, 2 h, 4 h, 8 h and 16 h. Drug quantification was performed as described in Section 2.3.2 and expressed as % cumulative release relative to the initial amount of drug encapsulated.

2.9 Stability Studies

SUV were stored at 4 °C, 25 °C (60%RH) and 40 °C (75%RH) in pharmaceutical grade stability cabinets over the required period of time. Samples were taken at specific time points for measurement of particle characteristics (Section 2.5). For assessment of the drug loading, samples were dialysed against 500 mL Tris buffer (10 mM, pH7.2, sink conditions) at each time point to remove non-entrapped drug after which quantification was performed as described in Section 2.3.2.

2.10 Solvent evaporation of polymer-based nanoparticles

Polymer (PLA or PLGA) was dissolved in chloroform by magnetic agitation over 2 hours, followed by emulsification in phosphate buffer solution over 15 minutes by using a tip sonicator. To form the second emulsion a 2% PVA solution was added to the first emulsion over a 30 minutes sonication process. The emulsion was mixed with a 0.2% PVA solution by magnetic stirring overnight prior to centrifugation by using spin columns (Section 2.4.2). Nanoparticles were collected on the retentate side and characterisation was performed as described in Section 2.5.

2.11 *In-vitro* studies

2.11.1 Culture and maintenance of continuous cell lines

African green monkey kidney cells (COS-7) and human cervical carcinoma cells (HeLa) were cultured in DMEM media supplemented with 10 % foetal bovine serum (FBS) and 1 % penicillin-streptomycin-58 glutamine (PSG). Cells grew as an adherent monolayer in T75 flasks and were passaged at 70-90% confluence. Media was removed and cell monolayer was washed three times with PBS to remove any residual media. Trypsin (1:4 diluted) was added to the monolayer and flasks were incubated for approximately 5 minutes at 37°C in a shaking incubator. Cell detachment was confirmed by microscopy. 5 mL of fresh media was added to cell suspension, which was transferred into a 15 mL flacon tube. Cells were separated from the supernatant by centrifugation (200 x g, 5 minutes) at room temperature. Supernatant was carefully removed and cell pellet was resuspended in pre-warmed media. Cells were then seeded at desired concentration into new flasks. All cell lines were maintained at 37°C, 5 % CO₂ and 95 % relative humidity and were feed with fresh media every 2-3 days.

2.11.2 Determination of cell number

During routine cell passage, the approximate cell number was estimated from the level of confluence. The exact cell number was determined prior to freezing cells for a cell bank, and determined by a trypan blue exclusion. 20 µL of resuspended cells was mixed with an equal volume of trypan blue, and cells were counted using a hemocytometer. Cells were quantified and the number of cells/ml was calculated using the average of 10 squares in the hemocytometer, the dilution factor and the multiplication factor related to the volume of the hemocytometer grid, Equation 2.4.

$$\text{Number cells} \left(\frac{\text{cells}}{\text{mL}} \right) = \frac{\text{Cell number}}{\text{Square}} * \text{Dilution factor} * 10^4 \quad \text{Equation 2.4}$$

2.11.3 Cryopreservation

Adherent cells were brought into suspension and quantified as described Sections 2.11.1 and 2.11.2. Cells were centrifuged at 200 x g for 10 minutes at 15 °C and the pellet resuspended in ice-cold media containing 10 % DMSO with a cell concentration of 4×10^6 cells/mL. 1 mL aliquots of cell suspension were stored in cryopreservation ampoules and frozen at -70 °C overnight prior to transfer into a liquid nitrogen storage container.

2.11.4 Transfection of COS-7 Cells

COS-7 cells were maintained at 37 °C and 5% CO₂ in Delbecco's modified Eagles medium (DMEM), which was supplemented with 4 mM L-glutamine, 10% (v/v) FBS, penicillin (100 mg/mL) and streptomycin (100 mg/mL). Cells were plated at a concentration of 1×10^5 cells/mL in 1 mL of medium in a 12-well plate 24 h prior to the transfection and incubated overnight. SUV (16 μ moles) were incubated with 0.35 mL Opti MEM and incubated for 40 min at room temperature after which 0.35 mL of Opti-MEM containing 3.5 μ g plasmid DNA (luciferase plasmid (gWiz-Luc) and a GFP plasmid (pEGFP-C3) was added and incubated for a further 15 min at room temperature. The resultant lipoplex mixture was diluted to a final volume of 3.5 mL with Opti-MEM. Before the lipoplex solution was added, cells were washed with 1 mL of Opti-MEM. 0.0078 μ mole total lipid content containing 1 μ g plasmid DNA was added to each well and each transfection performed in triplicate. Incubation time was 5h at 37 °C in 5% CO₂, after which the medium was replaced with growth medium (DMEM) containing 10% FBS and the cells were incubated for further 48 h.

2.11.5 Luciferase Assay

The transfection efficiency was assessed by a luciferase assay system. The transcriptional activity of cells transfected with the DNA, emitting light which can be quantified by a luminometer. Transfected cells were exposed to 80 μ L/well of lysis buffer and detached from the well using cell scraper. Detached cells were centrifuged at 12,000 x g for 15 seconds at room temperature to remove cell debris. 10 μ L of the supernatant was removed onto a new 96-well plate. The plate was read using luminometer with 30 reads/well, prior to addition of luciferase reagent in order to quantify the luciferase activity. 100 μ L/well of the luciferase assay reagent was added and the plate was read again. The luciferase activity was related to the activity achieved with Lipofectin™, which acted as the control transfection reagent.

2.11.6 Detection of fluorescent protein expression

Cells were transfected with the GFP plasmid as described in Section 2.11.4. Transfection was qualitatively assessed under a fluorescent microscope (DMI400B, Leica Microsystems).

2.11.7 Cytotoxicity study

COS-7 or HeLa cells were seeded at 1×10^5 c/mL on a 96-well plate and incubated for 24 h at 37 °C, 5%CO₂ in DMEM medium. The medium was replaced by 200 µL of supplemented DMEM (containing the lipoplex formulation as described in Section 2.11.4 or Section 2.8) and incubated for 5 h, after which 20 µL of Thiazolyl Blue Tetrazolium Bromide (MTT) reagent, was added to each well. The MTT gets bio-reduced by the cells into a red formazan product, indicative of metabolically active cells. Cells were incubated for 4h at 37°C, in a 5% humid CO₂ atmosphere, after which medium was removed. 100 µL DMSO was added in each well to lyse the cells. The absorbance of the produced formazan was measured on microplate reader at A490. The absorbance was, directly proportional to the number of living cells in the medium. cell viability was calculated and expressed as a percentage to the positive control (i.e., cells and medium).

2.11.8 *In-vitro* association assay

Liposomes were manufactured and labelled with 1,1'-dioctadecyl-3,3,3',3'-tetramethylindocarbocyanine perchlorate) (DiIc) (0.1 mol %) by inclusion of the lipid (dissolved in solvent) in the solvent evaporation stage of liposome production (as described in Section 2.2.1 and 2.2.4). Un-entrapped dye was removed by dialysis as described in Section 2.4.1.

Phagocytes at 1×10^6 /ml and fluorochrome tagged liposomes (1mg/ml) were mixed at 1:1 and incubate at 37°C until sampled (5, 15, 30, 60 and 120 min). At each time point, samples were gently mixed and 200 µL of the phagocyte-liposome mix was extracted. The extracted cell culture was washed by addition of 200 µL PBS/BSA (1% w/v) and centrifuged at 1200 rpm for 3 min. Cell pellets were resuspended in 500 µL PBS/BSA (1% w/v). Cell samples were analysed immediately on flow cytometer by taking 5000 events minimum in 'cell' region. For the analysis, MFI (mean fluor intensity - amount of fluorescence per cell) and % positive cells (% of MØ or DC that are positive for liposome) were considered. This assay was performed by Vinod Nadella at Aston University.

2.11.9 *In-vitro* migration assay

Liposomes were manufactured as described in Section 2.2.1 and 2.2.4. 1 mg/mL of liposome formulation was placed in 24 well trans-well plates. 8µm transwells (BD) were inserted in each well in the correct position to make sure no air bubble were left between the transwell and the medium. THP-1 cells (monocyte cell from human blood) at 1×10^6 /mL were stimulated with VD3 or with IL4 & GM-CSF (differentiation into macrophages or iDCs respectively) and were loaded at 300 µL into each trans-well. Empty wells or empty spaces between adjacent wells were partly filled with distilled water to maintain humidity within the plate. Trans- well plate was sealed with thermal tape and placed in plate holding chamber of Cell IQ unit while connecting to the CO₂ inlet. The migration of macrophages or iDC towards liposomes placed in the trans-well plate was assessed using the Cell IQ automated cell tracking system. This assay was performed by Vinod Nadella at Aston University.

2.12 *In-vivo* studies immunisation study

All experiments mentioned under “in vivo studies” were performed by Jubair Hussain.

2.12.1 Vaccination of mice

Work was undertaken in accordance with the 1986 Scientific Procedures Act (UK), (project license number PPL 30/2743). Female C57BL/6 mice, 6-8 weeks old were obtained from Charles River, UK. Liposomes were prepared according to Section 2.2.1, increasing levels (25, 50, 75 mol%) of the saturated phosphatidylcholine, 1,2-distearoyl-*sn*-glycero-3-phosphocholine (DSPC) was incorporated into the DDA-TDB formulation, at a locked DDA-TDB molar ratio of 8:1 with the addition of Ag85B-ESAT-6-Rv2660 (H56) antigen to a final concentration of 0.1 mg/mL (5 µg/vaccine dose). All mice, (exception of the naive group), were immunised intramuscularly (i.m.) with 0.05 mL/dose three times, with two week intervals between each immunisation.

2.12.2 Sera collection

The seven-week immunisation study included five scheduled bleeds, blood samples were taken at regular intervals prior to termination. A small incision the tail vein was used to draw blood (50 µL) with micropipette capillary tubes lightly coated in heparin solution (0.1% w/v in PBS). The blood was subsequently added to 450 µl PBS and centrifuged using a centrifuge (13,000 RPM, 5 minutes). The supernatants were stored at -20 °C for further analysis.

2.12.3 Mice termination and in vitro spleen cell culture

Suspensions of spleen cells were produced into 10 mL RPMI 1640 cell culture medium (w/o Glutamine) containing 10% (v/v) FBS and 1% (v/v) PSG. Each suspension was centrifuged twice (1000 RPM, 10 min, 15 °C) and the final pellet was resuspended in 5 mL RPMI. Single cell suspensions assessed the splenocyte proliferation and antigen specific cytokine responses. To assess splenocyte proliferation, H56 was added to sterile 96 well cell culture plates at various concentrations (0-5 µg/mL), using concanavalin A (2 µg/mL) as a positive control. 100 µL of the spleen cell suspensions were added and incubated at 37 °C, 5% CO₂. After 72 hours incubation, 40 µL of [³H] thymidine at 0.5 (µCi) in supplemented RPMI was added to each well and incubated for further 24 hours. A cell harvester was used to harvest onto quartz filter mats and solutions were transferred to 20 mL scintillation vials containing 5 mL scintillation cocktail. A scintillation counter measured the incorporation of [³H] thymidine in cultured cells.

2.12.4 Assessment of H56 specific antibody isotype titres

Antibody isotypes (IgG, IgG1 and IgG2b) were measured in serum samples using a enzyme-linked immunosorbent assay (ELISA). The ELISA plates (96 well, flat bottomed, high binding) were coated with 3 µg/mL H56 antigen, after which plates were incubated at 4 °C overnight. Plates were washed three times with PBST wash buffer (40 g NaCl, 1 g KCl, 1 g KH₂PO₄, 7.2 g Na₂HPO₄, (2H₂O) per 5 litres of ddH₂O, incorporating ~0.4 mL of Tween 20) using a plate washer, any unbound antigen was removed by blotting. Each well was coated with 100 µL of Marvel in PBS for blocking and incubated for one hour at 37 °C, after which plates were washed three times with PBST buffer. 140 µL of serum sample was serially diluted in PBS (70 µL sequentially), and added to the plates for one hour incubation at 37 °C. Plates were washed five times with PBST buffer, after which 60 µL/well of horseradish peroxidase (HRP) conjugated anti-mouse isotype specific immunoglobulins of IgG, IgG1 and IgG2b was added to each well, diluted to 1/750, 1/4000 and 1/4000 in PBS respectively. Plates were washed five times with PBST buffer, after which 60 µL/well substrate solution (colouring agent: 6x 10 mg tablets of 2,2'-azino-bis (3-ethylbenzthiazoline-6-sulfonic acid) in citrate buffer (0.92g Citric Acid + 1.956g Na₂ HPO₄ per 100 mL) was added to each well, incorporating 10 µL of hydrogen peroxide (30% H₂O₂/100 mL). Plates were incubated for further 30 min at 37 °C prior to measuring the absorbance at 405 nm using a microplate reader. Positive and negative controls incorporated Known positive serum and pooled naïve mice sera respectively.

2.12.5 Quantification of cytokine production by the sandwich ELISA

Splenocyte cell suspensions were harvested and plated onto 96 well cell culture plates as described in Section 2.7.3. The cells were incubated for 48 hours (37 °C, 5% CO₂), after which supernatant was removed and stored at -70 °C for further analysis. Cytokines (IL-2, IL-5, IL-6, IL-10 and IFN- γ) were quantified within cell culture supernatants using a specific DuoSet ELISA development kit. Each well was coated with 100 μ L capture antibody and incubated at room temperature overnight. Prior to blocking, the plates washed three times with PBST buffer. The plates were incubated (room temperature, minimum of one hour) after which plates were washed three times. 100 μ L/well of sample or standards was added to each well and incubated for two hours (room temperature.) after which plates were washed three times. 100 μ L of cytokine specific detection antibody was added per well and incubation for two hours (room temperature). Plates were washed for three times and 100 μ L of Streptavidin-HRP was added per well (diluted 1/200). The plates were covered to avoid exposure to direct light and incubated for 20 min (room temperature). Plates were washed for three times and 100 μ L substrate solution was added to each well (1:1 mixture of colour reagent A and B: stabilised hydrogen peroxide and stabilised tetramethylbenzidine respectively) after which the covered plates were incubated for a further 20 min (room temperature). 50 μ L stop solution (2N H₂SO₄) was added per well and the optical density was immediately determined at 450 nm.

2.13 Scalability assessment of the nanoprecipitation method

2.13.1 Scale-up by increase of channel diameter

The channel diameter was increased in a scale-up format in order to assess the scalability by increasing the throughput through the mixer. The mixer was obtained from Precision NanoSystems Inc. and included a SHM with moulded channels in PDMS, which were 300 μ m x 130 μ m (width x height), the herringbone features remain IP protected.

2.13.2 Scale-out by mixer parallelisation

All experiments were performed at Precision Nanosystems, Inc. in Vancouver, Canada. The 300 μ m design as described in Section 2.13.1 was used in a scale-out platform for further scalability assessment, using a 2x and 4x syringe driven platform (Figure 2.2A and B) and a 1x and 4x continuous flow system (Figure 2.2C and D).

The syringe driven system operated with syringe pumps for the solvent and aqueous stream respectively and disposable syringes between 5-20 mL. Aqueous and solvent phase was split into the 2x or 4x system using two fluid manifolds. For the 2x syringe driven system, a total sample volume of 10 mL was collected, with 5 mL was collected as waste and 5 mL as the core of the formulation. For the 4x system, a total sample volume of 12 mL was split into 8 mL waste and 4 mL of core sample.

The continuous flow system operated with two continuous flow pumps for the solvent and aqueous stream respectively, a glass reservoir was used for each phase. The tubing for the solvent phase was manually purged over the pump heads and recycled back into the solvent reservoir prior to operation. Aqueous and solvent phase was split using two fluid manifolds for the 4x system. For the 1x continuous flow system, a total sample volume of 55 mL was collected, with 5 mL was collected as waste and 50 mL as the core of the formulation was split in 5 batches of 10 mL. For the 4x continuous flow system, a total sample volume of 135 mL was split into 10 mL waste and 125 mL of core sample was split into 5 batches of 25 mL. The total sample volume was split into consecutive batches, verifying variation throughout the continuous process. Low solubility model drug was solubilised (Section 2.8), and after dialysis (Section 2.4.1) samples were analysed as described in Section 2.3.2 and 2.5.

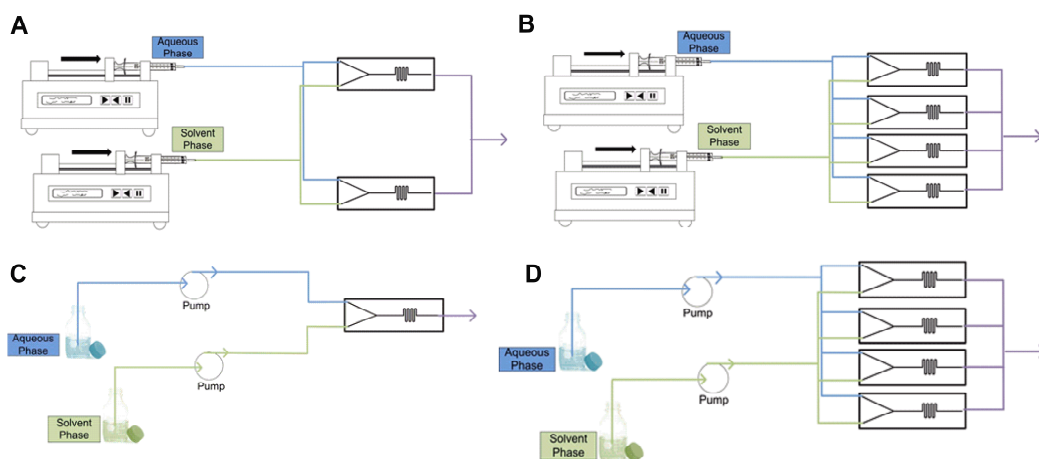


Figure 2.2: Schematic of the scale-out layout for A) 2x syringe driven, B) 4x syringe driven, C) 1x continuous flow and D) 4x continuous flow.

2.14 Tangential flow filtration for liposome purification

2.14.1 Filtration unit manufacturing

Poly(methylmethacrylate) (PMMA) was used to manufacture the rigid parts of the filtration unit, as previously reported (O'Sullivan et al., 2012); also the clamping system for the SHM chip using a micromilling machine. The gasket for the filtration unit was

manufactured from PDMS, according to the manufacturer's instructions and cast in PMMA moulds, manufactured as described above. Interconnect ports (milled from 5 mm PMMA), with two holes tapped with an M3 thread, were used for connection to the filtration unit; an M6 threaded hole was used for standard connection fittings (P-221).

2.14.2 Filtration device

The filtration system was designed to seal membranes in place by means of clamping (O'Sullivan et al., 2012). Two PMMA plates, with a straight channel (1 mm width, 1 mm depth, 45 mm length) and a 1 mm hole milled at each end were clamped together using M3 screws along the edges (Torque 10 Ncm). A 1 mm wide and 0.75 mm deep cutting was used to hold the PDMS gasket in place, which was used to secure the membrane in place. Different commercially available membrane sheets were cut to the required size using a CO₂ laser marking head. The membrane used in this set of experiments had a cut-off of 10kDa or 300kDa, for drug or protein filtration, respectively. The membrane was cleaned after each experiment by back-flushing with water and stored inside the TFF system in 0.8M saline solution. Thus the device was ready to use in another experiment.

2.14.3 Backpressure regulation

Constricting capillaries (internal diameters of 50, 63 and 100 µm, length 2.5 – 5 cm) were attached to the retentate outlet of the filtration device. Backpressure was related to the dynamic viscosity (µ) of medium at 25°C, length (L) and diameter (d) of the restricting capillary and the volumetric flow rate (Q) using Hagen-Poiseuille Law, (Equation 2.5).

$$\Delta P = \frac{128 \mu L Q}{\pi d^4} \quad \text{Equation 2.5}$$

Verification of the calculated backpressure was performed by measuring the pressure with an inline pressure sensor (40PC100) on the retentate side and the data logged with a LabVIEW virtual instrument.

2.14.4 Membrane fouling

Membrane fouling was assessed by comparing the cumulative permeate volumes of a filtered liposome formulation (concentration 5x10¹⁰ p/mL) to a normalized water permeability, NWP, (cumulative permeate volume of filtered water) for 150 minutes. Membrane fouling during filtration of the liposome sample was indicated by deviation of the slope of the accumulated permeate volume from the NWP over time.

2.14.5 Integrity testing

For the integrity testing, backpressure was set at 80 psi (0.1 mL/min, 50 μ m capillary ID, 0.05 m). Ovalbumin at 1 mg/mL and 0.5 mg/mL was filtered through the TFF and permeate and retentate were analysed by SDS - PAGE, Section 2.7.2.

2.14.6 Liposome formulations for spiking the filtration system

Multilamellar vesicles (MLV) were prepared using the lipid film hydration method (Bangham et al., 1965) as described in Section 2.2.1. Cationic liposomes comprised DDA-TDB (8 : 1 molar ratio) and anionic liposomes comprised DPPG, DPPC, Chol (1:1:1.3 molar ratio). Small liposomes were formed via probe sonication, Section 2.2.2. (5 min at an amplitude of 5). Vesicles were freeze dried (pre-freezing at -70°C for 4h, followed by drying in two stages, -50 °C for 48 h and at -30 °C to a final temperature of 20 °C for 6h) (Mohammed et al., 2010) and stored at -20°C until use. The vesicles were rehydrated with distilled water prior to filtration experiments. Ethanol was manually added to the liposome formulation to a final concentration of 20% (v/v). Aqueous model protein (ovalbumin, 100 μ g/mL) and model drug (propofol, 1 mg/mL) were manually added to the liposome formulation in order to mimic the conditions post liposome manufacturing by microfluidics, Figure 2.3.

2.14.7 Filtration

Filtration was performed in a diafiltration mode. Liposomes (Section 2.14.6), spiked with drug, protein or solvent were introduced into the filtration device by means of syringe pumps (Figure 2.3). Retentate and permeate volumes were assessed (by weight), collected in eppendorf tubes and used for further analysis. 10 mM pH 7.2 TRIS buffer, equivalent to the permeate volume, was added manually to the remaining retentate allowing for a washing process (diafiltration cycle). For particle concentration, no buffer was added on the retentate side.

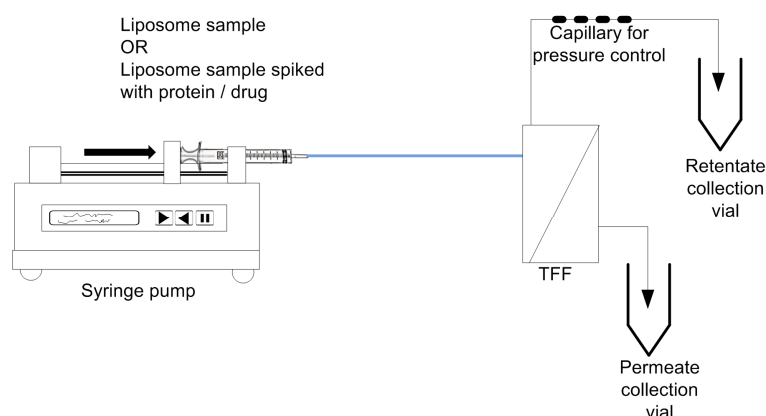


Figure 2.3: Filtration mode with a syringe pump driving the sample through the TFF. Retentate and permeate were collected manually.

2.14.8 Micromixer for liposome formation in combination with TFF purification

To achieve liposome formation and purification a SHM and a TFF device were connected in line (Figure 2.4). The SHM was as described in Section 2.2.4.1.

Luer-lock fitting and polytetrafluoroethylene (PTFE) tubing (1/16 in. x 0.031 in., Sigma-Aldrich Int.) were used to link disposable 1 mL syringes with the two inlet ports of the chip; flow rates and flow rate ratios were controlled by a syringe pump and the whole system was primed with Tris buffer (10mM, pH 7.2) prior to operation. Organic phase, weighed amounts of lipids in ethanol, was injected into the first inlet of the SHM device, while in the second inlet aqueous phase (TRIS buffer, 10mM, pH 7.2) was injected. The micromixer was clamped in place using a PMMA holding device.

It was connected to the tangential flow filtration (TFF) unit (Figure 2.4A) *via* an intermediate collection vial (1.5 mL Eppendorf) to allow for a direct input of microfluidics-manufactured liposomes into the filtration system for purification. Bi-directional milliGAT pump was connected in-line with the retentate loop of the TFF. Two different liposome formulations were produced using this set-up. For the preparation of neutral liposomes, PC and Chol (4:1 molar ratio) in ethanol were injected into the micromixer at 2 mL/min at a FRR 1:3, including 1 mg/mL of propofol in the solvent stream (Figure 2.4B). For the preparation of a cationic liposome formulation, DOPE and DOTAP (1:1 molar ratio) in ethanol were injected into the micromixer at a TFR of 2 mL/min at FRR 1:3. After formulation, the required amount of protein (ovalbumin, 100 µg/mL) was manually added to the collection vial, Figure 2.4C.

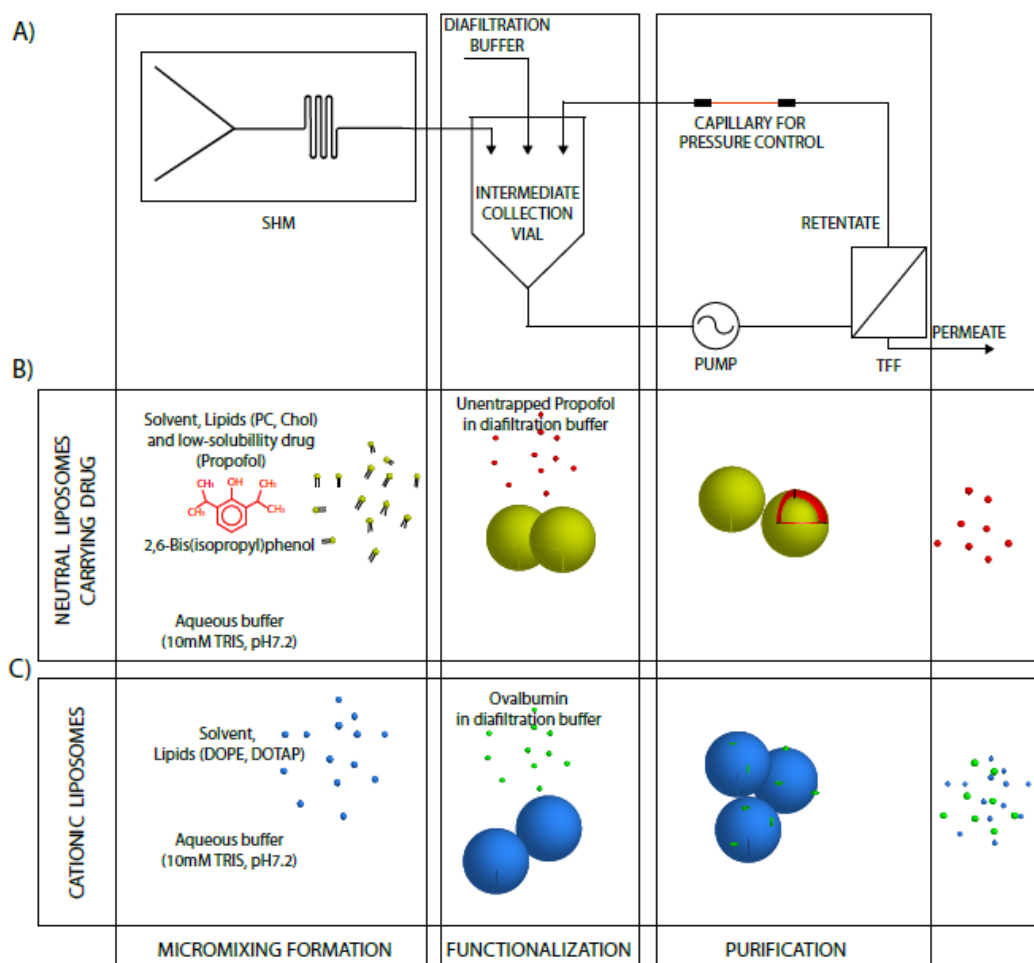


Figure 2.4: A) Schematic overview over the continuous manufacturing setup with B) loading of the low solubility drug and C) loading of the protein.

2.15 Statistical analysis

If not stated otherwise, results were reported as the mean \pm one standard deviation (SD). One- or two-way analysis of variance (ANOVA) was used to assess statistical significance, followed by Tukey's multiple comparing test and t-test was performed for paired comparisons. Significance was acknowledged for p values lower than 0.05 (marked with *). All calculations were made in GraphPad Prism version 6.0 (GraphPad Software Inc., La Jolla, CA, US).

2.16 Design of experiments

Chosen model depended on required outcome; screening design were used for initial testing and response surface modelling was used for optimization testing. Factors in selected ranges as well as desired responses were selected before the worksheet was produced. All runs were performed randomized. For evaluation, summary plot was evaluated for goodness of fit (R^2), goodness of prediction (Q^2) as well as model validity and reproducibility. Responses, which gave a poor model were removed and not

further investigated. Outliers were detected and removed if required using normal probability plot, observed vs. predicted and normal plot of residuals. Coefficients were assessed for significance and removed if required. Prediction plots (response surface or contour plot) were used for model interpretation and assessment of optimal regions in the model prediction. Sweet spot analysis determined the optimal region with pre-selected criteria (Eriksson, 2008).

2.16.1 Model evaluation

The first column presented the R^2 value, the fraction of the variation for the responses as explained by the model.

$$R^2 = \frac{SS_{REG}}{SS}$$

With

SS_{REG} The sum of squares of Y corrected for the mean, explained by the model

SS The total sum of squares of Y corrected for the mean

The second column displayed Q^2 , which represented the fraction of the variation of the response predicted by the model according to cross validation, expressed in the same units as R^2 .

$$Q^2 = 1 - \frac{PRESS}{SS}$$

With

$PRESS$ The predicted residual sum of squares

SS The total sum of squares of Y corrected for the mean

R^2 and Q^2 range between 0 and 1; values close to 1 indicate a very good model with excellent goodness of fit and predictive power. Furthermore, the predictive power should ideally be approaching the goodness of fit to a maximum of 100%, will however never outreach R^2 . The third column represented a measure of the validity of the model. A bar larger than 0.25 represents no lack of fit in the model, where the model error is similar to the pure error. A bar less than 0.25 indicates a lack of fit where the model error is significantly larger than the pure error. The fourth column represented the reproducibility of the model, comparing the total variation of the response under the same conditions (pure error), measured at the replicates (e.g. center points). A bar of 1 presents a perfect model for both, model validity and reproducibility.

$$Reproducibility = 1 - \frac{MS (pure error)}{MS (total SS corrected)}$$

With

MS Mean squares (or variance)

SS The total sum of squares of Y corrected for the mean

2.16.2 Normal probability and replicate plot

The normal probability plot displayed the residuals plotted on a normal probability scale, which allowed detecting the normality of the residuals. If the data follows a normal distribution, the residuals follow a straight line (in a 45° angle); outliers can be determined if residuals deviate from the normal probability line, i.e. larger than 4 standard deviations as indicated by the red line in the plot.

The replicate plots (residuals vs run number) compared the response values against the experimental runs. This displayed the variation in the responses for the replicated experiments. This was especially important if experiments have been performed over a prolonged time period where any effect on environmental change (e.g. temperature change in the lab) could impede the output measurements.

2.16.3 Coefficient plot

The coefficient plot (or regression coefficient plot), displayed the model terms, main effect and interaction terms, ranging from 0 to high, for a selected response with the confidence intervals as error bars. Confidence intervals cross zero in non-significant model terms. The most important factor had the highest range (positive or negative). Similar coefficients plots patterns were indicative of correlated responses.

2.16.4 ANOVA

An ANOVA was performed, as the basis for regression model evaluation. Here, two F-tests examined the probability value p ; firstly the significance of the regression model was assessed and determined as statistically significant for $p < 0.05$. The second test compared the model error and replicate error, with a sufficient low model error the model showed good fit to the data with no lack of fit (LOF). Hence, the LOF test was fulfilled for $p > 0.05$.

2.17 Multivariate Analysis

Studies using multivariate data analysis were made in SIMCA version 13.0 (Umetrics). Scaling and transformation of the data set prior to analysis was performed automatically.

2.17.1 Principal component analysis

Initially, all data was pre-processed in Principal Component Analysis (PCA). PCA included the assessment of scores (t) and loadings (p), representing the position of an observation on the model plane (score) and expressing how the original variable correlates to the model (loading). The goodness of fit (R^2) and goodness of prediction (Q^2) assessed the model fit, which was regarded as good for $R^2 > 0.5$. The score scatter plot was used to assess situation of the x observations with respect to each other. Possible outliers, groups or patterns were identified with using the tolerance ellipse around the observations.

2.17.2 Partial least square analysis

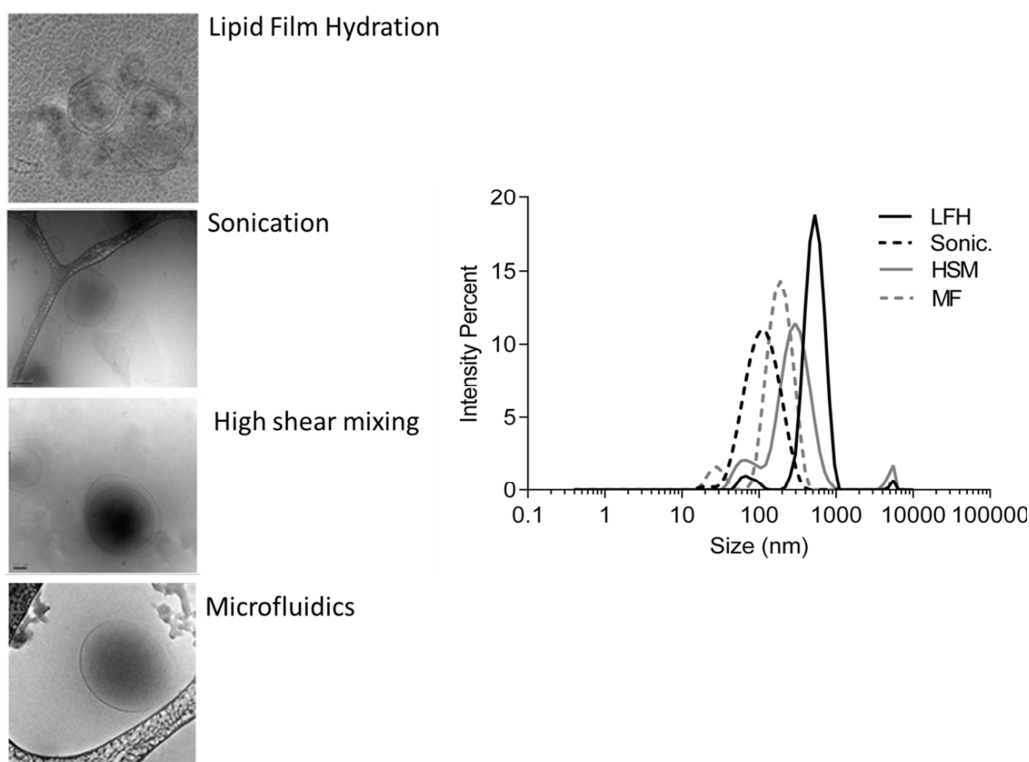
PCA was followed by Partial Least Square (PLS) as the quantitative modelling tool, for prediction of Y, correlation of X to Y matrix and regression. PLS modelled the relationship between X- and Y- variables and identified the importance of the X-variables (Eriksson, 2006). The X/Y Overview plot was used to evaluate the cumulated R^2 and Q^2 values for each variable of the data set. The number of components required were assessed and added or removed manually if required in order to avoid overfitting. DModX analysis was used for determination of the Dcrit in order to detect moderate outliers. The loading plot displayed the relation between the X-variables and the Y-variables. Weights were selected to maximize the correlation. The loading scatter plot identified relationships between the variables and the responses, and the relationships between the variables and the responses themselves. For interpretation, a line from a selected variable was drawn through the origin and X- and Y-variables were projected on the line. Variables opposite to each other were determined as negatively correlated, positive correlation was determined with variables adjacent to each other. The variable importance for the projection (VIP) plot was used to summarize the importance of the variables for explanation and prediction. The specific regression coefficients plots evaluated the X–Y relations in the computed PLS model. Correlated responses demonstrated similar coefficient profiles, uncorrelated responses showed different profiles in the regression coefficient plots (Wold et al., 2001a).

2.17.3 Validation

The model was validated using a permutations plots, which assessed the validity of the PLS model by evaluating the risk of invalidity and verified the validity not only for the current data set, but for new observations and predictions of Y. The X-data was left unchanged while permuting the Y-data, which was arranged it in a different order. new PLS models were fitted using the permuted data set and new R^2 and Q^2 verified the derived models by cross-validation, which were compared with real R^2 and Q^2 values of the model after random shuffling. Parallel models were generated over 40 permutations per model, assessing the validity of the initial PLS model (van der Voet, 1994) by comparing R^2 and Q^2 of the current model to the ones of the randomly permuted Y-observations at constant X-variables. A respective correlation line between permuted Y-vector to the original X-vector was shown and model validity was pre-set as the intercept of the Q^2 regression line at or below zero.

Chapter 3

Method development and evaluation: Quantification, particle sizing and microfluidics



Papers relating to this chapter:

Kastner E., Schmidt S. T., Wilkinson A., Christensen D. and Perrie Y. (2015). The Application of Liposomes as Vaccine Adjuvants. In Foged C., Rades T., Perrie Y. and Hook, S. Eds *Subunit Vaccine Delivery* Springer New York. pp. 77-94.

Kastner E. and Perrie Y. (2015). Particle size analysis for micro- and nanoparticles. In *Analytical Methods in Pharmaceutical Sciences* (submitted)

Kastner E., Lowry D. and Perrie Y. (2015). Rapid quantification of lipid concentrations within liposome systems (in preparation)

3.1 Introduction

Amongst all the methods available for liposome manufacturing, the lipid film hydration was the first described (Bangham, 1961; Bangham et al., 1965), and has since become one of the most commonly adopted methods for the manufacture of multilamellar vesicles (MLV). In addition to this method, sonication and high shear mixing (HSM) are used as down-sizing methods, categorised as “top-down” methods. In contrast, the microfluidics-based nanoprecipitation method has been described as a novel “bottom-up” method for vesicle manufacturing (Belliveau et al., 2012; Zhigaltsev et al., 2012) (Figure 3.1). The microfluidics-directed vesicle formation is based on a nanoprecipitation process; the controlled introduction of an aqueous phase to a solvent phase triggering the precipitation of lipids into liposomes.

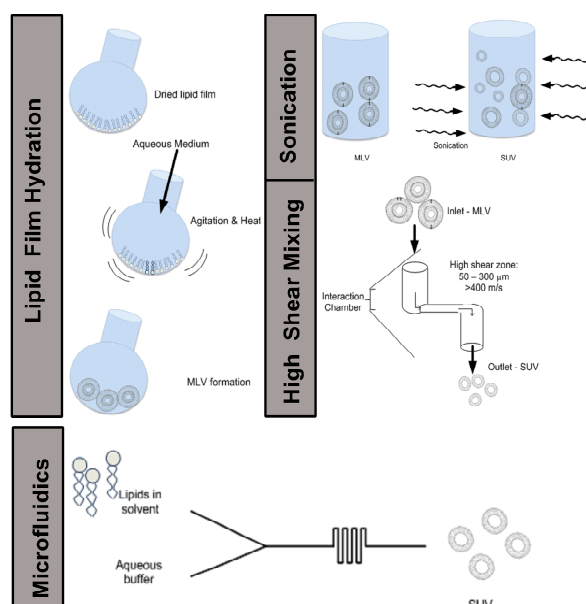


Figure 3.1: Schematic overview over the range of vesicle manufacturing methods investigated in this study.

It is well recognised that the size of drug delivery particles can dictate drug loading, drug release, biodistribution, cellular interactions and uptake, and biological function (Allen, 1994; Brewer et al., 1998b; Kirby et al., 1980; Mann et al., 2009). For example, in the design of vaccines, the vesicle size of liposomal adjuvants has been shown to influence the development of the immune responses towards a Th1 or Th2 cytokine profile via a range of routes (Brewer et al., 2004; Brewer et al., 1998b; Carstens et al., 2011; Mann et al., 2009; Manolova et al., 2008). Studies suggest that smaller particles promoted enhanced Th2 responses whilst larger particles promote IFN- γ and typical Th1 responses (Brewer et al., 1998a; Mann et al., 2009). This may be linked to differences in particle trafficking to local lymph nodes and uptake by antigen presenting cells (APCs). Improved antigen processing upon delivery in large (560 nm) vesicles, as

opposed to smaller (155 nm) vesicles, has been shown (Brewer et al., 2004). Similarly, uptake of particulates by dendritic cells was only observed at the injection site when large (0.5 – 2 μm) particles were used rather than small (20 – 200 nm) particles (Manolova et al., 2008) and significantly higher amounts of smaller liposomes were found at the popliteal lymph node 6 hours after injection (Henriksen-Lacey et al., 2011a) making the vesicle size a factor crucial for liposome exposure in the lymph nodes and recruitment of the innate immune system (Henriksen-Lacey et al., 2011a).

For particle characterisation light scattering techniques were used in the studies reported within this thesis. These methods are currently the most widely used techniques available to size micro- and nanoparticles. Based on the non-destructive methods, protocols can be adopted for a range of sample and molecules with a relatively quick analysis time. Here, two of the main light scattering techniques were compared, namely DLS and NTA. With methods highly applicable to determine the size liposome, typically SUV and LUV sizes ranging between 30 nm to 500 nm, each method was described first to consider the correct interpretation of measurement data. DLS (also known as photon correlation spectroscopy (PCS) and quasielastic light scattering (QELS)) determines the hydrodynamic diameter of particles typically below the micrometer range and down to a few nanometers in size. DLS assesses the time-dependent intensity scattering fluctuation of a particle in suspension. The method is based on determination of the diffusion constant (D) in order to derive the hydrodynamic diameter (d_H) of a particle; the measurement depends on the viscosity of the suspending media (μ), the absolute temperature (T) and the Boltzmann constant (k) as based on the Stokes-Einstein relationship, (Equation 3.1).

$$d_H = \frac{k T}{3\pi\mu D} \quad \text{Equation 3.1}$$

Based on collision between particles moving under the Brownian motion, the suspended particles scatter a light beam hitting on the suspension. A detector analyses the scattered light intensity, which strongly depends on the size of the particles. The measurement results in a correlation curve, which links the diffusion of the particles to the scattered light fluctuations over time (Figure 3.2) (Chu and Liu, 2000; Pecora, 2000). Measurements determine the hydrodynamic diameter (Stokes-Diameter), determining the translational diffusion coefficient of the measured particle by relation to a hypothetical sphere (Chu and Liu, 2000).

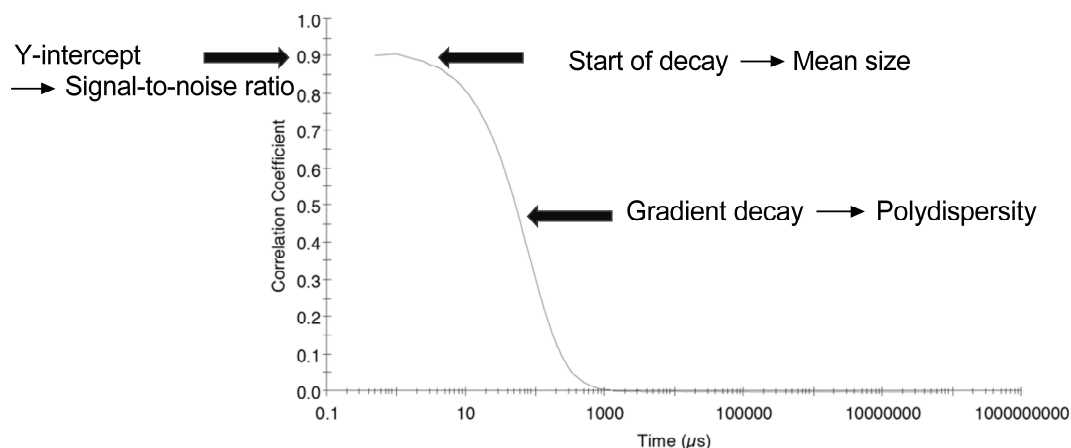


Figure 3.2: Schematic of a correlation function as obtained from a DLS measurement with indicated qualitative properties of suspended particles. Adapted from (Kastner and Perrie, 2015).

A monomodal size distribution is represented by an ideal single exponential decay correlation function, which fits the decay to the particle diffusion allowing derivitisation of the diffusion coefficient (D). The correlation function is assessed by the steepness and the gradient of the decay function, reflecting the heterogeneity of the sample and the Y-intercept, a qualitative indication of the signal-to noise ratio, ideally located at 1 and acceptable within the range of 0.6-0.9. The z-average size (cumulants mean) is the primary and most accurate measurement obtained. By definition, the z-average represents the intensity averaged particle diameter, which is difficult to directly compare with a number-based size as obtained by e.g. microscopy imaging. For a monomodal size distribution the z-average is highly applicable as it is defined in ISO standards (ISO, 2008). Nevertheless, the presence of a small number of larger aggregates will substantially influence the measurement outcome, which generally makes the z-average value less applicable in a multimodal size distribution. A measurement typically results in an intensity-based distribution, which can be converted into a number and volume distributions using the Mie theory (Fu and Sun, 2001). This aids in approximation of the relative proportions of the particles in a sample (Chu and Liu, 2000; Ito et al., 2004), given the distribution bias towards larger particles. The intensity of the scattered light is proportional to the molecular weight of the particle squared and the diameter of the particle to the power 6. Given this bias towards larger particles, the conversion into a volume-based distribution is often more applicable as the volume is proportional to the diameter of the particles cubed. Besides using DLS for particle size determination, the heterogeneity of the particle suspension is simultaneously determined and reported as the polydispersity index (PDI), ranging to a maximum of 1 for a very heterogeneous sample. Generally, any value > 0.7 is

representative of a very broad size distribution, where resulting particle size measurements based on DLS are not reliable (Berne and Pecora, 2000).

Similar to DLS, NTA relies on the measurement of scattered light and Brownian motion to determine particle size distributions of a suspension. During NTA analysis, a camera captures the scattered laser light and a video file allows separate tracking of each particle as they move under the Brownian motion (Carr et al., 2009; Carr and Wright, 2008; Gardiner and Dragovic, 2014). In addition to single particle sizing, NTA also allow for the particle concentration to be determined. Measurement commences with selecting the view field using a camera and projections onto a computer for the live tracking system. A video file of typically 30-60 seconds is recorded, where the localization of the centre of each particle allows tracking on a frame-by-frame basis (Figure 3.3). The travelled distances (x and y directions) are used to determine the diffusion coefficient using the Stokes-Einstein equation, based on the viscosity of the media (μ), the absolute temperature (T) and the Boltzmann constant (k), used to determine the hydrodynamic diameter (d_H) of the particles (Equation 3.1).

$$d_H = \frac{kT}{3\pi\mu D} \quad \text{Equation 3.1}$$

Travelled distances are converted into a particle size distribution, intensity and number based distributions are fitted and the concentration of the particles is extrapolated based on the known volume of the view field (Carr et al., 2009; Carr and Wright, 2008). As opposed to DLS, the hydrodynamic diameter of each particle is tracked rather than the sum of particles motion, thereby circumventing intensity-based bias seen with larger particles or aggregates present in a sample during a DLS measurement.

Whilst the advantage of the DLS measurement lies in its good accuracy for monodisperse samples along with a quick and user-friendly measurement, NTA analysis generally requires a higher level of operator training. However NTA generally results in a higher resolution (Bell et al., 2012). Nevertheless, the selection of the frame is user bias and the equipment requires a higher degree of maintenance, Table 3.1.

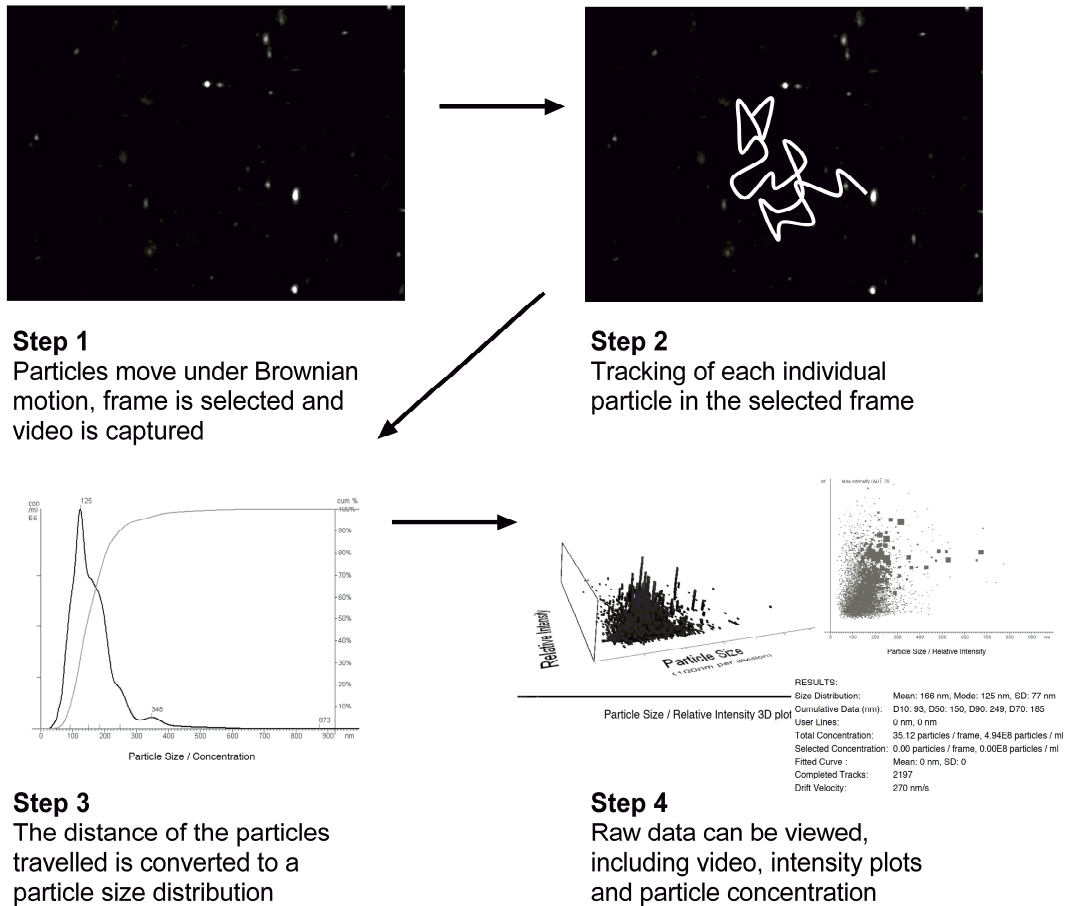


Figure 3.3: Stepwise procedure during NTA analysis. Adapted from (Kastner and Perrie, 2015).

Table 3.1: Direct comparison of DLS and NTA.

	DLS	NTA
Size Range	1-8 000 nm	10 – 2 000 nm
Concentration Range	Max 40% w/v (dependent on refractive index and particle size)	$10^7 - 10^9$ particles / mL
Sample volume	10 – 500 μ L	10-100 μ L
Accuracy	Good accuracy for monodisperse samples, inaccurate at higher polydispersities	Good accuracy for low and high polydispersity samples
Resolution	Low at less than 3 fold difference in diameter	High, higher than 0.5 fold in diameter
Reproducibility	High	Lower (frame selection by user)
Sample preparation	Removal of large contaminants by filtration or centrifugation	Removal of large contaminants by filtration or centrifugation
Contamination	Large particles influence measurements (intensity measurements)	Appropriate dilutions required Contaminants more easily detected, lower influence of larger particles
Output	Z-Average, intensity, volume and number distribution, polydispersity	Absolute particle diameter Particle concentration
Visualisation	No	Yes (video recording over measurement period)
Device	User-friendly, little sample preparation, disposable cuvettes	Several adjustments required (dilutions, microscope settings), cleaning of chamber after each measurement, operator experience required
Average recording time	2-5 min per measurement	5-10 min per measurement
Application	Sizing, size distribution	Sizing, size distribution, particle concentration

Thus it can be seen that in the development of a new process of liposome production, size analysis as well as drug and lipid concentrations are key factors. Therefore, within this chapter the two main methods for sizing nanoparticles, both based on light scattering techniques, have been investigated. DLS and NTA were used to assess the homogeneity of the particle population and for determining particle concentration. To

quantify lipid concentration, an ELSD coupled to a HPLC was used. An ELSD detector is based on a light scattering detection of solids with a lower volatility than the mobile phase, and was chosen to allow for lipid quantification due to lack of UV adsorption of most lipids (Brouwers et al., 1998).

3.2 Aim and Objectives

The aim of this chapter was to investigate the initial development, optimisation, evaluation and validation of the core methods based on lipid quantification, particle sizing and microfluidic-directed manufacturing of liposomes. To achieve this, quantification methods for the lipid, drug and protein molecules used throughout this thesis were based on development of HPLC protocols, with quantification based on an ELSD. Each developed method underwent extensive validation to align with current ICH guidelines (ICH, 2005). Two main methods for particle sizing, DLS and NTA, were described and compared. Both methods were assessed for the sizing of liposomes, which ultimately defined how each method was used throughout this thesis. Vesicle manufacturing methods based on lipid film hydration, sonication, HSM and microfluidics were compared and design of experiments for a lipid adjuvant formulation which combines the cationic lipid dimethyldioctadecylammonium (Bromide Salt) and the immunomodulator trehalose-6,6-dibehenate (DDA-TDB) were adopted to support the development of statistical regression models for the prediction and correlation of particle size in each method.

3.3 Results and Discussion

3.3.1 Development and validation of quantification methods based on HPLC and ELSD

The initial focus of this work was to establish quantification methods for a range of molecules. Therefore HPLC methods were developed, optimised and validated in terms of: linearity, accuracy, precision (intermediate precision and repeatability), limit of detection (LOD), limit of quantification (LOQ) and robustness. The separation of all compounds was achieved using a C18 reverse-phase column. The composition of the mobile phase, the flow rate and gradient flow was optimised for each compound. Detection was performed by UV (propofol, CM2) or ELSD (PC, Cholesterol, DOPE, DOTAP, DDA, TDB, ovalbumin). As an example, the complete validation protocol for cholesterol is shown below; thereafter the same protocols were adapted for all other molecules. For quantification of cholesterol, a gradient elution method was optimised,

which resulted in the elution of the lipid at 10 minutes and quantified by ELSD (Figure 3.4).

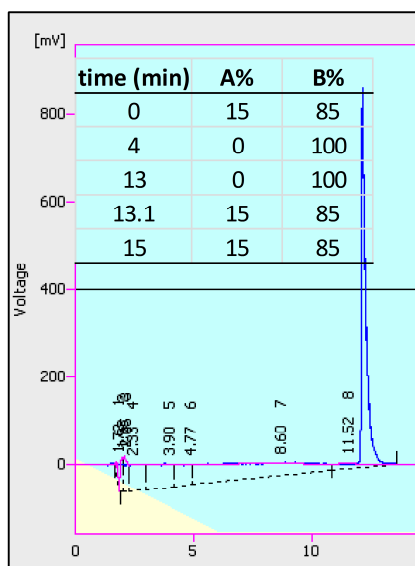


Figure 3.4: Elution peak for cholesterol detected by ELSD with the elution protocol. The flow rate was 1 mL/min throughout. Mobile phase A was 0.1%TFA water, B was methanol.

3.3.1.1 Linearity

Standard solutions (in chloroform) were prepared (with a minimum of at least five different concentrations), ranging from 0.25% to 200% of the target concentration (Shabir, 2003, 2005). If overshooting of the elution peak occurred at higher concentrations, respective dilution of the standards was adopted. For each concentration, three replicates were analysed. A calibration curve was constructed to assess the linearity for cholesterol over the concentration of 0.025 to 1 mg/mL. The peak area was determined and plotted against the known concentration of cholesterol standards. The mean and standard deviation was calculated for each concentration. Regression coefficients (R^2) was deemed to be sufficient at ≥ 0.99 . For example, for cholesterol the equation for the resulting calibration curve was $y = 63664x + 1192.3$, with a linear regression coefficient of 0.993, passing the pre-set acceptance criteria (Figure 3.5).

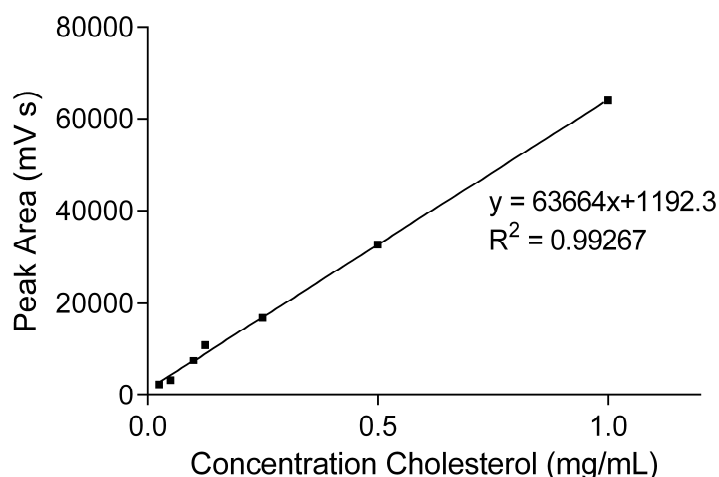


Figure 3.5: Linearity assessment of cholesterol (0.025 to 1 mg/mL) used to determine the calibration curve to assess the cholesterol concentration.

3.3.1.2 Precision

Intraday precision (repeatability) and interday precision (intermediate) were determined for cholesterol at concentrations from 0.025 to 1 mg/mL. Again for each concentration, three replicates were analysed and a calibration curve was constructed. The peak area was determined and plotted against the known concentration of cholesterol standards. The mean, standard deviation and relative standard deviation (%RSD) were calculated for each concentration. A %RSD of $\leq 5\%$ was set as the acceptance criteria. The interday precision determined the %RSD over the course of 3 days, intraday precision within one day. Examples of this for cholesterol are shown in Figure 3.6, with both criteria passing the pre-set acceptance criteria.

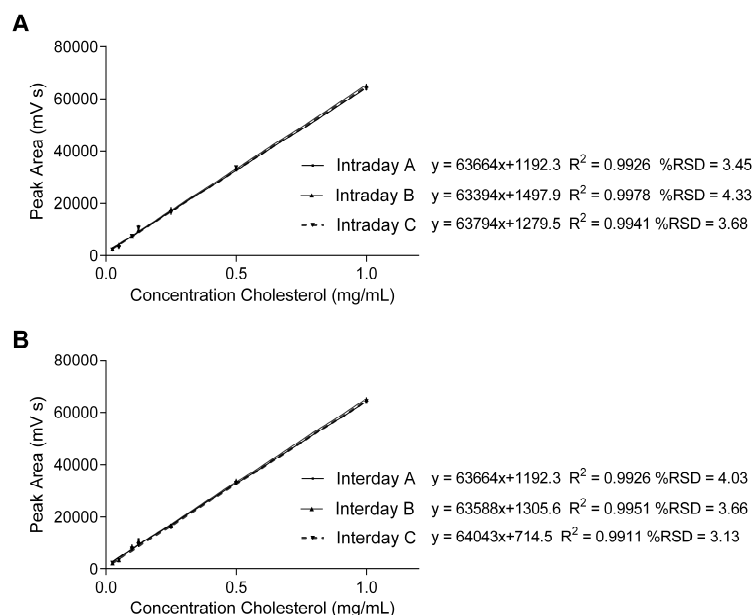


Figure 3.6: Cholesterol quantification - assessment of A) intraday and B) interday variability with linear regression coefficients and %RSD.

3.3.1.3 Accuracy

To assess the accuracy of the method, spiked samples of a known concentration of standard were prepared over the range of 50 to 150% of the target concentration (Shabir, 2005). Three prepared replicates were injected three times ($n = 9$), with for example, cholesterol concentrations of 0.05, 0.1 and 0.25 mg/mL. The mean, standard deviation and relative standard deviation (%RSD) was calculated for each concentration. Table 3.2 outlines the %RSD and recovery for cholesterol based on the method developed. The %RSD was found sufficient at $\leq 5\%$ at a recovery ranging from 90 – 110%, passing the pre-set acceptance criteria (Shabir, 2005).

Table 3.2: Evaluation of %RSD and recovery during the validation of the assay accuracy.

Concentration standard (mg/mL)	Average determined concentration (mg/mL)	%RSD	Recovery (%)
0.05	0.0512	4.7	104.5 \pm 5.1
0.10	0.1043	5.0	102.3 \pm 4.0
0.25	0.2522	3.1	96.4 \pm 6.2

3.3.1.4 Robustness

Robustness assesses the capacity of the method to remain unaffected by small variations, and informs on the reliability of the method during normal usage (Shabir, 2005). Investigated parameters included the variation in column temperature and flow rate. The column temperature was varied by $\pm 5^\circ\text{C}$ and the flow rate was varied by \pm

0.2 mL/min. When tested with cholesterol, the increase in temperature accelerated the elution, explained by increase in molecule diffusion by temperature increases (results not shown). The increase in flow rate also accelerated the elution profile, due to increased volumes of elution buffer through the column promoting dissociation of the compound from the column (results not shown). Both investigated parameters produced acceptable chromatograms, nevertheless effected elution time and area under the curve. Thus, the column temperature was fixed at 35°C and controlled throughout each measurement. Moreover, the flow rate of the mobile phase remained constant and was not altered post method validation.

3.3.1.5 Level of detection and level of quantification

Limit of detection (LOD) and limit of quantification (LOQ) were calculated by assessing the signal to noise ratio in the method and were determined from the standard deviation of the response and the slope from the calibration curve established during the linearity assessment. Calculations are based on the assumption of a signal to noise ratio of LOD 3:1, LOQ 10:1 (ICH, 2005), which may vary with ageing, model, manufacturer of detector or column. The slope is determined from the calibration curve and Equation 3.1, 3.2 and 3.3 are used to derive the LOD and LOQ. The LOD was below the reporting threshold (ICH, 2005) for all lipid protocols established. If the LOQ was found above the specification limit, a concentration of the sample was performed prior to quantification.

$$\sigma = \sqrt{\frac{\sum (Y - Y_i)^2}{n-2}}$$
Equation 3.2

$$LOD = \frac{3\sigma}{S}$$
Equation 3.3

$$LOQ = \frac{10\sigma}{S}$$
Equation 3.4

With

σ	Standard deviation determined in calibration curve
S	Slope determined in calibration curve
Y	Intercept
n	Number of standard solutions on the calibration curve

In the case of cholesterol, a concentration of 0.77 mg/mL was used in a standard formulation (Table 2.1) and the LOQ determined was 0.15 mg/mL and within the acceptance criteria. The slope is determined from Figure 3.3 and Equation 3.1, 3.2 and 3.3 were used to derive the LOD and LOQ as follows:

$$\sigma = \sqrt{\frac{\sum (Y - Y_i)^2}{n - 2}} = \sqrt{\frac{4540011.86}{5}} = 952.89$$

$$LOD = \frac{3\sigma}{S} = \frac{3 * 952.89}{63664} = 0.044 \frac{mg}{mL}$$

$$LOQ = \frac{10\sigma}{S} = \frac{10 * 952.89}{63664} = 0.150 \frac{mg}{mL}$$

3.3.1.6 Summary of validation criteria for lipids used

The overall summary of each validation procedure is shown in Table 3.3. As noted, it is important to verify both lipid and drug recovery throughout any work undertaken, first to assess the cost-effectiveness and verify concentrations of lipid and drug at ratios defined prior to formulation. In contrast to the time and equipment-intensive lipid quantification by mass spectrometry (Moore et al., 2007), the here-developed lipid quantification method based on HPLC separation and evaporative light scattering detection was found to be a simple and robust method, allowing quantification of any solids in the elute with a lower volatility than the mobile phase in validated methods.

Table 3.3: Overview over the validation of lipids, drug (propofol) and protein (ovalbumin).

Compound*	Linearity	LOD	LOQ	Precision		Accuracy	
	R ²	mg/mL	mg/mL	%RSD interday	%RSD intraday	%RSD	Recovery (%)
Cholesterol	0.993	0.044	0.150	3.607	3.820	4.277	101.1 ± 4.2
PC	0.989	0.104	0.349	4.633	4.554	4.333	96.4 ± 3.3
DOPE	0.996	0.051	0.168	3.543	4.983	2.544	98.6 ± 3.5
DOTAP	0.995	0.061	0.204	2.987	4.544	4.765	105.3 ± 2.6
DDA	0.998	0.024	0.079	5.043	4.765	3.433	107.3 ± 2.0
TDB	0.995	0.102	0.341	5.033	4.654	3.547	103.5 ± 4.6
Propofol	0.996	0.047	0.159	2.472	2.345	2.433	99.3 ± 5.9
Ovalbumin	0.991	0.014	0.046	4.554	3.433	2.512	100.9 ± 6.3
CM2	0.987	0.056	0.187	3.567	3.233	3.159	101.4 ± 3.6

*PC = Phosphatidylcholine, DOPE = 1,2-dioleoyl-sn-glycero-3-phosphoethanolamine, DOTAP = 1,2-dioleoyl-3-trimethylammonium-propane, DDA = Dimethyldioctadecylammoniumbromide, TDB = Trehalose 6,6'-dibehenate, Propofol = 2,6-Bis(isopropyl)phenol, CM2 = 1,1'-(decane-1,10-diyl)bis(9-amino-1,2,3,4-tetrahydroacridinium) diiodide.

3.3.1.7 Bimodal populations measurement by DLS

Throughout this thesis, a range of particulate systems will be studied, which may be mono-, bi- or even multimodal populations. This may not only have an impact on therapeutic outcome of the system but may also impact on the measurement results

from particle size analysis techniques. To consider the modality of the particle size distribution, liposome suspensions (DDA-TDB, 1.25 mg/mL and 0.25 mg/mL respectively) containing a mixture of two different liposome size populations were prepared and the particle size measured using DLS. Two populations of liposomes were manufactured; initially using a rotary evaporation process for generating a larger population of ~500 nm vesicles (Table 3.4, Figure 3.7B). Subsequently, vesicles were sonicated to generate a smaller sized liposome population (~80 nm; Table 3.4, Figure 3.7A). Both formulations contained equal lipid concentrations, therefore it follows that the 80 nm population comprised a larger number of vesicles.

Table 3.4: Particle size and polydispersities measured from various liposome mixtures to assess the impact of bimodal size distributions on the measurement outcome.

80:500 nm size ratio	z-average diameter (nm)	PDI
1:0	78.1 ± 5.5	0.196 ± 0.005
0:1	502.2 ± 15.5	0.704 ± 0.086
1:1	175.6 ± 17.8	0.594 ± 0.008
1:2	298.0 ± 22.1	0.595 ± 0.052
1:4	407.0 ± 11.3	0.636 ± 0.046
2:1	117.9 ± 8.5	0.413 ± 0.085
4:1	101.1 ± 5.4	0.387 ± 0.057

Subsequently, the two populations were mixed at different ratios in order to prepare bimodal populations (Table 3.4). Almost equal-sized intensity plot were obtained once mixing the 500 nm and 80 nm populations in a 1:1 lipid weight ratio, 51 % and 47% of the distribution at 500 nm and 47% of the distribution and 80 nm respectively (Figure 3.7C). The representation in a volume % showed a larger proportion of the smaller sized vesicles (34% for the 500 nm sized population and 65% for the 80 nm sized population; Figure 3.7C). Reporting the z-average here would not reflect the actual size as shown in Table 3.4. Once the concentration of the larger-sized vesicle population is increased, good peak separation was still given and the changing ratios between intensity and volume peaks highlighting on the increase in the larger sized population (Figure 3.7C). With the z-average diameter increasing with a higher amount of larger-sized population added (Table 3.4), highlighting on the inappropriate representation of the two populations by simply using the z-average. The 1:4 ratio of 80:500 nm liposomes resulted in approximately equal distribution plots (by volume) for both sub-populations. Following, an approximately 4 times higher concentration of the smaller (80 nm) relative to the larger (500 nm) particles could be anticipated (Figure 3.7C). In

addition, the resolution between the populations decreased upon increasing the ratio of the smaller liposomes (Figure 3.7D). The larger-sized population became difficult to accurately detect, represented by peak broadening in intensity and volume based distributions, once the ratio was increased to 4:1 for 80:500 nm liposomes (Figure 3.7D). The determined z-average approached the size of the smaller liposome population (80 nm), whereas the high degree of heterogeneity was still represented by a higher polydispersity (Table 3.4). The results in Figure 3.7 highlight the importance of evaluating both the intensity- and volume-based distribution plots for understanding particle size distribution during DLS measurements.

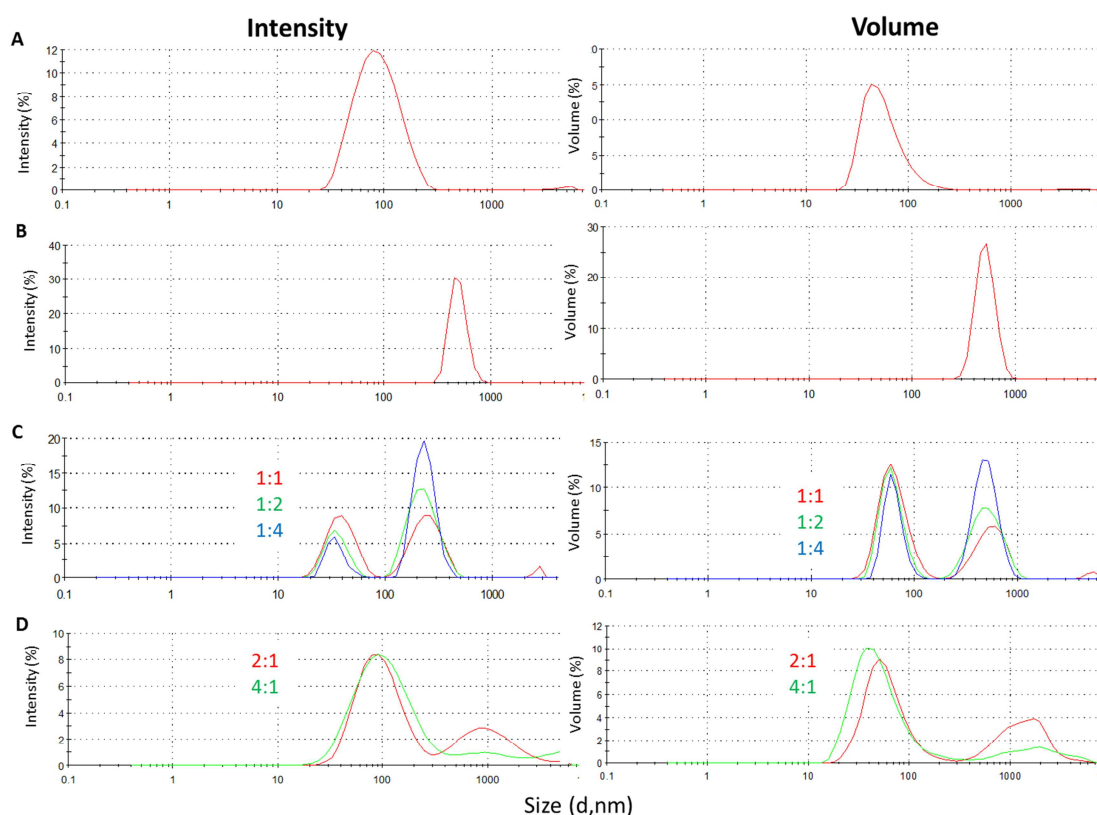


Figure 3.7: Resulting intensity and volume based size distribution plots for the A) 80 nm sized and B) 500 nm sized population, C) increasing the ratio of the larger 500 nm population and D) increasing the ratio of the smaller 80 nm sized population. Adapted from (Kastner and Perrie, 2015).

3.3.1.8 Direct comparison DLS and NTA measurement of liposomes

To consider the two different particle size analysis methods (DLS and NTA) a direct comparative study between both techniques for a SUV formulation (PC-Chol, 6.06 mg/mL and 0.77 mg/mL respectively) was undertaken. DLS analysis revealed a z-average of 119 nm, with a polydispersity of 0.121 (Figure 3.8A) for the SUV formulation. The intensity and volume based distribution plots revealed a monomodal size distribution, with 100% intensity at 126 nm and 100% volume at 116 nm (Figure

3.8A). The same liposome batch was then analysed via NTA, which yielded a mean diameter of 147 nm, a mode of 118 nm and a standard deviation of 60 nm (Figure 3.8B). In addition to the size distribution, the concentration of the particles was determined (8.9×10^8 particles/mL). A visual image and video were recorded throughout the measurement, showing the scattered laser light in the selected frame (Figure 3.8B).

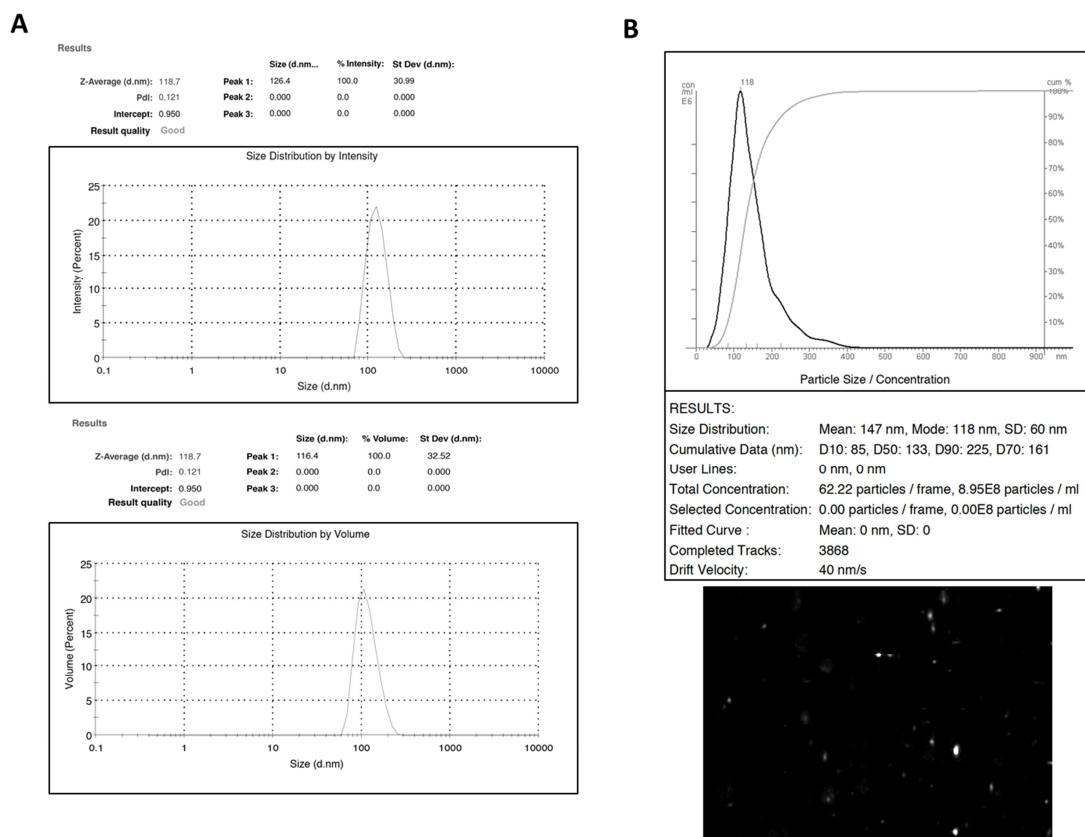


Figure 3.8: Direct comparison of a monomodal liposome size determination as measured by A) DLS and B) NTA with particle imaging by light scattering. Adapted from (Kastner and Perrie, 2015).

Based on these initial results, the z-average resulting from a DLS measurement was found to correspond the most closely to the mode diameter as obtained by NTA for a monomodal size distribution. Furthermore, the correct particle size can be assessed as mode or mean, whereas the NTA measurement was mainly used as a visual particle confirmation in subsequent studies.

Whilst the above described methods based on light scattering techniques are rapid and easily adopted, accurate size analysis of multi-modal size populations may be difficult and requires detailed analysis of intensity-, volume-based distribution. In order to validate measurements additional microscopy remains the most important reference method to be implemented for additional validation (Bootz et al., 2004). Therefore, an accurate and robust characterisation of suspended particles relies on selecting an

accurate measurement principle, accurate sample preparation and analysis. Likewise, both particle sizing techniques are based on a number of assumptions, which may not match the true attributes of the particles being sized. Throughout this work the size of particles was assessed by the z-average for monomodal size distributions, and the intensity-weight particle diameter for bi- or multimodal size distributions by DLS. Additionally, the comparison between intensity and volume-based distributions was used to qualitatively assess any ratios between bimodal size distributions. During NTA analysis, the mode diameter was recorded and the imaging tool was used as a visual confirmation of particles when required.

3.3.2 Methods for liposome manufacturing: sonication, high shear mixing and microfluidics.

To initially consider different methods of liposome production, a direct comparison of the four main methods for manufacturing liposomes (lipid film hydration, sonication, high shear mixing, microfluidics) was undertaken using protocols established within the laboratory. Liposomes composed of DDA-TDB (1.25 mg/mL and 0.25 mg/mL respectively) were prepared using each of the four methods and their size analysed by DLS (Figure 3.9). Here, the vesicles prepared by lipid film method (LFH) resulted in a population of around 500 nm \pm 50 nm, sonication (Sonic.) produced vesicles of 120 nm \pm 25 nm, high shear mixing (HSM) produced vesicles of 230 nm \pm 37 nm and vesicle produced by microfluidics were around 160 nm \pm 25 nm and polydispersities were relatively unaffected by the respective methods (Figure 3.9). The sizes obtained and displayed in Figure 3.9 represent the averages sizes obtained within the initial method development phase, which have been further defined throughout the thesis. This early comparison demonstrates the effect of the liposome production method on vesicle size.

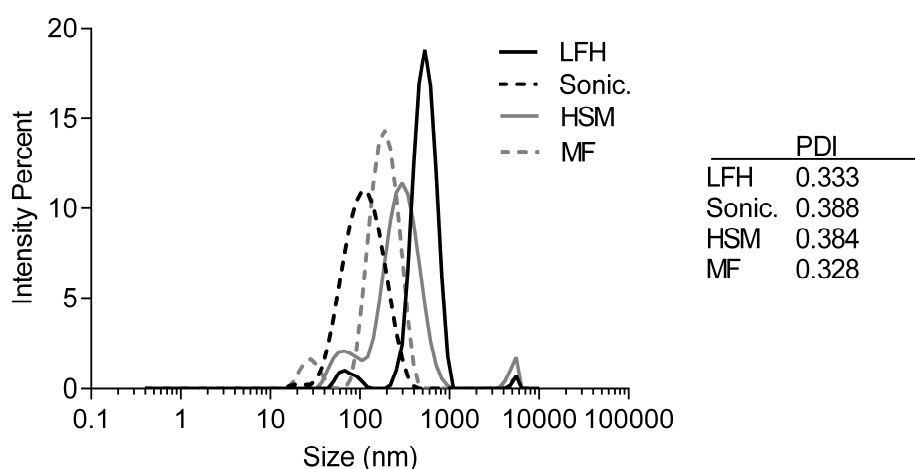


Figure 3.9: Overlay plot showing the difference in liposome population in size and PDI produced by high shear mixing (HSM), sonication (sonic.) and microfluidics (MF) compared to liposomes produced by lipid hydration (LFH) method.

The morphology of these vesicles was considered using cryo-transmission electron microscopy (cryoTEM) (Figure 3.10). CryoTEM showed that multilamellar vesicles were manufactured in the lipid film hydration method (Figure 3.10A), and unilamellar liposomes were generated in the microfluidics method (Figure 3.10B), whereas the vesicles produced in the HSM method generated vesicles with multiple bilayers (Figure 3.10C). Vesicles prepared by the sonication method were as unilamellar as would be anticipated (Figure 3.10D). However these vesicles do not appear spherical in nature as would be expected (Bibi et al., 2011). This may be due to disruptive mechanical forces in the process (Wagner and Vorauer-Uhl, 2010). Here, the average size based on cryoTEM differed from the size obtained by DLS measurement. Due to differences in underlying measurement principles and requirements, average vesicles sizes obtained by cryoTEM should not be directly compared to the size averages obtained by DLS measurement (Almgren et al., 2000) and an extensive comparison of particle size by cryoTEM and DLS has been done by Egelhaaf (Egelhaaf et al., 1996).

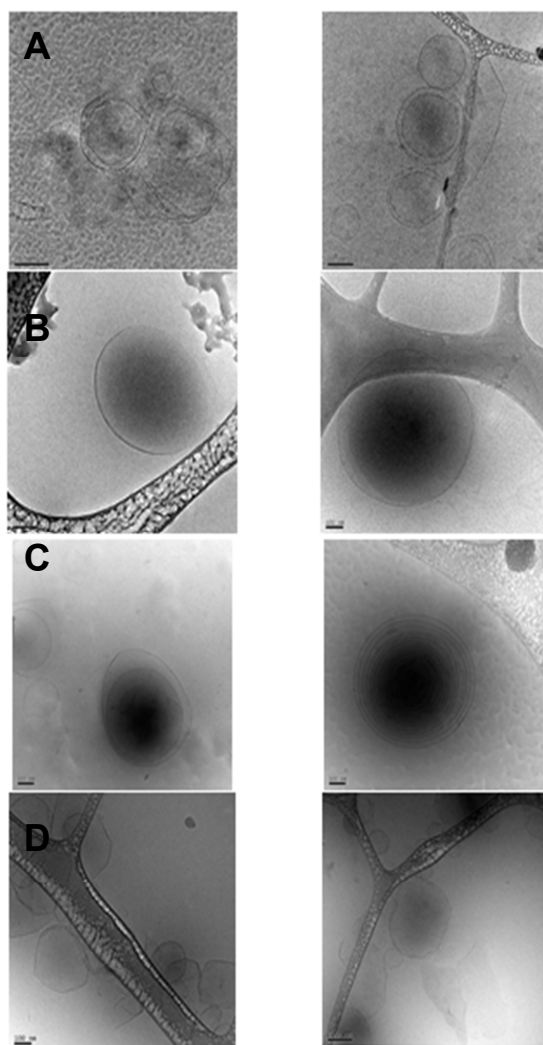


Figure 3.10: CryoTEM pictures obtained of A) MLV produced by lipid hydration B) SUV microfluidic mixing C) high shear mixing D) sonication. Bar represents A) 200 nm, B-D) 100 nm.

The lipid film hydration is a relatively easy, simple, quick and well-established method (Bangham, 1961). Nevertheless, despite flushing with N₂ after forming the lipid film, solvent residues may remain, making the method less applicable based on safety concerns. Moreover, the vesicle population is multilamellar and heterogeneous in size (ranging up to several microns), often resulting in low encapsulation achieved (Bangham, 1961). The vesicle size is influenced by the amount and type of lipids used and for a controlled vesicle size consecutive downsizing methods are required. Methods such as homogenisation, extrusion or HSM are relatively easy methods that allow for a bulk production with the possibility to run in a continuous mode. Nevertheless, these processes can require high pressures and/or generate heat, which may be damaging to lipids, drugs or proteins. With extrusion methods, filter clogging is an often-mentioned disadvantage (MacDonald et al., 1991) and the resulting sizes usually depend on the number of recirculation cycles or exposure times to shear or pressure (Bally et al., 1991). Sonication, based on a probe tip or a bath sonicator, is a quick and easy method, which mainly finds application in a laboratory setting only. Common reported problems are linked to contamination with metal residues from the probe tip and lipid degradation. The main disadvantage is the lack of scalability, making the method less viable for a large scale industrial process setting (Wagner and Vorauer-Uhl, 2010).

To address these issues, microfluidics-based liposome production has been explored. The advantage of the microfluidics-based nanoprecipitation method lies in the controlled environment, leading to a reproducible process setup. Due to mixing in the micro-channels, the mixer has been designed to introduce a controlled mixing environment in a chaotic advection mixing profile (Stroock et al., 2002). The method is flexible and allows for screening over a range of concentration in a high-throughput setup, given time for formulation is drastically reduced. Nevertheless, solvent residues remain in the process, which require an additional purification process based on dialysis or filtration. Here, a spin column process was implemented for purification and concentration of the vesicles. The type of chip material dictates the solvent compatibility, and the precipitation process is based on a high volume of aqueous flow, which results in a dilution of the final formulation based on the settings chosen (Belliveau et al., 2012; Zhigaltsev et al., 2012).

3.3.2.1 *Design of experiments for method investigation and validation*

The results reported in Figure 3.9 were based on protocols within the laboratory. To further optimise these, each method was evaluated using a DoE approach. Here, the previously described manufacturing methods, sonication, HSM and microfluidics were investigated in relation to the ability for controlling the size of the vesicles. The DDA-TDB liposome formulation was again used for this optimisation process as it is a well-established cationic adjuvant formulation (Christensen et al., 2007b) and has been further investigated in Chapter 8. Models included the variables:

- Sonication - time (1-2 minutes) and amplitude (1 – 10) in the sonication method.
- HSM - mixing time (1-10 minutes) and rotational speed (1000 – 25000 rpm).
- Microfluidics - flow rate ratio (FRR, 1:2 – 1:5) and total flow rate (TFR, 1.2 – 2.5 mL/min).

The effect of respective factors to the size of DDA-TDB liposomes was evaluated.

Model evaluation commenced with assessment of the summary plot, which displayed R^2 , Q^2 , model validity and reproducibility for all three methods: sonication, HSM and microfluidics (Figure 3.11A, 3.12A, 3.13A, respectively). Acceptance criterion were pre-set at: $R^2 \geq 0.5$, $Q^2 \geq R^2 - 0.3$, validity ≥ 0.25 and reproducibility ≥ 0.5 for an excellent model. Close situation of R^2 and Q^2 values indicated that the models were highly predictive. Summary plot for the sonication method (Figure 3.11A) showed excellent model properties with $R^2 = 0.91$, $Q^2 = 0.85$, validity = 0.97, reproducibility = 0.73. Evaluation of the summary plots revealed a high amount of noise in the data set for HSM (Q^2 of 0.25), with a goodness of fit of 0.81, validity = 0.5, reproducibility = 0.93, which was still evaluated and used as a control to the microfluidics method (Figure 3.12A). The microfluidics method revealed an excellent fit ($R^2 = 0.92$) with an acceptable predictability ($Q^2 = 0.39$), indicative of noise in the data set similar to the HSM process. Nevertheless, the validity of 0.85 and reproducibility of 0.80 were considered good with no lack of fit present in the model and hence additional model evaluation was performed (Figure 3.13A).

Given the excellent model fit and acceptable prediction along with good valid and reproducible models, further diagnostic tools were performed for outlier detection. The observed vs. predicted plots (Figure 3.11B, 3.12B, 3.13B) indicated good models in each method, as the points for the observed vs. the fitted values sat close to the straight 45° line. One outlier was detected in the microfluidics method (N8) and removed for model evaluation. A systematic effect was excluded in each model, as no

pattern was seen in the replicate plots (Figure 3.11C, 3.12C, 3.13C). Here, the replicate centre points showed a lower variation in each model compared to the experimental runs, with the sonication method showing the highest variation compared to the HSM and microfluidics model. The response surface plots showed liposome size predictions as a function of the factors in each method. Predictions in the sonication method showed minimal vesicle sizes of 90 nm and maximum vesicle sizes of 150 nm. The sonication amplitude was evaluated as the most important coefficient during the sonication process, whereas, the sonication time was found more important at low sonication amplitudes only (Figure 3.11D). The model predicting the vesicle size in the HSM method revealed the rotational speed as the factor with the biggest impact in the process (Figure 3.12D). Here, minimum vesicle sizes predicted were larger than the ones obtained in the sonication method, reaching a minimum of 160 nm, with maximum vesicle sizes of 320 nm. Overall, the HSM method showed an almost linear trend in the response surface with the smallest size achievable for the maximum mixing time (10 minutes) and rotational speed (25 000 rpm) and the largest size achievable for the minimum mixing time (1 minute) and rotational speed (1000 rpm). In the microfluidics method, vesicle sizes ranged between a maximum vesicle size of 200 nm down to a minimum of 90 nm. Here, both factors, TFR and FRR were found as strongly influencing the model predictions, where the effect to size at higher aqueous FRR (above 1:3) and at constant TFR showed only limited effect to the size. The TFR was found an important factor even at constant FRR, where the smallest liposome size was predicted for a FRR of 1:3 to 1:4 at the highest TFR of 2.5 mL/min (Figure 3.13D).

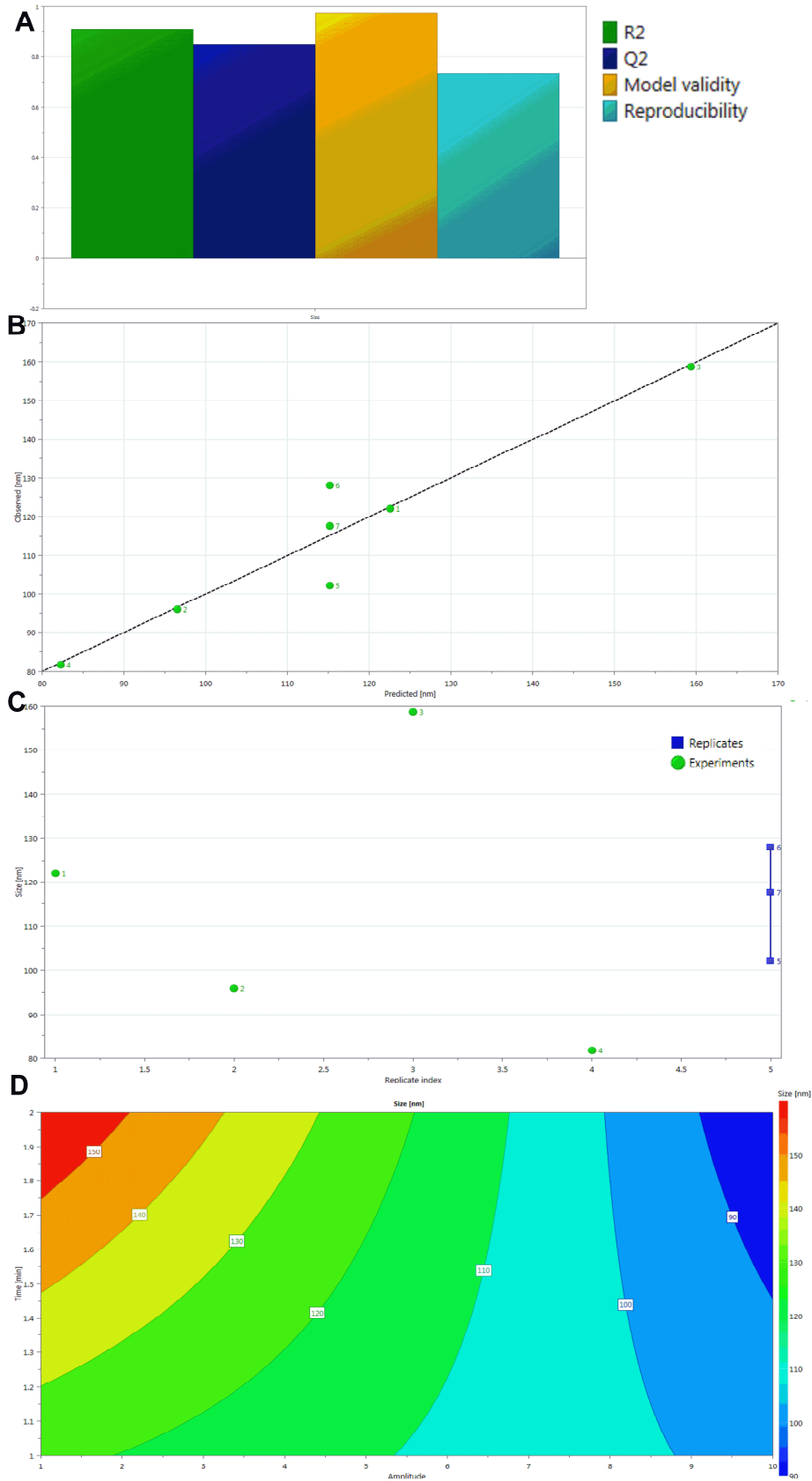


Figure 3.11: Design of Experiments predicting the liposome size in the sonication process dependent on the factors sonication time (1-2 minutes) and amplitude (1-10). Model type was a screening design (full factorial) with 3 centre points. Depicted is A) Summary plot ($R^2=0.91$, $Q^2=0.85$, Validity=0.97, Reproducibility=0.73), B) Observed vs. predicted, C) Replicates plot and D) Contour Plot.

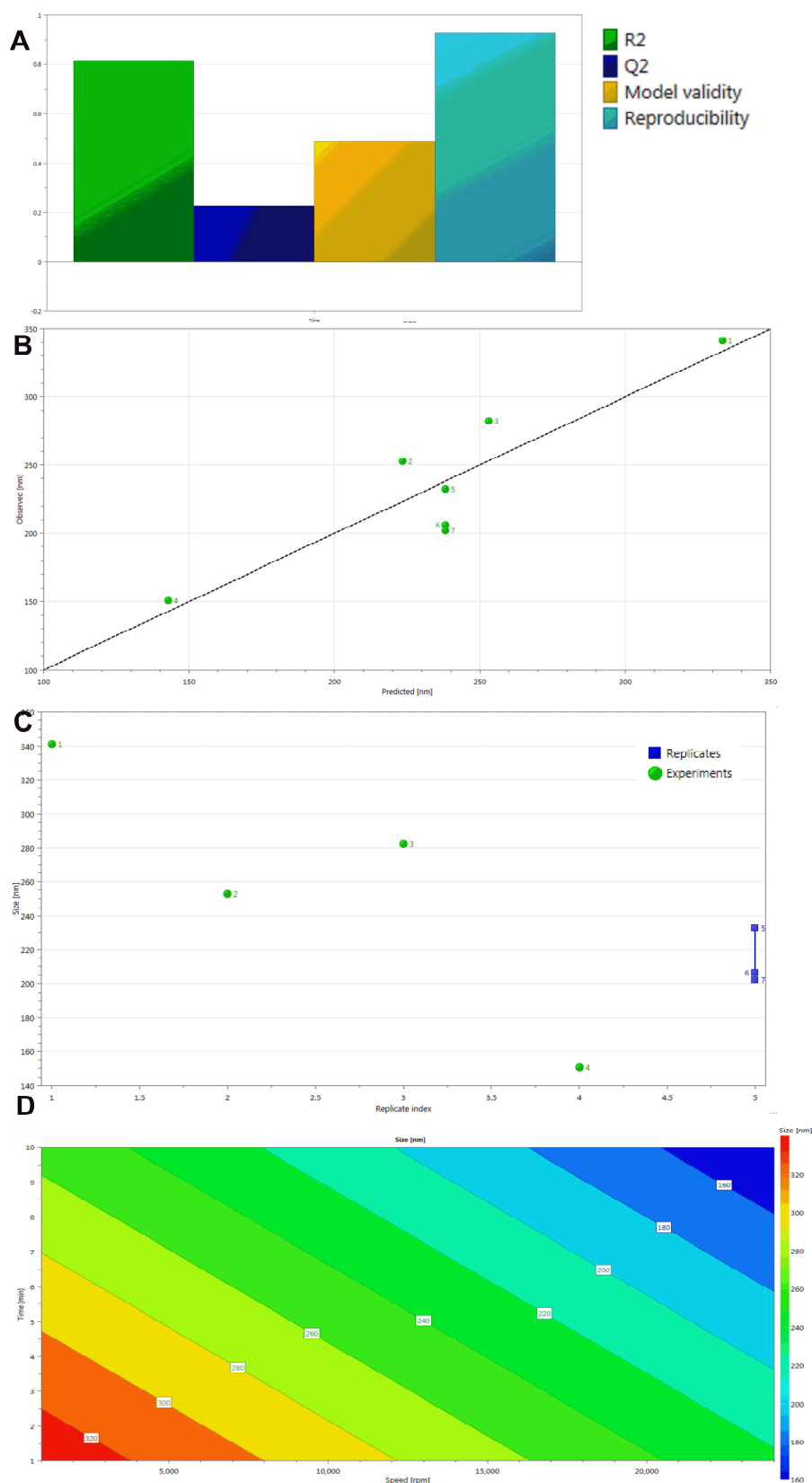


Figure 3.12: Design of Experiments predicting the liposome size in the HSM process dependent on the factors mixing time (1-10 minutes), rotational speed (1 000-25 000 rpm). Model type was a screening design (full factorial) with 3 centre points. Depicted is A) Summary plot ($R^2=0.81$, $Q^2=0.25$, Validity=0.5, Reproducibility=0.93, B) Observed vs. predicted, C) Replicates plot and D) Contour Plot.

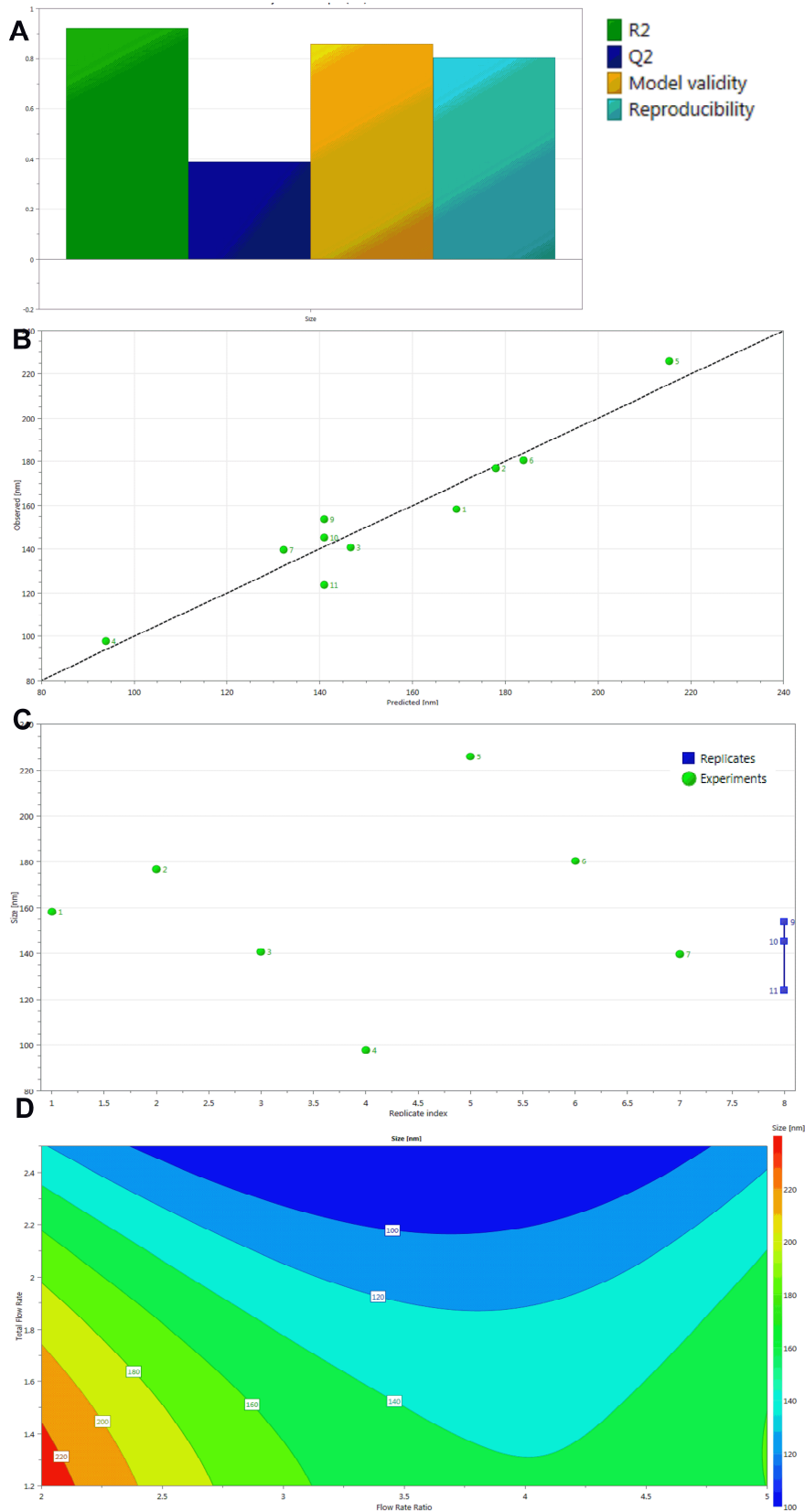


Figure 3.13: Design of Experiments predicting the liposome size in the microfluidics process dependent on the factors flow rate ratio (1:2 to 1:5) and total flow rate (1.2 to 2.5 mL/min). Model type was a response surface model (full factorial, CCC) with 3 centre points. Depicted is A) Summary plot ($R^2=0.92$, $Q^2=0.39$, Validity=0.85, Reproducibility=0.80, B) Observed vs. predicted, C) Replicates plot and D) Contour Plot.

Furthermore to model interpretation (Eriksson, 2008), the ANOVA analysis was linked to the replicate experiments; the centre points and all three models (sonication, HSM, microfluidics) were determined as statistical significant in the regression model ($p < 0.05$) and the LOF test ($p > 0.05$), Table 3.5.

Table 3.5: ANOVA for the response size in the sonication, HSM and microfluidics method. The p-statistics were analysed as well as the Lack-of-fit (LOF), together with fit power (R^2) and predictive power (Q^2).

ANOVA	Sonication	HSM	Microfluidics
Regression p	0.045	0.034	0.024
LOF p	0.906	0.130	0.568
R^2	0.910	0.81	0.923
Q^2	0.848	0.25	0.388
Model Significant?	Yes	Yes	Yes

Other than evaluating the model significance, the actual regression model was determined. Here, the response surface model (microfluidics method) was represented by a quadratic model, relating the responses (y) and factors (x), Equation 3.5.

$$y_1 = \beta_0 + \beta_1 x_1 + \beta_2 x_2 + \beta_{11} x_1^2 + \beta_{22} x_2^2 + \beta_{12} x_1 x_2 + \varepsilon \quad \text{Equation 3.5}$$

The screening models (sonication, HSM) were represented by an interaction model, Equation 3.6.

$$y_{1 \text{ and } 2} = \beta_0 + \beta_1 x_1 + \beta_2 x_2 + \beta_{12} x_1 x_2 + \varepsilon \quad \text{Equation 3.6}$$

Here, y_1 represented the response liposome size in the microfluidics method. x_1 represented the factor FRR and x_2 the TFR. y_2 represented the response liposome size in the sonication method. x_1 represented the factor sonication amplitude and x_2 the sonication time. y_3 represented the response liposome size in the HSM method. x_1 represented the factor mixing speed and x_2 the mixing time. In all models, β_0 was the constant term (representing the intercept), β 's were the effect coefficients, which were determined throughout the model evaluation (Eriksson, 2008). ε was the residual response variation, which could not be explained by the model. Insignificant model terms were removed during model evaluation and the remaining significant coefficients generated the regression models for each response (Table 3.6).

Equation 3.5 represents a quadratic model, as not only the model terms are evaluated (x_1 and x_2), but also their quadratic (x_1^2 and x_2^2) and combinatorial effect ($x_1 * x_2$) is evaluated. The interaction model (Equation 3.6) is a simplified version, only

investigating the model terms (x_1 and x_2) and their combinatorial effect ($x_1 * x_2$). Linking this to the investigated liposome manufacturing methods, the quadratic effect (x_1^2) of the factor FRR had the biggest impact on the resulting liposome size (Table 3.6). For the sonication method the factor amplitude (x_1) showed a bigger impact to the resulting liposome size than the factor sonication time (x_2) and the respective combinatorial effect ($x_1 * x_2$). Similar, for the HSM process, the factor speed (x_1) showed the biggest impact, with no combinatorial or synergistic effects detected throughout the model evaluation (Table 3.6).

Table 3.6: Determined significant coefficients and respective regression model in each method, predicting the liposome size. Amp = amplitude

Method	Significant Coefficients	Regression model
Microfluidics	TFR, FRR*FRR, TFR*TFR, FRR*TFR	$y_1 = 140.968 - 26.724x_2 + 29.34x_1^2 - 23.29x_2^2 - 15.34 x_1 x_2 + \varepsilon$
Sonication	amp, time, amp*time	$y_2 = 115.179 - 25.787x_1 + 5.637 x_2 - 12.767x_1 x_2 + \varepsilon$
HSM	speed, time	$y_3 = 238.207 - 55.025x_1 - 40.275x_2 + \varepsilon$

In addition to the model evaluations and predictions made by the respective response surfaces, each model was validated in an additional experimental setup. For each method, various points were selected from the model prediction, which were compared to the experimentally obtained values. In all methods, three points were chosen and experimentally obtained vesicles sizes directly compared to the ones predicted with the respective DoE model. The validation revealed that all three models predicted well the actual vesicle size obtained, with the error in the experimentally obtained values generally exceeding the ones obtained from the model, with increasing error with increasing vesicle size (Figure 3.14A, B, C). In the microfluidics as well as the HSM method, predicted vesicles sizes were generally underestimated as the experimentally obtained sizes exceeded the predicted ones by 15-30 nm (Figure 3.14A, C).

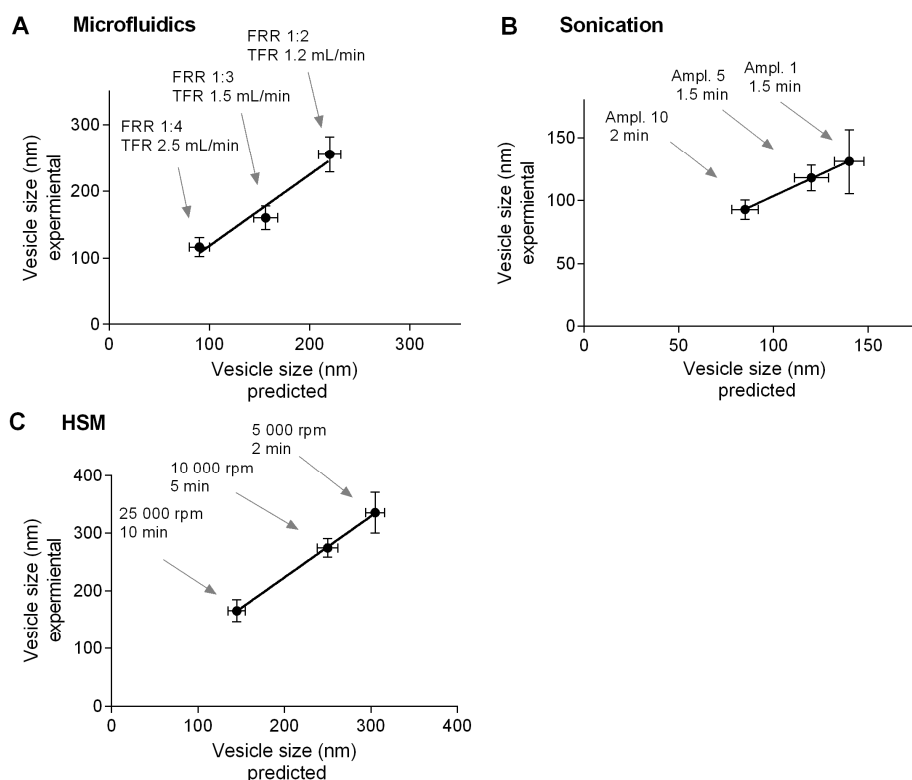


Figure 3.14: Validation of the DoE models generated by direct comparison of experimentally obtained vesicle sizes against predicted vesicle sizes at different set points.

For the well-established sonication method, vesicle sizes predicted ranged from 90 nm to 150 nm for the here used high transition temperature lipids (DDA-TDB), coinciding with averages sizes reported in literature using probe sonication (Kaur et al., 2012a; Milicic et al., 2012; Wagner and Vorauer-Uhl, 2010). Overall, the method was found to be quick with reproducible vesicle sizes obtained. However, the removal of metal contaminants by centrifugation post manufacturing requires additional time. The model evaluated sonication amplitude as the most important factor to be optimised once sonication has been chosen as the method of manufacturing. Therefore, for achieving small vesicles, it is more beneficial to choose a high amplitude but short duration process, which could be considered beneficial for the vesicles themselves being exposed to the sonication power only for a minimized period of time. The model predicted vesicle sizes in the HSM method ranging from 160 nm to 320 nm depending on the HSM time and rotational speed, overall coinciding with literature reporting on HSM methods (Bally et al., 1991). Here, the rotational speed was found as the most important variable in the process, highlighting on the need to carefully evaluate the speed in the process rather than extending the time in the mixing process to achieve smaller vesicles, similar to the sonication time a short exposure to the mechanical stresses would benefit the vesicles rather than choosing an extended process an intermediate or low power input and prolonged exposure time.

In the microfluidics method both factors, the TFR and the FRR had a significant impact, suggesting that both terms impacted on the resulting liposome size, with the ratio between solvent and aqueous stream having a significant impact, emphasized by the quadratic term $FRR \cdot FRR$. The microfluidics method was shown to manufacture small vesicles down to 90 nm in size. Previous work on a SHM method for lipid nanoparticle manufacturing reported sizes down to 20 - 40 nm as well as emulsions within the range of 20 - 50 nm (Belliveau et al., 2012; Zhigaltsev et al., 2012). This highlights the importance of the solvent to aqueous flow rate for producing vesicles of a defined size, and highlighted on the methods being less disruptive than a sonication method with higher reproducibility than the ethanol dilution method (Batzri and Korn, 1973). Noise in the microfluidics method, as detected in the DoE, could be explained by the process settings. In each formulation, the first sample stream was collected in the waste, whether only the core of the sample should be collected to achieve the most accurate and reproducible sizes, according to the manufacturer. Noise in the data set here could be explained by this waste volume initially not being optimised for the formulation. In all following conducted studies, the waste volume was optimised for each formulation, allowing for collecting the most reproducible sample core, but reducing the overall yield.

Deviation from model predictions and underestimated predicted vesicle sizes may be associated with the flexibility of the vesicles and sensitivity to manufacturing temperatures. Furthermore, all model predictions strongly depend on the accuracy of the method for analysing the particle characteristics, which here was DLS. The HSM as well as the microfluidics method were found with a higher level of noise in the data set, represented by the lower Q^2 values obtained (Figure 3.12A, 3.13A). Nevertheless, model evaluation (Table 3.6) and validation (Figure 3.14) confirmed the accuracy of each model predictions made, where presumably variation in noise levels was related to the choice of lipids. Here, the high transition temperature lipid DDA, with a transition temperature of $T_m \approx 47^\circ\text{C}$ (Christensen et al., 2010) was used. In the microfluidics method, a heating block was used to maintain this temperature during the vesicle manufacturing process. Nevertheless, given the solubility of the lipids being lower in isopropanol might have resulted in solubility difficulties, overall adding a larger variation and ultimately resulting in a lower predictive power in the respective model. The temperature during the HSM process was maintained by a water bath, where heat transfer might have been impeded overall leading to the larger noise level in the HSM model. In contrast, the probe sonication has been in direct contact with the vesicle

suspension, where the sonication process itself generated heat overall aiding the solubility of lipids and the formation of SUV. Above results confirmed the statistical validity of the models and allowed to generate regression models and response surface plots.

The noise in the models predicting liposome size could furthermore be linked to the molecular basis; bilayer fluidity dependency on temperature fluctuations, nucleation effect, pH changes, aggregation (Ellens et al., 1984; Sunamoto et al., 1980; Yoshioka, 1991), all known parameters to influence liposome size and leading to a higher noise level than in a completely described and fixed process (Eriksson, 2008). Based on this, a certain level of noise can always be expected in a liposome-based DoE study (Ducat et al., 2010; Stensrud et al., 2000).

3.3.2.2 Lipid quantification for process recovery

In addition to evaluating the vesicle sizes, the recovery of the lipids in each method was assessed using established HPLC protocols (Section 3.3.1). Here, the DDA and TDB lipids were quantified in the DoE optimised lipid film hydration process, HSM, sonication and microfluidics method. The quantification of the lipids throughout the microfluidics process highlighted the initial dilution of the liposome formulation in the aqueous phase, based on the high aqueous flow introduced into the process. Vesicle concentration was performed in a spin column process step, which countered the initial dilution, $p > 0.05$ (Figure 3.15), with an overall recovery of 82% achieved. The lipid quantification revealed a lipid recovery of 80% in the sonication method, remaining statistically insignificant on comparison to the lipid amount available prior vesicle manufacturing. The high shear mixing method showed a final recovery of 84%, $p > 0.05$, (Figure 3.15).

The dialysis protocol was based on a buffer exchange every hour for a total processing time of 4 h, with a solvent residue of $< 1\%$ (v/v) remaining as quantified by gas chromatography (results not shown). The developed purification process based on a spin column technique resulted in successful removal of solvent within less than one hour.

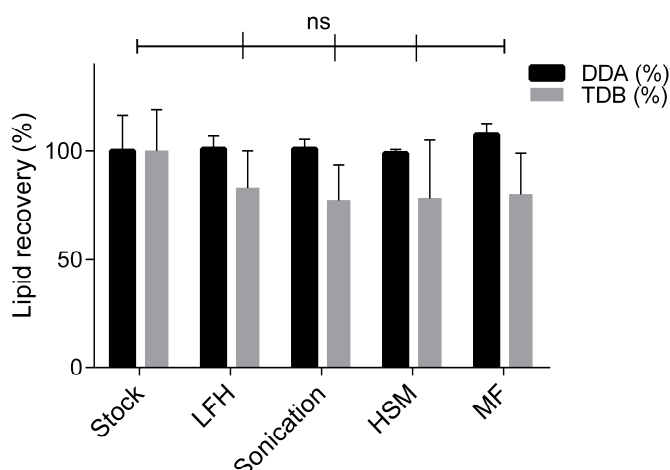


Figure 3.15: Recovery of DDA (%) and TDB (%) within the lipid film hydration (LFH), sonication, HSM and microfluidics (MF) process. Lipids were quantified using HPLC and expressed as % relative to the initial amount of lipids dissolved in the stock solution.

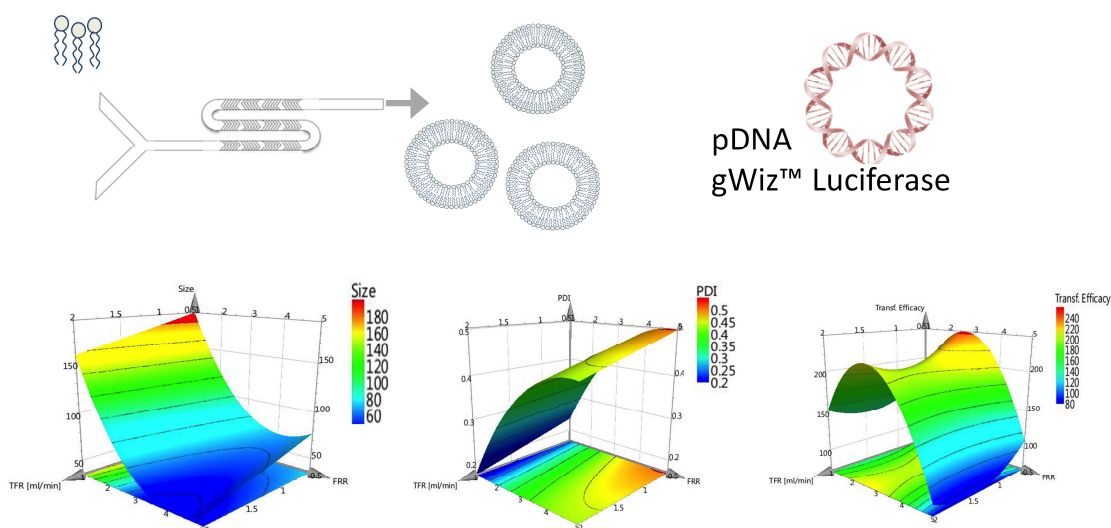
3.4 Conclusion

Within this chapter the methods to prepare liposomes and to characterise them were evaluated. Size characterisation protocols were established as were lipid recovery protocols. DoE models were used to give an initial overview of the size ranges obtainable in each method (sonication, HSM and microfluidics) whilst evaluating advantages and disadvantages of each method. DoE models were validated, which confirmed the accuracy and validity of predictions made overall allowing for a good comparison within the different methods. These models were verified by comparing predicted values to experimentally obtained results. The HSM process was shown to be a relatively quick method for the production of liposomes; however, noise in the data set has to be minimized by concise process control. Smaller vesicles are produced using the sonication method, but this method is compromised by potential lipid degradation or contamination. In the microfluidics method, the optimisation of the waste to sample ratio was found important for reducing noise. Also, the time associated with dialysis to remove residual solvent was found as the main disadvantage in the microfluidics method.

The aim of this work was to identify the most effective way of manufacturing small vesicles, and the DoE approach aided the process robustness and validation for the methods investigated. Based on the validity of all models generated and the advantages of each method being highlighted, the microfluidics method was chosen to be taken further into subsequent studies.

Chapter 4

Manufacturing of cationic liposomes by microfluidics for *in-vitro* transfection and assessment of statistical tools for process development



Papers relating to this chapter:

Kastner E., Kaur R., Lowry D., Moghaddam B., Wilkinson A. and Perrie Y. (2014). High-throughput manufacturing of size-tuned liposomes by a new microfluidics method using enhanced statistical tools for characterization. *International Journal of Pharmaceutics*, 477(1), 361-368.

4.1 Introduction

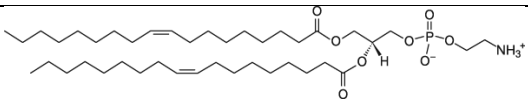
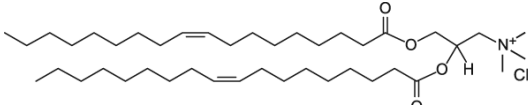
The efficient delivery of genetic material to a target site remains challenging. Factors like the size, charge and *in-vivo* degradation by nucleases impede the intracellular delivery of 'naked' DNA (Al-Dosari and Gao, 2009) and hence vehicles for delivering genetic material to a target site are used. Viral vectors promote high transfection efficiencies but are limited by their associated toxicity and immunogenic reactions, which leads to the preferred application of non-viral delivery systems, amongst which liposomes are well explored as non-viral delivery vehicles for genetic material (Bedi et al., 2011; Gjetting et al., 2011; Gregoriadis et al., 2002; Perrie et al., 2003). Along with enhanced safety profiles, liposomes can be manufactured easily, cost effectively and in a variety of sizes, thus overall fulfilling many requirements of an ideal delivery vector (Lui and Huang, 2003). As anionic charges dominate on cell surfaces due to presence of negatively charged membrane lipids like phosphatidylserine (PS) and sphingomyelin (Ohvo-Rekilä et al., 2002), cationic liposomes have been extensively investigated and reported as efficient transfection agents, based on their electrostatic interaction with cell surfaces. The term 'lipoplex' relates to the fusion product of cationic liposomes with negatively charged DNA, which is based on electrostatic interaction and achieves high *in-vitro* transfection rates with low cellular toxicity (McNeil et al., 2010). As such, several constraining factors have been investigated for the *in-vitro* transfection by lipoplexes, including the structure of the lipids, net positive charge, structure of the complexes formed, lipid/DNA charge ratio, type of lipid, electrolytes used and size of the liposomes themselves (Congiu et al., 2004; Moghaddam et al., 2011).

Current methods of liposome manufacturing for lipoplex production comprise top-down methods such as sonication or extrusion (Congiu et al., 2004; Moghaddam et al., 2011), where the control of the resulting liposome size requires time-intensive optimisation. This present chapter investigated microfluidics-directed nanoprecipitation as a new method for manufacturing cationic liposomes, with reported high *in-vitro* transfection efficiency and ideal immune response (Ciani et al., 2007; Liu and Huang, 2002; McNeil et al., 2010) and the systems produced via this new production method were compared to previous studies.

Here, the on-chip chaotic advection mixer was evaluated and the effect of flow rate and flow ratio on liposome physicochemical properties and transfection efficiencies *in-vitro* was investigated. Furthermore two statistical-based tools, design of experiments (DoE) and multivariate analysis (MVA) were implemented in order to aid process understanding. These optimisation tools were used to build knowledge around the

microfluidics-controlled manufacturing of lipoplexes, which ultimately supported the development, confidence, understanding, and robustness of the process.

Table 4.1: The chemical structure and key characteristics of lipids used to formulate liposomes in this study.

	Charge	Lipid structure*	Molecular Weight	Transition Temperature
DOPE	Neutral		744.03	-16°C
DOTAP	Cationic		698.54	-12 °C

Structure obtained from avantilipids.com.

4.2 Aim and Objectives

The aim of this chapter was to investigate the use of microfluidics to prepare cationic liposomal systems that are used as transfection agents. To achieve this, cationic liposomes were prepared using two commonly adopted lipids: 1,2-dioleoyl-*sn*-glycero-3-phosphoethanolamine (DOPE) and 1,2-dioleoyl-3-trimethylammonium-propane (DOTAP) (Table 4.1). To consider the parameters controlling their manufacture using microfluidics the total flow rate through the system and flow rate ratio between the solvent and aqueous phase were studied and their effect on particle characteristics and *in-vitro* transfection rate were investigated. To study and develop the manufacturing process, design of experiments and multivariate analysis were adopted to support the development of statistical regression models for the prediction and correlation of particle characteristics and transfection efficiency.

4.3 Results and Discussion

4.3.1 In-process control of vesicle size using microfluidics-directed nanoprecipitation

Liposomes, consisting of DOTAP and neutral fusogenic helper lipid DOPE were formulated using the microfluidics nanoprecipitation method with a SHM design. Initially, the two factors total flow rate (TFR) and flow rate ratio (FRR) were related to the resulting particle characteristics by varying the TFR from 0.5 mL/min to 2 mL/min and varying the FRR of the solvent/aqueous phases from 1:1 to 1:5. The effect of both parameters were explored in a one factor at a time (OFAT) method, varying only one factor while keeping the other one fixed.

The solvent to aqueous ratio substantially affected the size of the resulting liposomes (Figure 4.1); a decrease in vesicle size from 200 nm to 80 nm was linked to an increase in aqueous FRR from 1:1 to 1:5 (Figure 4.1A). The smallest liposome size was detected at a FRR of 1:3 and 1:5 with around 50 - 75 nm whereas the 1:1 solvent/aqueous formulation resulted in significant larger vesicle sizes of 175 – 200 nm (Figure 4.1A). The change in TFR did not significantly affect the resulting liposome size when increased from 0.5 mL/min to 2 mL/min at constant FRR of 1:1, 1:3 or 1:5 (Figure 4.1A). The PDI, a measure of the heterogeneity of the formulation, ranged between 0.2 and 0.5, with a notable link to the FRR (Figure 4.1B); the lowest PDI of 0.2 was observed for a FRR of 1:1, increasing to a maximum value of 0.5 for a FRR of 1:5. In contrast, the zeta potential of the liposomes formed by micromixing was independent of flow rates and ratios suggesting that surface characteristics of the liposomes were not altered by these factors (Figure 4.1C). This would be expected for these cationic formulations, a strong cationic zeta potential of around 45 - 60 mV was measured (Figure 4.1C), linked to the cationic polar head group of the lipid DOTAP and in agreement with previous work on DOPE-DOTAP vesicles prepared by the lipid-hydration method followed by sonication (McNeil et al., 2010).

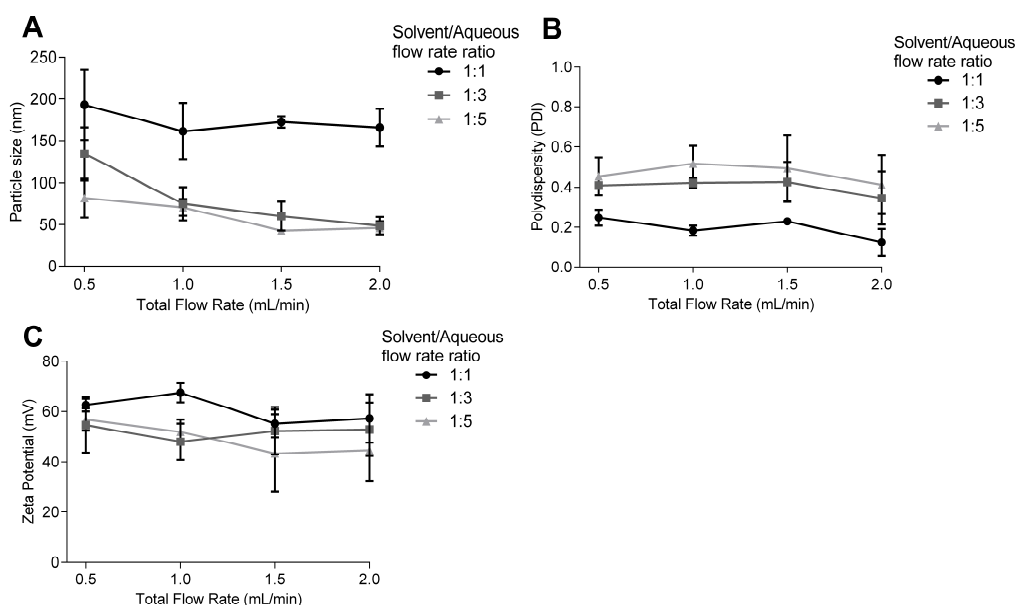


Figure 4.1: Liposome characteristics. A) Vesicle size, B) polydispersity and C) zeta potential of DOPE-DOTAP formulations manufactured by microfluidic mixing. Results denote the mean of triplicate formulations \pm SD.

The factor FRR is directly linked to the polarity increase throughout the chamber, which is the driving mechanism behind the precipitation reaction (Dong et al., 2012). At high aqueous buffer ratios, the mixing rate of the lipid phase with the buffer is enhanced. At higher aqueous FRR the fluid velocities between both streams differ dramatically,

which decreases the effective diffusion layer thickness of the solvent stream in the mixing profile. Additionally, enhancing the ratio of alcohol to buffer reduces the width of the solvent stream in the mixing profile, further diminishing the diffusion distances (Zook and Vreeland, 2010). Mixing in a chaotic micromixer is primarily dominated by enhancing the diffusion due to alterations of the fluid flow profile as here achieved by the herringbones in the floor of the mixing chamber (Stroock et al., 2002). The enhanced mixing process at FRR with high aqueous content, decreases the solvent concentration drastically, leading to the formation of lipid bilayers (Zook and Vreeland, 2010). With less solvent available for solubilisation of the hydrophobic chains, the closure time for the vesicle decreases with smaller vesicles expected at higher FRR (Zook and Vreeland, 2010). As seen in Figure 4.1A, the smallest vesicles correspond to higher aqueous volumes introduced into the precipitation process. At lower aqueous content FRR (here 1:1), more solvent remains present during the mixing process, allowing for prolonged stabilisation of the hydrophobic components. The slower depletion rate leaves more time for the bilayers to grow before vesicles are formed, leading to overall larger vesicles, as seen here for a FRR of 1:1 (Figure 4.1A). Furthermore, higher aqueous content FRR reduce the final solvent concentration, thus decreasing the synthesis of larger particles due to particle fusion and lipid exchange (Ostwald ripening) after complete mixing is achieved. Nanoprecipitation of lipids based on microfluidics has been reported based on hydrodynamic flow focusing, where a stream of solvent is hydrodynamically focused between two aqueous streams. Similar to the chaotic advection micromixer investigated within these studies, the flow focusing technique reported a decrease in liposome size with the increase in aqueous ratio present in the mixing process (Jahn et al., 2010; Zook and Vreeland, 2010). The larger-scale precipitation method based on an adapted ethanol-injection method reported the significance of the buffer flow rate, where a lower buffer flow rate was linked to a broader size distribution and polydispersity (Wagner et al., 2002b). The increase in PDI by increasing the FRR (to 1:5), as seen in Figure 4.1C, may be a result of partially incomplete mixing due to the higher aqueous volume inputted into the chamber, which may be countered by extending the channel length. However, polydispersity remained independent of the flow rate applied at constant FRR. The effect of flow velocity to the polydispersity was also studied by Balbino et al.; similar to the results reported in Figure 4.1, these studies showed that flow velocity remained independent of the polydispersity of the formation, which ranged from 0.2 to 0.3 for cationic using egg PC, DOPE and DOTAP in a 50/25/25 % molar ratio (Balbino et al., 2013a; Balbino et al., 2013b). These differences in PDI may be subject to the formulations used; for example

it has been reported that the inclusion of PEGylated lipids can reduce PDI (Fang et al., 2012).

This preliminary screening work reported in Figure 4.1 emphasized that particle size is strongly dependent on the ratio of aqueous to solvent rate, thereby offering an ability to control the resulting particle characteristics in the microfluidics method. This suggests that vesicle size can be in-process controlled. Furthermore, the flow rate was shown as an independent variable for cationic DOPE-DOTAP liposomes, indicating on the potential of the method to generate a higher production throughput, one of the main advantages of using microfluidics controlled liposome manufacture.

In contrast to multi-step “top down” methods like lipid film hydration, sonication, mixing or extrusion, the microfluidics-directed nanoprecipitation method is a relatively new and quick “bottom-up” method of vesicle manufacturing (Hood et al., 2014b). The nanoprecipitation method based on microfluidics has been reported by hydrodynamic flow focusing (Hood et al., 2014b; Jahn et al., 2010; Jahn et al., 2007; Jahn et al., 2004), which was based on the same principle of mixing of aqueous and solvent phase. However, flow focusing methods reported significant lower total flow rates, ranging from 0.08 to 0.4 mL/min, extrapolated from reported fluid velocities of 100 to 500 mm/s (Balbino et al., 2013b). Jahn and co-workers presented the hydrodynamic flow focusing method for controlled vesicle assembly, using flow rates between 1 to 90 μ L/min (Jahn et al., 2007), magnitudes lower than the reported flow rates in the here presented SHM method. Opposed to flow focusing methods, the here evaluated SHM mixer allowed for significant higher TFRs, ranging up to 2.5 mL/min, increasing throughput up to 30 times. Furthermore, the ratios between solvent to aqueous flow in the hydrodynamic flow focusing method ranged from 5 (Balbino et al., 2013b) up to 30 (Jahn et al., 2007), leading to a significant lower particle concentration post manufacturing. This high aqueous ratio has two major impacts; first, solvent residues are reduced, which might benefit storage and use of proteins/peptides. Second, the effective concentration of the particles is significantly reduced, necessitating an additional concentration step, which will increase the total process time. In this here-presented SHM method, higher solvent concentrations remained after the formulation, which ranged between 15 to 25% dependent on the FRR chosen (1:5 to 1:3) and were removed by dialysis; however, this increased the processing time. Both the flow focusing and SHM methods were previously shown to allow for the control of the nanoparticle size, where the SHM method was reported for lipid nanoparticles with an

electrodense core for siRNA delivery only (Belliveau et al., 2012; Leung et al., 2012; Zhigaltsev et al., 2012).

4.3.2 Evaluating the microfluidics-based manufacturing for process recovery - Lipid quantification by ELSD

Further to the above assessment on the effect of TFR and FRR on particle characteristics, their effect on the recovery of the lipids was also assessed. Therefore, the lipids DOPE and DOTAP were quantified in the core of each sample. Similar to Section 4.3.1, the factor TFR and FRR were investigated separately in an OFAT method. Lipid recovery was expressed as the average of DOPE and DOTAP recovery and related to the initial amount of lipids present in the ethanol stock (and considering the dilution factor based on the FRR). The recovery of the lipids was above 87% for all preparation factors considered; this was not significantly different from initial amounts in the ethanol stocks and was independent of the TFR and FRR chosen and (Figure 4.2A). Furthermore the DOPE-DOTAP ratio was maintained in all preparations (Figure 4.2B). These results suggested that the syringe driven system accurately introduced the solvent volumes into the chip even at higher ratios (1:5). Given that the increase in FRR increased the polydispersity in the formulation (section 4.3.1), FRR higher than 1:5 were not considered.

Whilst no significant loss of lipids was noted here, lipid loss due to adsorption onto the chip material was important to consider. Polydimethylsiloxane (PDMS) is a transparent, elastomeric polymer, with wide application in microfluidics. Chip manufacturing with PDMS is relatively cost-effective and the moulding process easy. Nevertheless, it is known for its adsorption properties of biologic materials, including proteins, mainly due to its porosity and hydrophobicity (Monahan et al., 2002; Toepke and Beebe, 2006). Studies have shown that a PDMS matrix adsorbed hydrophobic compounds up to four-times higher compared to glass or polystyrene (Li et al., 2009). At the time point of this study, the PDMS chips and mixer platform were part of a beta-test version. The available technology underwent a material change throughout its commercialisation process, with chip material changed to cyclic olefin copolymer (CoC), a thermos-plastic polymer, with better material properties and manufacturing processes compared to PDMS (Jeon et al., 2011). The quantification of lipids was based on the developed ELSD technique (Chapter 3), a quick and effective method, circumventing time-intensive mass spectrometry or assays. Maintaining the lipid content and the lipid ratio is important in the overall process yield and the process economy.

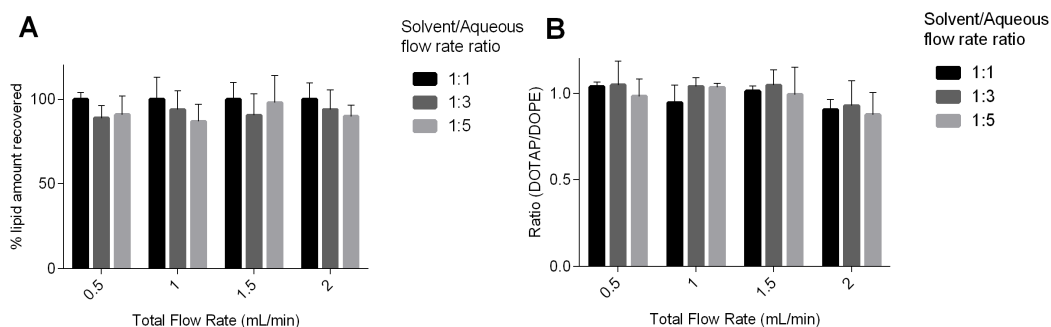


Figure 4.2: Quantification of total lipid content (DOPE + DOTAP) by HPLC, shown as A) recovery (%) and B) ratio of both lipids, DOTAP/DOPE. Results are the mean of triplicate formulations \pm SD.

4.3.3 *In-vitro* transfection efficiency and the effect of vesicle size

Given that above studies indicated the effect to the resulting vesicle characteristics, the ability of those vesicles to act as a transfection agent was explored *in-vitro* with a plasmid containing the luciferase gene (gWiz™ Luciferase). Lipofectin™ has been reported in various cell lines for *in-vitro* transfection and acted as a transfection control (Fortunati et al., 1996; Malone et al., 1989). Each formulation varied in TFR and FRR as described previously, and respective transfection efficiency was assessed as the percentage of luciferase activity to the control (Lipofectin™) and reported as luciferase activity (%). The highest transfection was determined for a solvent:aqueous ratio of 1:3, increasing the transfection outcome to 250% compared to the commercial Lipofectin™ (Figure 4.3A). Formulations made at a FRR of 1:1 gave a 150-200% increase in transfection whereas the formulations at a FRR of 1:5 gave the lowest transfection, matching the transfection rates of the commercial Lipofectin™ product (Figure 4.3A). Despite the differences in transfection outcome due to changes in FRR, changes in TFR were independent of the transfection activity, which, similar to above, demonstrates the microfluidics-method as a highly applicable method for high-throughput production of liposomes (Figure 4.3A). Furthermore, the potential toxicity of these formulations verified that transfection efficacy was independent of cell viability. For all experiments and formulations made, the cell viabilities ranged between 60-85% with no significant ($p > 0.05$) difference between the formulations (Figure 4.3B). Flow rates and ratios were also independent variables of the cell viability (Figure 4.3B).

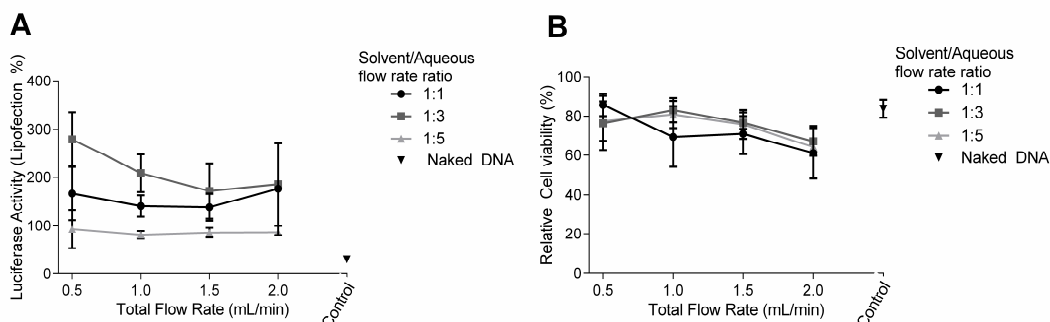


Figure 4.3: A) Comparison of transfection efficiency of cationic nanoparticles. Liposomes were complexed with gWiz plasmid DNA expressing firefly luciferase. B) Relative cell viability of nanoparticles formulated. Results are the mean of triplicate formulations \pm SD.

Published transfection efficiencies from our laboratories obtained with the cationic DOPE-DOTAP lipoplexes were approximately 250% in comparison to the Lipofectin™ (Moghaddam et al., 2011). These transfection efficiencies and cell viabilities (up to 90%) coincided with the results presented in Figure 4.3, confirming that the method of manufacturing was independent of the resulting biological performance. The *in-vitro* transfection efficacy of lipoplexes has been well explored; the size, charge and lipid/DNA ratio are all crucial factors for successful transfection (Aljaberi et al., 2007; Caracciolo et al., 2007). Here, the lipids/DNA ratio, as well as the cationic zeta potential was maintained throughout the formulation, which consequently links the resulting transfection efficacies to differences in vesicle sizes (Figure 4.1A). The vesicle size has previously been investigated (Esposito et al., 2006; Felgner et al., 1987; Kawaura et al., 1998; McNeil et al., 2010), with the lowest transfection rate correlating to a smaller vesicle size. Additionally, the ideal transfection reagent should be simple to manufacture in a reproducible setup (Lui and Huang, 2003).

4.3.4 Statistical impact of the factors flow rate and flow ratio in a design of experiments study

The results from Section 4.3.1 showed that vesicles manufactured by microfluidics were size controlled and acted as an efficient delivery system for genetic material. However, the variables TFR and FRR were investigated separately in an OFAT method, where only one factor was varied while the other one was fixed. Such OFAT methods often require a substantial amount of time/resource and may overlook local optima along with poor cover of the experimental space. Therefore, a design of experiments (DoE) approach investigated the effect of the factors TFR and FRR on liposome size, polydispersity and transfection efficiency (luciferase activity), with good coverage of the experimental space to determine optima that might have been

overlooked in the OFAT method. Thus the next step was to determine the statistical effect, along with exploring the significance and interaction between variables while generating a regression model. Based on the knowledge developed in the previous screening of the factors in the OFAT method, a response surface model (RSM) was chosen. This in-depth analysis investigated the factors TFR and FRR, as well as their interaction and quadratic terms $TFR \cdot TFR$, $FRR \cdot FRR$ and $TFR \cdot FRR$ in a quadratic regression model (Figure 4.4). In addition to 3 replicates acting as centre points (N11, N12, N13), a further replicate set was added to aid the reproducibility of the model (N1, N2). The experimental space was chosen to match the exact values of the FRR and TFR as investigated earlier, ranging from 1:1, 1:3 to 1:5 and FRR and 0.5, 1, 1.5 and 2 mL/min for TFR.

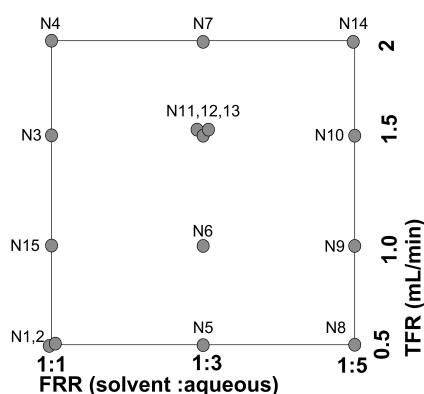


Figure 4.4: Design space in a two factorial design including 2 Factors (TFR and FRR) with a total 15 experimental points, triplicate centre point (N11, 12, 13) and replicate experimental point (N1, N2) were added.

Model evaluation commenced with assessment of the summary plot, which displayed R^2 , Q^2 , model validity and reproducibility and revealed a valid model for all three responses: liposome size, PDI and transfection efficiency (Figure 4.5). Acceptance criterion were pre-set at $R^2 \geq 0.5$, $Q^2 \geq R^2 - 0.3$, validity ≥ 0.25 and reproducibility ≥ 0.5 for a good model. Close situation of R^2 and Q^2 values indicated that the models were highly predictive, e.g. the Q^2 value of 0.97 in the size model revealed that 97% of the model is predictive, which represented an excellent model prediction with only 3% of the data not being predictive.

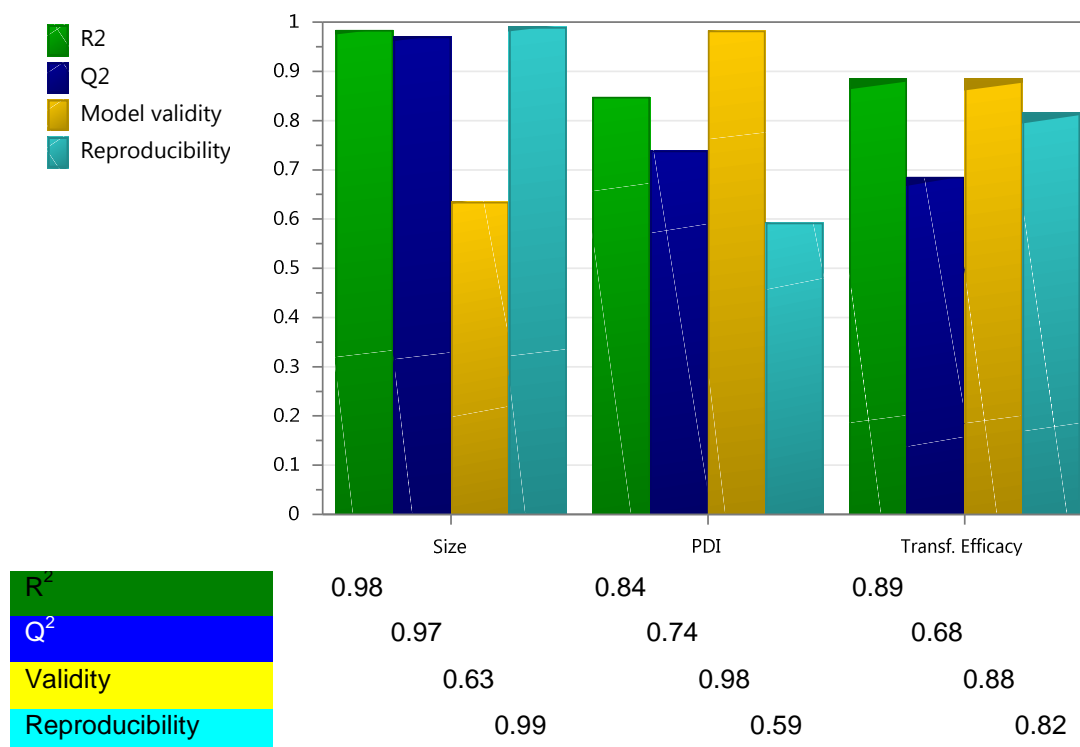
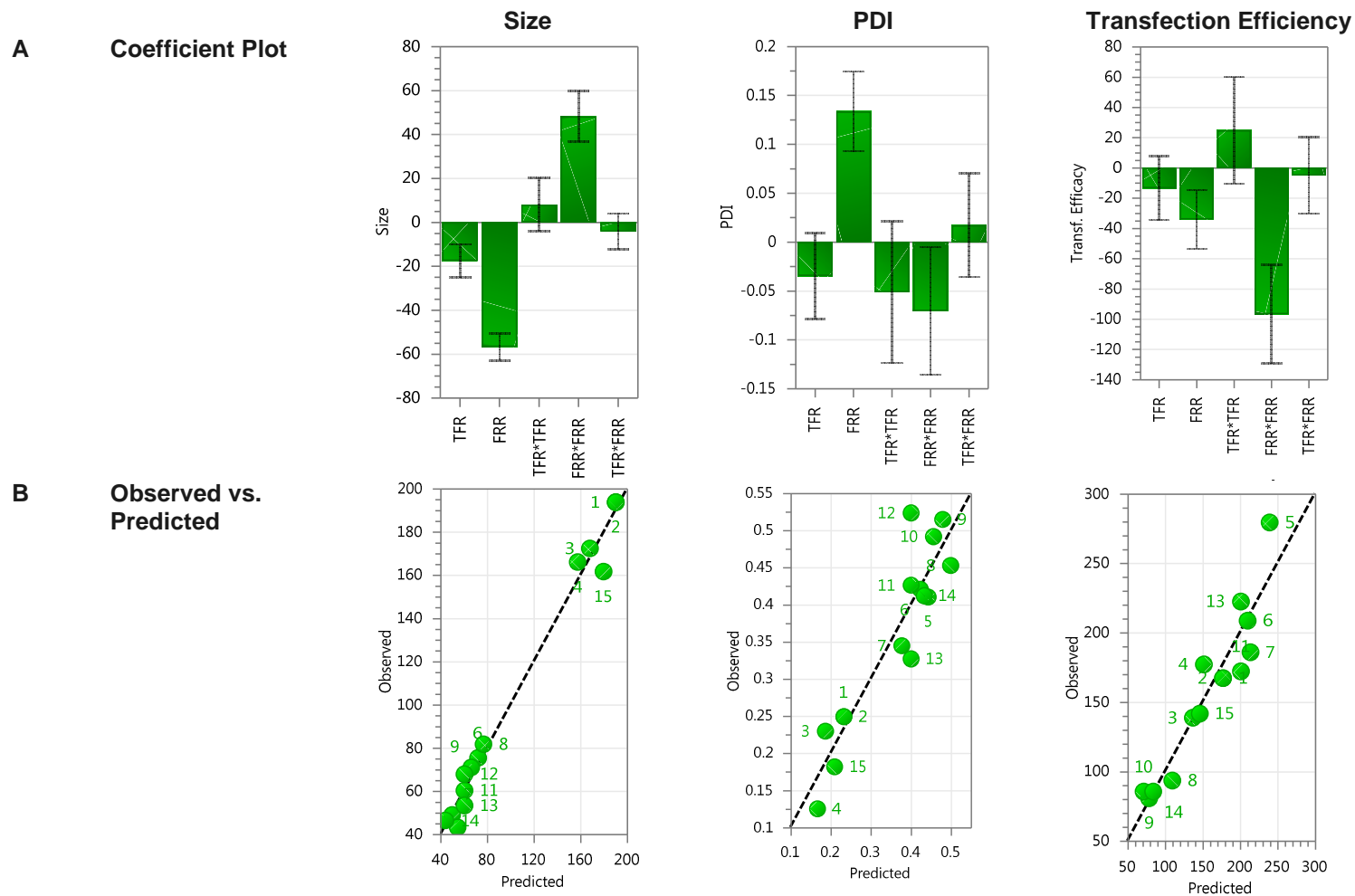


Figure 4.5: Summary plots to evaluate the model fit (R^2), prediction (Q^2), validity and reproducibility for the responses liposome size, polydispersity and transfection efficiency. For an excellent model, all values are approaching 1.

Given the excellent model fit and prediction along with valid and reproducible models, further diagnostic tools were performed for outlier detection. The model terms TFR*TFR and TFR*FRR in the size model were not significant, as confidence intervals crossed zero (Figure 4.6A). The most important factor with the highest range was the factor FRR in the size model (Figure 4.6A). Here, the terms FRR and FRR*FRR showed an inverse profile comparing the size and the PDI model, which gives an initial indication of an inverse correlation between size and PDI, e.g. the decrease in size may correlate to an increase in PDI. However, this initial model interpretation required further confirmed throughout the analysis. Statistical significance terms were determined for all responses, where a nonlinear relationship was predicted for all three responses, given the significant quadratic interaction term of the FRR, Table 4.2.

The observed vs. predicted plots (Figure 4.6B) indicated a good model for the responses size, PDI and transfection efficiency as the points for the observed vs. the fitted values sat close to the straight 45° line. Nevertheless, the removal of the outlier N5 along with excellent summary plot for size response was indicative of a good model. The normal probability plot (Figure 4.6C) displayed the residuals plotted on a normal probability scale, which showed the normality of the residuals. Here, N5 was

removed in the size model and N12 removed in the transfection model, both showed strong deviation in the normal probability plot, whereas the PDI model showed no outliers. Furthermore, no pattern or time dependency was given, with all data points randomly distributed in the residuals vs. run number plot (Figure 4.6D), which displayed the variation in the responses for the replicated experiments. A systematic effect was excluded in the model, as no pattern was seen in the replicate plots. Here, experiments 11, 12 and 13 were the replicate centre points; with a lower variation in the centre points for all three responses compared to the experimental runs. The PDI model had the largest variation, indicated by a lower reproducibility as seen in the summary plot (Figure 4.5), which had to be considered in further model evaluation. The additional replicates (N1, N2) implied a high reproducibility in the experimental setup for all responses. Overall, the size model showed smallest error in the replicates (Figure 4.6D), which was an indication of its excellent summary plot (Figure 4.5). The outlier detection in the normal probability plot removed one of the triplicate centre points in the transfection model, where the addition of the experimental replicates (N1, N2) gave further confidence in the replicate error in the model. The evaluation for model significance above was followed by the model interpretation. Here, the coefficient plot (or regression coefficient plot), displayed the model terms, main effect and interaction terms.

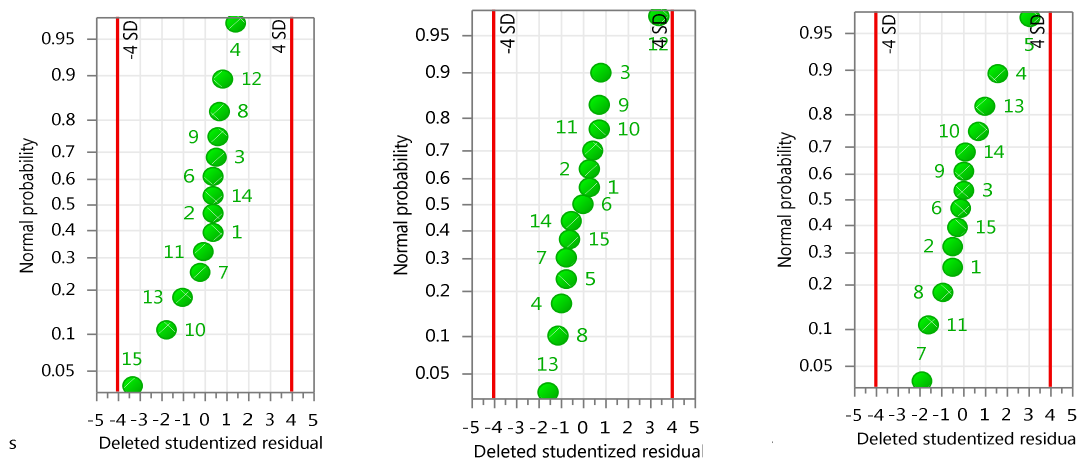


Displays regression coefficients with 95% confidence interval. Significant coefficients (different from noise) if confidence interval does not cross zero,

Displays the observed versus predicted values of the responses. A good model shows the points falling on a 45° line

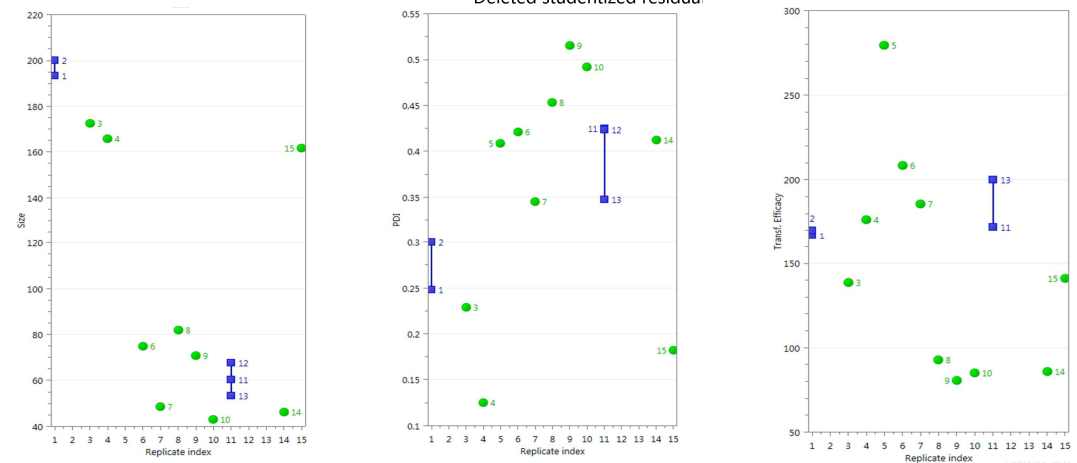
Figure 4.6: Results from the analysis of the DoE study for the prediction of the liposome size, PDI and transfection efficiency with A) Coefficient Plot B) Observed vs. Predicted C) Residuals vs. Normal Probability, D) Replicate plots.

C **Residuals** **Normal**
Probability



Displays the residuals on a double log scale. The plot is used to detect outliers and assess the normality of the residuals. In a good model, residuals are random and normally distributed, lying on a 45° line between -4 and +4.

D **Replicate plot**



Displays the response values against the experimental runs. The plot is used to assess the variation in the replicate experiments. Replicates are presented in blue, experimental points in green.

Figure 4.6: Results from the analysis of the DoE study for the prediction of the liposome size, PDI and transfection efficiency with A) Coefficient Plot B) Observed vs. Predicted C) Residuals vs. Normal Probability, D) Replicate plots.

Table 4.2: Coefficient list for the responses size, PDI and transfection efficiency. Coefficients were determined as statistically significant ($p < 0.05$).

Response	Significant coefficients
Size (nm)	TFR, FRR, FRR*FRR
PDI	FRR, FRR*FRR
Transfection Efficiency	FRR, FRR*FRR

Further to model interpretation (Eriksson, 2008), the ANOVA analysis was linked to the replicate experiments; the centre points (N11, 12, 13) and replicate experimental points (N1, 2). All three models (size, PDI and transfection efficacy) were determined as statistical significant in the regression model ($p < 0.05$) and the LOF test ($p > 0.05$) (Table 4.3).

Table 4.3: ANOVA for the responses size, PDI and transfection efficiency. The p-statistics were analysed as well as the Lack-of-fit (LOF), together with fit power (R^2) and predictive power (Q^2).

ANOVA	Size	PDI	Transfection Efficiency
Regression p	0.000	0.001	0.001
LOF p	0.255	0.973	0.585
R^2	0.989	0.845	0.889
Q^2	0.965	0.749	0.682
Model Significant?	Yes	Yes	Yes

Other than evaluating the model significance, the actual regression model was determined. Here, the RSM was represented by a quadratic relationship between responses (y) and factors (x), Equation 4.1.

$$y_{1,2 \text{ or } 3} = \beta_0 + \beta_1 x_1 + \beta_2 x_2 + \beta_{11} x_1^2 + \beta_{22} x_2^2 + \beta_{12} x_1 x_2 + \epsilon \quad \text{Equation 4.1}$$

The regression model with two factors (TFR, FRR) and three responses (size, PDI, transfection efficiency) was adapted with, y_1 represented the response liposome size, y_2 the response PDI and y_3 the response transfection efficiency. x_1 represented the factor TFR and x_2 the FRR, β_0 was the constant term (representing the intercept), β 's were the effect coefficients, which were determined throughout the model evaluation (Table 4.4). ϵ was the residual response variation, which could not be explained by the model.

Table 4.4: Coefficient list with coefficients (scales and centred), standard error, p-values and confidence intervals for three responses.

	Coeff. SC	Std Error	P	Conf. int (+/-)
Size				
Constant	66.5	3.99	1.27 e-008	8.89
TFR	-16.7	3.45	0.00069	7.69
FRR	-56.7	2.88	2.55 e-9	6.43
FRR*FRR	50.7	5.00	1.41 e-6	11.2
PDI				
Constant	0.411	0.022	1.44 e-9	0.049
FRR	0.134	0.018	1.73 e-5	0.040
FRR*FRR	-0.078	0.029	0.022	0.067
Trans. Eff.				
Constant	202.9	12.6	6.11e-8	28.5
FRR	-33.53	8.00	0.00233	18.1
FRR*FRR	-96.89	13.4	4.989 e-5	30.4

With insignificant model terms removed by help of the coefficient plot (Figure 4.6A), the remaining significant coefficients (Table 4.2) generated the regression models for each response.

$$y_1 = 66.5 - 16.7x_1 - 56.7x_2 + 50.7x_2^2 + \varepsilon$$

$$y_2 = 0.41 + 0.13x_2 - 0.07x_2^2 + \varepsilon$$

$$y_3 = 202.95 - 33.53x_2 - 96.9x_2^2 + \varepsilon$$

Equation 4.1 represents a quadratic model, as not only the model terms are evaluated (x_1 and x_2), but also their quadratic (x_1^2 and x_2^2) and combinatorial effect ($x_1 * x_2$) is evaluated. Linking this to the investigated microfluidics method, the factor FRR (x_1) had the biggest impact on the resulting liposome size (Table 4.4), which coincided with results obtained in Chapter 3. Same factor FRR (x_1) showed a bigger impact to the resulting polydispersity than the factor TFR (x_2) and no combinatorial effect ($x_1 * x_2$) was determined. Similar, the quadratic term (x_1^2) of the factor FRR showed the biggest impact on the resulting transfection efficiency, elucidating on the importance of the ratio between aqueous and solvent stream in the microfluidics directed nanoprecipitation method (Table 4.4).

These regression models were used to mathematically determine the liposome size, PDI and transfection efficiency as a function of the TFR and FRR in the microfluidics-based nanoprecipitation process for DOPE-DOTAP lipids. Having determined model significance, outliers and significant terms, factor interaction was visualised in a response surface plot (Figure 4.7). Given the quadratic interaction RSM, a curved response surface was expected underlying the chosen design (Eriksson, 2008).

Respective response surface plots showed the predicted response values over the two factors, depicting their combinatorial effect in the microfluidics-based vesicle manufacturing process with regards to the liposome size, PDI and transfection efficacy. Here, minimal vesicle sizes of 60 nm were predicted for high flow rates (2 mL/min) and at high flow rate ratios (1:5). Maximum sizes predicted were 200 nm for 0.5 mL/min and a low FRR (here 1:1; Figure 4.7A). Evaluating the respective response surface plot, minimum PDIs of 0.2 were predicted for low FRRs (1:1) (Figure 4.7 B), with an increase in PDI linked to an increase in FRR. Maximum PDIs predicted were around 0.5, for the highest FRR of 1:5. Furthermore, the response surface plot visualised that a change in TFR provided a minimal impact to the resulting PDI, emphasised by the insignificance of respective factor, as determined in above model evaluations and the coefficient plot (Table 4.3). The link between FRR and PDI was already observed in previous OFAT method (Figure 4.1), model prediction confirmed this direct correlation. Maximum luciferase activities around 250% were predicted for a FRR of 1:3, efficiencies were predicted above 180% for FRR between 1:2 and 1:4, independent of the TFR used (Figure 4.7C). Minimum transfection efficiencies were predicted for the highest FRR (1:5) ranging between 80-100%.

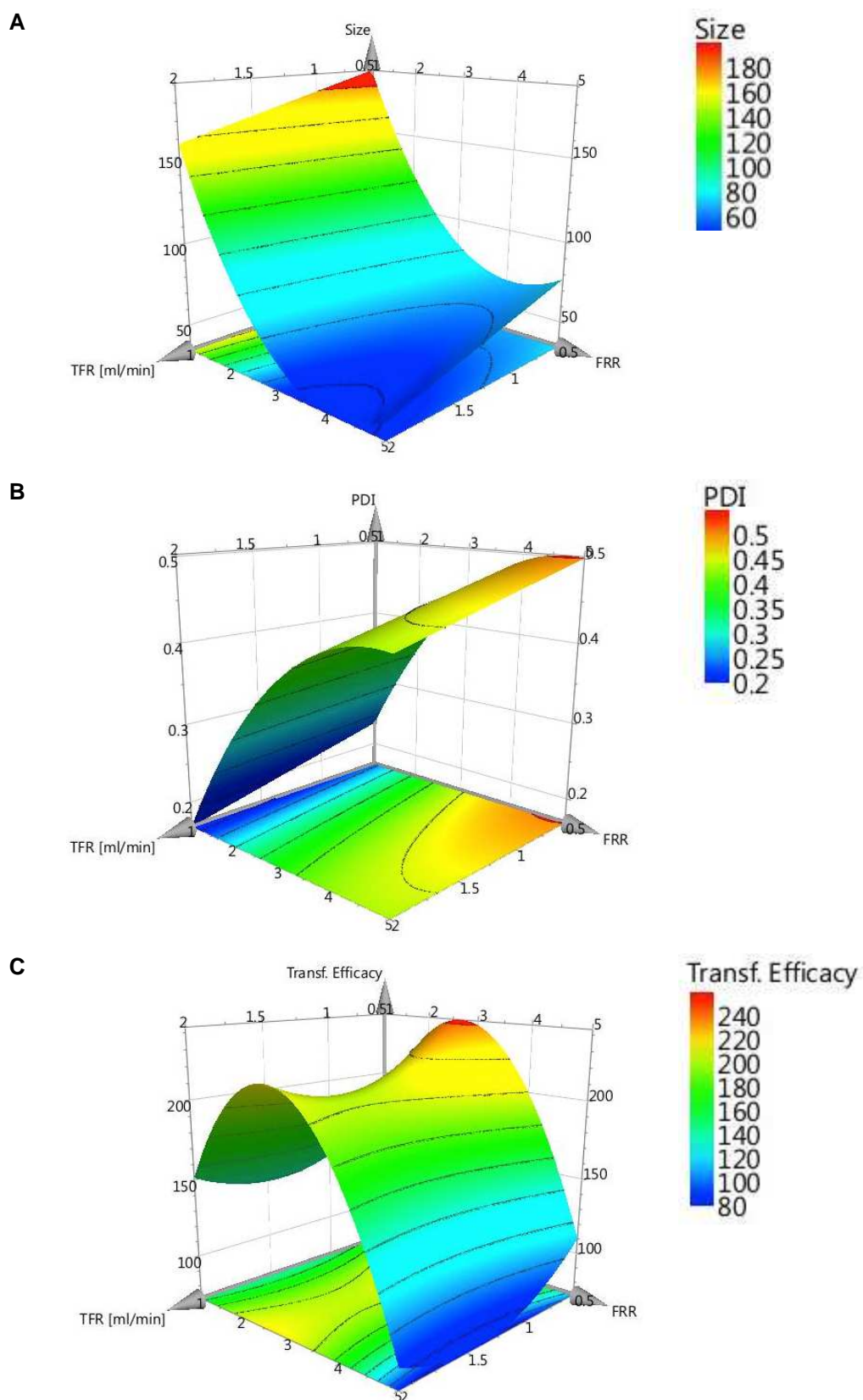


Figure 4.7: Response surface predictions for A) liposome size, B) polydispersity and C) transfection efficiency as a function of TFR (0.5 – 2 mL/min) and FRR (1:1 to 1:3 in the microfluidics-directed manufacturing of DOPE-DOTAP liposomes.

Predicted values for the liposome size, minimum and maximum of 60 nm and 200 nm respectively, coincided with previous determined liposome sizes by a one-factor-variation method (Figure 4.1), verifying the model predictions. Furthermore, predictions reassured the theory of liposome formation by microfluidics-triggered nanoprecipitation method, where the increase in aqueous phase (volume) increased the polar phase available and thus accelerated the rate of polarity increase, indicated by the significant interaction term $FRR \cdot FRR$ (Table 4.2). As a high ratio of aqueous phase present triggered a quicker precipitation reaction, smaller vesicles could be expected, as seen for the predictions for a FRR of 1:5. The predictions for the transfection efficiency coincided with previous observations, where the highest transfection was achieved for a FRR of 1:3 (Figure 4.3). Furthermore, these results may allow for targeted selection of flow properties (TFR and FRR) depended on desired vesicle characteristics and transfection efficiencies anticipated. Response surface evaluations further elucidate on the factor TFR being the primary impact on the overall throughput, with minimum effect to vesicle characteristics and transfection outcome.

Additionally, a sweet spot analysis was performed, exemplifying the use of DoE predictions. For exemplification, selected criteria comprised a liposome size of 80-150 nm, a PDI of 0.125 – 0.3 (minimize) and a transfection efficiency of 150-280% (maximize). The area shown in green in Figure 4.8 depicts the sweet spot for a FRR between 1:1 and 1:2 at a TFR between 1.4 and 2 mL/min. This tool, together with the possibility to generate vesicles of different sizes using the microfluidics-directed vesicle manufacturing, underlined the usefulness of the DoE method, as the characteristics and *in-vitro* performance of the vesicles can be predicted using the models generated.

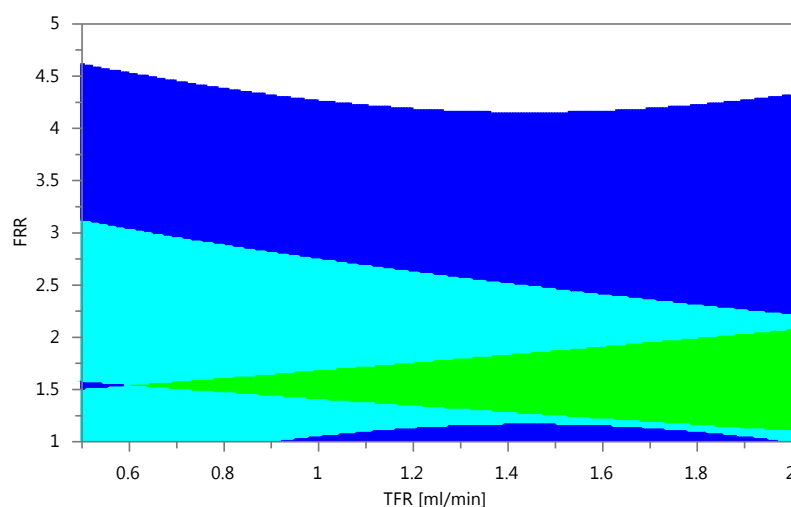


Figure 4.8: Sweet spot analysis for the desired criteria 1, size (80-150 nm); criteria 2, PDI (0.125-0.3) and criteria 3, transfection efficiency (150-280%). Dark blue = criterion 1 met, light blue = criterion 2 met, green = sweet spot.

To validate the model, predicted values from the regression model were compared to the responses obtained in an additional experimental study. Using the optimiser tool, predicted size, PDI and transfection efficiency at targeted TFR and FRR were determined, and compared to the values of size, PDI and transfection efficiency obtained experimentally post model performance. The comparison of the model prediction (minimum to maximum values predicted) to the experimental obtained results showed close alignment, with excellent predictions for settings at 2 mL/min, FRR 1:3 (Table 4.5). Here, predicted liposome size ranged between 49.8 to 55.0 nm, with good correlation with the experimental obtained sizes of 49 ± 11 nm. Additionally to the size model, predictions for the PDI and transfection efficiency coincided well with results obtained experimentally, with smaller errors in the model predictions.

Table 4.5: Validation of the regression models built during the DoE analysis. Predicted values are compared to experimentally obtained results for two process settings; 1 mL/min, 1:1 and 2 mL/min 1:3 (TFR, FRR).

		TFR, FRR	
		1 mL/min, 1:1	2 mL/min, 1:3
Size (nm)	Model predictions (min – max)	171.8 – 181.8	49.8 – 55.0
	Experimental validation	162.1 ± 34.0	49.5 ± 11.3
PDI	Model predictions (min – max)	0.21 – 0.23	0.37 – 0.38
	Experimental validation	0.18 ± 0.024	0.35 ± 0.13
Tranf. Eff. (% Luciferase activity)	Model predictions (min – max)	146.6 – 158.69	210.2 – 215.9
	Experimental validation	142.3 ± 22.5	186.5 ± 80.1

The above results confirmed the statistical validity of the model and supported the generation of regression models and response surface plots. Overall, the DoE analysis generated three statistical significant regression models that reproducibly predicted the size, PDI and transfection efficiency of cationic DOPE-DOTAP liposomes prepared by microfluidics. Model evaluations emphasized on the suitability of the microfluidics method for particle manufacturing, given that the mixing process was very rapid and offers high throughput. This decreases the risk of introducing experimental error over time, in contrast to time-intensive manufacturing methods like lipid-film hydration (Wagner and Vorauer-Uhl, 2011). The size model showed that both factors, the TFR and the FRR had a significant impact. The DoE analysis showed that the term FRR had a more significant impact, including a significant interaction term of FRR*FRR, suggesting the importance of the solvent/aqueous ratio to the overall liposome size. The model developed was additionally used in a sweet-spot analysis to select the FRR and TFR to target a specific size and transfection efficiency of the resulting vesicles. Overall, the DoE section developed, analysed and validated a set of predictive

regression models. In contrast to the OFAT method in Section 4.3.1, this method developed a response surface, useful for future predictions and detection of the statistical impact of the factors TFR and FRR in the microfluidics-directed liposome manufacturing method.

DoE studies were previously investigated for liposomal products in recent trends in the pharmaceutical sector involving Quality by Design (QbD) principles. Similar to the studies presented in this chapter the aim was the generation of a robust and reproducible design space to control liposome quality characteristics. Along with evaluating the critical variables in a process, those principles aided the formulation and product quality. Using DoE, the effect of lipid chain length, lipid concentration and drug concentration was related to the drug encapsulation efficiency, linking to the particle characteristics (size, zeta potential). The resulting physicochemical particle characteristics were linked to the manufacturing method, ultimately relating to the amount of drug encapsulated (Xu et al., 2011). An additional study further increased the number of variables, linking the lipid concentration, drug concentration, cholesterol concentration, buffer concentration, hydration time, sonication time, freeze–thaw cycles and extrusion pressure to the physicochemical vesicle characteristics, along with their stability and drug encapsulation. Here, the lipid and drug concentration were found as the variables with the highest impact on the drug encapsulation (Xu et al., 2012). Along with those examples, the application of DoE for QbD principles was underlined, ultimately aiding the optimization of a formulation process. Multivariate tools were described in pharmaceutical applications, which overall reported improved processes and product quality (Gabrielsson et al., 2002).

4.3.5 Statistical impact of the factors flow rate and flow ratio in a multivariate study

The above DoE study detected the local optima in a design space that predicted the liposome size, PDI and transfection efficiency. To strengthen the theory behind the microfluidics-based liposome manufacturing method, a multivariate study based on PCA and PLS was performed as an additional statistical analysis tool. Here, all variables were analysed simultaneously, which identified patterns within those variables whilst detecting the relationship amongst input variables (X) and output responses (Y). As a predictive tool, the change in one variable was linked to the respective effect to the response. This is a method frequently applied in data analysis, data mining, classification (e.g. cluster analysis or outlier detection), regression analysis and predictive modelling (Eriksson, 2006). Here, two MVA methods were

applied; PCA dealt only with X-variables, whereas PLS involved X and Y variables and was used for regression modelling. PLS was used for predictions of Y from X, and additionally for identifying if and how variables and responses were linked to each other. This was achieved by fitting principal components (PC) through the multidimensional data set, which generated coordinates for each data point. Those coordinates allowed for plotting the data set onto a plane in a so-called loading plot, which was subsequently used for data interpretation.

Here, two PCs were fitted, which together evaluated the effects of the factors TFR and FRR to the responses liposome size, PDI and transfection efficacy (Figure 4.9). The size model indicated that the data set contained approximately 10% noise, similar to the noise level in the PDI model, and both were considered good enough for further evaluating the model. The transfection model yielded the lowest fit with a predictive power of ca. 50%, which was anticipated sufficient for further evaluation.

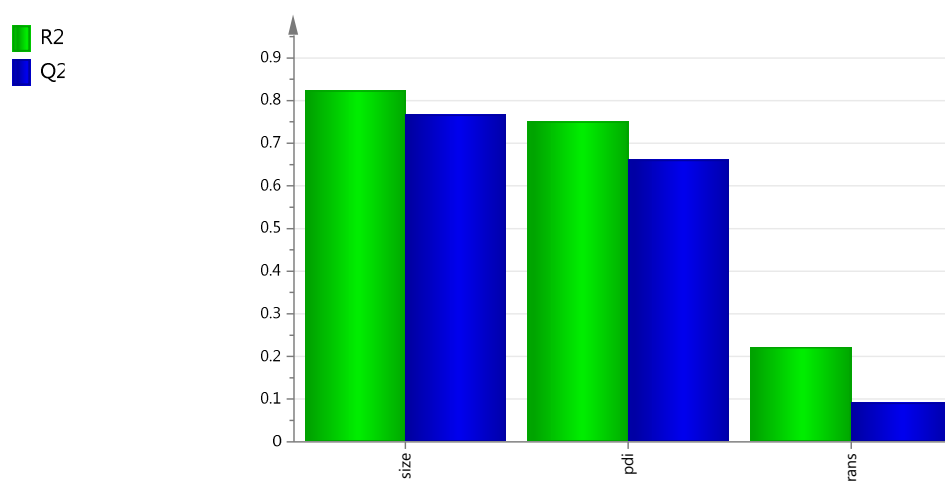


Figure 4.9: Summary plot with two principal components added, showing the model fit (R^2) and predictive power (Q^2).

The initial performed PCA analysis was represented in a score plot (Figure 4.10), which shows a summary of the relationships among the observations. Two PCs were fitted to model the systematic variation of the data set to approximate the X-data and define the plane of the variable space. All observations were projected onto the space of lower dimensions to visualize the data set and by approximation of the two PCs. The score plot showed how the observations were situated with respect to each other, revealing no outliers as all observation remained in the 95% confidence interval ellipse. The structural arrangement of the data points reflected the setup as derived from the DoE study, with a total of 15 observations (Figure 4.10). A colour coding was used for cluster analysis for visualization help. Groups according to FRR (1:1, 1:3 and 1:5) trended from the right to the left with increase in FRR (Figure 4.10A). The same trend

was given once coloured according to PDI, with the increase in PDI trending from the right to the left, matching the trend seen for the FRR (Figure 4.10B). Once coloured according to the TFR, the data points trended from the two lower to the two upper quadrants (Figure 4.10C). The colouring according to size depicted a trend from large to smaller sizes trending from the right to the left quadrants (Figure 4.10D). Similar colour trends (right-to-left) were seen in the plots coloured according to size (Figure 4.10D), PDI (Figure 4.10B) and FRR (Figure 4.10A); the largest size and lowest PDI was depicted in the same quadrant as the lowest FRR of 1:1. Here, the cluster analysis revealed a clear link between FRR, PDI and size, a similar trend seen in above DoE study, where a decrease in liposome size was predicted for an increase in FRR along with the increase in PDI (Figure 4.7A, B).

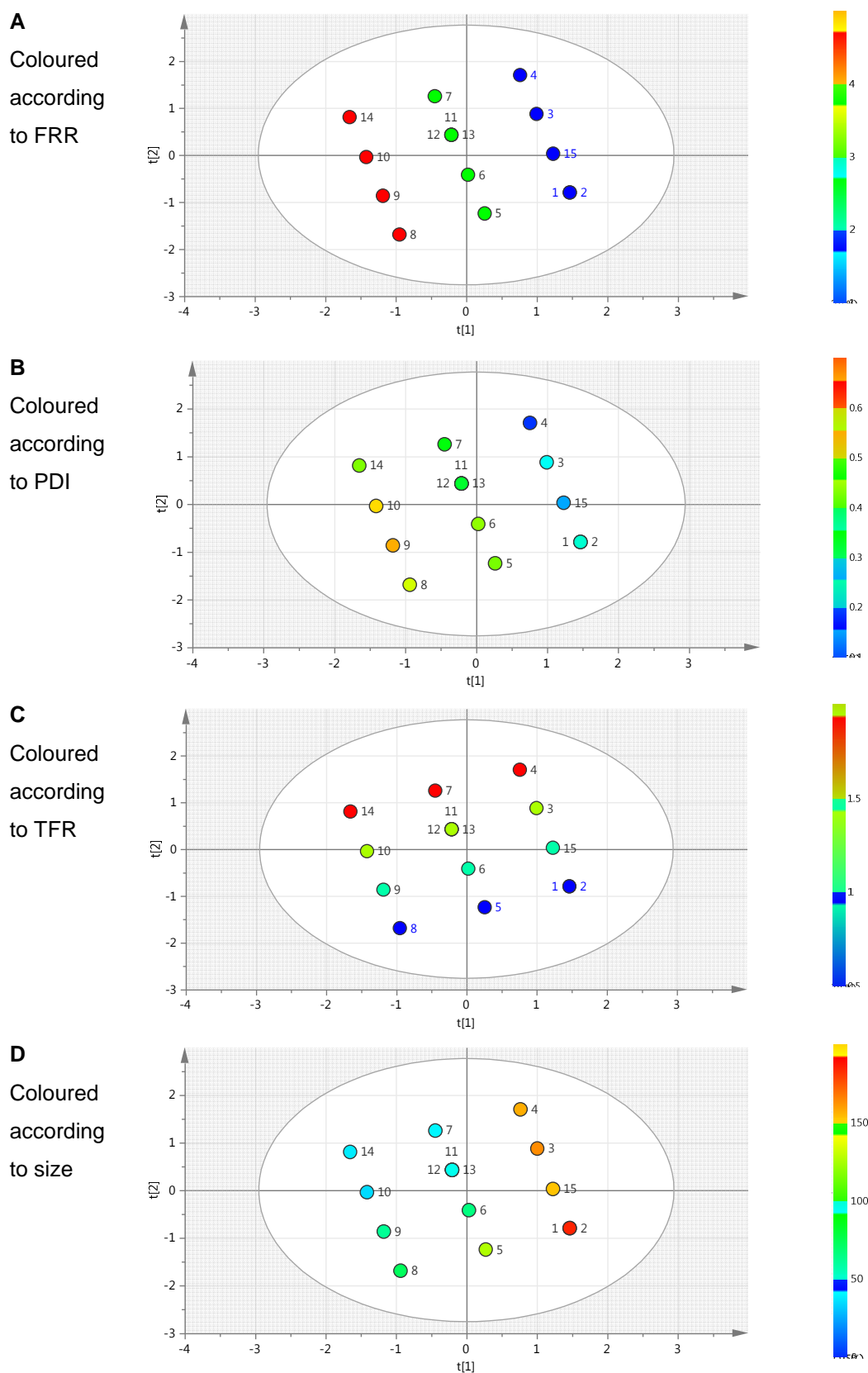


Figure 4.10: Score scatter plot as identified during the PCA. Colour coding simplifies the cluster analysis and trending in the data set with A) coloured according to FRR, B) coloured according to PDI, C) coloured according to TFR and D) coloured according to liposome size. The numbers represent observations as obtained from the DoE study.

The PLS analysis included the Y-variables as an extension to the performed PCA. Here, the Y-variables (size, PDI, transfection efficiency) were related to the X-variables (TFR and FRR) by a multivariate model (Wold et al., 1984; Wold et al., 2001a; Wold et al., 2001b). The PLS model was interpreted by respective coefficients, represented in the coefficient plot (Figure 4.11), which showed the importance of the variables TFR and FRR linked to the responses (size, PDI and transfection efficiency) for the two PCs fitted. The factor TFR was found only significant in the second PC, whereas the factor FRR, along with the responses transfection efficacy and size were shown to be highly statistical significant in the first principal component (Figure 4.11A). Both PCs were found significant for the response PDI. The relationship between the factor TFR and the response size was visualized in the loading scatter plot (Figure 4.11B). Here, the factor TFR was found in the upper left quadrant, opposite to the response liposome size. The coefficient plot for same variable and response indicated their significance in different PCs, indicating no correlation between the factor TFR and the response size. The factor TFR was found to be independent of the response size and transfection efficiency, as indicated by their significance in different PCs in the coefficient plot.

A direct correlation between FRR and PDI was indicated by their significance in the first PC (Figure 4.11B). This correlation was observed in above PCA analysis (Figure 4.10) as well as in the performed DoE model (Table 4.2). The results from the PLS analysis correlated an increase in PDI with the increase in FRR. A correlation between the size and the transfection efficiency was indicated with their close situation in the loading scatter plot and matching significance of the first PC in the coefficient plot (Figure 4.11A). This direct correlation predicted the increase in transfection efficiency with larger liposomes.

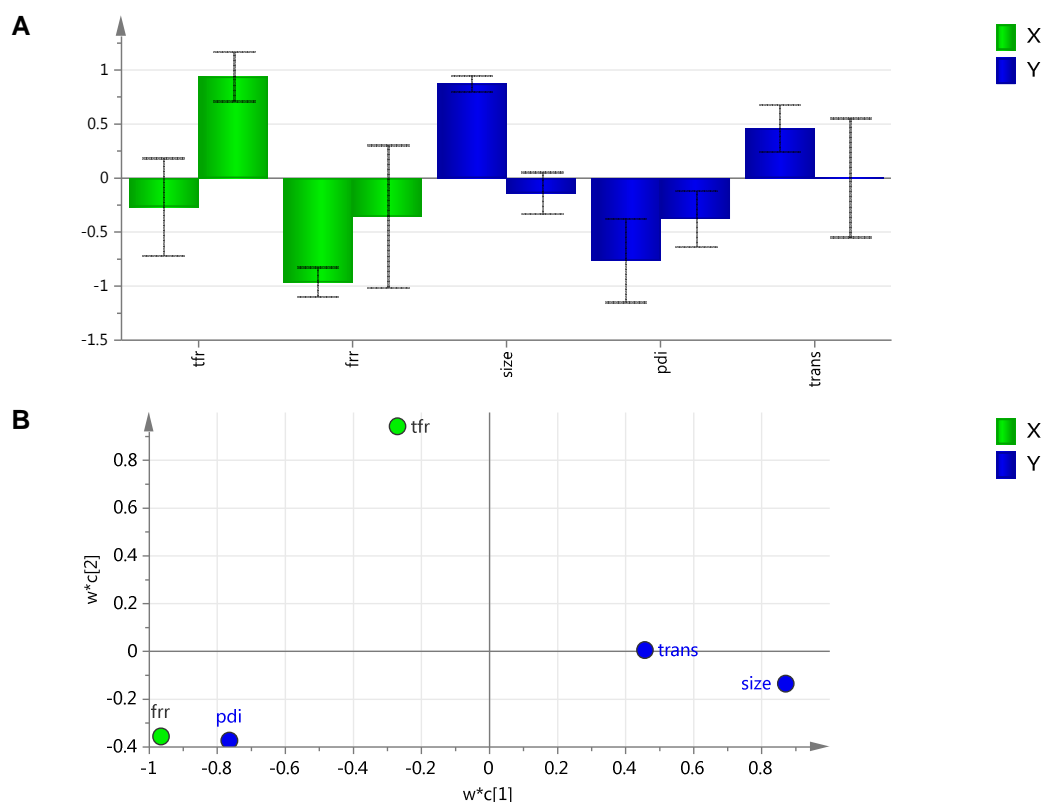


Figure 4.11 Results from the PLS regression analysis coloured according to model term. A) Coefficient plot including 95% confidence interval for the two principal components. B) The loading scatter plot indicating significance of the factors (X) and responses (Y) to each other.

Loading and score plot are complementary and superimposable and can be used to interpret the patterns seen. A direction or cluster in a score plot corresponds to a variable seen in the same direction in the loading plot (Eriksson, 2006). The points for larger sized vesicles lie on the right hand side of the score plot (Figure 4.10D), which corresponded to the response size and transfection efficiency situated closely together in the loading plot. The size response was situated far away from the origin (lower right-hand quadrant, Figure 4.11B), overlapping with the same area of the score plot for the vesicles with the highest size (Figure 4.10D). The variable FRR was situated on the opposite side in the lower left-hand quadrant (Figure 4.11B), indicating an inverse relationship to the response size and corresponded to the vesicles with the lowest size in and the highest PDI in the score plot (Figure 4.10B, D). The loading plot revealed a direct correlation between the PDI and the FRR, with both terms situated in the same lower left-hand quadrant. The strong link between particle characteristics (size, PDI) and FRR was revealed in both scores and loading plots, as seen in above DoE evaluations (Figure 4.10, 4.11B, Table 4.2).

As with other models, the validation of the developed MVA models is crucial. Here, permutation plots assessed model validation and the risk of a fault in the PLS model and eliminated the risk that the model developed just fitted the data set in this study without predicting the responses well for new observations. Here, the goodness of fit (R^2) and prediction (Q^2) of the original model were compared to the ones of several models based on data where the Y- observations were randomly permuted, while the X-matrix was kept constant. The respective permutation plots showed the original R^2 and Q^2 values on the vertical axis far to the right, which coincided with the values from initial model summary, Figure 4.9. The values for the permuted models were shown on the left. A horizontal axis between respective values showed the correlation between the permuted and the original Y-vectors for a selected response. The criterion for a valid model was pre-set for a Q^2 regression line intercept the vertical axis at or below zero. For all responses, 40 permutations were added and the original value had a correlation of 1 on the horizontal axis. Here, all three permutation plots strongly indicated valid models, given that the intercept of the predictive regression line intercepted below zero (Figure 4.12A, B). Furthermore, higher original R^2 and Q^2 in the plots for the response size and PDI, were indicated in the summary plot (Figure 4.9). Most importantly, the here developed permutation analysis confirmed the validity of transfection model, which showed overall lower R^2 and Q^2 values in the initial summary plot (Fig 4.12C, Figure 4.9).

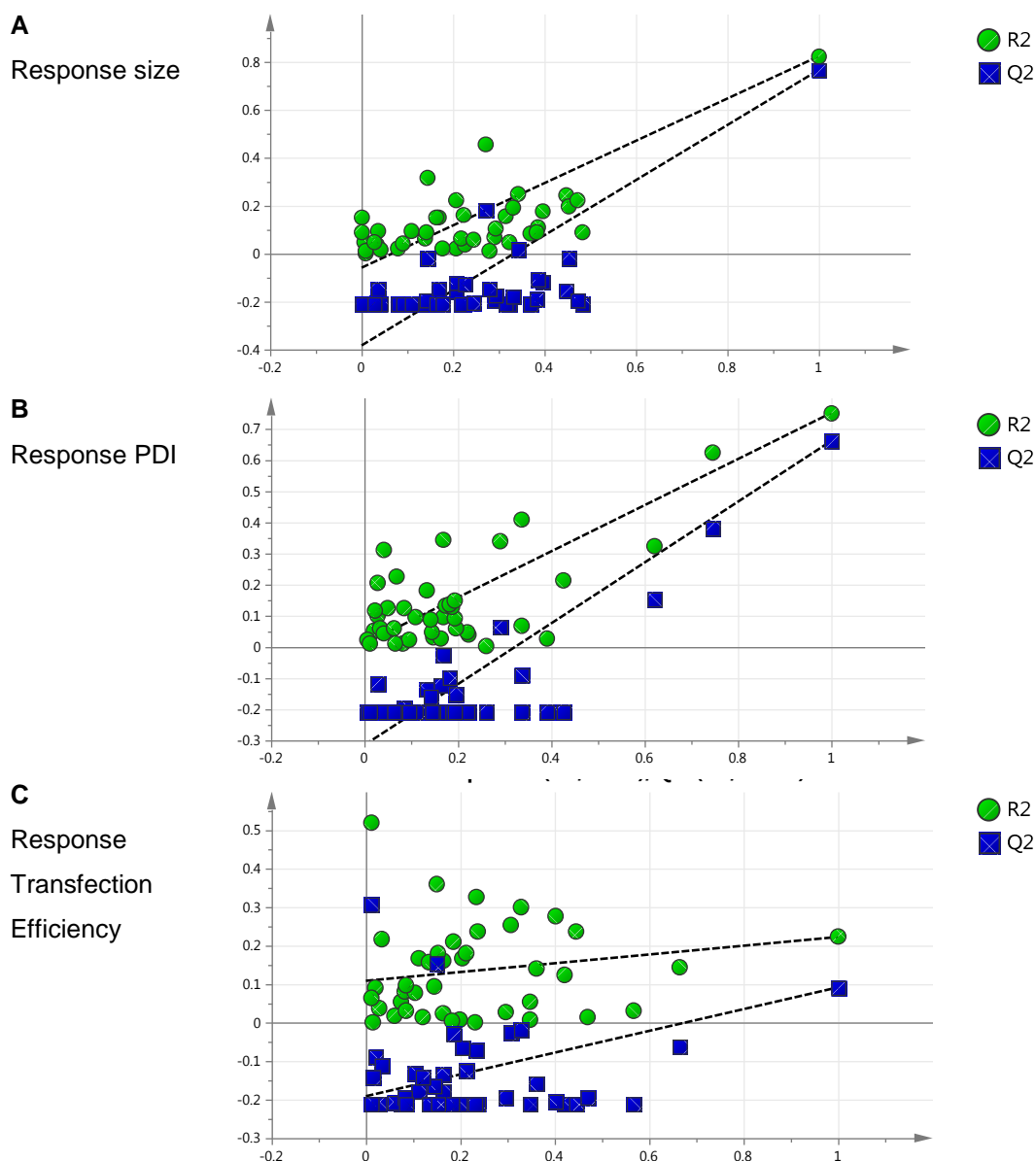


Figure 4.12: Permutations plot for A) size, B) PDI and C) transfection efficiency. Model validity was assessed for 40 permutations. The correlation between permuted Y-vector to the original X-vector is depicted by the horizontal correlation axis. The criterion for model validity was selected as the intercept of the Q^2 regression line at or below zero.

The MVA results verified the outcome of the DoE study, giving a mathematical proof that a better transfection results may be expected for vesicles with a larger size at a constant lipid/DNA ratio (Esposito et al., 2006; Felgner et al., 1987; Kawaura et al., 1998; McNeil et al., 2010). The coefficient plot further revealed the smallest 95% confidence interval for the factor FRR, as seen in the DoE study, the factor FRR was shown to be highly significant in the size, PDI and transfection efficiency model. Together with the results from the DoE study, it can be concluded that the factor FRR is the most crucial factor in the microfluidics-based nanoprecipitation process, requiring detailed optimisation once the lipid combination is altered. The FRR directly affects particle characteristics (size and PDI) but also in the case of the lipid combination used

here, the anticipated transfection efficiencies for *in-vitro* gene delivery and application of lipoplexes.

4.4 Conclusion

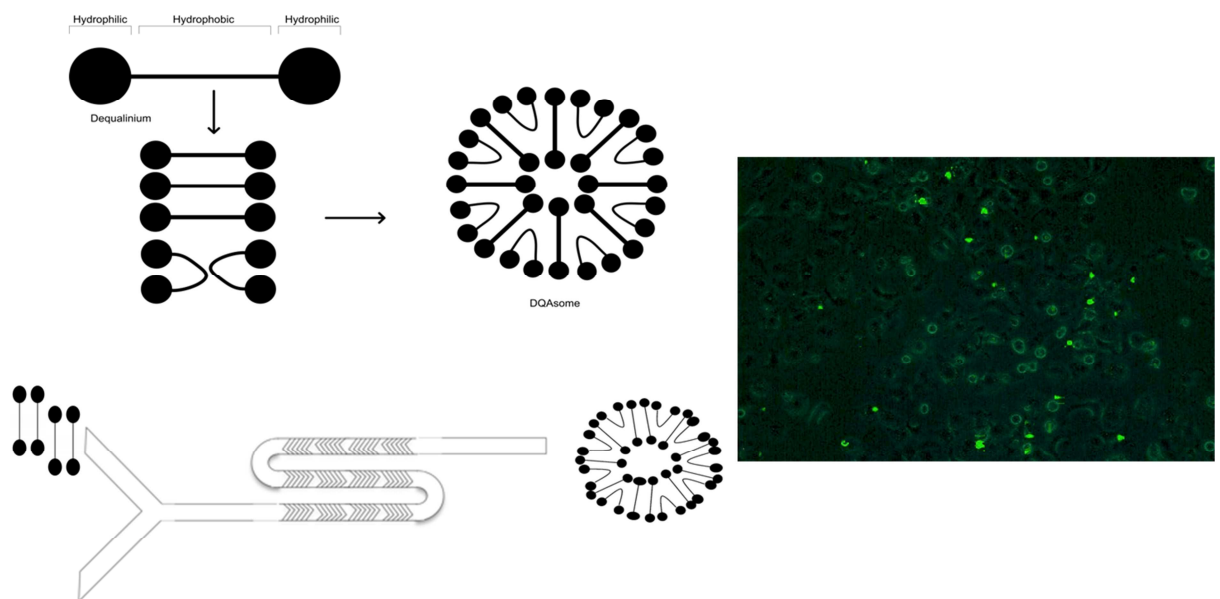
In this chapter, the microfluidics-based liposome manufacturing method was explored by variation of the process parameters TFR and FRR to produce liposomes of defined sizes, which gave reproducible transfection results in standard transfection protocols. This SHM method generated homogenous liposomes suspensions in a high-throughput setup. The advantage of the microfluidics-based method is its high-throughput and small footprint, allowing for a high number of formulations to be screened in a short time period. Here, a series of statistical tools to model the process and the effect of vesicle size for an *in-vitro* transfection were also exploited. The implemented statistical-based methods (design of experiments and multivariate data analysis) revealed the mathematical relationship and significance of the factors TFR and FRR in the microfluidics process to the liposome size, PDI and transfection efficacy. The systematic application of statistical based process control determined local optima. Furthermore, it revealed how variable interactions and clustering can be used for process simulations and predictions. Model predictions coincided with the initial performed OFAT experiments, reassuring the suitability of predictive tools in pharmaceutical process development. These tools deepen the process understanding, assist in development work and possible scale-up (Singh et al., 2005) and further enhance the reproducibility of a process for the generation of a design space.

The large-scale counterpart of the here-presented nanoprecipitation method is the ethanol injection method described in the 1970s (Batzri and Korn, 1973), which is based on the principle of precipitation reaction. Its replicate on a smaller footprint was developed (Jahn et al., 2008; Pradhan et al., 2008), however injection into a vortexed aqueous solution impeded on controlled mixing conditions and resulted in polydisperse liposome formulations (Jahn et al., 2008). The development of the crossflow injection techniques as an improvement over the ethanol injection method provided better process control and improved reproducibility at flow rates between 500 to 2700 mL/min; clearly a high-throughput and large footprint operation (Wagner et al., 2002b). In contrast, the mixing in microchannels is highly controlled, driven by diffusion and chaotic advection in a small-footprint lab-scale technique. Those unique properties allow for a precise process control of fluid flow patterns, resulting in a robust mixing profile, the key for a controlled vesicle manufacturing on micro-scale.

Overall, the FRR in the microfluidic process was verified as the most crucial parameter to the formation of size-controlled vesicles, confirmed by predictive modeling tools. The successful combination of experimental screening work, multivariate methods and experimental design is a powerful tool in any pharmaceutical or biopharmaceutical process development, for the development and optimization of new processes and finding optima within a defined region of factors and speeding up a developing process. Overall, process understanding and confidence is enhanced which gives predictive and correlative comparisons between the critical process parameters and their influence on desired critical quality attributes, leading to a desired and robust product quality.

Chapter 5

Microfluidics-directed manufacturing of a gene delivery system made from dequalinium™



Papers relating to this chapter:

Kastner E., Ingham AJ. and Perrie Y. Microfluidics-directed manufacturing of a gene delivery system made from dequalinium™ (in preparation)

5.1 Introduction

Dequalinium, 1,1-decamethylene bis (4-aminoquinaldiniumchloride), is a di-cationic compound, which is symmetrical with two charge centres that belongs to the “bola”-form electrolytes (Figure 5.1). Those bola-amphiphiles comprise two quinaldinium rings which are connected by methylene groups, comprising a delocalized charge centre (Figure 5.1A). The lipophilic drug dequalinium (DQA) has been used for more than 50 years as a compound with antimicrobial (Weissig, 2015; Weissig et al., 1998; Weissig and Torchilin, 2001), antifungal (Berlin et al., 1998) and anticarcinoma activities (Christman et al., 1990). Its antitumour activities have been linked to the preferential accumulation in carcinoma cells (Berlin et al., 1998; Rotenberg et al., 1990; Weissig et al., 1998). In comparison to cisplatin, a frequently applied chemotherapeutic agent, DQA was found to be more efficacious and less toxic for the treatment of ovarian cancer (Christman et al., 1990). Furthermore, an associated delay in tumour growth has been linked to the drug-induced loss and depletion of mitochondrial DNA (mtDNA) along with its associated functions (Berlin et al., 1998). In addition to its anticancer activity, antifungal and antimicrobial properties, DQA is currently used in a variety of creams and topical applications for treating infections (Babbs et al., 1956; Jones, 1995; Schneider-Berlin et al., 2005; Weissenbacher et al., 2012; Weissig et al., 1998). In this study, a DQA derivative compound 1,1'-(decane-1,10-diyl)bis(9-amino-1,2,3,4-tetrahydroacridinium) diiodide (CM2) (Figure 5.1B) was obtained from Procatra Biosystems Ltd. It is structurally related to dequalinium where the positive charges in two tetrahydroacridinium rings are connected by an alkyl chain of 12 atoms, with similar *in-vivo* activities to that of DQA (Tischer et al., 2012).



Figure 5.1: A) 1,1-Decamethylene bis (4-aminoquinaldiniumchloride) and its derivate B) 1,1'-(decane-1,10-diyl)bis(9-amino-1,2,3,4- tetrahydroacridinium) diiodide (CM2). Adopted from (Weissig, 2015).

Given the structure of bola-amphiphiles, either a U-shaped or a stretched confirmation can be adopted (De Rosa et al., 1986; Gulik et al., 1988; Luzzati et al., 1987), (Figure 5.2). Initial experiments demonstrated that upon solubilisation in aqueous vehicles, DQA formed colloidal particles between 70-700 nm with freeze fracturing imaging showing convex and concave structures suggesting the formation of liposome-like vesicles, termed DQAsomes (Weissig et al., 1998). DQAsome/DNA complexes (also known as DQAplices) offer high DNA binding capacity and mediated cellular uptake, delivery and release of DNA in mammalian cells (Weissig, 2015). Furthermore, DQAsomes are considered as quite a unique delivery system based on their *in-vivo* selectivity of carcinoma cells, their affinity for accumulation in mitochondria, and the potential of organelle-targeted drug or DNA delivery (Weissig and Torchilin, 2001).

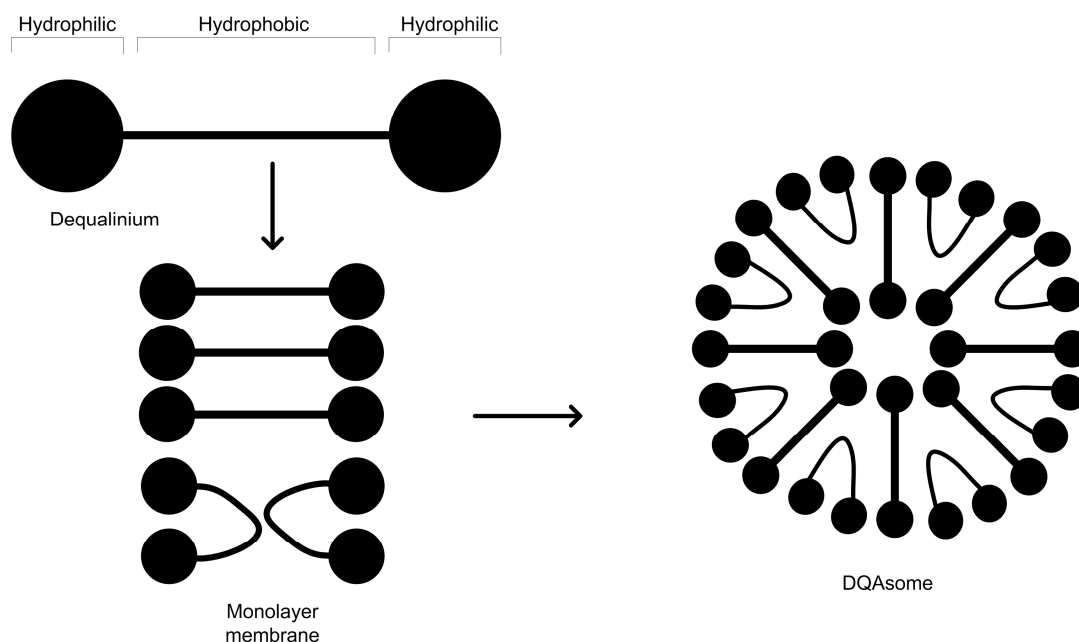


Figure 5.2: Assembly of a liposome-like vesicle comprising U-shaped and stretched-confirmation of bola-form amphiphiles. Adapted from (Gregoriadis, 2007).

Nevertheless, the manufacture of DQAsomes is challenging, and the applied lipid-film hydration and sonication processes do not provide acceptable reproducibility in industrial manufacturing (Wagner et al., 2002a). Traditional manufacturing methods rely on vesicle self-assembly after a sonication step; the lack of appropriate and reproducible methods is one of the current limitations for a process transfer from a laboratory setting into a large-scale process. Lipid-film hydration is associated with heterogeneous liposome population, whereas sonication may not be applicable for sensitive products and might result in protein and or lipid degradation and limited control during self-assembly might lead to a poor reproducibility and process control (Wagner and Vorauer-Uhl, 2011).

5.2 Aim and Objectives

The aim of this study was to assess the microfluidics-directed manufacturability of vesicles consisting of dequalinium-derivate (CM2), a bola-amphiphile with delocalised charge centres. To achieve this, the objectives were:

- Physicochemically characterise the particles formed using this microfluidics.
- Assess the stability of vesicles formed.
- Compare vesicles manufactured by methods relying on sonication and microfluidics.
- Investigate the *in-vitro* transfection of the systems to assess the ability of the microfluidics-manufactured particles to act as a delivery vehicle for genetic material.

Throughout this chapter, all work was performed on the dequalinium-derivate (CM2) compound, and the dequalinium-derivate (CM2) derived nanoparticles were termed “DQAsomes”.

5.3 Results and Discussion

5.3.1 A feasibility study of DQAsome manufacturing by microfluidics

Initial work focused on the manufacturability of bola-amphiphile nanoparticles by microfluidics-directed nanoprecipitation. Initially, a proof-of-concept study was performed where three independent batches were manufactured (and each batch assessed in triplicate) at the same flow rate conditions on different days, verifying the intra-day and inter-day variability. Flow rate conditions (TFR 2 mL/min, FRR 1:3) were extrapolated from previous work (Chapter 4). Results (Figure 5.3) show that vesicles with an average vesicle size of 250-300 nm were formed, with a polydispersity (PDI) around 0.4 and zeta potential highly cationic around +30 mV. In addition to low inter-day variability (variability between the trials), the intra-day variability (variability within one trial) was low, ranging between 20-50 nm in size, 1-5 mV in zeta potential and 0.04-0.07 in PDI (Figure 5.3). The cationic zeta potential measured coincided with recent published work on dequalinium-based vesicles for drug delivery (Zupančič et al., 2014), linked to its cationic tetrahydroacridinium rings. In comparison, DQAsomes were prepared by the lipid film hydration followed by sonication, as initially described and patented by Weissig et al. in the mid-1990s upon discovery of DQA-specific assembly into nanoparticles (Weissig et al., 1998). Using this method and sonication for 30 minutes (amplitude 5) yielded an average size of 300 nm (Figure 5.3) coinciding with previously published work on vesicles manufactured by sonication (Weissig et al.,

1998; Zupančič et al., 2014); these vesicles were overall larger in size with a higher PDI than vesicles prepared by microfluidics.

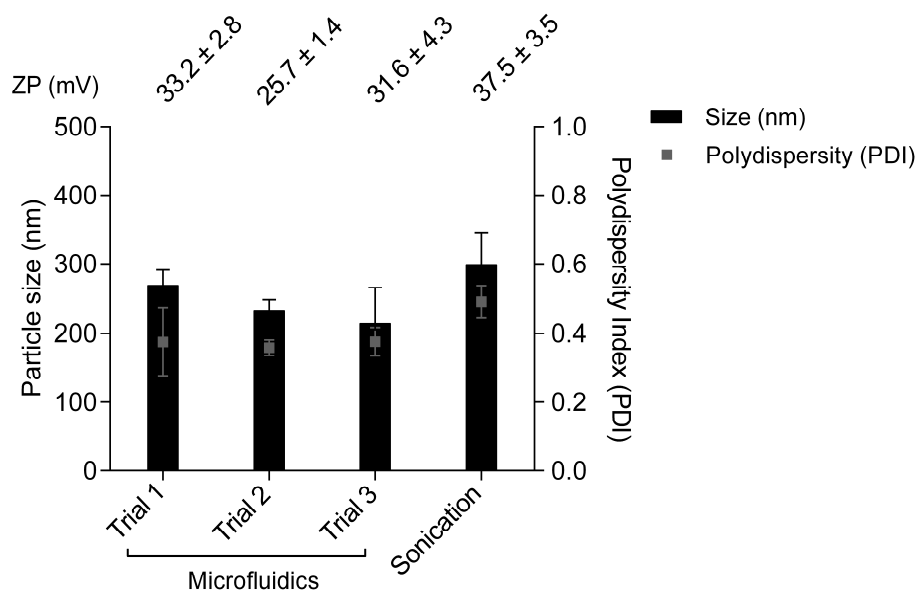


Figure 5.3: Reproducibility (intra-day variability) and inter-day variability of DQAsomes manufactured by microfluidics (TFR 2 mL/min, FRR 1:3) and sonication (30 min, amplitude 5) showing the particle size, polydispersity and zeta potential. Results denote mean \pm SD of 3 separate batches.

Investigation of the DLS vesicle size data by comparison of intensity- and volume-based size distribution plots and correlograms (Figure 5.4) reveal low variability within the three trials performed (inter-day variability, %RSD =13.2 for size and 14.5 for PDI). The intensity-based size distribution plot (Figure 5.4A) revealed an intensity-based average particle diameter $\geq 90\%$ intensity. A subpopulation of particulates in the micrometer range was visible for all three trials, with significance in the volume pot ranging within 3-9 volume% at a size of 4-6 μm (Figure 5.4B); a shoulder in the decay function indicated the sub-population in the respective correlograms (Figure 5.4C). The intensity-based size distribution showed higher variability in the sonication method, due to subpopulation visible below and above the average particle size (Figure 5.4D), with larger significance in the volume-based size distribution plot showing multi-modal populations (Figure 5.4E), which ranged within 9-30 volume % with a higher variability in the associated correlation plots (Figure 5.4F). The volume-based distribution of the sonicated vesicles revealed a sub-population around 20 nm in size, which may be indicative of micelle formation by the respective method (Figure 5.4E). Given the sub-populations in both methods, microfluidics and sonication, the presence of larger aggregates or contaminants was found independent of the manufacturing method, possibly deriving from contaminants based on compound specific aggregation

behaviour. Furthermore, correlation functions of sonicated vesicles were suboptimal, with a shallow decay referring to a higher PDI and wider size distribution (Figure 5.4F).

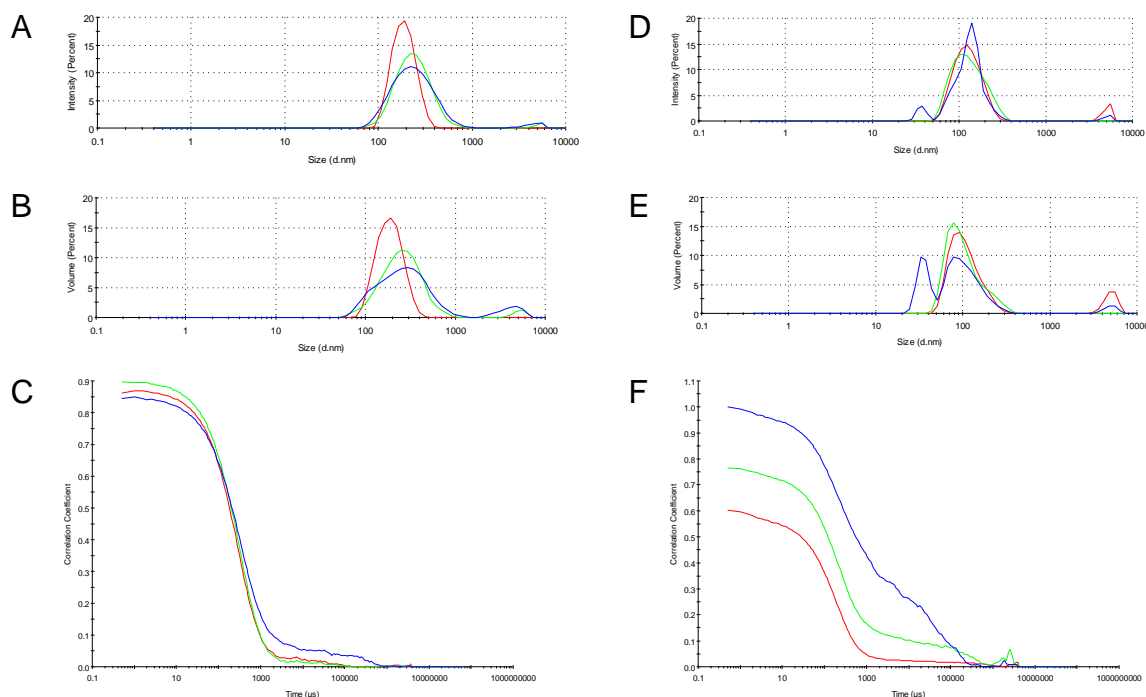


Figure 5.4: A) Intensity-based, B) volume-based size distribution and C) correlogram of particles manufactured via microfluidics-based nanoprecipitation. D) Intensity-based, E) volume-based size distribution and F) correlogram of particles manufactured via lipid film hydration followed by sonication. Plots show the average out of three batches and the inter-day variability for the microfluidics-manufactured vesicles.

5.3.2 The effect of flow rate ratio and total flow rate on vesicle characteristics

Given that previous investigations demonstrated that both the total flow rate (TFR) and flow rate ratio (FRR) in the microfluidics process can impact on vesicle characteristics (e.g. as shown in Chapter 3), the effect of these factors on DQAsomes was also investigated (Figure 5.5). The adjustment from FRR 1:1 to 1:3 resulted in a significant ($p < 0.001$) decrease in DQAsome size, with a minimum size of ~250 nm (Figure 5.5A). Vesicle size plateaued at a FRR greater than 1:3 ($p > 0.05$), suggesting that the smallest size achievable was ~250 nm. All alterations in flow ratios remained independent of the PDI (Figure 5.5A), which ranged within 0.3 to 0.5; given the presence of a sub-population in above correlograms (Figure 5.4), a PDI higher than 0.2 would be expected. The zeta potential remained above +25 mV and was not significantly influenced by any of the factor variations tested. The effect of increasing throughput in the microfluidics-method was evaluated at a constant FRR (1:3) by increasing the TFR from 1 mL/min to 8 mL/min; the results show that TFR did not significantly change DQAsome characteristics (Figure 5.5B).

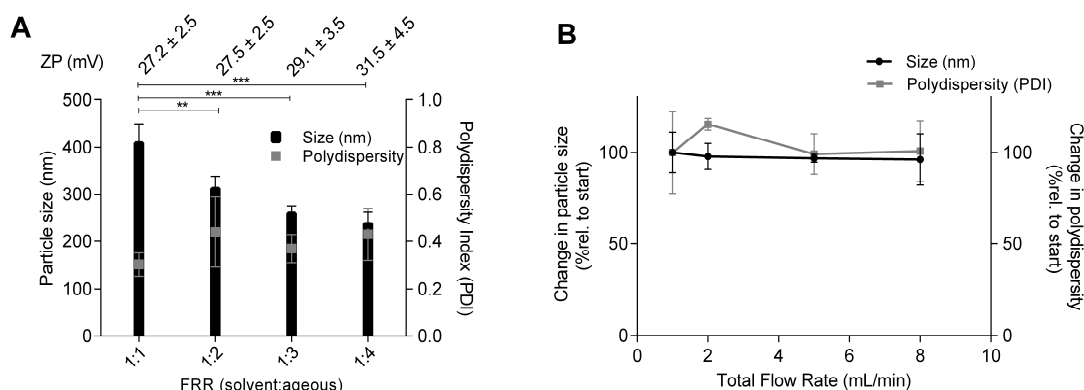


Figure 5.5: Effect of increase in A) FRR at constant TFR of 2 mL/min and B) TFR at constant FRR of 1:3 to DQAsome characteristics. Change is represented in % relative to the start size of 250 nm, PDI 0.3. Where shown, significance between data is against results at a FRR 1:1 ($p < 0.01$, *** $p < 0.001$). Results denote mean \pm SD of 3 separate batches.**

The initial work based on the DQAsome formation, patented by Weissig et al., referred to a vesicle size between 70 – 700 nm (Weissig et al., 1998) where size was presumably controlled by alterations in sonication parameters. More recent work on DQAsomes manufacturing by lipid-film hydration and sonication techniques reported sizes between 170 – 200 nm dependent on the ratio of lipophilic drug incorporated into the DQA-based vesicles (Zupančič et al., 2014). The here-presented microfluidics-directed manufacturing method allowed for vesicle sizes between 250 – 400 nm, with the major advantage of an in-process control of vesicle size dependent on flow conditions selected. Similar to work performed on cationic double-chain lipids (Chapter 4), the FRR factor was most influential regarding the resulting particle characteristics. Results in Chapter 3 highlighted on the importance of both, TFR and FRR for influencing the vesicle size; however, this was with high transition temperature lipids opposed to lipids used in this chapter and in Chapter 4, where the FRR was found the most contributing factor for controlling vesicle size. The microfluidics-directed nanoprecipitation method uses the advantages of a controlled ratio of aqueous to solvent phase to specifically influence the closing time of vesicles formed (Dong et al., 2012). A high aqueous content FRR allows for a high aqueous volume to be introduced in the mixing process, which ultimately enhances the mixing process. This controlled alteration first decreases the diffusion layer thickness between both streams and reduces the width of the solvent stream, both reducing diffusion distances in the mixing profile. The mixing profile itself is enhanced by the herringbone structures in the floor of the channel (Stroock et al., 2002), which overall allows for a lower FRR compared to the hydrodynamic flow focusing method, resulting in more concentrated vesicles manufactured (Jahn et al., 2007). The reduction in solvent concentration below the

solubility limit for the CM2 component leads to reduced closure time for the vesicles and subsequently smaller vesicles formed at higher aqueous content FRR (Zook and Vreeland, 2010). As seen in Figure 5.5A, smallest vesicles correspond to higher aqueous volumes, which plateaued at a FRR higher than 1:3, suggesting the smallest size possible in the nanoprecipitation method was 250 nm. Additionally, the remaining solvent in the final formulation is reduced with increase in FRR, which influences the synthesis of larger particles due to particle fusion and lipid exchange (Ostwald ripening) after complete mixing is achieved. At lower aqueous FRR (here 1:1), more solvent remains present during the mixing process, allowing for prolonged stabilisation of the hydrophobic components of the CM2 component, which leaves more time for the bilayers to grow before vesicles are formed, resulting in overall larger vesicles formed, here 400 nm (Figure 5.5A). A tailored vesicle size dependent on selection of flow properties may be advantageous for a specific application of DQAsomes with size-specific *in-vivo* performance.

The advantage of the microfluidics based nanoprecipitation method lies in the generation of controlled mixing profiles throughout a chamber. Microfluidic devices allow for a tight control of mixing efficiencies, which are based on molecular diffusion processes. The increased surface-to-volume ratios create fast mixing times, emphasized by reducing dimensions and diffusion lengths (Lee et al., 2011; Mengeaud et al., 2002). Such on-chip setups allow for tailored and controlled alterations in polarities throughout a mixing chamber. These constant mixing profiles are key for a reproducible manufacturing process with minimal inter-day variability, as seen in Figure 5.3, 5.4. Furthermore, results highlighted an 8-fold increase in throughput by increasing the TFR, emphasizing on the suitability of using this method for high-throughput manufacturing.

5.3.3 The effect of CM2 concentration in the microfluidics-directed DQAsome formation

In addition to the studies evaluating the particle characteristics, the CM2 concentration was assessed as a further variable during the microfluidics-directed manufacturing step and was increased, aiming for an overall higher concentration of DQAsomes generated within the method.

Quantification of the CM2 compound was performed by the HPLC method as described in Chapter 3. Here, the CM2 concentration was increased approximately 8-

fold from initial 0.6 mg/mL to 5 mg/mL (0.7 mM to 6.1 mM respectively; Figure 5.6). This allowed for simply manufacturing vesicles at a higher concentration, which showed a linear trend in quantification of the CM2 component (Figure 5.6A). Recovery, expressed in % and related to the initial amount of CM2 compound available in the stock as well as the FRR applied, remained above 87% for all formulations ($p>0.05$; Figure 5.6B). No difference in particle size was noted with the increase in concentration from 0.6 to 3 mg/mL (Figure 5.6C), whereas the highest CM2 concentration (here 5 mg/mL, 6.1 mM) resulted in a significant larger particle size with an additional significant increase in PDI ($p<0.05$), (Figure 5.6C and D). The zeta potential remained unaffected throughout ($p>0.05$, Figure 5.6E).

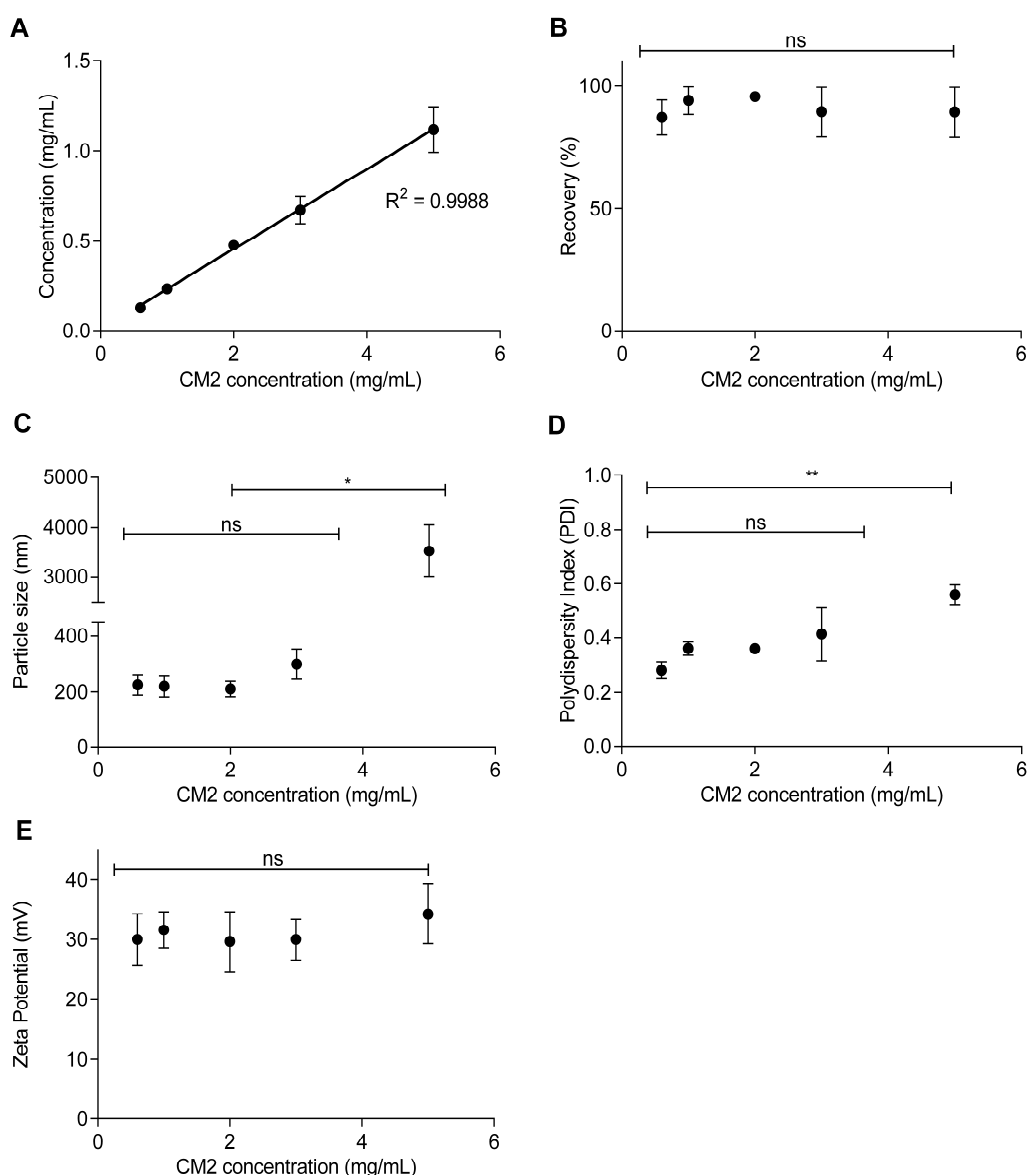


Figure 5.6: Effect of increase in CM2 concentration to A) quantification, B) recovery (%), C) DQAsome size, D) PDI and E) zeta potential. The heating block was used for formulations ≥ 3 mg/mL to maintain solubility. Where shown, significance between data is against results at a concentration of 0.6 mg/mL (* $p<0.05$, ** $p<0.01$). Results denote mean \pm SD of 3 separate batches.

The higher PDI and sizes at a CM2 concentration of 5 mg/mL (Figure 5.6B) might be explained by solubility difficulties of CM2. Solubility at room temperature was limited to 1 mg/mL and a heating block was used to heat the chamber inlets to 60°C for all stock solutions exceeding 1 mg/mL. Nevertheless, the ability to form DQAsomes with nanometer size was restricted to a CM2 concentration of up to 3 mg/mL (Figure 5.6C). Previous work has also shown that an increase in amphiphile concentration can lead to the formation of larger vesicles (Henriksen-Lacey et al., 2011a). In this study, the lipid film hydration method was used for manufacturing vesicles of a larger size by decreasing the amount of rehydration buffer. Ten-fold higher concentrated vesicles were manufactured, which resulted in an increase the size of the vesicles from initially 500 nm to 1.5 μ m. Studies also showed that the alteration of the hydration buffer furthermore increased the size to 2-3 μ m by addition of saline PBS buffer, which resulted in vesicle aggregation (Henriksen-Lacey et al., 2011a). Here, the movement of the liposomes to the lymph nodes was strongly related to the size of the vesicles, with small vesicles down regulating splenocyte proliferation rates and the vesicle size overall effecting the cell mediated immune response (Henriksen-Lacey et al., 2011a).

5.3.4 DQAsome stability and integrity upon manufacturing by microfluidics

Given the novelty of microfluidics-directed nanoprecipitation manufacturing of DQAsomes, the stability of the vesicles formed upon this method was verified over 5 hours and 8 days at two storage conditions (4°C and room temperature (RT)). The investigation of the vesicle stability was anticipated crucial for two reasons; the novelty of the manufacturing method and previous reported instability of DQAsomes (Weissig, 2015). DQAsomes were manufactured by microfluidics (FRR 1:3, TFR 2 mL/min) and kept under controlled temperature conditions throughout the stability study with no post-processing steps (e.g. dialysis) performed. Results (Figure 5.7) show the particle characteristics expressed as % compared to the vesicles directly after manufacturing, with an initial size of ca. 250 nm and a PDI of 0.35. No major effect to the particle size was noted upon storage for 5 hours (Figure 5.7A) and 8 days (Figure 5.7B), independent of storage temperatures. A slight increase in PDI at 1h was noted (Figure 5.7A); however, this remained overall insignificant throughout the 8-day study (Figure 5.7B). Throughout the study, the zeta potential remained highly cationic, ranging between 25 – 35 mV (Figure 5.7C).

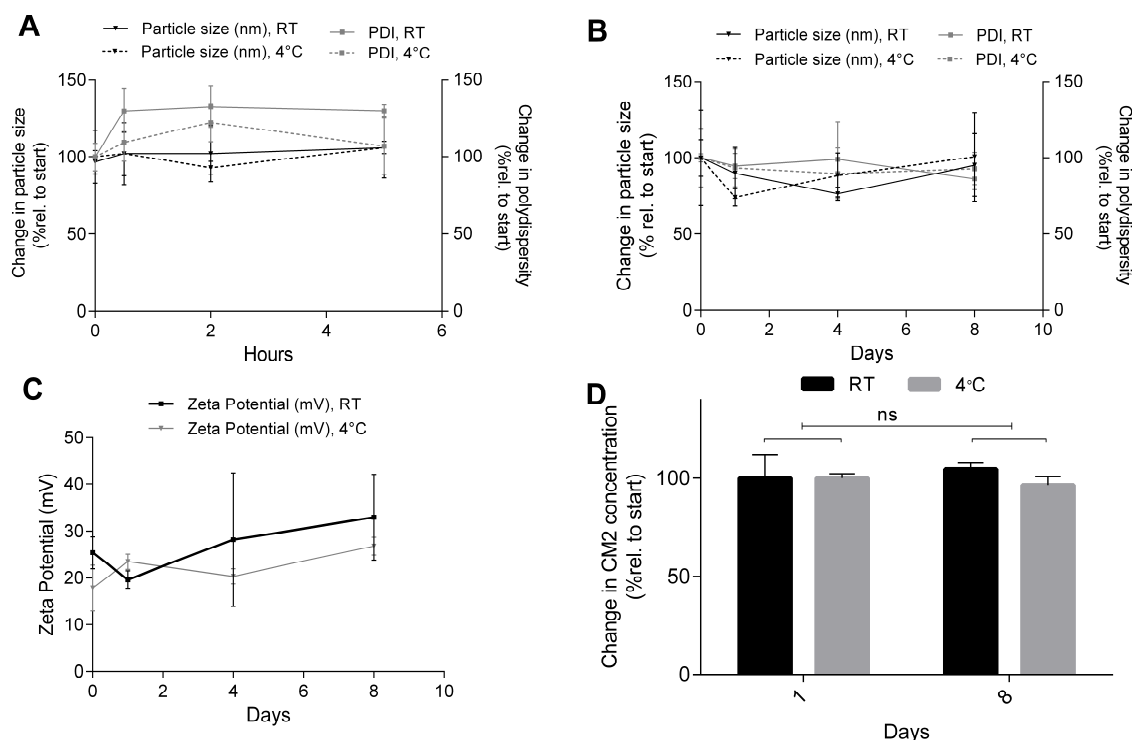


Figure 5.7: Effect of storage temperature to DQAsome size and PDI over A) 5 hours, B) 8 days and respective effect to C) zeta potential. D) Effect of storage temperature on stability of the CM2 compound over 8 days. RT = room temperature. Results denote mean \pm SD of 3 separate batches.

In addition to the physical stability of the vesicles, the CM2 component was simultaneously quantified. Results indicated a complete recovery of the CM2 component in the formulations (above 95%), indicating no physical degradation or unspecific adsorption of the CM2 compound, independent of the storage conditions (4°C and room temperature; Figure 5.7D).

The manufacture of the vesicles by microfluidics resulted in a residual solvent amount (here methanol) that may impact on the stability of the vesicles if not removed prior to storage. Whereas dialysis was used as a simple post-processing method for removal of residual solvent (e.g. in Chapter 4), dialysis attempts resulted in poor retention of the vesicles in the dialysis bag based on loss of the CM2 compound into the dialysis buffer (results not shown). Stability problems have been reported in literature, where the vesicle disintegration over several hours has been linked to the chemical structure of the dequalinium molecule (Weissig, 2015). Published stability data confirmed vesicles integrity up to 96 hours only (Weissig et al., 1998). The critical vesicle concentration of dequalinium ranges between 3-7 mM and especially upon dilution loss of colloidal structures has been reported (Weissig, 2015). Concentrations below 3 mM did not result in vesicle formation and only chemical modifications of the amphiphiles impacted

the stability (Weissig and Torchilin, 2001). Here, concentrations ranged within 0.7 mM to 6.1 mM, allowing for vesicle assembly and presumably loss of colloidal structure upon dilution in the dialysis method at concentrations below 3 mM. Poor chemical stability along with formation of micelles upon dilution might be associated with poor retention throughout a dialysis procedure. Nevertheless, data here showed that DQAsomes manufactured by microfluidics remain stable over the course of 8 days, no significant changes in population characteristics and stability.

5.3.5 DQAsome purification and recovery upon manufacturing by microfluidics

Following the verified short-term stability in the presence of residual solvent, an additional post-processing purification method was considered. Given that dialysis was not applicable for DQAsome purification, a method based on spin columns was investigated. A spin column process was found applicable for concentration and removal of residual solvent for liposomes (data not shown), and the same method was explored for the applicability of DQAsome purification. This method relies on membrane separation by centrifugal forces, often used in post processing of colloids or proteins (Chapman, 2005). Here, the spin column process was related to particle characteristics, along with possible purification ability by membrane retention.

The ability of the membrane to retain the DQAsomes was tested and the CM2 component was quantified before and after the spin column process in the retentate (concentrate) and permeate (filtrate) respectively. The spin column process acts as a dead end filtration process, a separation process based on a membrane. The concentrate was recovered on the retentate side of the membrane, containing components too large to penetrate through the membrane. In contrast, the filtrate contains the wash-through part, components small enough to penetrate through the membrane pores.

Both, concentrate and filtrate were recovered independently after membrane separation by aids of centrifugal forces. Unfortunately, the CM2 component permeated through the membrane, indicative of a failed retention (30kDa and 2kDa cutoff, polyethersulfone membrane) (Figure 5.8A). The anticipated membrane separation process was based on the retention of the DQAsomes by the membrane and removal of solvent residues into the permeate. Based on detection of the CM2 compound in the filtrate, this anticipated purification process failed. Despite the lower cut-off membrane, the DQAsomes were not retained and were found present in concentrate as well as filtrate side (Figure 5.8A).

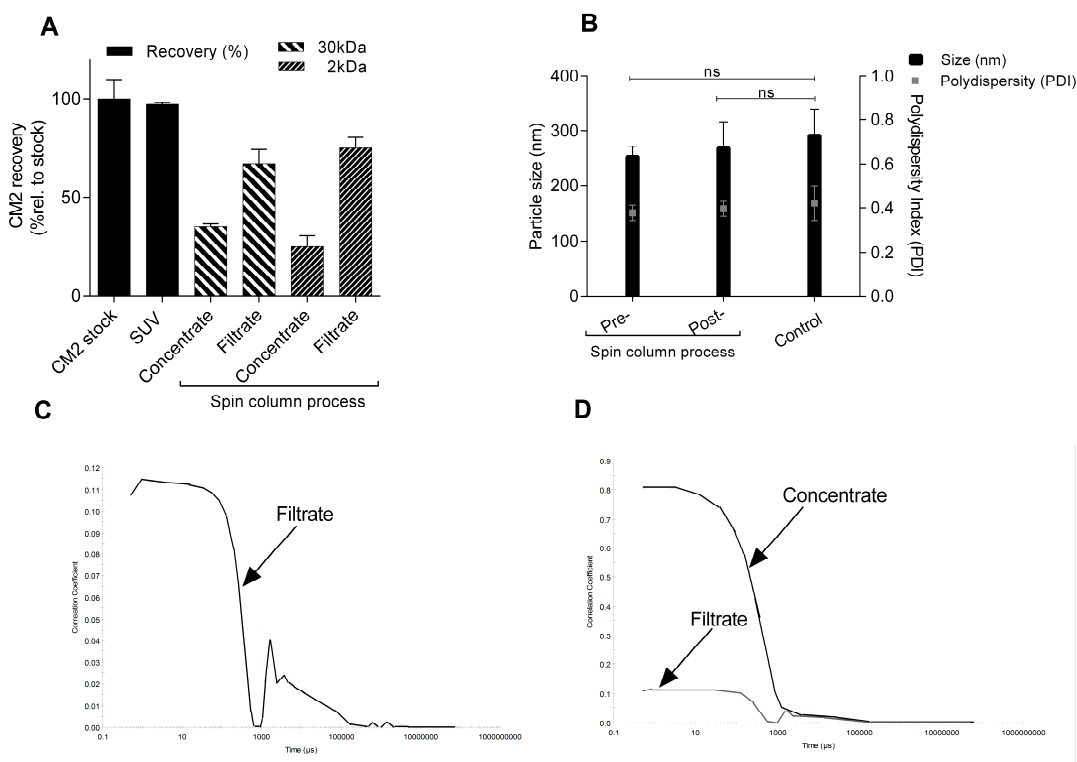


Figure 5.8: A) Effect of a spin column process on vesicle characteristics. B) Effect of membrane cutoff to recovery of the CM2 compound. Results denote mean \pm SD of 3 separate batches and purification cycles. Correlogram of the filtrate C) in comparison to the concentrate side of the spin column membrane D).

DQAsomes were recovered on the retentate side of the membrane and particle characteristics compared to the vesicle characteristics before centrifugation remained around 250 nm, with a PDI around 0.4 ($p > 0.05$), 2kDa cutoff, polyethersulfone membrane. The control was vesicles manufactured by the microfluidics method that did not undergo a centrifugation process (Figure 5.8B). Despite the centrifugation forces applied, the vesicles on the retentate side remained intact. Nevertheless, the quantification of CM2 revealed its presence in the concentrate as well as the filtrate (Figure 5.8A), with majority of the CM2 recovered in the filtrate, indicating that the membrane failed to retain the vesicles despite variation in membrane cutoff. Given that the permeate did not show the presence of colloids (as revealed in DLS by poor correlation function, Figure 5.8C and D), the centrifugation process was found to physically disrupt the vesicles once passed through the membrane. Hence, the CM2 amount detected in the permeate was not related the actual vesicles permeating the membrane, which instead broke down into the initial CM2 component once passed through the membrane pores.

Depending on the DQA concentration and manufacturing temperatures, computer simulations have revealed a variety of possible DQAsomes confirmations, including micelles, vesicles, cylinders, disks and planar aggregates, U-shaped and stretched confirmation (Gregoriadis, 2007; Grinberg et al., 2008; Weissig and Torchilin, 2001). This flexibility of the CM2 compound may have resulted in conformational changes throughout the centrifugation process and membrane penetration, resulting in poor retention of the vesicles. The filtration membranes (2 kDa and 30 kDa) failed to retain DQAsomes and any concentration attempts were unsuccessful. Limited stability in an aqueous environment and upon concentration has been previously reported (Weissig, 2015). This was related to the structural instability of the DQAsomes, which may have been challenged here by additional centrifugal forces applied. In response to this data, the CM2 component has been chemically altered to tackle the limited stability upon concentration and dilution in aqueous medium. This work is on-going.

5.3.6 *In-vitro* transfection efficiency of DQAsomes

In addition to evaluating the microfluidics-manufactured vesicles regarding their particle characteristics and stability, their biological activity was studied *in-vitro*. The ability of DQAsome-directed gene transfer was described and patented by Weissig in the 1990s (Weissig et al., 1998); numerous researchers have since used dequalinium as a delivery system due to its selectivity for organelle directed uptake, which is well reported in literature (Christman et al., 1990; Steichen et al., 1991; Vercesi et al., 1991; Weiss et al., 1987). Therefore to consider the biological activity of microfluidics-manufactured DQAsomes, the system were tested as a non-viral delivery vehicle of genetic material using two pDNA structures; a luciferase plasmid (gWiz-Luc) and a GFP plasmid (pEGFP-C3) (Figure 5.9).



Figure 5.9: Two plasmids used in the *in-vitro* study evaluating the transfection potential of the microfluidics-manufactured DQAsomes. Structures obtained from www.aldevron.com.

The *in-vitro* transfection was tested with DQAsomes manufactured from different CM2 concentrations, linking to above study that higher concentrated vesicles may be manufactured (Figure 5.6). The transfection efficiency achieved by microfluidics-manufactured DQAsomes yielded ca. 70% of that achieved by cationic liposomes, with no difference between the vesicles manufactured at different CM2 stock concentrations ($p>0.05$; Figure 5.10). As the CM2 to DNA ratio and the DQAples to cell ratio was kept constant during the transfection studies, these results emphasize that vesicles can be manufactured at a higher concentration, without impeding on their *in-vitro* activity. Given that vesicles manufactured at a stock concentration of 5 mg/mL showed a significant increase in size (Figure 5.6), the transfection efficiency here was found to be independent of the vesicle characteristics. In contrast to the results in Chapter 4, the organelle-targeted transfection was found independent of the vesicle size, anticipated as the main reason behind the difference to the nucleus-directed transfection (Weissig and Torchilin, 2001). Overall, transfection achieved by the vesicles manufactured by microfluidics was higher compared to vesicles formed by sonication ($p<0.05$), which may be related to suboptimal vesicle characteristics (Figure 5.4).

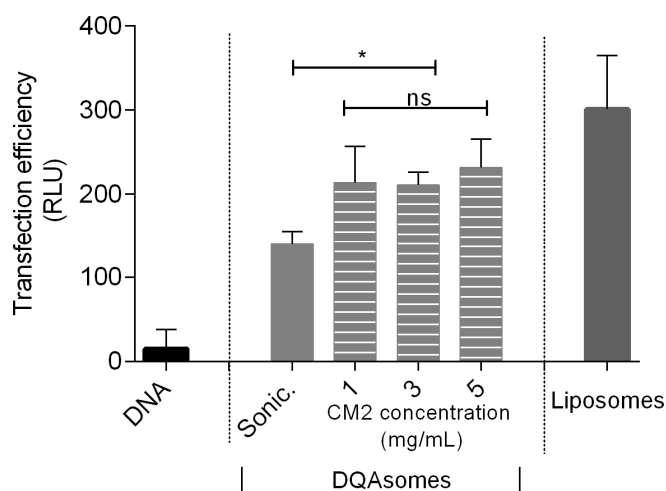


Figure 5.10: Transfection efficiency (RLU, relative light units) as obtained by microfluidics-manufactured DQAsomes (FRR 1:3, TFR 2 mL/min), sonicated DQAsomes (30 min, amplitude 5) as compared to cationic liposome transfection efficiency (DOPE-DOTAP, FRR 1:5, TFR 1.5 mL/min). Significance between data is against the transfection efficiency achieved by vesicles manufactured in the sonication method ($*p<0.05$). Results denote mean \pm SD of 3 separate transfections.

In addition to the transfection studies performed with a luciferase-encoding plasmid, a GFP-encoding plasmid was used for a visual detection of protein expression. Figure 5.11 shows the expression of the GFP protein, delivered by microfluidics-manufactured DQAsomes post transfection. Images verified the expression of a fluorescent protein

in-vitro (Figure 5.11A, B). With the fluorescence signal corresponding to the correct conformation and full protein folding, the protein has been found small enough (29kDa) for secretion into the medium (Tanudji et al., 2002) as seen in images obtained in this study.

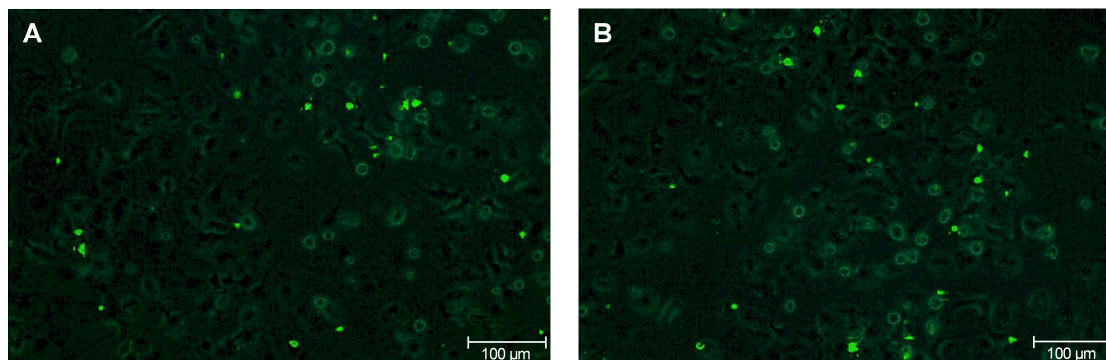


Figure 5.11: A, B) Confocal microscopy images showing the *in-vitro* expression of the fluorescent protein in transfected COS-7 cells.

The *in-vitro* transfection was performed with a COS-7 cell line, a cell line often used in liposome and DQAsome mediated transfection (Jain et al., 2012), allowing for a comparison to previous published work. Here, the CM2 component was the only amphiphile used for the formation of DQAsomes. To improve transfection efficacy, Jain et al. have shown that the inclusion of a helper lipid like DOPE (as used within the liposome formulation) enhanced the *in-vitro* transfection efficiency >100-fold compared to dequalinium alone, using a luciferase-encoding plasmid (Jain et al., 2012). Nevertheless, *in-vitro* transfection by DQAsomes formed by microfluidics was promoted with both plasmids tested, indicating the biological activity of the vesicles manufactured by microfluidics.

Weissig and co-workers first described the application of DQAsomes as transfection vehicles (Weissig et al., 2000; Weissig et al., 1998). DQAsomes were found to bind DNA and act as transfection vehicles with selectivity for carcinoma cells and targeted accumulation in the mitochondria (Christman et al., 1990; Steichen et al., 1991; Vercesi et al., 1991; Weiss et al., 1987). Lipophilic cationic compounds preferentially localise in mitochondria due to the electric potential of the mitochondrial membrane, making DQAsomes an ideal intramitochondrial gene delivery system (Johnson et al., 1981). Enhanced by the fact that carcinoma cancer cells have a higher negative mitochondrial surface potential, DQA is preferentially taken up, accumulated and also retained intramitochondrially (Berlin et al., 1998; Summerhayes et al., 1982). The similarity between a mitochondrial and a bacterial cell wall allows DQAsomes not only to bind and deliver DNA, but also treat bacterial infections. Opposed to cationic bola-

amphiphiles, cationic lipids (Chapter 4) have been well described for the delivery of genetic material into the nucleus, where the protein is expressed in the cytoplasm allowing only for an indirect mitochondrial targeting. The delivery of genetic material by DQAsomes however is a direct method, where the DNA is directly delivered and followed by transcription and translation in the organelle itself. This direct delivery takes into account that the mitochondrial genetic code differs by four codons from the universal code (Barrell et al., 1979). Additionally, the proteins encoded by the mitochondrial DNA are highly hydrophobic and hence their transport into the organelle is unlikely; in fact, the hydrophobicity of mtDNA encoded proteins has been reported as a restricting factor for the transport from the cytoplasm into the organelle (Owen Iv et al., 2000). Following, a synthesis at the location of function is highly desired (Scheffler, 1999). The here presented work showed that such organelle-targeted nanoparticles may be manufactured in a reproducible and high-throughput method based on nanoprecipitation in a chaotic advection micromixer. Work in this chapter additionally verified that DQA-vesicles manufactured by microfluidics deliver genetic material intracellular, allowing for protein expression and confirming that the biological activity has not been compromised by the method of manufacturing.

5.4 Conclusion

This work verified the suitability of the microfluidics-directed nanoprecipitation method for the manufacturing of DQAsomes, assembled from bola-amphiphiles with delocalized charge centres. Overall, vesicles manufactured in the microfluidics method showed lower variation and better correlation plots for particle size measurement, aligning with ideal intercept range (Chapter 3). Results suggested the presence of a larger sub-population between 2-4 μm , which may have resulted due to component specific aggregation behaviour and was found independent of the method of manufacturing. The FRR was evaluated as a crucial variable to influence the resulting size of the vesicles, which were shown to remain stable over 8 days. DQAsomes, as manufactured here by microfluidics, act as non-viral vectors, highly applicable in gene therapy procedures. Several diseases have been linked to mtDNA deficiencies (Taylor and Turnbull, 2005) including alzheimers, dementia, Parkinson's disease, and the targeted delivery of genetic constructs may treat those diseases associated with mitochondrial gene deficiencies (Weissig, 2015; Weissig and Torchilin, 2000). DQA is currently used in tumour growth inhibition, by specific destruction of tumour mtDNA, related to loss or delay of mtDNA function (Berlin et al., 1998). The variety of potential application necessitates a robust and reproducible manufacturing technique, where DQAsome manufacturing by microfluidics has been evaluated in this chapter. The

microfluidics method generated size-controlled DQAsome vesicles in a robust process setting, vesicles were stable, and had *in-vitro* activity. Nevertheless, the chemical instability was noticed throughout concentration and purification techniques employed; an issue currently addressed by Procarta Biosystems Ltd.. Results here further emphasize on the usefulness of the microfluidics-directed nanoprecipitation method. The high-throughput method allows screening over a range of concentrations and settings in a relative short period of time, compared to the time associated with lipid-film hydration and sonication. Relating this work to the previous chapter, results show that the microfluidics-method is not limited to “standard” phospholipids (Chapter 4) but further amphiphilic compounds, here bola-amphiphiles with delocalized charge centers, can be used to yield nanoprecipitated vesicles, highlighting on the versatility and applicability of respective method. Recent work based on DQAsomes showed that other than the amphiphilic compounds itself, lipophilic drugs are often required to be associated within the lipophilic compartment of a vesicle (Zupančič et al., 2014). Following, the next chapter focused on the encapsulation of lipophilic compounds within the nanoprecipitation method.

Chapter 6

Microfluidics-controlled solubilisation of a low-solubility drug and scale-up considerations



* Structure obtained from sigmaaldrich.com

Papers relating to this chapter:

Kastner E., Verma V., Lowry D. and Perrie Y. (2015). Microfluidic-controlled manufacture of liposomes for the solubilisation of a poorly water soluble drug. *International Journal of Pharmaceutics*, 485(1), 122-130.

Kastner E., Ou K., Ramsay E. and Perrie Y. Scale-up considerations for the microfluidics-directed manufacturing of liposomes (in preparation)

6.1 Introduction

Of all new chemical entities in discovery, currently more than 40% have limited aqueous solubility and subsequently related bioavailability issues (Savjani et al., 2012; Williams et al., 2012). Given the amphiphilic structure of lipids, liposomes are well placed as solubilisation agents for drugs with low aqueous solubility. The encapsulation of low solubility drugs into the bilayer of liposomes is well described (Allen, 1998). In addition to offering solubilisation in an aqueous media, liposomes can offer a drug protection from degradation, control over its pharmacokinetic distribution profile and improved therapeutic efficacy. The drug encapsulation in lipid bilayers has been linked to a range of factors including the properties of the drug, the composition of the liposomes, the lipid choice and concentration (Ali et al., 2010; Ali et al., 2013; Mohammed et al., 2004). Besides research focusing on the optimisation of formulation parameters on the application of liposomes as solubilising agents, more focus may be required into the manufacturing process itself. Microfluidics-based methods have been described for the manufacture of liposomes and lipid nanoparticles (van Swaay, 2013) and previous work investigated the manufacturing of size-controlled liposomes as transfection agents (Chapter 4).

6.2 Aim and Objectives

The aim of this chapter was to investigate the microfluidics-based nanoprecipitation method for simultaneous liposome manufacturing and drug encapsulation. To achieve this, the drug encapsulation process was incorporated into the vesicle assembly by incorporation of a low-solubility model drug into the solvent phase (Figure 6.1). The ability of the method to encapsulate a low solubility model drug was evaluated and compared the drug encapsulation achieved by a top-down method based on sonication. The effect of flow rates, ratios and drug concentration was related to the efficiency of drug encapsulation, which was verified over a stability period of six months. In addition, the developed microfluidics-directed vesicle manufacturing method underwent a scale-up study, by a process transfer into a design with an increased channel diameter. Final scalability studies were undertaken at Precision Nanosystems Inc. in Vancouver, CA, where the process of drug encapsulation was evaluated in a scale-out system based on planar chip parallelisation.

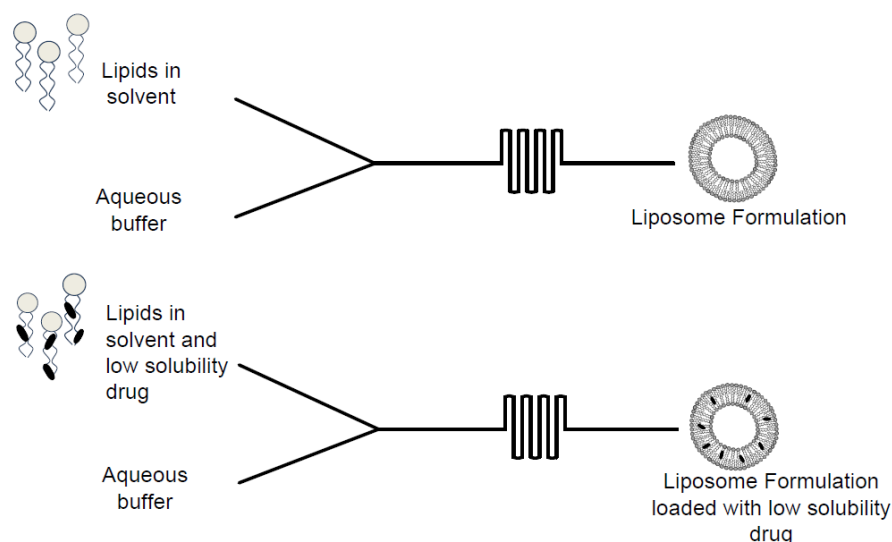


Figure 6.1: Schematic depiction of the proposed drug encapsulation methodology by incorporation of a low solubility drug into the solvent stream during the microfluidics-directed nanoprecipitation reaction of liposome formation.

6.3 Results and Discussion

6.3.1 Influence of the flow rate ratio of the aqueous and solvent streams on particle characteristics

Similar to investigations in previous chapters (Chapters 4 and 5), the rate of mixing as well as the ratio of aqueous to solvent stream was anticipated as crucial factors in the formation of here neutrally-charged liposomes. Liposomes were prepared from PC and Cholesterol (16:4 molar ratio, 8:1 w/w) (based on previous studies; Ali et al., 2010) at different total flow rates (TFR) and flow rate ratios (FRR), ranging from 2 to 6 mL/min and 1:1 to 1:5 without loaded drug and the vesicle size, polydispersity (PDI) and zeta potential (ZP) were measured.

The largest size of around 450 nm was linked to a low FRR (1:1), where the increase of the aqueous content FRR resulted in smaller liposomes (around 40 - 50 nm) at constant flow rates of 2 mL/min (Figure 6.2A). Liposome sizes remained between 40-55 nm ($p > 0.05$) within a FRR 1:2 to 1:5, with no notable influence on resulting ZP (Figure 6.2A). Similar to previous studies (Chapters 4 and 5), the PDI was found to increase significantly ($p < 0.05$) with increasing aqueous FRR to a maximum of 0.4, (Figure 6.2B). In contrast, the sizes obtained by the top-down sonication method were significantly ($p < 0.05$) larger, remaining above 150 nm for all sonication times tested, with the lowest PDI obtained via sonication coinciding with the largest PDI obtained by microfluidics (around 0.4); (Figure 6.2 C, D respectively). ZP remained independent of sonication times tested, coinciding with the ones obtained in the microfluidics method (Figure 6.2A and C).

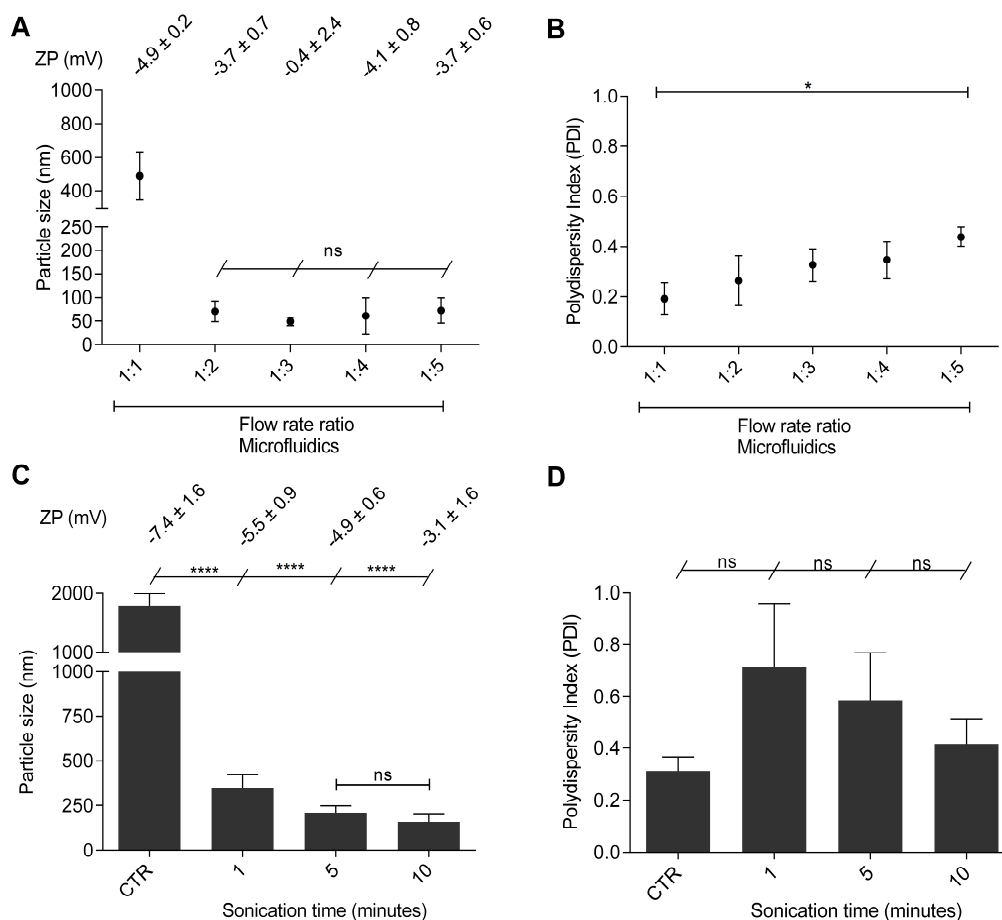


Figure 6.2: Particle size, polydispersity and zeta potential of empty liposomes. The effect of increasing flow rate ratio (FRR) in the microfluidics method on A) particle size and zeta potential and B) polydispersity. Where shown, significance between data is against results of the FRR 1:1 (* $p < 0.05$). The effect of increase in sonication time on C) particle size and zeta potential and D) polydispersity. Where shown, significance between data is against the control (**** $p < 0.0001$). ns, not significant; CTR, control. Results denote mean \pm SD of at least 3 separate batches.

The impact of FRR on vesicle size was in agreement with previous work (Chapter 4 and 5) showing that the increase in FRR reduced the resulting size of the liposomes (Jahn et al., 2010; Zook and Vreeland, 2010). The SHM design has been developed to primarily enhance the diffusion and advection due to alterations of the fluid flow profile by the herringbones in the floor of the mixing chamber (Stroock et al., 2002). The mixing process is further enhanced by high aqueous content FRR, which decrease the solvent concentration drastically (Zook and Vreeland, 2010). With less solvent available for solubilisation of the hydrophobic chains, the closure time for the vesicle decreases. Here, the mixing rate of the lipid phase with the buffer was enhanced at high solvent to aqueous ratios, where the differences in fluid velocities between both streams decreased the effective diffusion layer thickness of the solvent stream in the mixing profile. In addition, reduced width of the solvent stream in the mixing profile

further diminished the diffusion distances. Decreased closure time for the vesicle leads to the formation of smaller vesicles at higher FRR (Zook and Vreeland, 2010). The nanoprecipitation-directed vesicle formation reported a correlation between FRR and particle size for liposomes composed of 1-palmitoyl, 2-oleoyl phosphatidylcholine (POPC), cholesterol and the triglyceride triolein; a higher aqueous content FRR was linked to overall smaller particles, ranging from 140 nm to 40 nm and triglyceride emulsions between 20 – 50 nm in size with nonpolar cores (Zhigaltsev et al., 2012). The authors noted that the higher aqueous content FRR employed decreased the particle fusion (Ostwald ripening), which lead to the formation of smaller particles (Zhigaltsev et al., 2012). The link between FRR and PDI, as seen in earlier Chapters (Chapter 4 and 5), may be a result of increased dilution at higher FRR, which reduces the rate of diffusional mixing within the micromixer. Given the correlation between diffusion to concentration, the decreased lipid concentration reduced the rate of diffusion at higher aqueous content FRR, which lead to partly incomplete nucleation and a lower rate of liposome formation inside the micromixer (Balbino et al., 2013b). Overall, these findings demonstrated that the liposome size plateaued at a FRR greater 1:2, which suggested that the smallest vesicle size achievable was 40-50 nm.

6.3.2 Influence of flow rate on throughput and particle characteristics

Besides the FRR, the effect of the TFR on particle characteristics was studied and linked to the overall method-throughput. Here, the TFR was increased 3-fold from 2 to 6 mL/min whilst maintaining the ratio between solvent and aqueous stream constant (1:3). Liposome size was independent of the applied flow rate, with no significant change in vesicle size, PDI and ZP ($p>0.05$) throughout the TFR alterations (Figure 6.3).

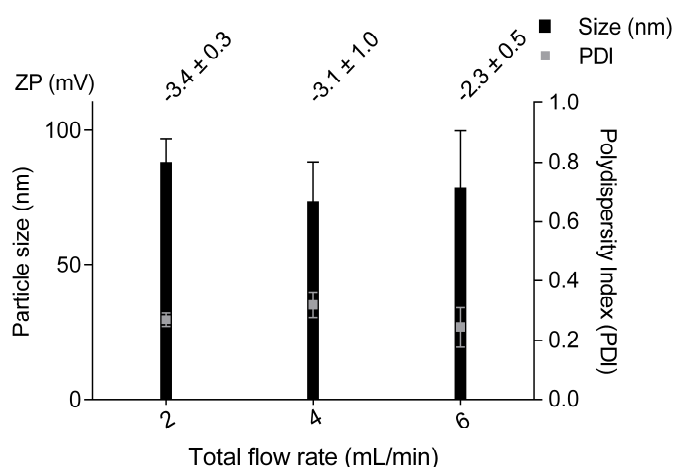


Figure 6.3: The effect of increasing total flow rate (TFR) on vesicle size, polydispersity and zeta potential. Results were not significant compared to the vesicle characteristics obtained at 2 mL/min. Results denote mean \pm SD of 3 separate batches.

Liposome characteristics were maintained with increasing TFR, which demonstrated the suitability of microfluidics manufacturing for a high-throughput bench-top liposome manufacturing. Results further confirmed previous finding (Chapter 4) with the FRR as the most crucial variable impacting on liposome size, which has been demonstrated with other formulations (Balbino et al., 2013a; Balbino et al., 2013b; Jahn et al., 2007; Jahn et al., 2004). Nonetheless, the FRR is directly linked to the resulting vesicle concentration, where an increase in FRR will inevitably dilute the final formulation manufactured. Liposome concentration processes have been proposed, relying on either filtration (Pattnaik and Ray, 2009), chromatography (Ruyschaert et al., 2005) or centrifugation, with all methods adding processing time. In order to circumvent this additional step, the lipid concentration was increased according to the FRR chosen. Results showed that liposomes up to a 6-fold higher concentration could be manufactured, with no significant influence to their characteristics at FRR of 1:3 and 1:5 compared to the standard lipid concentration (Figure 6.4A, B). However, the two-fold increase in lipid concentration did result in a significant ($p < 0.05$) decrease in vesicle size at a FRR of 1:1, which may be linked to the low aqueous content FRR, where an increase in lipid concentrations may affect the particle fusion, which lead to the formation of smaller particles (Zhigaltsev et al., 2012).

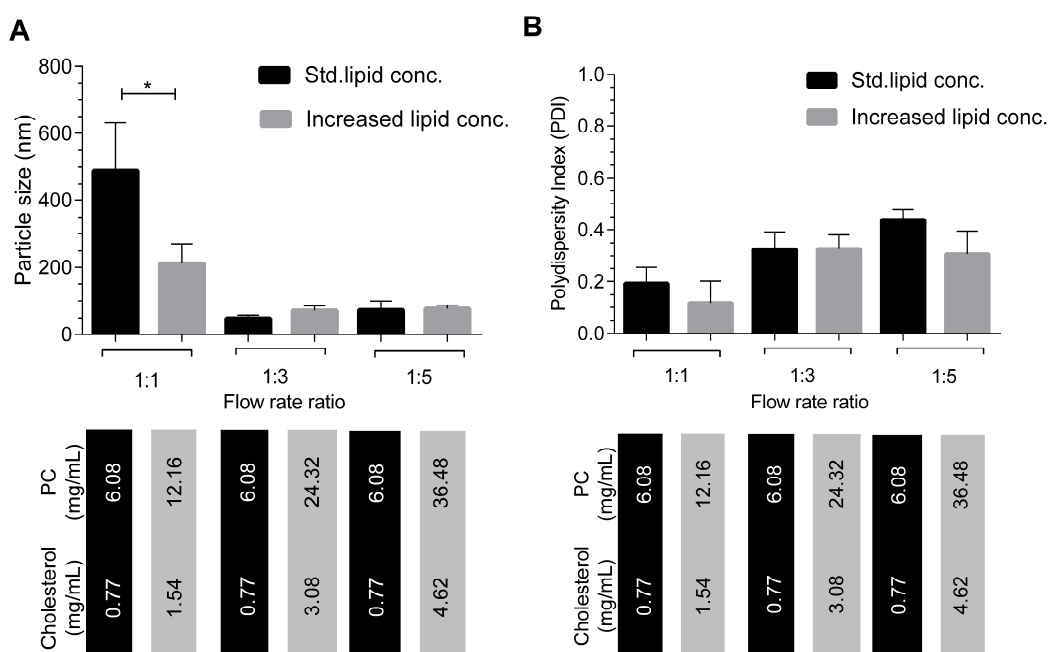


Figure 6.4: The effect of increased lipid concentration on A) vesicle size and B) polydispersity for the standard lipid concentration and increased lipid concentrations. The lipid concentration is shown in the table below the graph, which was tailored to the FRR. Where shown, significance between data is against results of standard lipid concentration ($*p < 0.05$). Results denote mean \pm SD of 3 separate batches.

Based on the advantage of diffusional mixing, the final liposome concentration could be increased according to the FRR in the method, with minimal effects on vesicle characteristics (Figure 6.4). This method allowed for manufacturing vesicles at a higher concentration, circumventing time intensive post-processing concentration techniques. In comparison to the microfluidics-counterpart, the flow-focusing method, dilution factor (due to flow ratios chosen involved in the SHM method) are overall lower, which can reach up to 60 in the flow focusing method (Jahn et al., 2010; Jahn et al., 2007; Jahn et al., 2004).

6.3.3 Drug loading studies: The effect of drug encapsulation by the liposome manufacturing method

In addition to the particle characteristics studied, the method was evaluated for its ability to produce liposomes as solubilising agents by assessing the loading capacity. A low-solubility model drug, propofol, was included in the solvent stream while liposomes were manufactured at a FRR of 1:3 and a TFR of 2 mL/min, based on previous studies (Figure 6.2, 6.3). Initially, the drug loading was examined as a function of propofol concentration in the solvent stock, which ranged from 0.5 to 3 mg/mL. The propofol concentration in the solvent stream strongly influenced the resulting particle characteristics; a particle size of ~50 nm and a low PDI was observed at a propofol concentration of 0.5 and 1 mg/mL (Figure 6.5A, B), which matched the characteristics seen at same TFR/FRR without the drug incorporated in the process (Figure 6.2A, B). The highest propofol concentration of 3 mg/mL in the solvent stream increased particle size and PDI notably to ca. 600 nm and 0.8 respectively (Figure 6.5A, B). Drug loading was highest at a propofol concentration of 1 mg/mL and reduced when the initial propofol concentration increased to 3 mg/mL (Figure 6.5C). This suggests a saturation or destabilisation at higher propofol concentrations (drug-to-lipid ratio 1.72 mol/mol). Propofol encapsulation (mol%) in liposomes was found independent of the FRR tested, ranging from 1:1, 1:3 and 1:5 and remained at approximately 50 mol% ($p > 0.05$), Figure 6.5D. In comparison to the sonication method, drug loading was overall significantly higher ($p < 0.0001$) in the microfluidics method (Figure 6.5D). The recovery of the drug was reduced at a propofol concentration of 3 mg/mL in the solvent stream, with the lowest recovery of 67% corresponding to the FRR of 1:5 (significantly lower than at the FRR of 1:1; $p < 0.01$; Figure 6.5E). The recovery of both, lipids and drug in the nanoprecipitation method was linked to the cost-effectiveness of the process and the importance of maintaining the lipid to drug ratio (here, 1 mg/mL propofol in solvent stream). The drug was recovered between 88 - 92% (Figure 6.5F), independent of the FRR ($p > 0.05$). The highest lipid recovery was at FRR of 1:1 and 1:3 (97% and 89%;

respectively; Figure 6.5F). Reduced lipid recovery of 79% at FRR 1:5 ($p < 0.05$), which suggested that higher FRR may impede lipid recovery due to enhanced dilution in the chamber (Figure 6.5E). Given that the lowest vesicle size was found at a FRR 1:3, the increase in FRR beyond that point would not benefit the formulation (size, PDI and drug encapsulation).

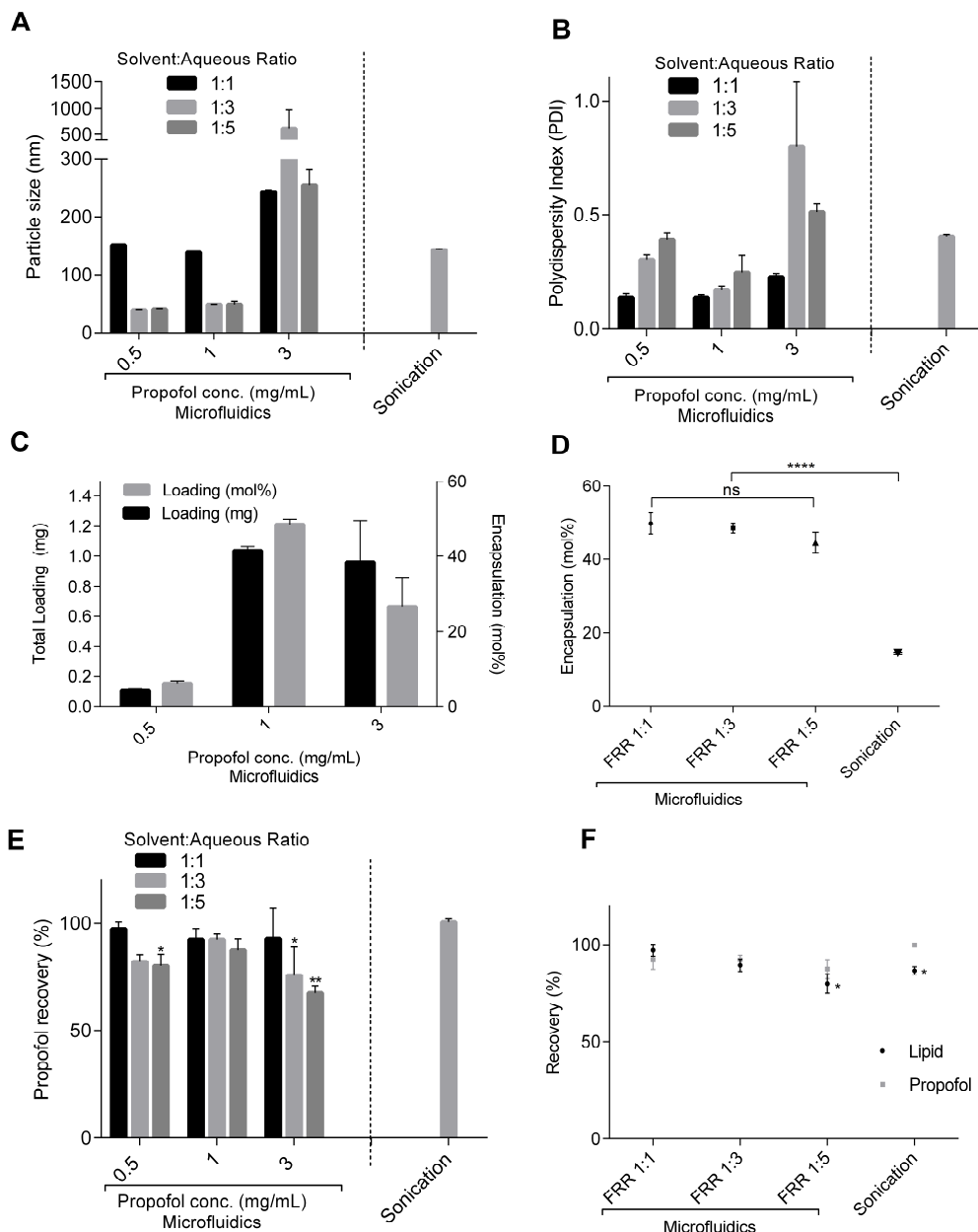


Figure 6.5: The effect of incorporating a low solubility model drug (propofol) at 0.5, 1 and 3 mg/mL in the solvent stream on A) particle size, B) polydispersity, at different FRR and C) total loading (mg) in 3 mL formulation and encapsulation (mol%). D) Direct comparison of the loading (mol%) at different FRR to the loading in the sonication method, achieved with a propofol concentration of 1 mg/mL in the solvent phase for both methods. Significance between data is against results of loading achieved in the sonication method (**** $p < 0.0001$). E) Recovery of propofol in the formulations at different FRR and in comparison to the recovery obtained in the sonication method. F) Recovery of lipids and propofol at different FRR employed (TFR 2 mL/min, 1 mg/mL propofol in solvent stream). Significance between data is against the recovery achieved in at the FRR of 1:1 (* $p < 0.05$, ** $p < 0.01$). Results denote mean \pm SD of 3 separate batches.

The larger vesicle sizes and PDI of vesicles manufactured with high drug concentrations in the solvent stream highlights the importance of screening for the ideal starting drug concentration, which was found to be best at 1 mg/mL and was independent of the FRR applied. Based on these results, all subsequent studies adopted a propofol concentration at 1 mg/mL in the solvent stream at a FRR of 1:3. Here, the control method was a top-down method involving lipid-film hydration and sonication. This control method was chosen for comparison to published data on the encapsulation of low solubility drugs into liposomes. Here, the encapsulation of ~20 mol% by the sonication method coincided with literature values (Ali et al., 2013). Overall, loading of the drug into the bilayer by the microfluidics method was significantly higher compared to the top-down method. The efficient mixing process, based on chaotic advection and diffusion in the channel, was anticipated as the key mechanism behind drug encapsulation, which was favoured and occurred simultaneously with the synthesis of the vesicles themselves. Overall, the propofol encapsulation reached ~50 mol%, which represented a total propofol amount of ~300 mg/mL in the final liposome formulation. In comparison to the published aqueous solubility of propofol (150 µg/mL), the chaotic advection nanoprecipitation method yielded a 2000-fold increase in solubility (Altomare et al., 2003). Following these recovery studies, a FRR of 1:3 was maintained throughout a long-term stability study. The here-developed quantification method verified that desired lipid to drug ratios were maintained and opposed to time intensive mass spectrometry, allowed for a quick quantification of any solids in the eluate with a lower volatility than the mobile phase (Moore et al., 2007).

The use of liposomes as solubilising agents for low solubility drugs is well explored (Ali et al., 2010; Ali et al., 2013; Mohammed et al., 2004); however this is the first time that the manufacturing method itself was linked to the overall increased amount of drug solubilised within the bilayer. The log P and molecular weight were often considered to impact on bilayer loading, where the molecular weight was shown as an important factor (Ali et al., 2013). With regards to the design of liposomes, a range of parameters were shown to impact the bilayer loading efficacy; the increasing the bilayer lipophilic volume (by adopting longer alkyl chain lipids within the liposomes) was linked to an increase in the loading ability of liposomal systems (Mohammed et al., 2004; Ali et al., 2013). Similarly, the lipid charge within the liposomal system was found important based on electrostatic repulsion of drugs with like-charged liposomal bilayers (Mohammed et al., 2004). Where the incorporation of cholesterol is known to stabilise

the liposomes, it was also shown to inhibit bilayer drug loading (Ali et al., 2010) due to the space-filling action of cholesterol in the liposomal bilayer.

Work also highlighted the current deficiencies in the SHM method. Firstly, reduced propofol recoveries at higher drug concentration (3 mg/mL) and reduced lipid recovery that a FRR of 1:5 (Figure 6.5E, F), which may be linked to the amount of waste volume collected prior to collecting the core of the sample. This effect can be countered by simply increasing the waste volume, making a process less economical. Also, drug or lipid adsorption onto the PDMS matrix might have occurred (Toepke and Beebe, 2006), turning significant at an overall lower amount of solvent present, as seen at a FRR of 1:5. The material affect has been addressed, by changing the chip material from PDMS to CoC (reference Precision NanoSystems Inc.).

6.3.4 Microscopy images for vesicle verification

To investigate the morphological nature of these vesicles, liposomes were studied using free fracture microscopy. Images taken by freeze fracturing electron microscopy verified the small unilamellar nature of vesicles manufactured by microfluidics, found in agreement with average sizes of the vesicle diameters obtained via dynamic light scattering (~40 nm), Figure 6.6A-D, with no notable difference in images obtained between empty and drug loaded vesicles manufactured by microfluidics (Figure 6.7A-D). Furthermore, an aqueous fluorescent dye, carboxyfluorescein (CF) was included in the aqueous phase in both methods, sonication and microfluidics. Particles were visualised by confocal microscopy after removal of any untrapped drug by dialysis. Vesicles manufactured showed bright green fluorescent cores, where particles produced by lipid film hydration/sonication (Figure 6.8A, B) acted as a control method and images verified the formation of liposomes in the microfluidics method (Figure 6.9A, B).

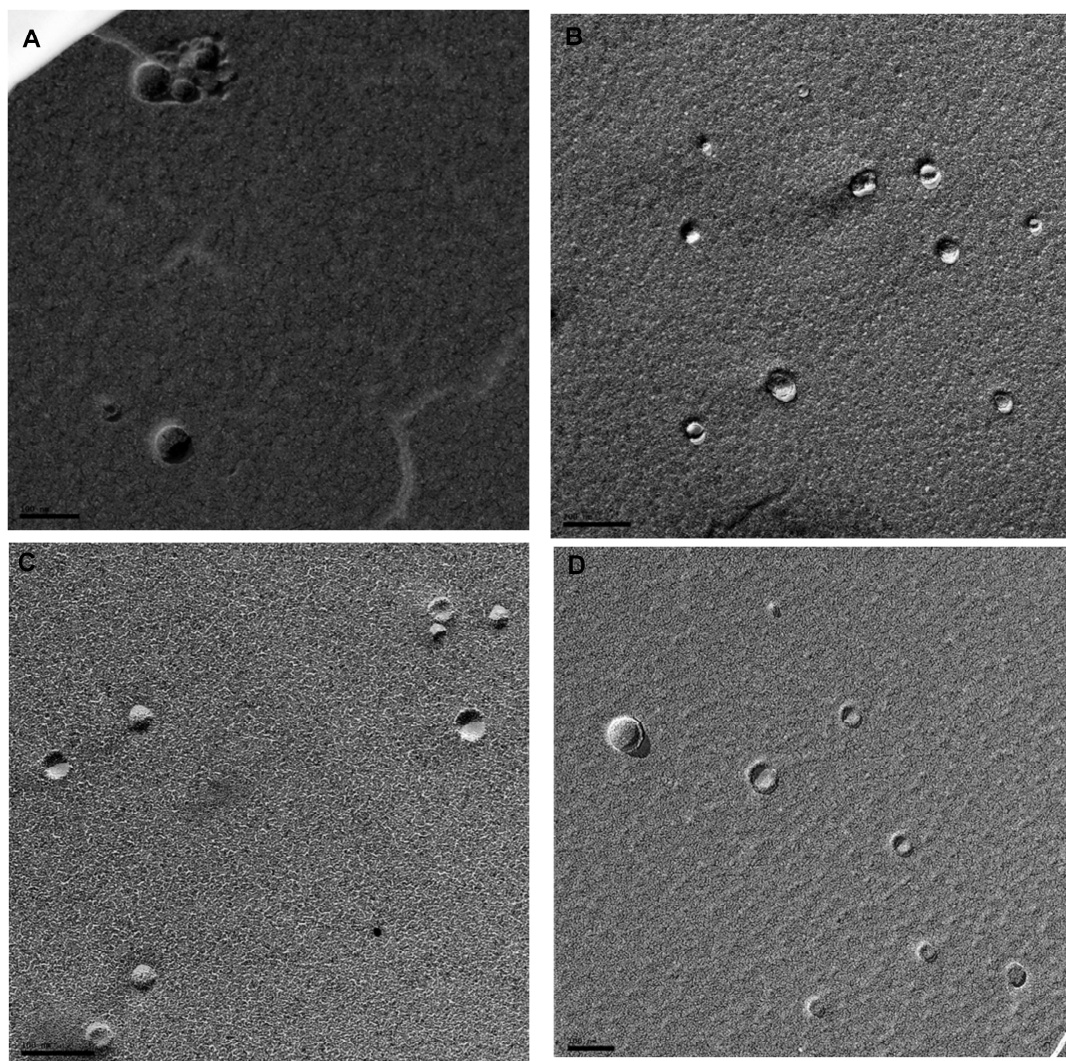


Figure 6.6: Freeze fracturing electron microscopy images (A-D) obtained of PC-Chol liposomes manufactured by microfluidics (TFR 2 mL/min, FRR 1:3).

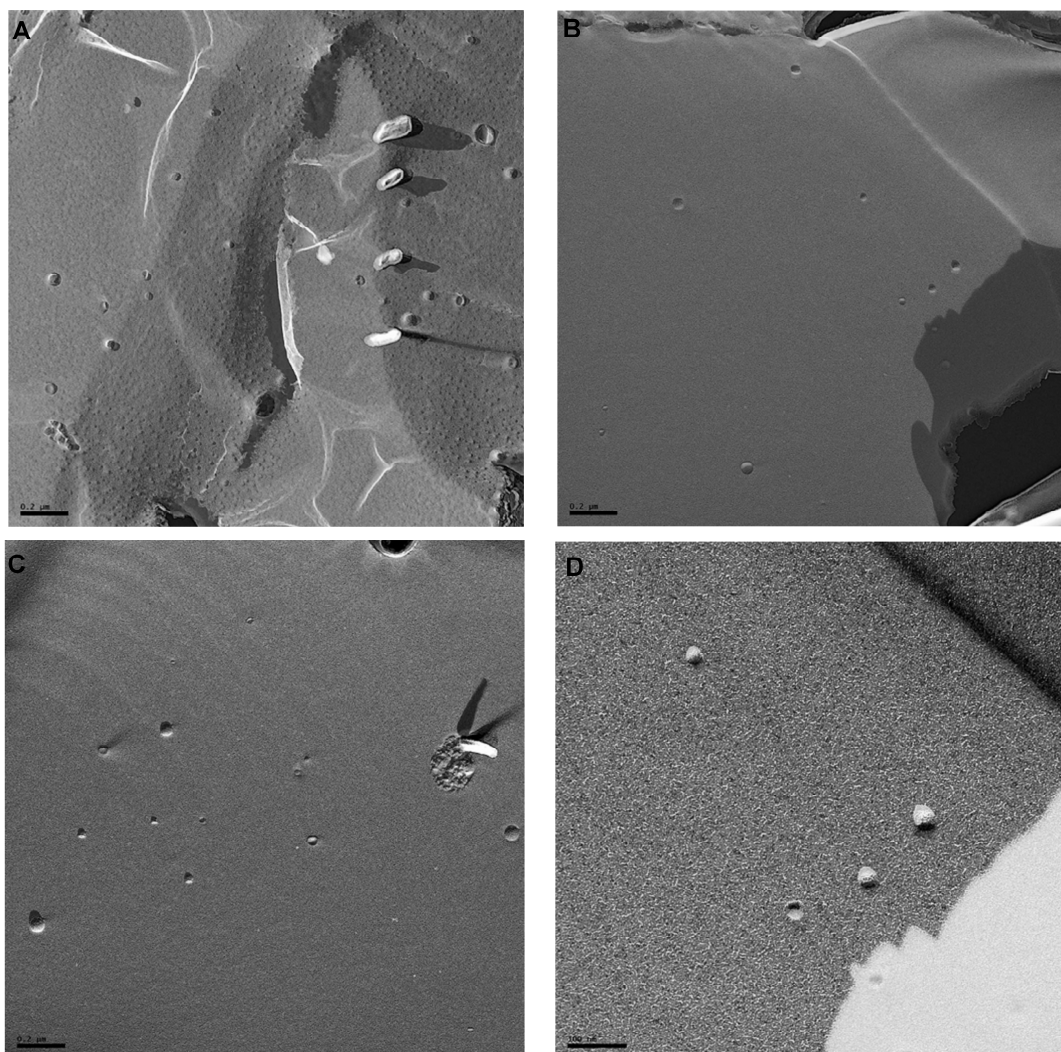


Figure 6.7: Freeze fracturing electron microscopy images (A-D) obtained of PC-Chol liposomes loaded with propofol manufactured by microfluidics (TFR 2 mL/min, FRR 1:3, 1 mg/mL propofol in solvent stream).

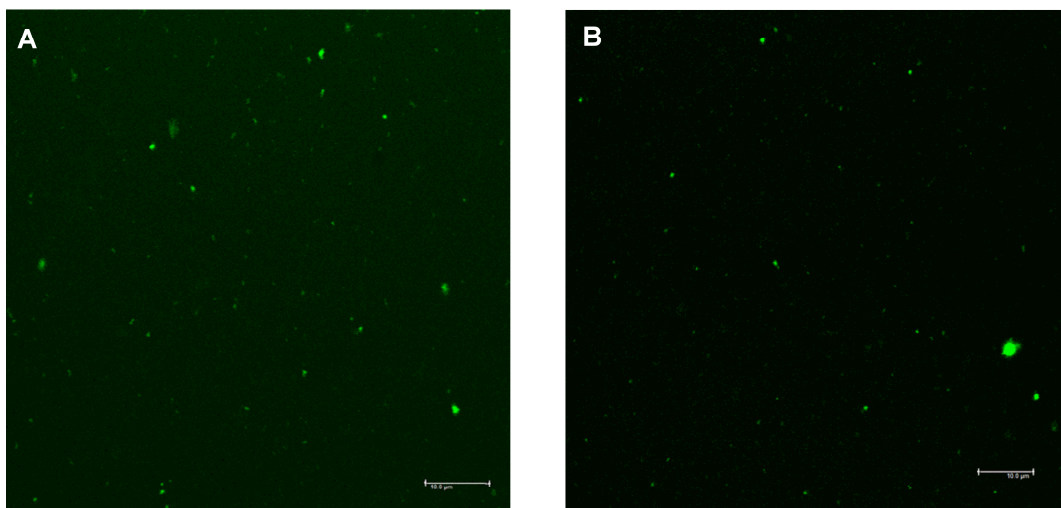


Figure 6.8: Images obtained by confocal microscopy showing liposomes manufactured by (A, B) lipid film hydration/ sonication, encapsulating the aqueous marker (carboxyfluorescein). Note that fluorescence spot size does not correspond to actual vesicle size as liposomes in this sample were below the optical resolution.

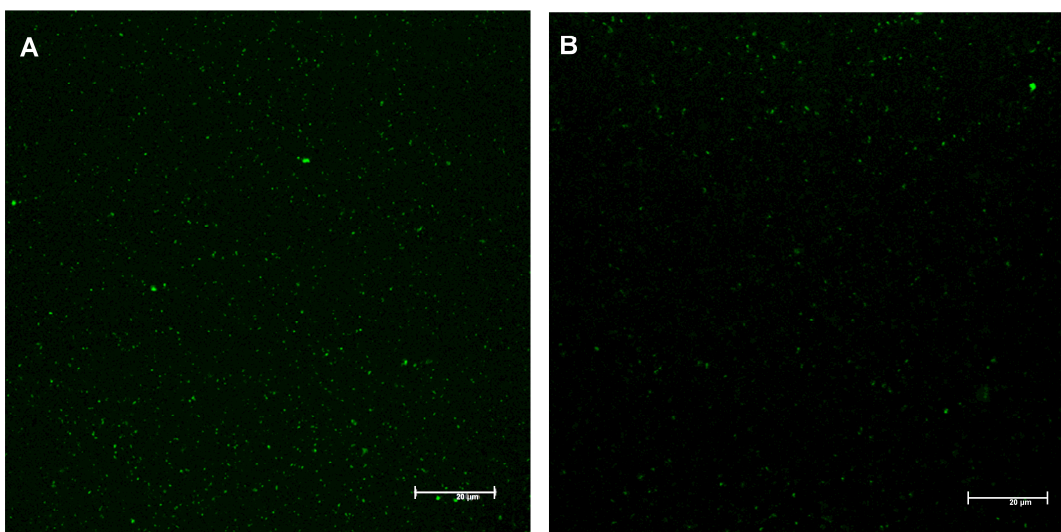


Figure 6.9: Images obtained by confocal microscopy showing liposomes manufactured by (A, B) microfluidics (TFR 2 mL/min, FRR 1:3), encapsulating the aqueous marker (carboxyfluorescein). Note that fluorescence spot size does not correspond to actual vesicle size as liposomes in this sample were below the optical resolution.

6.3.5 The effect of manufacturing method to drug release

In addition to the drug loading, the *in-vitro* release profile was monitored at 37°C over 16 h and compared to vesicles manufactured by the top-down sonication method (Figure 6.10). At the start of the release study, vesicles manufactured by microfluidics (2 mL/min, 1:3) showed a higher drug encapsulation (~55 mol%) compared to vesicles formed by sonication (~20 mol%). Results showed an initial drug release of ca. 40% at 1 h independent of the manufacturing method followed by a continuous release of 90% of the encapsulated drug over 8 h and drug release rates were independent from the manufacturing method when plotted as % cumulative release of total amount loaded (Figure 6.10A), other than plotting the mol% release (Figure 6.110B). Previously published work demonstrated that PC liposomal bilayer-loaded propofol followed a zero-order release kinetics (Ali et al., 2013), and the incorporation of cholesterol into the liposomal systems shifted the release rates towards a first-order release model (Ali et al., 2010). The authors described that bilayers containing cholesterol are more condensed and less permeable, where without cholesterol the bilayer can be thought of as more 'porous' in nature (Ali et al., 2010). This suggests that the release rates are dictated by the formulation rather than the method of manufacture. Given the independence of the manufacturing method from the release profile, the microfluidics-directed vesicle manufacturing may prove advantageous in the development of an IV formulation due to its high-throughput and robustness. Pharmacokinetic release profile of propofol has been studied in a colloidal dispersion between 20-100 nm (Cai et al., 2012), where data compared the distribution of propofol to the commercial product Diprivan®. The authors showed that propofol in a microemulsion required less time to be released from the oil phase compared to a commercial product. Besides the rapid distribution of propofol, it also penetrated quickly into the tissue (Cai et al., 2012). The authors emphasised on the need for new technologies, given current drawbacks of the commercial product like instability (Park et al., 2003) and pain upon injection due to free propofol (Sim et al., 2009).

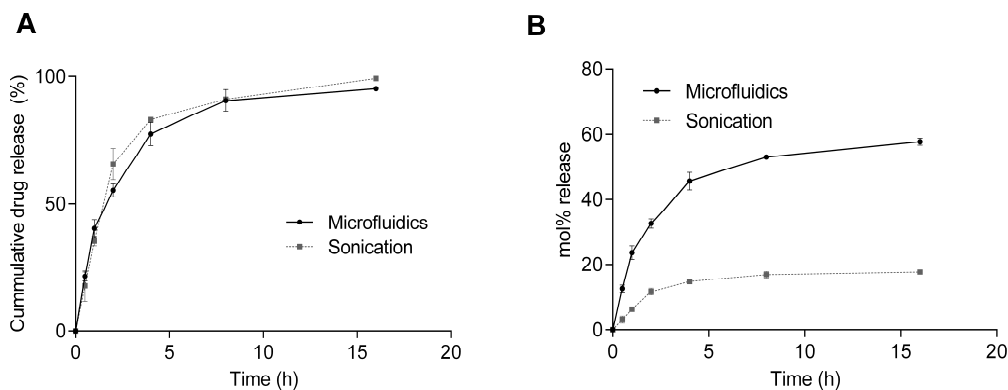


Figure 6.10: *In-vitro* drug release profile for propofol-loaded liposomes manufactured by microfluidics and sonication. Release profiles show A) the cumulative drug release and B) the release of the drug in mol% over 16 hours. Results denote mean \pm SD of 3 separate batches.

6.3.6 The effect of manufacturing methods on liposome stability and drug encapsulation over 6 months

The stability of the vesicles manufactured by microfluidics at different storage temperatures was assessed, in addition to a stable and long term drug encapsulation. Vesicles were prepared using the microfluidics-nanoprecipitation method as described above (FRR 1:3, 1 mg/mL propofol in solvent stream). After removal of the encapsulated drug by dialysis, the initial amount of propofol encapsulated was quantified and the liposomes were stored at 4°C, 25°C/60%RH and 40°C/75%RH (as per ICH guidelines) in pharmaceutical grade stability cabinets for a storage period of 6 months. Vesicles manufactured by the sonication method acted as the control and were stored at 25°C/60%RH.

Vesicle size remained constant throughout the storage over 6 months at 4°C and 25°C for liposomes prepared by microfluidics, with a slight increase noted for the vesicles stored at 25°C at the end of the study (Figure 6.11A). In contrast, vesicles stored at 40°C significantly increased ($p < 0.05$) in size from initially 55 nm to 800 nm throughout the study, with no notable effect on PDI (Figure 6.11A, B), suggesting that the whole liposome population has changed in size rather than a sub-set of the vesicles. Similar to above results, vesicles manufactured by the microfluidics-directed method were smaller with a lower PDI than those obtained by lipid film hydration / sonication (Figure 6.11A, B). The liposomes manufactured by sonication (stored at 25°C) showed good stability in terms of size retention over the initial 50 days of around 100 ± 20 nm, after which a size increase was noted (Figure 6.11A). The formulations at 4°C and 25°C showed minor (but not significant) drug loss after the first 7 days of storage, after which

the formulations remained stable with final drug encapsulation values of 43 ± 10 mol% and 29 ± 12 mol% at 4°C and 25°C storage conditions respectively (Figure 6.11C). Similarly, liposomes manufactured by the sonication method showed an initial drug loss when stored at 25°C/60%RH, which plateaued out approaching complete drug loss over the storage period of 6 months (Figure 6.11C). Notable drug loss from the microfluidic-based vesicles was seen at elevated storage temperatures (40°C), which resulted in almost complete drug loss over the course of the stability study, with only 3 ± 1 mol% drug remaining encapsulated after 6 months, still higher than the final drug encapsulated in the sonicated liposomes which were stored at 25°C/60%RH (Figure 6.11C). In addition to the stability of propofol-loaded vesicles, the drug itself was subjected to same storage duration and temperatures, which showed complete recovery of the drug independent of the storage condition (Figure 6.11D), which verified its physical stability. The drug loss over time could hence be linked to its diffusion over the lipid membrane, and not its physical degradation throughout the storage period. Given the dependence of solubility on temperature and enhanced diffusion at elevated temperature, the aqueous solubility of the drug increased, resulting in reduced drug encapsulation at higher storage conditions (here 40°C).

In addition, a microfluidics-manufactured formulation with a higher lipid concentration was subjected to the 6 months storage conditions (4°C), Figure 6.11E, linked to previous study where the lipid concentration was increased to counter the dilution (Figure 6.4). Here, both lipid and propofol concentration was increased four-fold, remaining the lipid to drug ratio. Vesicles showed identical particle characteristics (size, PDI) as well as loading (mol%) in comparison to the vesicles manufactured at a one-fold concentration (Figure 6.11A, B, C), with particle characteristics remaining throughout the stability study, the drug loading was reduced to ca. 30 mol%, overall lower compared to the one-fold concentration at similar storage conditions (ca. 43 mol%). Given the higher concentration gradient during dialysis, enhanced drug diffusion may be linked to the higher propofol concentration.

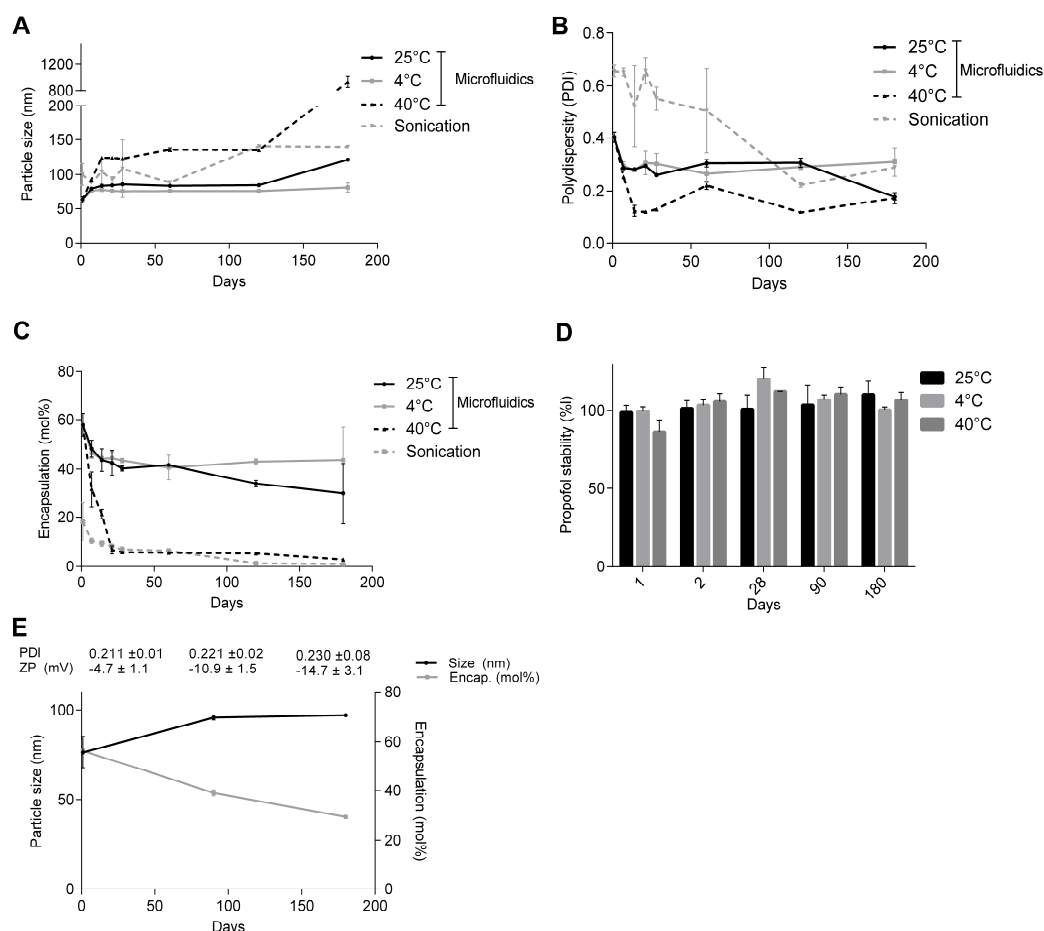


Figure 6.11: Results depicting the effect of long term storage conditions to A) vesicle size B) polydispersity, C) drug encapsulation, D) drug recovery and E) stability at 4-fold lipid and drug concentration. Results denote mean \pm SD of 3 separate batches.

No visual precipitation throughout the stability study for vesicles manufactured by microfluidics was seen, whereas the sonicated vesicles showed flocculants present after 14 days of storage (Figure 6.12), which however dissolved after vortexing the solution, not impeding on the respective size measurements (Figure 6.11A). Formulation stored at higher temperatures turned slightly yellow during the stability study (Figure 6.12), linked to the oxidation of propofol (Baker et al., 2003). A clear solution was only maintained at a storage temperature of 4°C (Figure 6.12), which also allowed for a stable drug encapsulation throughout the study (Figure 6.11C). Quantification of propofol was performed by HPLC, which does not distinguish between oxidization states of the drug, not impeding the measurements over the course of the stability study (Figure 6.11D).

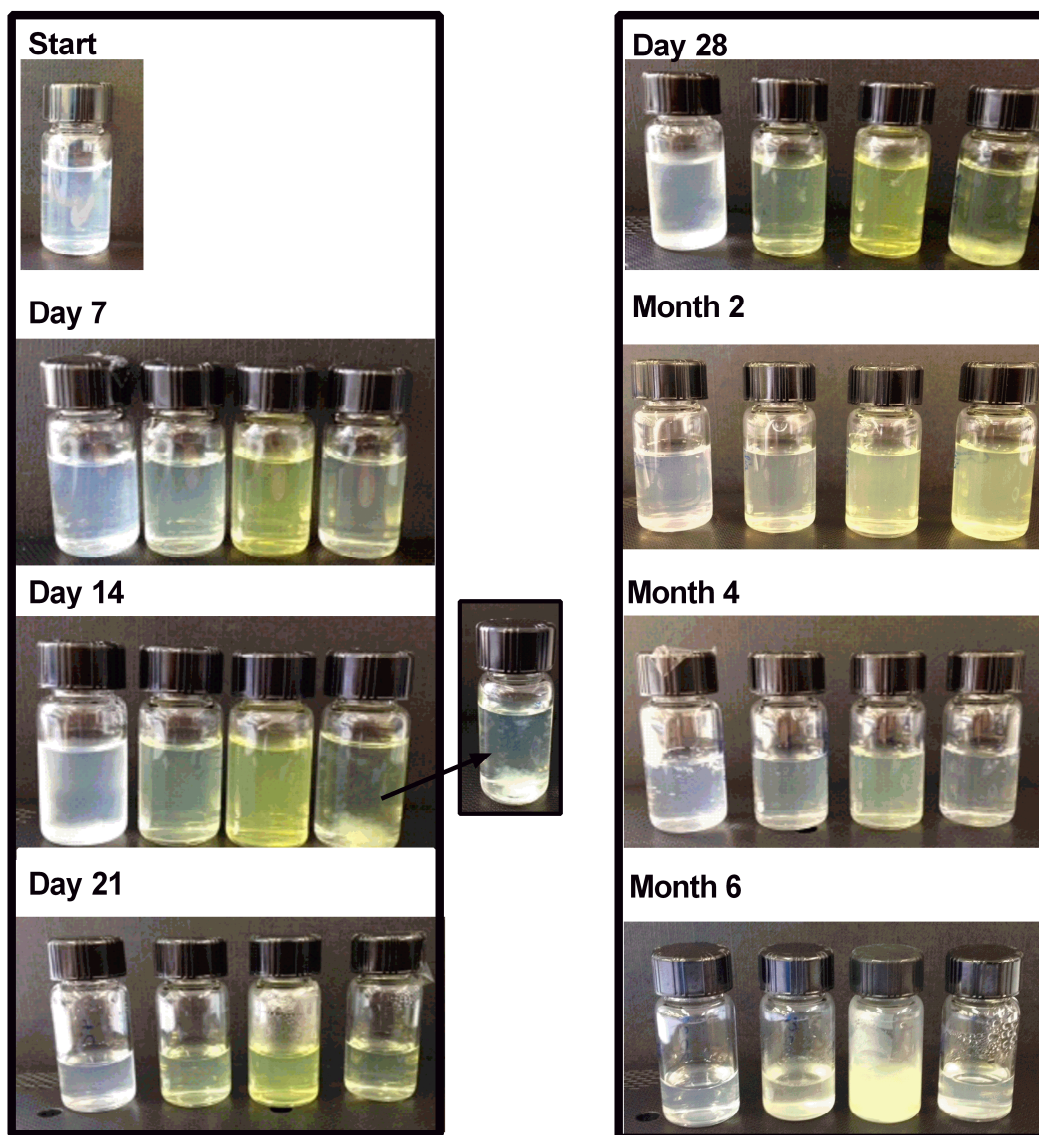


Figure 6.12: Images taken throughout the stability study duration, showing vials of microfluidics-manufactured vesicles stored at 4°C, 25°C and 40°C and sonication-vesicles (25°C), from left to right at respective time points.

The results in Figure 6.11 and 6.12 suggest that vesicles formed by microfluidics-directed nanoprecipitation and loaded with a low solubility drug remained stable over six months at conditions of 4°C. The SHM nanoprecipitation-method was previously investigated for the encapsulation of a highly water-soluble drug only, with approximately 100% loading efficiencies using doxorubicin as a model drug. The authors demonstrated high drug retention of the encapsulated drug in liposomes stored at 4°C over the course of eight weeks (Zhigaltsev et al., 2012). Despite widespread use of propofol emulsions e.g. Diprivan®, stability concerns are currently a major limitation (Baker and Naguib, 2005; Driscoll et al., 2002); were the microfluidics-based manufacturing was shown to potentially overcome this issue.

6.3.7 The effect of drug, drug loading and manufacturing method to the biological toxicity

In addition to the performed *in-vitro* drug release study, the biological effect of the vesicles manufactured was assessed in a toxicity assay. Initially, the toxicity of the drug itself, propofol, was investigated. Given a constant drug to cell ratio, no difference ($p>0.05$) was noted within the different drug concentrations tested (Figure 6.13), which linked to the previous study of determining the ideal drug/lipid ratio (Figure 6.5 A, B, C). Vesicles manufactured by microfluidics were tested in various combinations with (+) and without (-) drug at concentrations ranging from the standard lipid concentration (6.08 mg/mL PC, 0.77 mg/mL Chol), to the two-fold (12.16 mg/mL PC, 1.54 mg/mL Chol), four-fold (24.32 mg/mL PC, 3.08 mg/mL Chol) and six-fold lipid (36.48 mg/mL PC, 4.62 mg/mL Chol) concentration, which all remained insignificant ($p>0.05$) with a biological viability above 72% (Figure 6.13). Vesicles manufactured by lipid film hydration / sonication showed a reduced viability between 60 -70 %, significantly reduced compared to the control ($p<0.05$ and <0.001). The incorporation of the drug however had no significant impact ($p>0.05$) on the cellular viability, confirming its independence on the cellular toxicity (Figure 6.13).

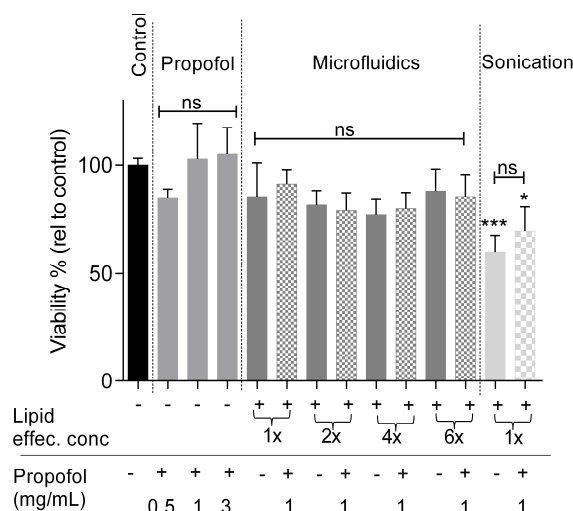


Figure 6.13: Viability (%) as determined by a MTT study. Significance between data is against the viability of the control (untreated cells) (* $p<0.05$, * $p<0.001$). Results denote mean \pm SD of 3 separate measurements in 3 independent cell passage numbers ($n=9$).**

The biological toxicity was independent of the incorporation of the drug, with the vesicles manufactured by microfluidics showing a higher viability compared to the vesicles subjected to sonication. Sonication is a method frequently applied for size reduction, which is however known for contamination due to direct contact of the probe tip and metallic residues (Wagner and Vorauer-Uhl, 2011). Despite centrifugation, metallic residues might not have been completely removed, impacting on the cellular

toxicity as seen in this study. These results further emphasize on the suitability of the microfluidics method for potential industrial application, as the method was shown to not only benefit the particle characteristics and drug loading, but also allowed for the manufacturing of a less contaminated sample, with beneficial biological impact, which may be advantageous for transferring this method in an industrial-scale process. Given the limited scalability of a lipid-film hydration method and potential contamination based on a sonication process, the microfluidic-based vesicle manufacturing process might be a viable option for a robust and controlled particle manufacturing for large-scale industry setting. In order to approach that, scalability studies are vital, not only for understanding the critical process parameters, but furthermore for a seamless transfer into a large-scale version of the respective method.

6.3.8 Assessment of the scalability of the microfluidics-directed nanoprecipitation method

In order to verify the suitability of the microfluidics method for industrial scale application, scalability studies were undertaken by firstly increasing the channel diameter and secondly parallelising the design in a planar scale-out platform, both aiming for an enhanced production throughput. Initially the channel width was increased from 200 μm to 300 μm and the height was increased from 78 μm to 130 μm , both designs with a similar aspect ratio and hydraulic diameter (design obtained from Precision NanoSystems Inc.). In order to determine the flow rates for the 300 μm design, scale-up calculations were performed. Therefore, dimensionless numbers (Re and Pe) were determined for the average flow rates applied in the 200 μm design, which ranged between 1-3 mL/min in the current used SHM design (200 μm width and 78 μm height). The average fluid velocities, Re and Pe numbers were determined as exemplified below (Equation 6.1).

$$u = \frac{Q}{A} \quad \text{Equation 6.1}$$

With

u Fluid velocity (m/s)

Q Volumetric flow rate (m^3/s)

A Cross sectional area of channel (m^2)

$$Q = 2 \frac{\text{mL}}{\text{min}} = 2000 \frac{\text{mm}^3}{\text{min}} = 33.3 \frac{\text{mm}^3}{\text{s}}$$

$$A = w * d = 200 * 10^{-3} \text{ mm} * 78 * 10^{-3} \text{ mm} = 15.6 * 10^{-3} \text{ mm}^2$$

$$u = \frac{Q}{A} = \frac{33.3 \frac{\text{mm}^3}{\text{s}}}{15.6 * 10^{-3} \text{ mm}^2} = 2134.6 \frac{\text{mm}}{\text{s}} = 2134.6 * 10^{-3} \frac{\text{m}}{\text{s}} \approx 2000 * 10^{-3} \frac{\text{m}}{\text{s}}$$

The dimensionless Re and Pe numbers were determined based on above determined fluid velocities (Equation 6.2, 6.3).

$$Re = \frac{\rho u L_o}{\mu} \quad \text{Equation 6.2}$$

With

- L_o Characteristic length = channel diameter = $200 \mu m = 200 * 10^{-6} m$
 u Fluid velocity (m/s)
 μ Dynamic viscosity = $10^{-3} Pa s$
 ρ Fluid density = $10^3 \frac{kg}{m^3}$

$$Re = \frac{u L_o \rho}{\mu} = \frac{2000 * 10^{-3} \frac{m}{s} * 200 * 10^{-6} m * 10^3 \frac{kg}{m^3}}{10^{-3} Pa s} \approx 400$$

$$Pe = \frac{u L_o}{D} \quad \text{Equation 6.3}$$

With

- L_o Characteristic length = channel diameter = $200 \mu m = 200 * 10^{-6} m$
 u Fluid velocity = $2000 * 10^{-3} \frac{m}{s}$
 D Diffusion coefficient lipid = $3 * 10^{-12} \frac{m^2}{s}$ (Almeida et al., 2005)

$$Pe = \frac{u L_o}{D} = \frac{2000 * 10^{-3} \frac{m}{s} * 200 * 10^{-6} m}{3 * 10^{-12} \frac{m^2}{s}} \approx 10 * 10^7$$

Above calculations determined Re and Pe for flow rates from 1 to 3 mL/min in the 200 μm design, Table 6.1.

Table 6.1: Determined Re and Pe numbers in the chip design with a channel diameter of 200 μm ranging at TFR between 1 to 3 mL/min.

Total Flow rates (mL/min)	Re	Pe
1	200	$6 * 10^7$
2	400	$10 * 10^7$
2.5	500	$17 * 10^8$
3	650	$20 * 10^8$

Based on a micromixer review, passive micromixers are recommended at either low Re (< 1) or high Re (> 50), Figure 6.14, (Nguyen and Wu, 2005). Given the Re numbers in the 200 μm design (Table 6.1), the mixing based on chaotic advection was anticipated feasible even at higher Re, which could be expected in the 300 μm design. Given the high Pe numbers, convection is the dominant way of mixing, here the

movement of the lipid particles by the fluid motion. If the mixing would be achieved solely by diffusion, a long channel length would be required due to high Pe (Squires and Quake, 2005). Here, the dominant convective forces allow for a shorter channel length (here $19 \cdot 10^3 \mu\text{m}$ in the $200 \mu\text{m}$ design and $14 \cdot 10^3 \mu\text{m}$ in the $300 \mu\text{m}$ design), as mixing is primarily dominated by convection. Given a linear pressure-flow relationship in a low-Re Newtonian fluid, the pressure drop in the design was anticipated as the scale-up factor to be maintained constant.



Figure 6.14: Overview over micromixers identifying the operating ranges for passive micromixers at low (< 1) and high (> 100) Re numbers. Adopted from (Nguyen and Wu, 2005).

Following the determination of Re numbers, scalability calculations were based on Hagen-Poiseuille Law (Equation 6.4).

$$\Delta P = \frac{128 \mu L Q}{\pi d^4} \quad \text{Equation 6.4}$$

With

- ΔP Pressure difference (Pa)
- μ Viscosity of medium (Pa s)
- L Length of channel (m)
- Q Volumetric flow rate ($\text{m}^3 \text{s}^{-1}$)
- d Diameter of channel (m)

Assumptions: Incompressible and Newtonian fluid, laminar flow, constant cross-section, no fluid acceleration.

For scale-up consideration, the pressure drop (ΔP) in the microfluidics system was anticipated as the crucial variable to maintain constant, given its key role in determining mixing times (Kockmann et al., 2011; Squires and Quake, 2005). Therefore Equation 6.4 simplifies to Equation 6.5

$$\Delta P \approx \frac{Q}{d^4} \quad \text{Equation 6.5}$$

Given a rectangular channel, equivalent pipe diameter was calculated, which estimated the diameter of a circular pipe with the equal pressure loss as obtained in the rectangular channel, Figure 6.15, Equation 6.6.

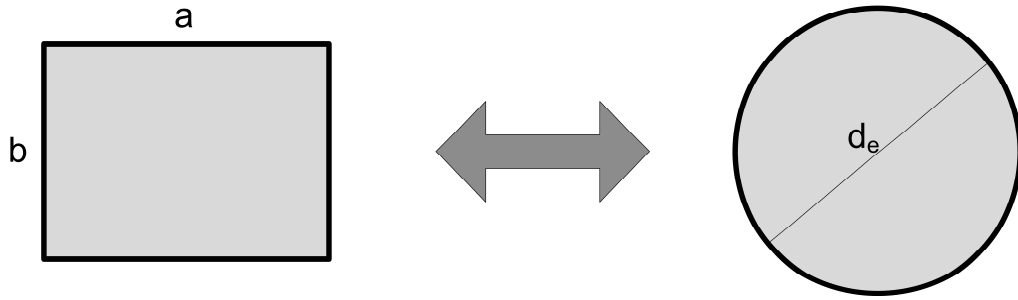


Figure 6.15: Depiction of rectangular cross section and equivalent diameter in a pipe.

$$d_e = 1.30 * \left(\frac{(a*b)^{0.625}}{(a+b)^{0.25}} \right) \quad \text{Equation 6.6}$$

With

d_e = Equivalent diameter (m)

a = Width of channel (m)

b = Height of channel (m)

The equivalent diameter for the 200 μm and 300 μm design (d_{e200} and d_{e300} respectively) was calculated and the pressure drop between both chips anticipated as the constant, leading to Equation 6.7.

$$\begin{aligned} \Delta P_{200} &\approx \Delta P_{300} \\ d_{e200} &= 1.30 * \left(\frac{(200 * 10^{-6} \text{ m} * 78 * 10^{-6} \text{ m})^{0.625}}{(200 * 10^{-6} \text{ m} + 78 * 10^{-6} \text{ m})^{0.25}} \right) \approx 0,00013 \text{ m} \approx 130 \mu\text{m} \\ d_{e300} &= 1.30 * \left(\frac{(300 * 10^{-6} \text{ m} * 130 * 10^{-6} \text{ m})^{0.625}}{(300 * 10^{-6} \text{ m} + 130 * 10^{-6} \text{ m})^{0.25}} \right) \approx 0,00021 \text{ m} \approx 210 \mu\text{m} \end{aligned}$$

$$\frac{Q_{200}}{d_{200}^4} \approx \frac{Q_{300}}{d_{300}^4} \quad \text{Equation 6.7}$$

Flow rates in the 300 μm design were calculated based on Equation 6.7 and equivalent channel diameters and flow rates in the 200 μm design (Table 6.1).

$$Q_{300} \approx \frac{d_{300}^4}{d_{200}^4} * Q_{200}$$

$$Q_{300} \approx \frac{210^4}{130^4} * Q_{200}$$

Table 6.2: Corresponding flow rates in the 200 µm and 300 µm design considering a constant pressure drop throughout scale up.

Q_{200}	Q_{300}	Re_{300}	Pe_{300}
0.5	3.4	360	$12*10^7$
1	6.8	750	$25*10^7$
1.5	10.2	1200	$40*10^7$
2	13.6	1650	$55*10^7$
2.5	17.0	2000	$70*10^7$
3	20.4	2500	$85*10^7$

Based on these calculations, the TFR in the 300 µm design ranged from 5 to 20 mL/min (Table 6.2) and resulting particle characteristics were compared to those obtained by the 200 µm design. The Re numbers indicated that flow remains laminar, entering the transition range to a turbulent flow at a TFR of 20 mL/min ($Re > 2300$), with a full turbulent flow expected at $Re > 4000$ (Kirby, 2010).

The increase in FRR at constant TFR of 10 mL/min showed the same profile as obtained in the 200 µm design (Figure 6.2A), where largest vesicles were obtained at a FRR of 1:1 and a minimum particle size of 50 nm obtained at higher FRR (Figure 6.16A). The increase in TFR from 5 to 20 mL/min did not influence resulting particle size, PDI and ZP, which remained insignificant ($p > 0.05$) in comparison the ones obtained with the 200 µm design (Figure 6.16B). Once incorporating the low solubility model drug in the solvent phase, encapsulation capacity was assessed in the 300 µm design at TFR of 5 to 20 mL/min, at constant FRR of 1:3. Physicochemical vesicle characteristics (size, PDI and ZP) of vesicles manufactured by the 300 µm design remained insignificant in comparison to those obtained with the 200 µm design. Additionally, and most important, the drug encapsulation was maintained at ca. 50 mol% throughout the scalability assessment, with no significant ($p > 0.05$) change in drug loading compared to the 200 µm design (Figure 6.16C).

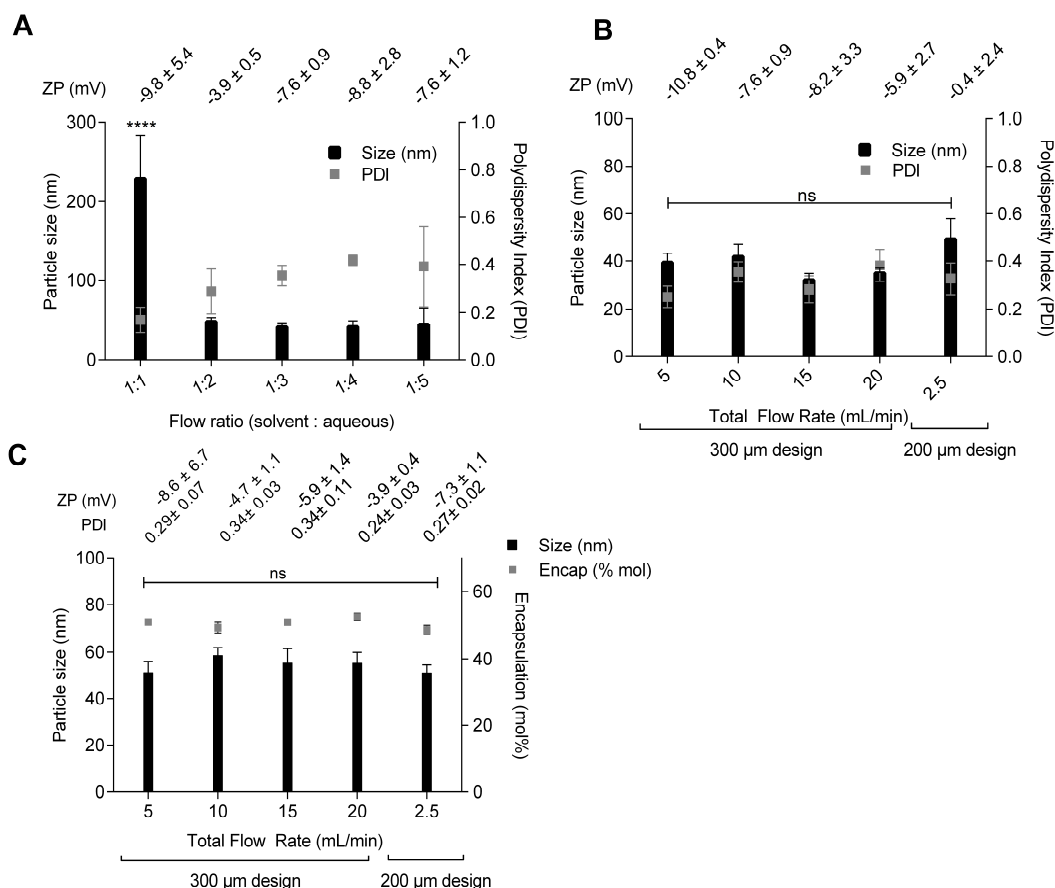


Figure 6.16: Evaluation of the scale-up design with a channel diameter of 300 μ m for effect of increase in A) FRR at constant TFR of 10 mL/min and B) TFR at constant FRR of 1:3 on vesicle size, PDI and zeta potential. Significance between data is against the FRR of 1:1 (* $p < 0.05$). C) Effect of increase in TFR at constant FRR (1:3) on drug loading and vesicle characteristics. Results denote mean \pm SD of 3 separate batches.

To further evaluate the 300 μ m scale-up design, the concentration of the lipids was increased to allow for a higher concentrated formulation. The TFR was based on previous results (Figure 6.16B) and maintained at 10 mL/min, whereas the concentration of the lipids was varied according to the FRR, with no significant effect ($p > 0.05$) on the physicochemical vesicle characteristics (Figure 6.17A). Given ideal particle characteristics at a FRR of 1:3, the previous determined lipid/drug ratio was maintained and both, lipid and drug concentration was increased four-fold to circumvent the dilution based on respective FRR. Besides maintaining the particle characteristics at a four-fold higher lipid and drug concentration, the overall drug loading was maintained (Figure 6.17B) with no significant difference ($p > 0.05$) to the loading achieved with the 1-fold lipid and drug concentration in the 300 μ m and the 200 μ m design.

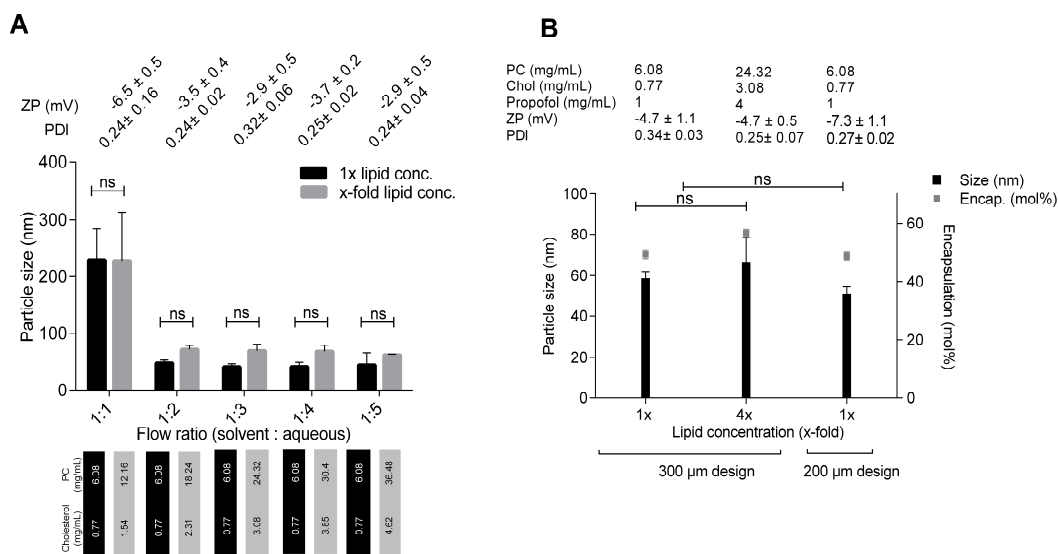


Figure 6.17: Evaluation of the scale-up design with a channel diameter of 300 µm for A) increase in lipid concentration to counter dilution of liposomes tailored to the FRR at constant TFR of 10 mL/min. B) Particle characteristics and loading achieved with a higher concentrated lipid/drug concentration compared to the 200 µm design, at constant FRR of 1:3. Results denote mean ± SD of 3 separate batches.

These initial results showed that determined TFR, based on the scale-up consideration of a constant pressure drop, maintained the critical particle characteristics as well as the drug loading capacity of those vesicles. Furthermore, the 300 µm design allowed for manufacturing of vesicles up to a six-fold higher concentration without adversely impacting on physicochemical characteristics. In addition, vesicles were not only manufactured at a higher throughput and a higher concentration, but also with constant drug loading capacities. Overall, the scale up from the 200 µm to the 300 µm design resulted in a 10-fold increase in throughput, up to a maximum of 20 mL/min.

In addition to increasing the channel diameter (scale-up), the setup was evaluated in a scale-out platform. Here, mixers, all with a channel diameter of 300 µm, were parallelised in a planar way (Figure 6.18A, B). Fluid manifolds were used to split the flow, solvent and aqueous respectively, in the parallelised chips, which were assembled into a 2-fold and 4-fold platform (Figure 6.18C, D), referred to as 2x and 4x scale-out platform in subsequent results and discussion section. Scale-out platforms were evaluated in syringe driven systems in 2x and 4x setup (Figure 6.18E) as well as in continuous flow pump system in a 1x and 4x setup (Figure 6.18F).

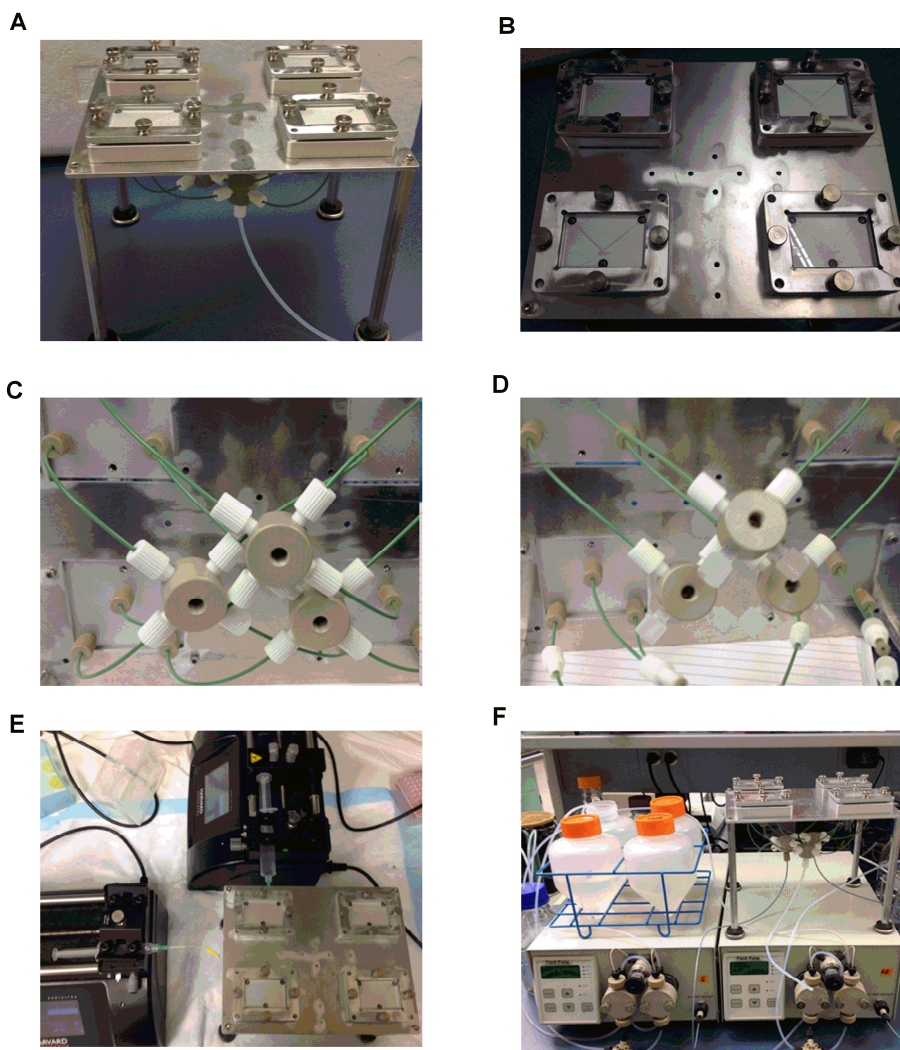


Figure 6.18: Scale-out platform from A) side and B) top view, fluid manifolds as set for a C) 4x and D) 2x flow, E) syringe driven and F) continuous flow pump system.

In comparison to the standard bench-top system, the syringe driven system allowed for a higher throughput by volume, with larger syringes connected to the inlet streams, but still remaining a batch-type process. Physicochemical characteristics (size, PDI and ZP) were maintained in the 2x and 4x syringe-driven scalability platform (Figure 6.19A), and the recovery of lipids and drug was found independent of the scale-out setup (Figure 6.19B). Vesicles were no significantly different in size once the drug (propofol) was incorporated into the manufacturing process (Figure 6.19A), with a comparable drug loading compared to the batch system (Figure 6.19B).

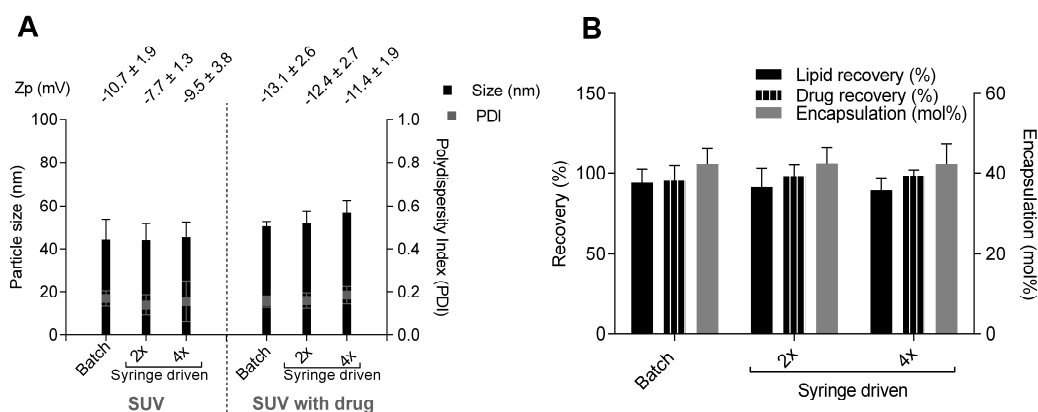


Figure 6.19: Effect of scale-out by a syringe-driven 2x and 4x setup to A) particle characteristics of empty and drug loaded liposomes and B) recovery of lipid and drug as well as overall drug encapsulation. All runs were performed at a FRR 1:3 and a TFR of 10 mL/min per chip. SUV, small unilamellar vesicles. Results denote mean \pm SD of 3 separate batches.

Further to the syringe driven scale-out platform, the platform was connected to continuous flow pumps, Figure 6.18F. The formulation was collected in cumulative batches in a 1x and 4x continuous flow system, with the initial 5 and 10 mL collected in the waste. A total of 50 mL was collected in the 1x continuous flow system, whereas a total of 125 mL was collected in the 4x continuous flow system. The collection of the waste volume in the 1x and 4x continuous flow system highlighted on the significance of collecting the core of a sample once the system reached a steady-state condition. Overall, particle characteristics throughout the 1x and 4x continuous flow system were maintained (Figure 6.20A, B), highlighting on the robustness of the process once operating in a steady-state condition. Similar to above, particle size increased once the drug was added into the manufacturing process in the continuous flow process (Figure 6.20C, D).

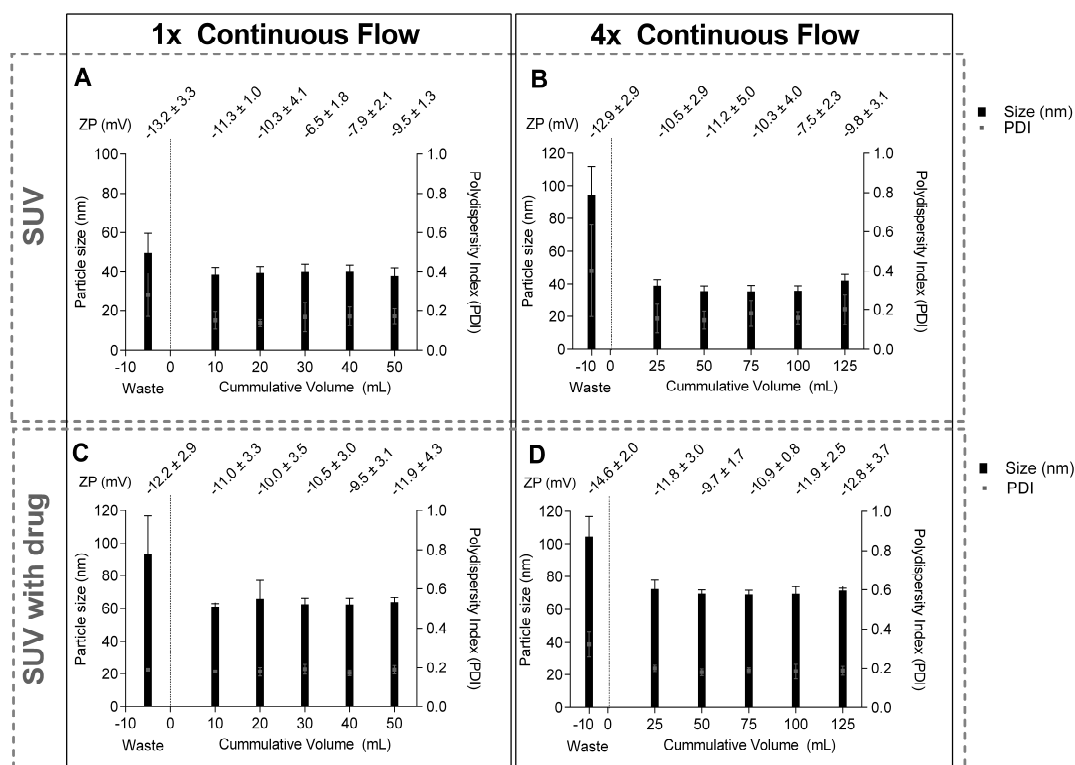


Figure 6.20: Effect of scale-out by a continuous flow setup to particle characteristics in a A) 1x and B) 4x setup as well as on drug loaded liposomes in a C) 1x and D) 4x setup. All runs were performed at a FRR 1:3 and a TFR of 10 mL/min per chip, 5 mL were collected as waste in the 1x setup, 10 mL in the 4x setup. SUV, small unilamellar vesicles. Results denote mean \pm SD of 3 separate batches.

In comparison to the batch process, recovery of lipids and drug was impeded (Figure 6.21). Both, lipids ($p < 0.01$) and drug ($p < 0.05$) recovery were found reduced in the 1x and the 4x continuous flow platform in comparison to the recovery in the batch system. Additionally, drug encapsulation reduced ($p < 0.05$) for both platforms tested, a reduction from ca. 50 mol% to 38 mol%, Figure 6.21.

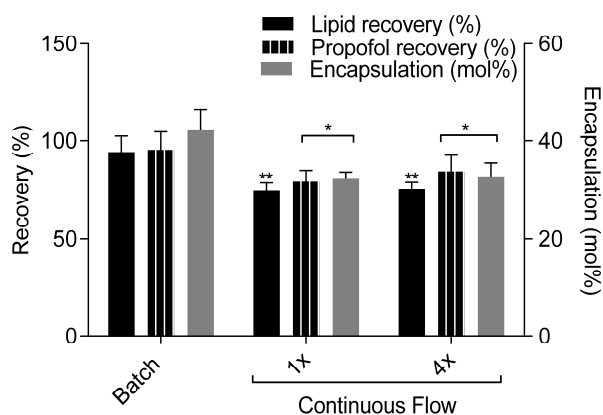


Figure 6.21: Effect of scale-out by a continuous flow 1x and 4x setup to the recovery of lipid and drug as well as overall drug encapsulation. All runs were performed at a FRR 1:3 and a TFR of 10 mL/min per chip. Significance between data is against the results obtained in the batch system (* $p < 0.05$, ** $p < 0.01$). Results denote mean \pm SD of 3 separate batches as the average out of the cumulative batches collected in the continuous flow setup.

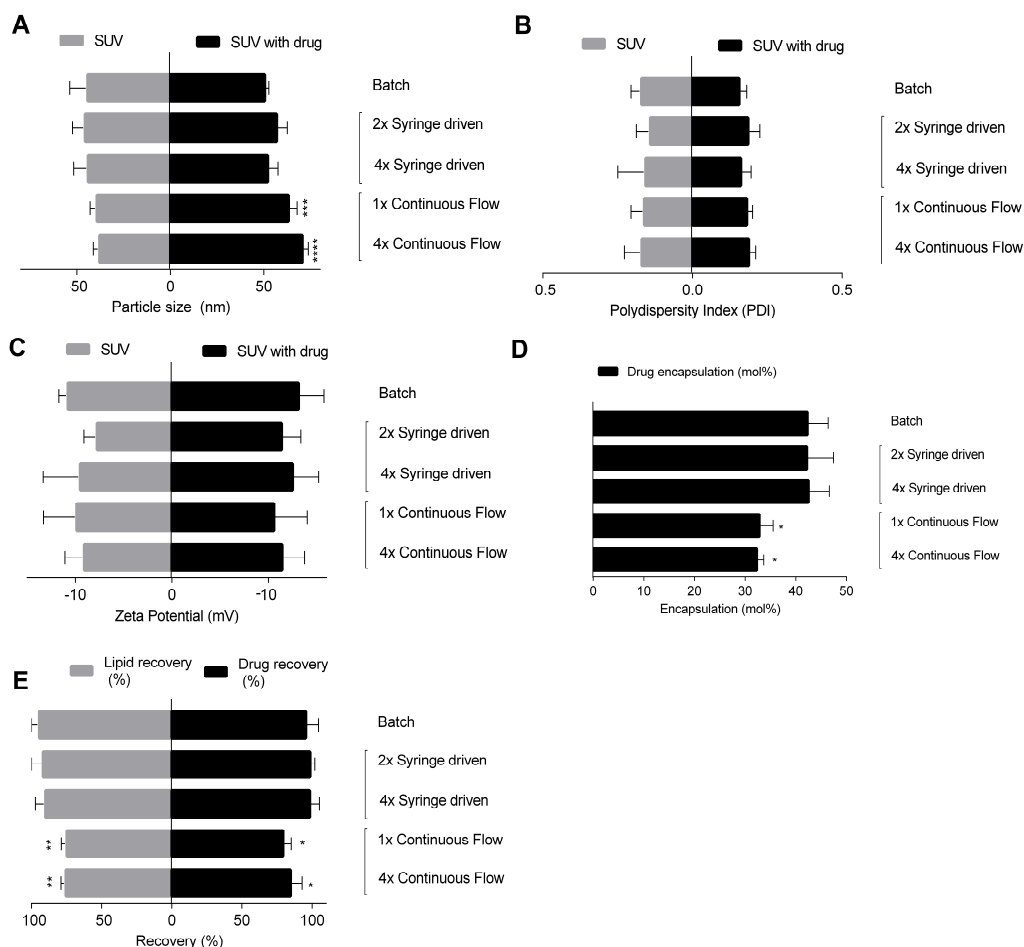


Figure 6.22: Overall comparison between the different scale-up platforms tested on A) size, B) PDI, C) ZP, D) encapsulation and E) recovery of lipids and drug. Significance between data is against the results obtained in the batch system (* $p < 0.05$, ** $p < 0.01$, * $p < 0.001$, **** $p < 0.0001$). Results denote mean \pm SD of 3 separate batches and the average out of the cumulative batches collected in the continuous flow setup.**

The reduced performance in the continuous flow system might be explained by the underlying principle. The transfer from batch to syringe driven 2x/4x system can be considered seamless, as both systems work with syringe pumps. However, the continuous flow system used pulsating pumps, which may have disturbed the flow in the tubing prior to reaching the SHM, visualised by air bubbles in the outlet stream. Additionally, pressures were higher in the continuous flow system, ranging up to 50 psi, and lipid solution remained in the tubing for a prolonged period due to a longer flow path (Figure 6.18F). Anticipated compression of lipids and drug in the tubing followed by sudden relaxation in the chip itself might have led to an alteration in fluid flow behaviours in the setup, resulting in larger sized particles with reduced drug encapsulation properties, as seen in Figure 6.22A and D. A change in the viscosity of the solvent stream due to the addition of the drug was anticipated as the reason for change in particle size, based on alterations in fluid flow behaviour under compression

(Figure 6.22A). Furthermore, the solvent solution was manually recycled over the pump heads prior to the start in the continuous flow system, which was anticipated as the main factor behind reduced lipid and drug recovery (Figure 6.22E). An additional study quantified respective recovery independently at different pressures and different tubing material, with the pressure being linked to the flow rate by Hagen-Poiseuille Law (Equation 6.4).

At constant tubing diameter/length a direct link between pressure and flow rate can be assumed and Equation 6.4 simplifies to Equation 6.8. Flow rates varied from 1 to 6 mL/h, which represented pressures of 0.08 to 0.5 psi.

$$\Delta P \approx Q$$

Equation 6.8

Whereas the tubing material itself was shown to be an independent factor of the recovery, a higher pressure in the process were indicative of a reduced lipid recovery (Figure 6.23), here up to a maximum of 0.5 psi only. Given higher pressures in the continuous flow system (max. 50 psi) compared to the batch and syringe driven system, results might be indicative of the importance of pressure and lipid adsorption to the tubing wall. Given a direct link between tubing diameter and pressure (Equation 6.4), a suggestion might be to alter the pump heads for operation with lower pressure and reduced pulsation or selecting the appropriate tubing diameter in the continuous flow system.

Small imperfections in a microchannel may result in variation of the hydraulic resistance, which especially in parallelised micro channels may result in flow variations. Furthermore bubbles should be avoided, which may block the channels (Vladislavljević et al., 2013). Such variations may have resulted in the alteration of the flow profile, ultimately leading to variations in physic-chemical particle characteristics and encapsulation efficiencies achieved in this study. The concept of microreactor parallelisation was found to result in a larger, but still considered acceptable, variation of 9% in particle size compared to the size obtained in a single reactor, which was found less than 5%. This deviation was linked to the variation in emulsion formation within the 10 parallelised reactors (Mbanjwa et al., 2014).

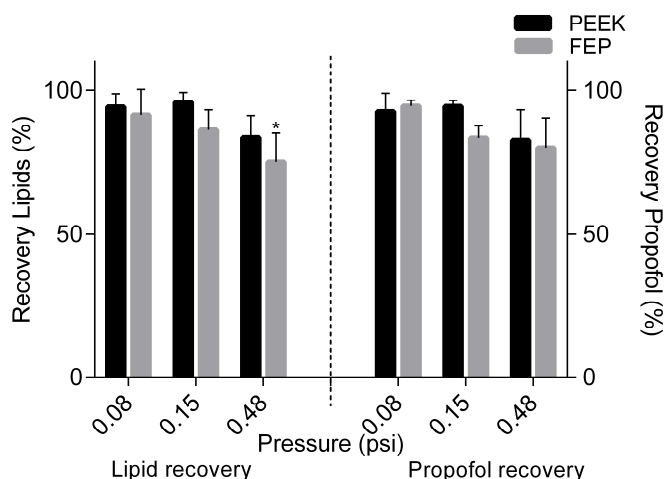


Figure 6.23: Effect of tubing material (PEEK vs. FEP) and pressure to the recovery of the lipids and drug. Significance between data is against the results obtained in the lowest flow rate and pressure (* $p < 0.05$). Results denote mean \pm SD of 3 separate batches.

Scalability and increase in throughput together demonstrate the industrial applicability comparable with scale-up options available (Wagner and Vorauer-Uhl, 2011), viable for any method aiming for industrial application. Considering commercial aspects of formulation development, the translation of a product to market at a reasonable price remains a key consideration (Holtze, 2013). The use of microfluidic devices is known for successful application in research and development for pharmaceutically relevant nanoparticles (Dittrich and Manz, 2006; van Swaay, 2013); however, the realisation of larger-scale microfluidic process depends on the technology deriving a product that is difficult to achieve with any other technology and strongly depends on the market need (Holtze, 2013). Considering the significant increase in drug encapsulation by the microfluidics technology achieved and presented in this chapter, the transfer of this method for a larger scale production might be economically justified.

Parallel-flow microfluidics has been suggested as one of the key methods in continuous manufacturing (Martel et al., 2015). The scale-up of microfluidic reactors is considered an ongoing challenge (Vladisavljević et al., 2013), where the two main approaches applied include parallelisation and internal scale-up. Scale-up based on internal scale-up is the less frequently applied approach (Vladisavljević et al., 2013). A successful version included a design with a higher available surface area, providing an overall 9-times higher power output (Fuerth and Bazylak, 2013). In this chapter, the change in diameter yielded an overall 10-fold increase in TFR from 2 to 20 mL/min, maintaining particle characteristics and drug loading. The alteration of the channel

diameter allowed for a seamless process transfer, which was based on a constant pressure drop in the channel.

For parallelisation, identical microchips are set in parallel, where flow-splitters are required to split the flow over the chosen number of reactors (Vladislavljević et al., 2013). This approach has the advantage, that still one pump per phase can supply multiple chips, rather than one pump per microchip (Holtze, 2013). This approach has been developed for the mass productions of droplets by planar microfabricated units to an overall throughput of 320 mL/h (Nisisako and Torii, 2008). The concept of parallel-flow microfluidics was further exemplified for the production of emulsions and microparticles in 10 microfluidic reactors, drastically increasing the throughput 10-fold by maintaining a small footprint (Mbanjwa et al., 2014). In this chapter, the syringe driven scale-out platform allowed for a four-fold higher throughput in comparison to the batch system. In combination with the 10-fold higher throughput by changing the channel diameter, an overall 40-fold throughput could be achieved. The TFR per chip was maintained at 10 mL/min, which gave an overall throughput of 40 mL/min in the 4x system. The collection of 125 mL sample in the continuous flow system required ca. 3 minutes. This transfer into a continuous flow system highlighted on the importance of achieving and maintaining a steady-state process, which resulted in reproducible particle characteristics.

Overall, advantages by parallelisation comprise the reduced number of pumps allowing to operate multiple chips, a smaller footprint than multiple systems, the ease of handling and diminished costs due to scale-up development work (Mbanjwa et al., 2014). The work on the continuous flow system highlighted on the necessity of a pressure control along with further future optimisation with regards to eliminating the manual recirculation process and optimising material. Possible non-uniformity of the micro- or nanoparticles formed, as found in this chapter, along with possible complexity in microchip fabrication, might be associated disadvantages (Mbanjwa et al., 2014).

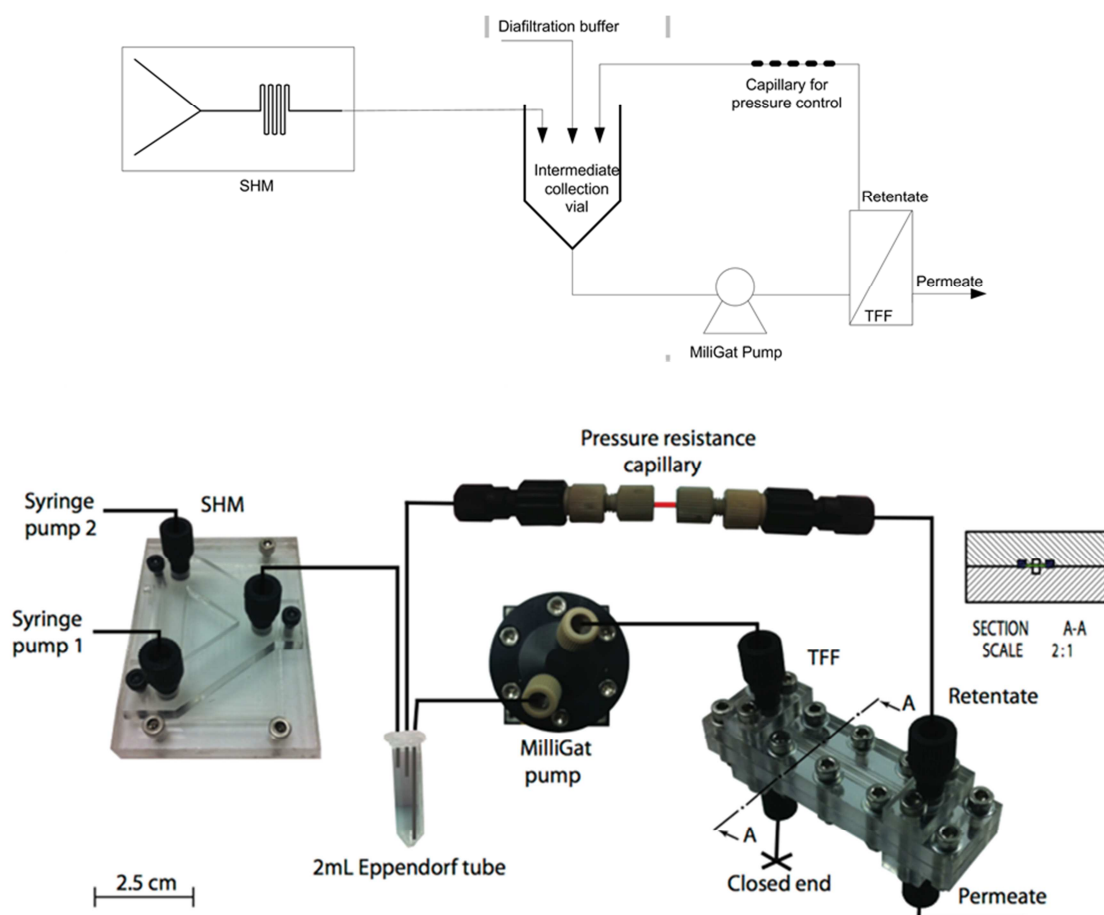
6.4 Conclusion

This chapter demonstrated a high-throughput, robust and scalable method of preparing liposomes as solubilising agents based on microfluidics-directed nanoprecipitation. Resulting particles have well defined, scalable and process controlled demonstrating this method is suitable for pre-clinical and clinical application (Biebuyck et al., 1994). Furthermore, the method combined liposome manufacturing and drug encapsulation in a single process step, circumventing an additional drug loading step downstream,

which overall diminishes the time for production of stable drug-loaded vesicles of specified physico-chemical characteristics. The results in this chapter showed that the microfluidics-directed nanoprecipitation method is well suited for a high-throughput batch-type processing, which allows screening over a range of drug and lipid concentration with minimum time requirements. Despite success in the scale-up format, the continuous flow system still requires optimisation, which is linked to optimizing the pressures and flow profiles in the system as well as the process of recirculating the solvent through the pumps. Overall, waste volumes were higher in the batch and syringe driven system, whereas the ratio of waste to total sample volume was significantly reduced once the system is used in a continuous flow mode, making a continuous flow system more economical. Most importantly, results here show that the method based on chaotic advection is scalable, by changing the channel diameter and parallelising the chip design. The scalability of a method is important for its consideration for an industrial large-scale process.

Chapter 7

Development of continuous microfluidic systems for manufacture and purification of liposomes



Papers submitted:

Kastner E., Dimov N., Ingham A., Perrie Y. and Szita N. (2015). Formation and purification of tailored nanoparticles for drug delivery using continuous microfluidics (in preparation).

7.1 Introduction

Besides the necessity of a robust process characterisation, quality control of the liposomal formulation and reasonable production and development costs, there remains a need for rapid, robust and reproducible development techniques. Indeed robust cost-effective manufacture of liposomes remains a key bottleneck in liposome technologies (Wagner et al., 2002a). With an increasing number of liposomal products in clinical trials and development (Chang and Yeh, 2012) the demand for rapid process development tools continues to rise. To address this several microfluidic-based methodologies are currently being exploited in drug development (Dittrich and Manz, 2006; Hood et al., 2014a; Weigl et al., 2003; Whitesides, 2006). Whilst reducing volumes during development processes, costs can be diminished whereas throughput is increased (Jensen, 2001; van Swaay, 2013; Weibel and Whitesides, 2006). Compared with process optimisation on a larger scale, process development with microfluidic devices allows for a better control of mixing efficiencies, which at this scale is predominantly based on molecular diffusion. The increased surface-to-volume ratios generate fast mixing times by minimising dimensions and diffusion lengths (Lee et al., 2011; Mengeaud et al., 2002).

Nevertheless for any liposomal-based process, be it industrial-, bench- or micro-scale, the separation of non-entrapped contaminant molecules, small molecule drugs or proteins, from the final liposome product is required (Wagner et al., 2002a). To date, separation is typically achieved by filtration (Pattnaik and Ray, 2009; Wagner et al., 2002a) or centrifugation. Centrifugation needs sufficient density gradients between particles and suspending fluid to be efficient. Therefore this method is more suitable for larger particles. For smaller vesicles, centrifugation is either prohibitive or very time consuming (Torchilin and Weissig, 2003). Furthermore, with time-intensive size exclusion chromatography, problems including reduced product yield by column equilibration and dilution of the final liposomal product is often reported (Ruysschaert et al., 2005). Dialysis is a simple alternative and is commonly employed following microfluidics-based liposome manufacturing (Chapter 4 and 6), removing solvent residues prior to an *in-vitro* or *in-vivo* applications. Yet dialysis is also relatively time-intensive, diminishing the time saving gained during particle manufacturing. Filtration of liposomes for purification is reported for large-scale manufacturing (Pattnaik and Ray, 2009; Wagner et al., 2002a).

Work in this chapter describes a microfluidic liposome purification process based on a tangential flow filtration (TFF) device (O'Sullivan et al., 2012) and explores on-chip process development. The on-chip TFF device relies on separation of liposomes and contaminants based on a membrane separation process. Components larger than the cut-off value of the membrane are retained on the retentate side of the membrane, whereas components small enough to penetrate through the membrane pores are found in the permeate. The setup is based on a clamping device, sealing the membrane sheet within a PDMS gasket, with an overall hold up volume of 50 μL , (Figure 7.1A and B). The resulting set-up reports on a fully microfluidic liposome formation and purification process train with exchangeable membrane.



Figure 7.1: A) 3D image of the TFF system with two PMMA plates used as in a clamping system to hold the membrane in place. B) Dimensions of the assembled TFF device. Adopted from (O'Sullivan et al., 2012).

7.2 Aim and Objectives

The aim of this chapter was to develop a continuous-manufacturing unit based on microfluidic systems (Figure 7.2). To achieve this, a purification method based on an on-chip tangential flow filtration unit was developed and optimised. To consider the parameters controlling the filtration unit, backpressure regulation was studied and its effect on particle characteristics was investigated. Furthermore, the filtration unit was challenged with a range of cationic, anionic and neutral liposomes and explored for purification of a model protein and a small drug molecule from these liposome systems. To study and develop a continuous flow microfluidics-based system, the upstream mixer for vesicle formation (Chapter 4, 5 and 6) was connected to the downstream purification unit supporting the development of microfluidics-tools in continuous manufacturing. Off-line monitoring verified the purification in comparison to vesicle characteristics and efficacy of drug encapsulation as described in Chapter 4 and 6.

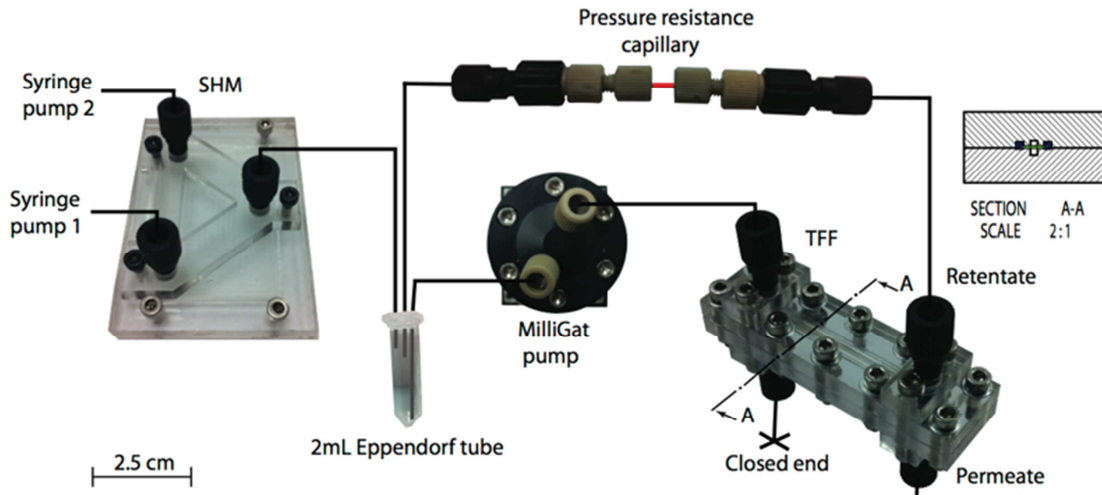


Figure 7.2: Overview over the continuous flow microfluidics-based liposome manufacturing and purification setup.

7.3 Results and Discussion

7.3.1 Backpressure regulation

The aim of this section was to implement a backpressure regulation for the purification of liposomes by a TFF membrane. The backpressure was controlled by attaching a constricting capillary (inner diameter 50, 63 and 100 μm) to the retentate outlet (Figure 7.2). The backpressure was regulated by relating the capillary inner diameter (I.D.) and the fluid flow to the pressure drop as described in the Hagen-Poiseuille Law (Equation 7.1), relating the theoretical pressure drop in a fluid flowing through a cylindrical pipe, assuming that an incompressible Newtonian fluid is used at a laminar flow with no acceleration in the pipe.

$$\Delta P = \frac{128 \mu L Q}{\pi d^4} \quad \text{Equation 7.1}$$

With

ΔP	Pressure difference (Pa)
μ	Viscosity of medium (Pa s)
L	Length of tubing (m)
Q	Volumetric flow rate ($\text{m}^3 \text{s}^{-1}$)
d	Diameter of tubing (m)

Equation 7.1 was used to determine the required capillary length whilst aiming for a backpressure between 5-80 psi. Pressure drop was calculated for the capillary and the tubing connecting the TFF unit to the capillary (Figure 7.2) respectively, and overall pressure drop included both values as additive values. Results highlighted on the linear relationship between backpressure, depended on the flow rates and the length of the

capillary (Figure 7.3). Backpressures determined for the tubing (ID 800 μm) were below 0.02 psi (Figure 7.3A), significantly lower than backpressures achieved by the capillaries. For maintaining a backpressure below 100 psi, a short capillary or low flow rates are desired (Figure 7.3B) and by increasing the capillary diameter (Figure 7.3C and D) a higher flow rate can be achieved by still remaining below 100 psi backpressure.

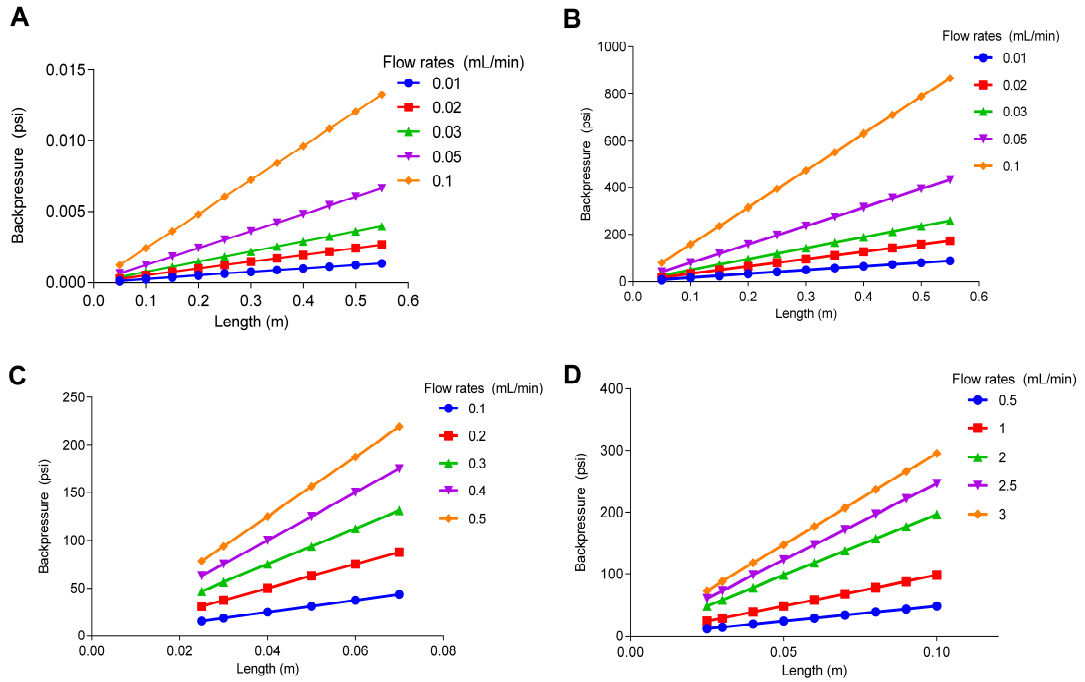


Figure 7.3: Determined theoretical backpressures at different flow rates from 0.01 to 3 mL/min at various capillary lengths and I.D. of A) 800 μm , B) 50 μm , C) 63 μm , D) 100 μm .

The validation of these theoretical backpressures was performed by connecting the TFF to a pressure transducer, which was connected to LabView, where a voltage signal was converted to a pressure. Actual pressures inside the TFF were recorded until a stable pressure reading was obtained. The direct comparison of theoretical and measured backpressure (Table 7.1) showed close match, with the theoretical pressure (Equation 7.1) slightly underestimating the pressures in the channel by 1 to 10 psi, with the difference getting bigger with higher flow rates applied (Table 7.1).

Table 7.1: Comparison of theoretical and actual backpressures in the TFF setup at increasing flow rates from 0.01 to 0.1 mL/min. Deviation in actual backpressure was extrapolated from fluctuations in the pressure recordings and expressed as \pm compared to the average pressure recording (5 cm capillary I.D. 50 μm).

Flow rates (mL/min)	Theoretical Backpressure (psi)	Actual Backpressure (psi)
0.01	7	8.4 ± 1
0.02	15	19.5 ± 1
0.03	23	27 ± 3
0.05	39	55 ± 3
0.1	80	86 ± 5

The maximum rated pressure of the selected membrane according to the manufacturer was 100 psi. Here, the ideal backpressures in the TFF was set between 5-80 psi (Van Reis and Zydney, 2001, 2007), which is a common range for backpressures in filtration processes in industry (Cheryan, 1998). The calculated theoretical back-pressures were found to correlate well with increasing flow rate and decreased capillary diameter (Figure 7.3 A and B), in line with previous backpressure regulation using the TFF (O'Sullivan et al., 2012). The overall pressure drop accounted by the tubing was negligible, with maximum values of 0.013 psi at the highest flow rate and the longest tubing length of 0.55 meters (Figure 7.3A). Here, the backpressures achieved by the capillary were found most contributing to the overall pressure drop (Figure 7.3 B, C, D). Overall, a shorter capillary was anticipated beneficial given the recovery of the vesicles from the retentate side. Furthermore, reduced residence time of the vesicles in the capillary might reduce any adverse effects to shear stresses. Generally, the control of back pressures with capillaries can be considered more reproducible compared to commercially available micrometering valves. Furthermore, controlling backpressure with a capillary is considerably cheaper, and any moving parts can be avoided (O'Sullivan et al., 2012).

Given the close overlap between theoretical and actual backpressure, the theoretical backpressure has been used throughout further development work. Also, the calculation based on Equation 7.1 was used to tailor the I.D. and the length of the capillary to the desired flow rate.

7.3.2 Membrane fouling

This section aimed to verify membrane fouling as a function of flow rates in the current filtration system. Based on work in section 7.3.1, the flow rate was investigated as a function of membrane fouling. Membrane fouling occurs once filtered products (liposomes) accumulate on the membrane surface and restrict flow through the membrane, determined by a reduced flux through the membrane. The resistance of the membrane can be assumed using Darcy's Law (Equation 7.2), which relates the transmembrane pressure (TMP) and the membrane resistance to the flow through the membrane (Bolton et al., 2006).

$$J = \frac{TMP * \Delta P}{R_m * \mu} \quad \text{Equation 7.2}$$

With

J Flux ($\text{l m}^{-1} \text{s}^{-1}$)

TMP Transmembrane pressure (psi) = $(P_{\text{feed}} - P_{\text{ret}}) / 2 - P_{\text{perm}}$

ΔP	Axial pressure drop (Pa) = $P_{\text{feed}} - P_{\text{ret}}$
R_m	Membrane resistance (m^{-1})
μ	Viscosity of fluid (Pa s)

Fouling was assessed by comparison of the normal water permeability (NWP) compared to the filtration performance using liposomes. Membrane fouling tested with water and liposomes filtered through the TFF at increasing flow rates of 0.01 mL/min, 0.02 mL/min and 0.05 mL/min. The slopes for the cumulative permeate volumes of water were compared to the one of liposomes filtered, where a deviation from the NWP-slope was an initial sign for reduced permeate volume, associated to reduced flux and hence membrane fouling. At higher flow rates of 0.05 mL/min and 0.02 mL/min, slopes of cumulative permeate volume of NWP and liposomes matched (Figure 7.4). Membrane fouling was indicated at the lower flow rate of 0.01 mL/min. Here, permeate volume levelled after 150 min filtration time, indicating built-up on the membrane surface and liposomes fouling the membrane (Figure 7.4, small insert).

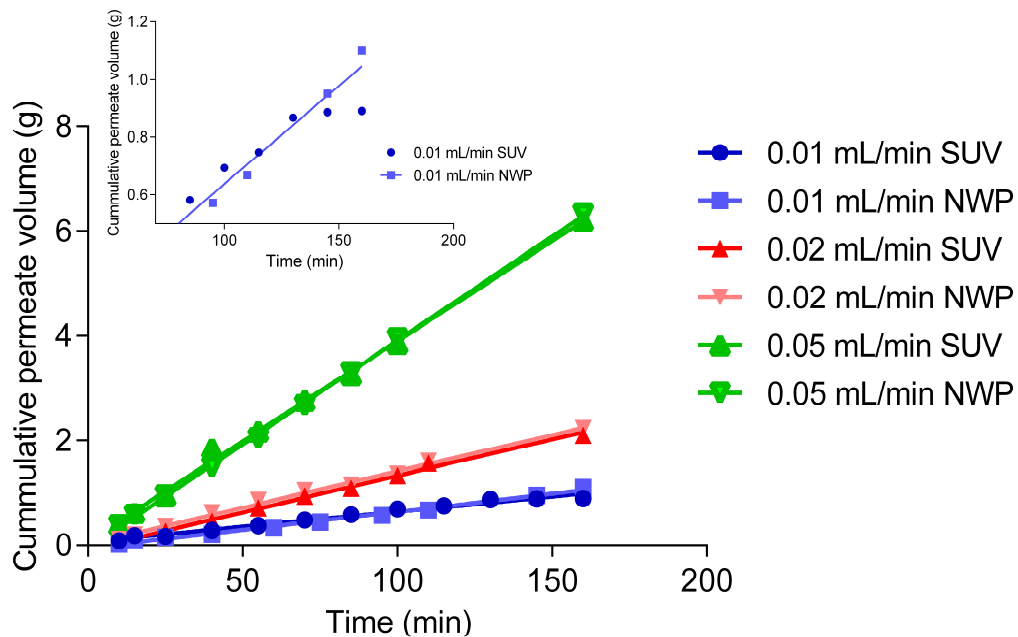


Figure 7.4: Determination of membrane fouling at flow rates of 0.01 mL/min, 0.02 mL/min and 0.05 mL/min for liposomes (SUV) and water (NWP). Smaller picture represents a zoom of NWP and SUV cumulative permeate volumes at the lowest flow rate of 0.01 mL/min, with initial indication of membrane fouling. All experiments were performed at a particle concentration of 5×10^{10} P/mL.

Given the indication of an inverse relationship between membrane fouling to the flow rate; fouling was anticipated reduced by increasing the flow rate through the filter. At higher flow rates liposomes may be swiped off the membrane surface, where at lower flow rates liposomes might be more prone on accumulating on the membrane surface

leading to membrane fouling over time. In order to maximize the recovery of the liposomes from the TFF system, low flow rates of 0.01 mL/min were avoided in all work. Here, a higher flow rate could be associated to a higher throughput in the TFF system, beneficial for a high throughput purification system for liposomes.

7.3.3 Batch -type purification of liposomes – pressure testing

The aim of this initial test was to assess the impact of purification by TFF on the physico-chemical properties including size, PDI, ZP and particle number of liposomes, whilst verifying the integrity of the liposomes at increasing flow rates and backpressures, maintaining previously determined flow rates to avoid membrane fouling (Section 7.3.2). The selection of capillary diameters and lengths allowed controlling the backpressure in the system and permeability through the membrane as a function of the flow rate (Equation 7.1) with the aim of achieving a high throughput in the TFF system as described in section 7.3.1.

Initial measurements assessed liposomes retention on the retentate side of the membrane, a vital criteria for a successful separation of liposomes from un-entrapped drug or protein. Liposome physico-chemical characteristics were found independent of increasing backpressures during filtration at backpressures ranging from 5 to 80 psi, with no significant alteration in size and PDI ($p > 0.05$; Figure 7.5A). The integrity of liposomes was evaluated at increasing backpressures between 5 – 80 psi, with a range of capillaries of different lengths and inner diameter tested (Figure 7.5B). At backpressure higher than 75 psi, particles were detected in the permeate (Figure 7.5C), with a significant ($p < 0.05$) increase in particle size from initial 115 nm to ~140 nm and a significant ($p < 0.05$) increase in PDI from 0.15 to 0.3 when compared with the initial formulation before filtration.

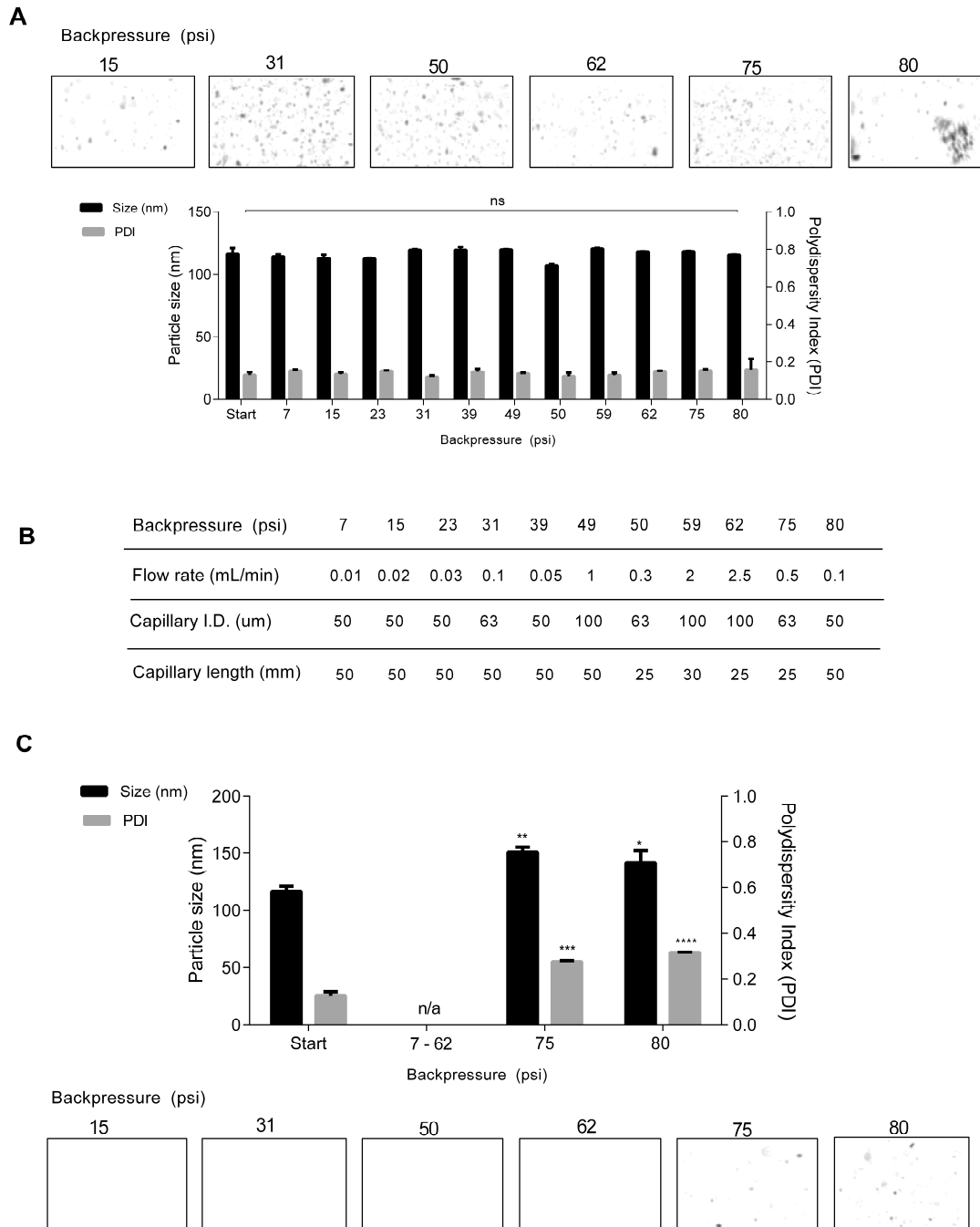


Figure 7.5: Particle size and polydispersity as a function of increasing backpressures in the TFF system. A) Samples collected and analysed on the retentate side including images obtained from NTA analysis and particle characteristics obtained via DLS. B) Backpressures were controlled with differently sizes capillaries, varying in inner diameter (I.D.) and length allowing different flow rates to be used in the system. C) Samples collected and analysed on the permeate side including images obtained from NTA analysis and particle characteristics obtained via DLS. n/a = not applicable. All runs are presented as average of three independent runs \pm SD.

The presence of particles within in the permeate side above a backpressure of 75 psi was confirmed by qualitative image-based NTA analysis (Figure 7.5C). Furthermore,

DLS measurement of collected retentate and permeate verified vesicles present based on an intensity-based (Figure 7.6A) and volume-based (Figure 7.6B) size distribution.

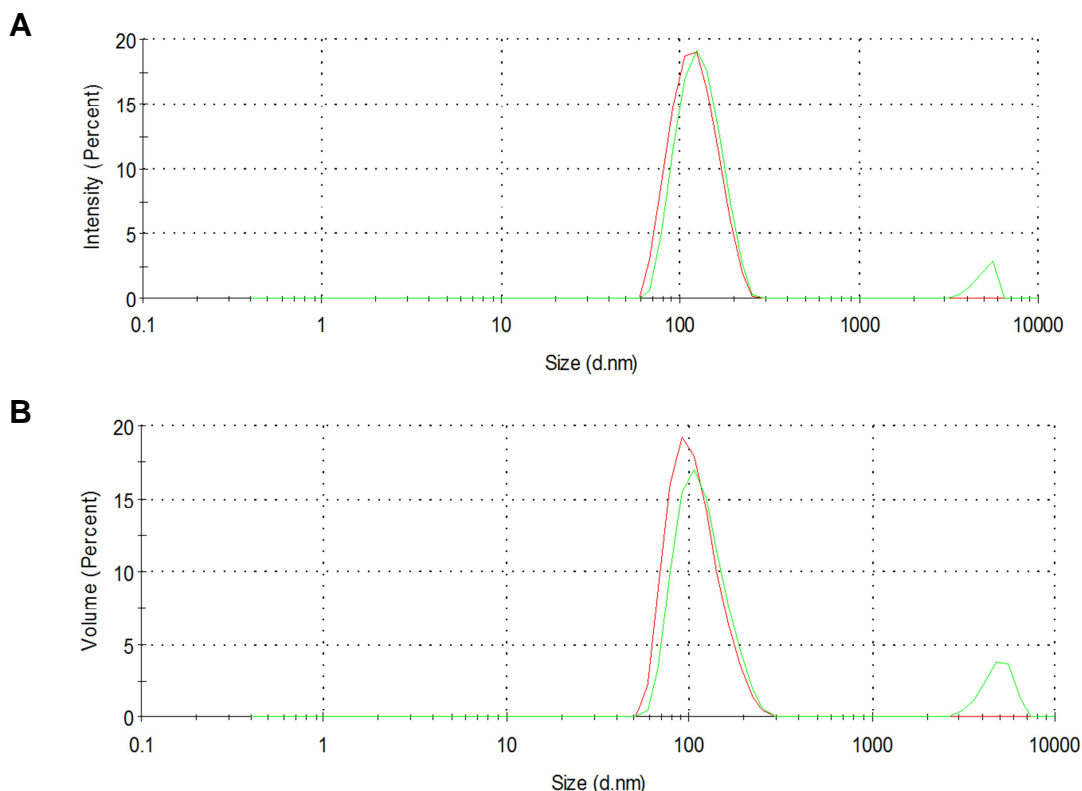


Figure 7.6: DLS measurement of A) intensity and B) volume based size distribution profiles comparing the retentate (red) and permeate (green) at 80 psi backpressure, confirming presence of particulates in the permeate.

Backpressures >75 psi resulted in extrusion of the vesicles through the membrane, altering physico-chemical particle characteristics as seen in the increase in size and PDI. Particle reformation on the permeate side may be associated to well-known liposome extrusion processes, which are reported to operate at pressures as high as 100-700 psi; where polycarbonate filters are reported for pressures less than 100 psi for lower lipid concentrations (Cullis et al., 1991; Olsen et al., 2001). Operating the TFF at 1-2 mL/min allowed faster operations with higher throughput and the flow rates matched the ones applied for liposome manufacturing (Chapter 4, 5 and 6). Results suggest the selection of backpressures in the TFF unit between 5-80 psi (Van Reis and Zydney, 2001, 2007) a common range for backpressures in filtration processes in industry (Cheryan, 1998).

Whereas commonly used separation techniques necessitate the formulation of larger vesicles to achieve separation (Torchilin and Weissig, 2003), vesicles at or below 300 nm have been shown to be difficult for separation by centrifugation and are hence often subjected to lengthy dialysis for removal of non-entrapped drug and solvent residues

(Belliveau et al., 2012; Zhigaltsev et al., 2012). In contrast purification of large multilamellar liposomes often use centrifugation to remove un-entrapped drug (Ali et al., 2013), where liposome range in the micrometer-size. The presented setup demonstrates that a range of capillaries with varying inner diameter and length can be easily applied for controlling the backpressures, with the ability to tailor resulting flow rates to desired throughput. Furthermore, the clamping mechanism of the filtration device allowed for simple membrane exchange, thereby supporting the use of different commercially available membrane sheets as required. Overall, the setup allows for continuous filtration of the liposomes, while collecting in the same vial. The increase in backpressure allowed screening over the ideal operational backpressure under which the desired liposome characteristics were maintained and maximum recovery yields obtained.

7.3.4 Membrane integrity testing

In order to verify the membrane integrity at a backpressure of 80 psi, the system was challenged with ovalbumin at two different concentrations (1 mg/mL and 0.5 mg/mL). Protein was filtered through the membrane at backpressures of 15 and 80 psi and the presence of protein in retentate and permeate was qualitatively verified by SDS-PAGE. Ovalbumin was detected in the retentate stream at 15 and 80 psi for both concentrations of ovalbumin (Figure 7.7, lane 4, 6, 9 and 11), with no protein detected in the permeate streams respectively (Figure 7.7, lane 3, 5, 8 and 10). Following, the membrane integrity remains at 80 psi with no rupture and subsequent leakage of the membrane. Furthermore, the retention of the protein in the retentate stream was found to be independent of the protein concentration in the inlet stream.

These results verify that liposome detection in the permeate stream at backpressures of 80 psi (Figure 7.5, 7.6) were associated solely to extrusion of the lipids through the filter at higher backpressures and reassembly of the liposomes in the permeate stream.

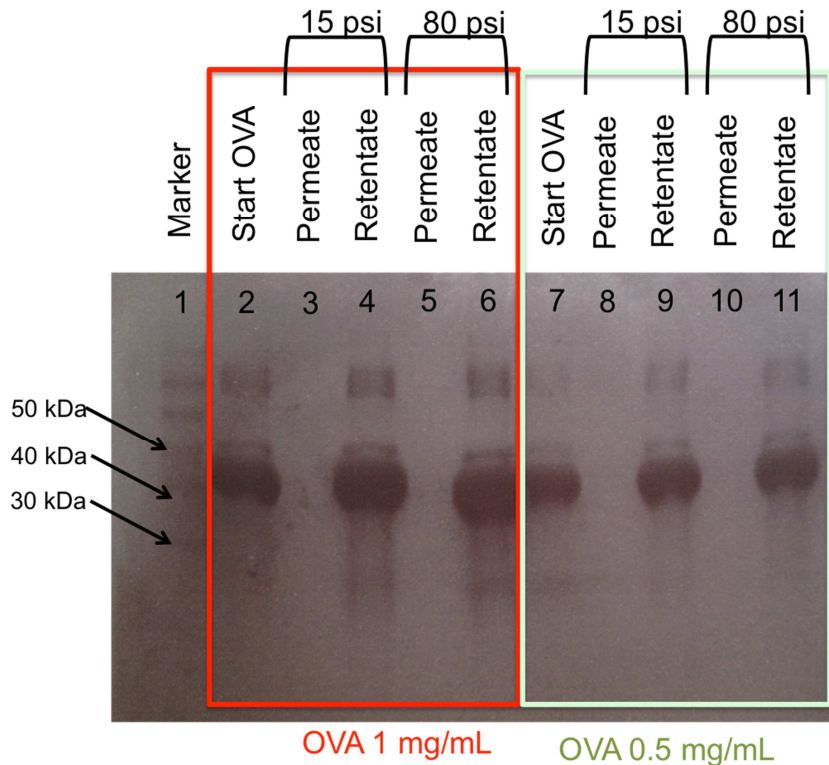


Figure 7.7: SDS-PAGE of ovalbumin filtered in the TFF system at 1 mg/mL (red) and 0.5 mg/mL (green) at backpressures of 15 and 80 psi.

A control of filtration backpressures by a capillary on the retentate side was required for purification of the liposomes and retention of the liposomes. Furthermore, backpressures of 80 psi were found to force extrusion of the liposomes through the membrane with vesicle resemblance on the permeate side of the TFF system, leading to increased polydispersities and vesicle sizes (Figure 7.5C). Furthermore it was shown that the membrane is capable of withstanding high backpressures of 80 psi without loss of its integrity (Figure 7.7).

7.3.5 The effect of filtration on particle characteristics for cationic and anionic liposomes

Based on the established backpressures during liposome purification (< 75 psi), the purification capabilities of the TFF device were explored with a variety of small liposomes, differing in size and charge (DDA-TDB vesicles, 250 nm, +50 mV; PC-Chol vesicles, <100nm, -5 mV; DPPC-Chol-DPPG vesicles, <150 nm, -50 mV;; DOPE-DOTAP vesicles, <100 nm, 60-80 mV). The objective was to study the capabilities of the on-chip filtration unit to purify broad range of liposomal products. The filtration process of a cationic liposomal adjuvant (DDA-TDB) in three diafiltration runs gave 91% particle recovered throughout three cycles of diafiltration (Figure 7.8) with no significant change in size or zeta potential for the cationic formulations, but with a small

increase in PDI, still remaining within the polydispersities obtained with DDA-TDB systems (Henriksen-Lacey et al., 2011a).

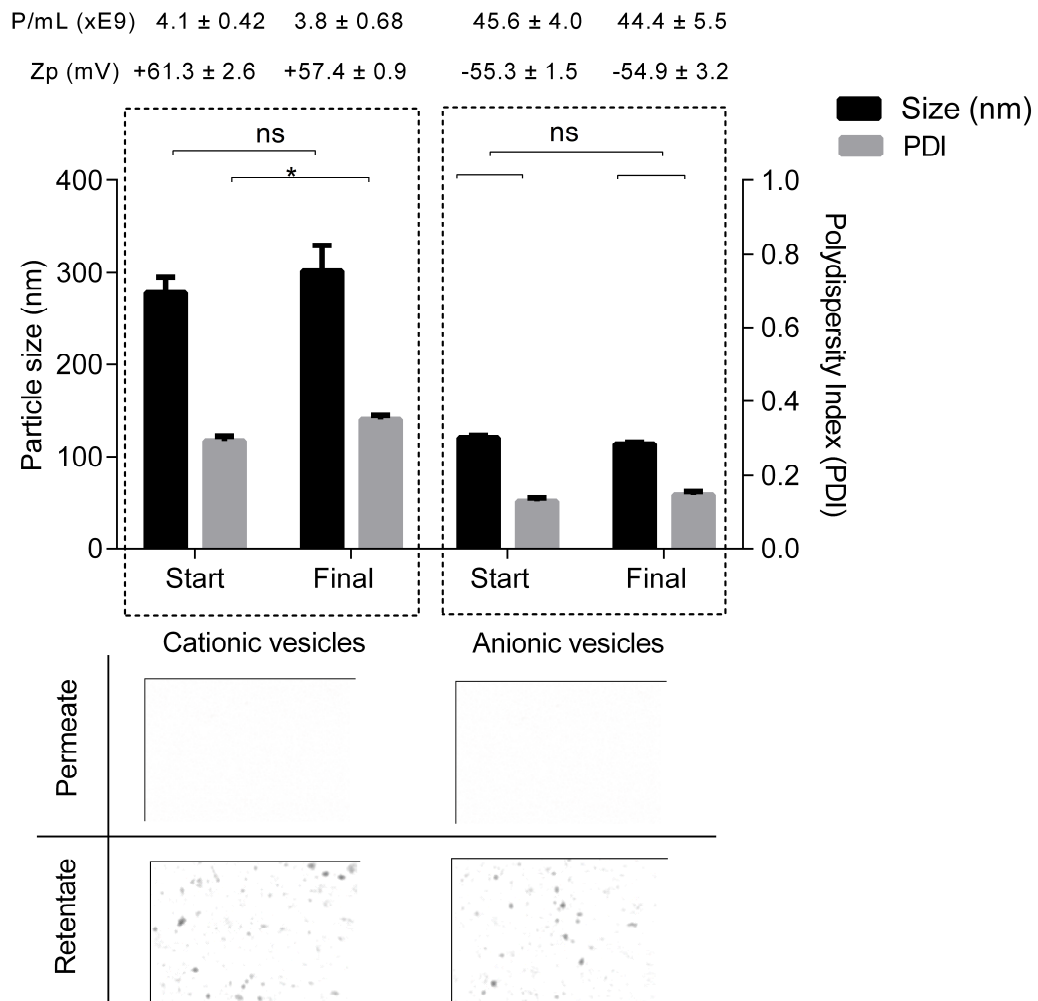


Figure 7.8: Vesicle size, polydispersity, zeta potential (zp) and particle concentration (P/mL) for cationic (DDA-TDB) and anionic (DPPC-Chol-DPPG) liposomes before and after the TFF purification. Images from NTA show vesicles present on the retentate side only.

Similarly, when anionic liposomes (DPPC-Chol-DPPG) were tested the vesicle size, PDI, ZP and particle concentration remained unaffected with vesicles being around 120 nm, with a PDI of 0.14 and a zeta potential of -55 mV. The concentration of the particles after filtration was 4.4×10^{10} P/mL, representing an overall particle recovery of 95% (Figure 7.8). Furthermore, NTA analysis in each diafiltration cycle verified that no liposomes were present in the permeate stream (Figure 7.8).

7.3.6 Purification of non-incorporated moieties from liposome formulations

With the system initially investigated for the filtration of liposomes only, the efficiency for removal of drug or protein not incorporated within the liposomes was investigated in three diafiltration cycles. At each cycle, liposome characteristics were assessed and the removal of contaminants (drug or protein and solvent residues) was quantified.

To consider the removal of non-entrapped protein from liposome formulations, liposomes (DPPC-Chol-DPPG) were also mixed with ovalbumin (OVA; 100 $\mu\text{g/mL}$); with repulsive forces prominent no electrostatic interaction between liposome and protein are expected and therefore all non-entrapped protein should be removed. The size and PDI of the liposomes remained unchanged through the course of three diafiltration cycles and 93% of the liposome particles were recovered (Figure 7.9A). The addition of OVA to the liposome formulation caused an initial reduction in the overall anionic ZP from -55 mV to -32 mV; however, upon removal of the free protein via filtration, the ZP reverted back to an more anionic nature (-43 mV; Figure 7.9A), with no qualitative indication of surface-adsorbed protein. Protein (OVA) and residual solvent was removed into the permeate stream throughout the filtration cycle, with a final removal of 70% of free protein and 95% solvent (Figure 7.9B). A residue of 10% free ovalbumin was found in the final retentate after three diafiltration cycles with no liposomes present (Figure 7.9C) which allows estimating a protein remain of 20% using the negatively charged liposomes. Electrostatic repulsion forces may have contributed to remaining free protein levels, which is anticipated to further decrease with additional filtration cycles.

The drug concentration was related to previous work on the encapsulation of a low solubility drug (propofol) in the liposomal bilayer by microfluidic mixing (Chapter 6). Drug was added post-liposome production at a concentration of 1 mg/mL in a liposome formulation containing negatively charged liposomes (DPPC-Chol-DPPG). Overall, 99% of free drug was removed in three diafiltration cycles (Figure 7.9D). The majority (90%) removed in the first diafiltration cycle, with further reductions (by 80%) in the second diafiltration run (effective remaining propofol ca 2.5%) (Figure 7.9D). The third diafiltration cycle further reduced the available free drug by 60%, with 1% of free drug remaining after three filtration cycles (Figure 7.9D). The TFF system was also validated by effectively removing residual solvent from the formulation. An initial starting concentration of 20% (v/v) ethanol was present in the sample; representing the average amount of solvent after a microfluidics-based liposome manufacturing at a FRR of 1:3 (Chapter 6). The amount of ethanol was reduced by ca. 50% in the first

diafiltration cycle, with a remaining effective ethanol concentration of 3% (v/v), (Figure 7.9D) after three filtration cycles. Liposome characteristics (size, PDI and ZP) remained throughout three diafiltration cycles (Figure 7.8).

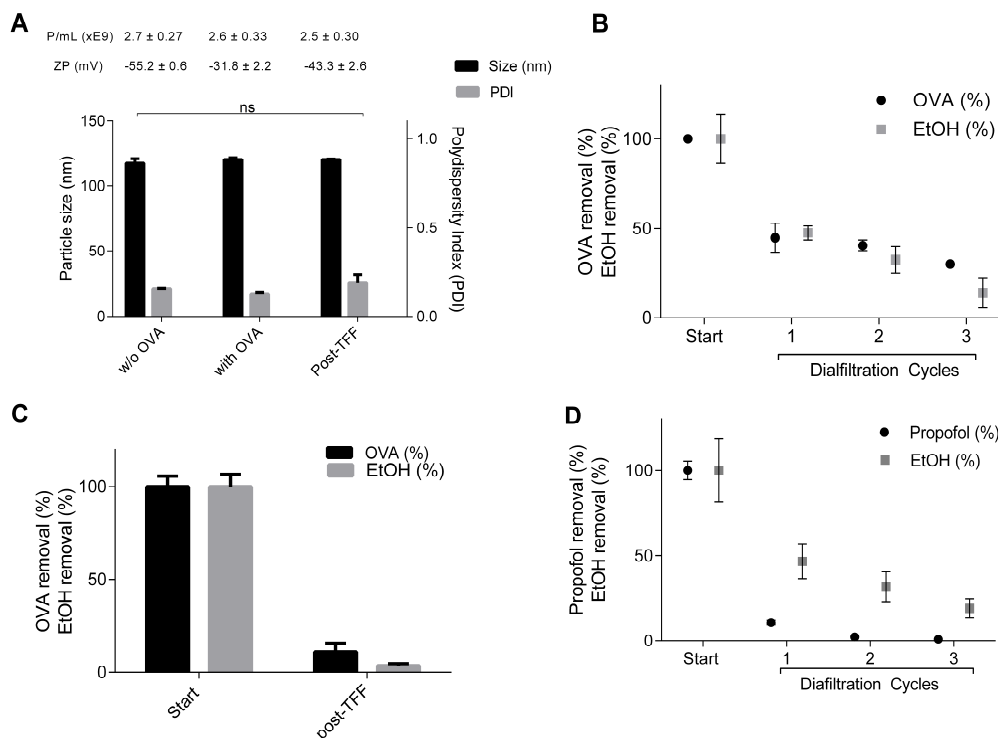


Figure 7.9: A) Vesicle size, polydispersity, zeta potential (zp) and particle concentration (P/mL) for anionic liposomes (DPPG-DPPC-Chol) prior and post ova-addition (ovalbumin, 100 $\mu\text{g/mL}$), and particle characteristics after the TFF purification. B) Protein (ovalbumin) and ethanol removal in three diafiltration cycles for anionic liposomes (DPPG-DPPC-Chol), expressed as % to the initial amount of contaminants present. C) Ovalbumin and ethanol removal in three diafiltration cycles with no liposomes present D) Propofol and ethanol removal in three diafiltration cycles for anionic liposomes (DPPG-DPPC-Chol), expressed as % to the initial amount of contaminants present. All runs are presented as average of three independent runs \pm SD.

The desired application of the liposomes will determine the required final purification level, which cannot be generalized, and results here suggest that the on-chip filtration unit copes with different levels of purification required. Overall, the on-chip purification system showed efficient removal of solvent, non-entrapped protein and drug from the liposome product, which fully retained in the TFF setup.

7.3.7 Purification of cationic liposomes with spiked model protein

The efficient protein delivery through cationic liposomes is well known, with electrostatic attractive force dominating and often leading to a surface-adsorption reaching close to 100% (Kaur et al., 2013). To challenge the on-chip TFF system, a high concentration of protein (100 $\mu\text{g/mL}$) was added, beyond levels that can be

effectively adsorbed onto the cationic liposome formulation (DDA-TDB) to demonstrate the ability of the filtration system to separate non-adsorbed protein from liposomes with surface-adsorbed protein.

The liposomes without protein had an average size of 230 nm and were highly cationic in nature (Figure 7.10A). As expected, the addition of excess protein (which adsorbs to the surface of the cationic liposomes) resulted in a decrease in zeta potential and an increase in measured vesicle size and PDI due to cross-linking and/or aggregation of liposomes, as seen in previous work with DDA-TDB liposomes where a drop in ZP by ca. 20 mV was linked to a 100% adsorption of protein onto the liposomes surface at a final concentration of 10 $\mu\text{g/mL}$ (Henriksen-Lacey et al., 2010a). When these liposomal-protein systems were subjected to TFF and removal of non-associated protein, there was no significant difference in the size, PDI and zeta potential of the system (Figure 7.10A). The polydispersity was shown to remain stable throughout the diafiltration process of cationic liposomes (Figure 7.10A), which following allows associating the increase in PDI to the addition of the protein rather than the filtration parameters (flow rate, backpressure). Particle recovery showed that 87% of the particle concentration (P/mL) (post protein loading) was recovered in the final retentate after three filtration cycles (Figure 7.10A).

Using TFF, ethanol residues were reduced to 4% (v/v) and 75% of free protein was removed in the filtration setup (Figure 7.10B). Given that the vesicle size and zeta potential were maintained throughout the filtration process, this suggests that protein adsorbed to these liposomes was effectively retained during the process, and the liposome-protein complexes were not compromised. These liposome-protein aggregates as analysed via NTA are shown in Figure 7.10C. A higher PDI post protein addition is known to impede effective particle size measurement by light scattering processes given the bias of a DLS measurement towards larger particles (Chapter 3). The reduction in particle concentration after the addition of protein may be associated to the increase in particle size by aggregation rather than the loss of lipids in the system, leading to a misleading poorer result for particle recovery.

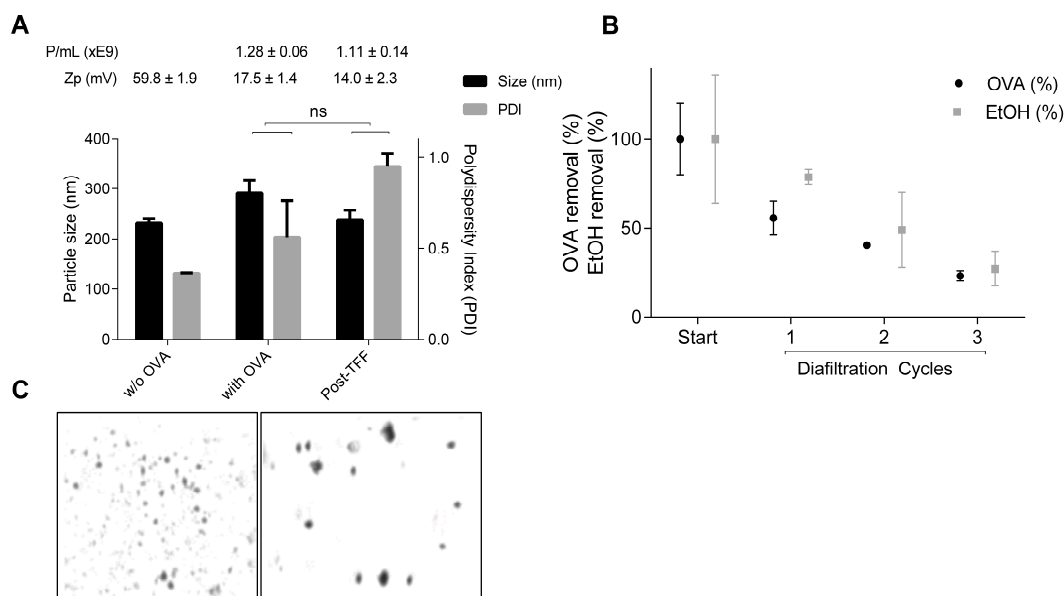


Figure 7.10: A) Vesicle size, polydispersity and zeta potential (zp) for cationic (DDA-TDB) liposomes prior and post ova-addition (ovalbumin, 100 µg/mL) and particle characteristics after the TFF purification. B) Protein (ovalbumin) and ethanol removal in three diafiltration cycles for cationic liposomes (DDA-TDB), expressed as % to the initial amount of contaminants present. C) NTA analysis for liposomes before (left) and after (right) loading with model protein (ovalbumin, 100 µg/mL). All runs are presented as average of three independent runs ± SD.

Aggregation upon exposure of DDA-TDB liposomes to protein has been reported, where a drop in ZP by ca. 20 mV was linked to a 100% adsorption of protein unto the liposomes surface at a final concentration of 10 µg/mL (Henriksen-Lacey et al., 2011a). The system was challenged by a protein addition of 100 µg/mL, representing a 10-fold increase in protein concentration usually encountered in *in-vivo* dosages (Henriksen-Lacey et al., 2010a). These results verify that an on-chip TFF system is capable of removing non-associated protein without influencing the liposome characteristics, providing an effective post-production purification step, with the option to recycle purified protein in further application.

Proof-of-principle studies performed in this study verify that liposomes maintain their particle characteristics with no significant alterations to particle size and PDI ($p > 0.05$) and overall recoveries from the filtration system are high (87-97%). A diafiltration setup (buffer exchange) was shown to successfully remove residual solvent as well as un-entrapped drug into the permeate side, elucidating the base of purification of liposomes based on on-chip TFF whilst providing guidance for backpressure control in a batch-type process.

7.3.8 Continuous setup

Next, the on-chip purification system was combined with the upstream on-chip liposome manufacturing method, as described in earlier chapters (Chapter 4, 5, 6), aiming for moving from conventional batch type processing to an on-chip continuous manufacturing setup for liposome synthesis and purification. A SHM micromixer was employed to directly supply the TFF system with liposomes (Figure 7.11A) in a continuous setup.

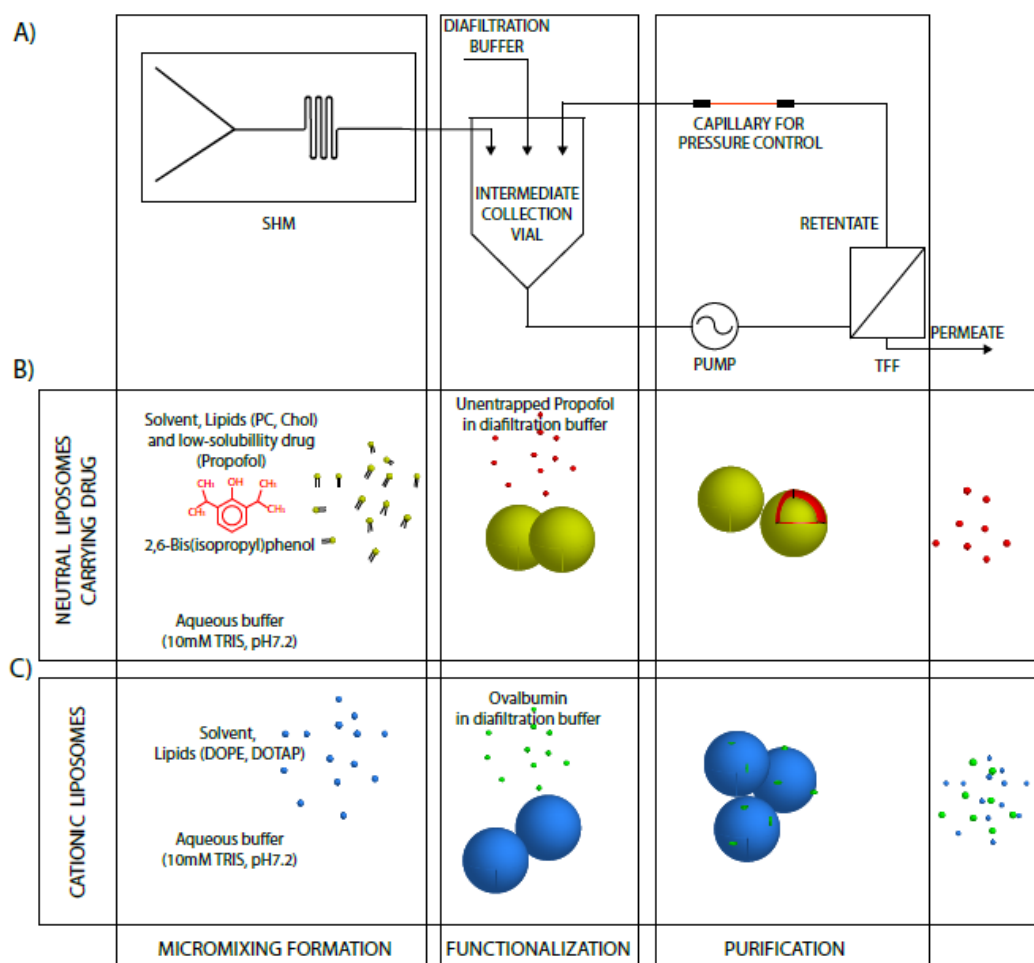


Figure 7.11: A) Schematic overview of the continuous on-chip liposome manufacturing. Liposomes were manufactured with a SHM mixer upstream and lead through the TFF system for consecutive on-chip purification. B) Schematic overview of the formation of liposomes loaded with a low-solubility model drug. Vesicle assembly and drug loading are performed with a SHM, non-entrapped (free) drug to be removed by consecutive TFF. C) Schematic overview of the formation of liposomes loaded with a protein model. Vesicle assembly is performed with a SHM, with protein addition post assembly, non-entrapped (free) protein to be removed by consecutive TFF.

However, to decouple the throughput from the two devices and to control independently the flow rates an intermediate collection vial was used. The setup allows for purification of the liposomes in a diafiltration mode, with complete recovery of lipid (Figure 7.12A). Furthermore, once the desired purification level was reached, the

formulation was concentrated, by stopping the manual top-up of permeate volume, here the filtration of four volumes without replenishing of fresh buffer allowed to double the lipid concentration (Figure 7.12B). The setup allows for continuous filtration of the liposomes, while collecting in the same vial. The process described here is continuous, as only one pump works at a time, allowing independent control over the flow rates in the SHM and TFF devices and the addition of the permeate volume was done manually. Moreover, multiple diafiltration cycles can run in the TFF until desired purity is reached. Adding manually fresh solution to the intermediate collection vial compensated for liquid passing into the permeate. The overall process described, enables independent control over the flow rates in the SHM and TFF devices both as separate or coupled units of operation. This system was then tested with two formulations: 1) neutral liposomes (PC-Chol, 4:1 molar ratio) incorporating propofol (Figure 7.11A) and 2) cationic liposomes (DOPE-DOTAP, 1:1 molar ratio) loaded with surface-complexed protein (Figure 7.11B).

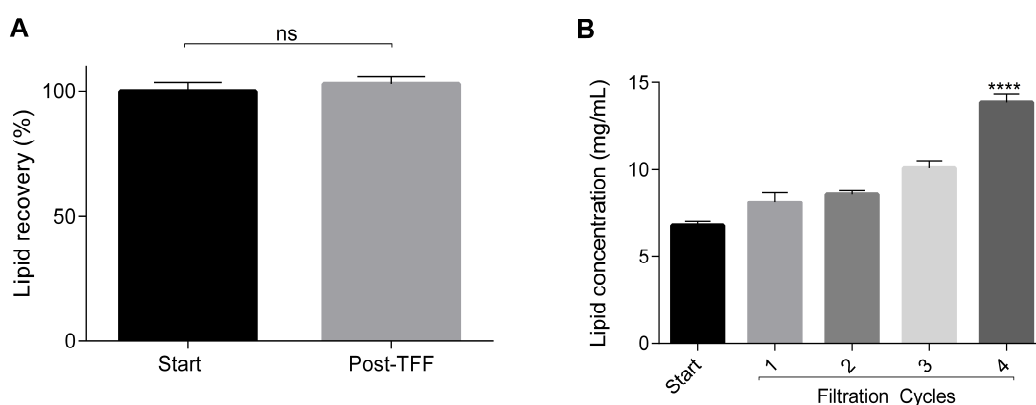


Figure 7.12: Lipid recovery in the continuous process setup for A) lipid recovery after four diafiltration cycles. B) Lipid concentration in four concentration cycles, related to the initial amount of lipids present prior to the concentration cycles. All runs are presented as average of three independent runs \pm SD.

7.3.8.1 Continuous manufacture and purification of liposomal solubilisation agents

The encapsulation and solubilisation of low aqueous drug in the bilayer of liposomes in a microfluidics based setup has been investigated previously (Chapter 6). The setup (Figure 7.11B) was applied here to compare drug encapsulation with previous studies in Chapter 6. In this work, the amount of free drug (untrapped) was removed by means of the previously-described on-chip filtration, replacing the earlier reported dialysis method (Chapter 6). The resulting particle size of 50 nm with a low PDI of 0.4 is in line with previously reported liposome sizes at given FRR and TFR (Figure 6.2, Chapter 6). The continuous filtration setup maintained particle sizes and PDI (Table

7.2) with no significant alteration. The continuous filtration setup was able to remove un-entrapped drug at a remaining solvent concentration of 3% (v/v) after three diafiltration cycles (Table 7.2). Encapsulation of the drug yielded 50 mol%, according to previous reported encapsulation values using the same SHM setup (Figure 6.5D, Chapter 6). The assembly presented here allows for complete removal of the free drug, which was previously achieved by dialysis, with the remaining amount of drug encapsulated in the liposome bilayer. Most importantly, the remaining drug encapsulation shows that the pressures applied in the system has no adverse effect on liposome integrity, successfully replacing time-consuming dialysis with a microfluidics-based filtration process.

Table 7.2: Continuous purification of PC-Chol liposomes loaded with propofol. Here, propofol and lipids were included in the solvent stream and liposome formation and drug encapsulation was performed in a SHM, run at 2 mL/min and a 1:3 solvent:aqueous ratio. na= not applicable.

	Liposome with drug after SHM	Liposome with drug after TFF
Size (nm)	49.8 ± 0.5	62.3 ± 11.6
Polydispersity	0.42 ± 0.003	0.35 ± 0.07
Loading (mol%)	na	49.3 ± 5.8
Effec. ethanol (% v/v)	16.1 ± 3.9	3.1 ± 1.5

7.3.8.2 Continuous manufacture and purification of cationic liposomes with adsorbed protein

The continuous setup for the production of cationic liposomes (Figure 7.11C) verified the removal of free protein in the given TFF setup. Here, vesicle size and PDI remained unchanged throughout the filtration process. Liposome sizes (before protein addition) of 60 nm are in line with sizes reported in a SHM design for production of DOPE-DOTAP liposomes (Figure 4.1A, Chapter 4). The continuous system allowed for a removal of 75% of free protein (Table 7.3), with the remaining protein adsorbed on the liposome surface, evidenced by reduced ZP (Table 7.3). Protein and solvent was removed to a final level of 24% and 4% (v/v) respectively (Table 7.3).

Table 7.3: Continuous purification of DOPE-DOTAP liposomes loaded with protein (ovalbumin). Here, lipids were included in the ethanol stream and liposome formation was performed in a SHM, run at 2 mL/min and a 1:3 solvent:aqueous ratio. Protein was added post-liposome synthesis. OVA = ovalbumin, na= not applicable.

	Liposome w/o OVA after SHM	Liposome with OVA in collection vial	Liposome with OVA after TFF
Size (nm)	62.8 ± 1.9	88.5 ± 5.7	89.3 ± 10.9
Polydispersity	0.44 ± 0.02	0.45 ± 0.008	0.42 ± 0.02
Zeta potential (mV)	83.9 ± 3.5	43.6 ± 1.6	69.2 ± 6.1
Loading (%)	na	100.1 ± 2.5	23.9 ± 0.8
Effec. ethanol (% v/v)	na	15.0 ± 6.9	4.1 ± 1.5

7.4 Conclusion

Overall, work demonstrated feasibility for on-chip purification of liposomal batches below 5 mL for developmental purposes. Liposome manufacture, drug loading and removal of contaminants (like un-entrapped drug or protein as well as of solvent residues) were performed in a continuous on-chip design, allowing for manufacturing, purification and concentration of liposomal drug products. The system was challenged with a range of liposomes, varying in lipid composition, surface potential, size and concentration, demonstrating on the ability of the on-chip filtration unit to be tailored to a broad diversity of lipid-based nanoparticles. The setup allows for an efficient and quick screening of several lipid or drug candidates, and that is able to cope with high throughput requirements of early stage development processes. The continuous setup may permit early determination of liposomal characteristics (e.g. size, surface potential, particle number) and encapsulation efficiencies of a wide variety of drug molecules, allowing for future integration of process analytical technologies to further aid reproducibility. Furthermore, the setup is of considerable interest for screening of cost-intensive drugs or protein, which require a quick and efficient development process. The system copes with a wide variety of protein products in development, together with its flexibility for incorporating different membrane types, aligned with recent trends in biopharmaceutical industry (Walsh, 2010). Nevertheless, scalability by parallelisation of mixer chips has been suggested, as highlighted in Chapter 6 and scalability of TFF membranes is reported which offers future application and scale-up for larger-scale production and purification of liposomal products in a continuous flow setup. Whereas large-scale continuous-based methods for liposome extrusion have been reported (Schneider et al., 1994), the here presented method shows applicability for a high-throughput and small-footprint early-stage development techniques for liposomal products.

Chapter 8

A multivariate analysis study to correlate liposomal adjuvant characteristics



*Lipid structure obtained from avantilipids.com

Papers relating to this chapter:

Kastner E., Hussain M. J., Bramwell V. W., Christensen D. and Perrie Y. (2015). Correlating liposomal adjuvant characteristics to in-vivo cell-mediated immunity using a novel *Mycobacterium tuberculosis* fusion protein: a multivariate analysis study. *Journal of Pharmacy and Pharmacology*, 67(3), 450-463.

8.1 Introduction

The new generation of vaccines, based on recombinant DNA or highly purified proteins, provide a safer but less immunogenic vaccination strategy (O'Hagan et al., 2001b). Subunit vaccines contain selected highly purified antigens, which can offer reduce side effects and specific immune responses are raised with an overall safer and more immunologically defined form of vaccination (Black et al., 2010; Mohammed et al., 2010). However, the administration of purified recombinant proteins induces only a low immunogenicity, necessitating the co-administration with a suitable immunostimulatory adjuvant to produce a more potent vaccine (Holten-Andersen et al., 2004; O'Hagan and De Gregorio, 2009). Amongst the particulate delivery systems, liposomes act as competent immune response stimulators and as immunological adjuvants already approved for human administration (Bramwell and Perrie, 2005). The key factors for interaction with the immune system and influencing the efficacy of liposomal adjuvant activity are vesicle charge, size, bilayer fluidity and liposomal composition (Henriksen-Lacey et al., 2011b). Their intracellular presence is important for effective vaccine delivery and has been linked to a cationic surface charge (Christensen et al., 2007b), which enhances antigen adsorption and retention due to electrostatic interaction (Perrie et al., 2008; Smith Korsholm et al., 2007). The combination of the cationic dimethyldioctadecylammonium bromide (DDA) with an optimised incorporation of the glycolipid trehalose 6,6-dibehenate (TDB) is used in an adjuvant system (CAF01), which is capable of stimulating powerful cell-mediated immunity against mycobacterium tuberculosis (MTB), upon delivery of the recombinant TB subunit protein Ag85B–ESAT-6 (H1 vaccine) (Davidsen et al., 2005).

However in the analysis of vaccines, a range of biological outputs are generated which may be interlinked in enhancing immune responses. Multivariate analysis (MVA) is a method that allows for analysing several variables at a time and represents a flexible and multipurpose tool for data mining and analysis. Other than linear regression tools, MVA deals with several variables and observation at a time, handles dimensionality problems and provides overview whilst classifying and comparing different groups of data, using regression modelling between variables (X) and responses (Y). Despite noise in a data set, MVA extrapolates even in limited data sets (Eriksson, 2006). Principal components (PC) are computed through the multidimensional space, which approximate the best data fit. Generally, at least two orthogonal PCs are required to approximate the data and model the systematic variation sufficiently. Principal component analysis (PCA) allows for a simple overview of the data allowing to group large data sets and identify trends and outliers (Jackson, 2005; Wold et al., 1984). The

addition of the Y-variables (responses or measurements) in a partial least square (PLS) analysis aims to predict Y from X. This identifies the influence of the variables to a response, correlations within the responses and factors responsible for achieving a desired response (Wold et al., 1984; Wold et al., 2001a; Wold et al., 2001b).

8.2 Aim and Objectives

The aim of this chapter was to investigate multivariate modelling for prediction of *in-vivo* liposomal vaccine efficiency from *in-vitro* measured physicochemical vesicle characteristics. To achieve this, a model was generated, which comprised the experimentally obtained data for predicting liposomal adjuvant *in-vivo* performance. Cationic liposomal adjuvants of well described activities were manufactured containing the lipids DDA and TDB (Christensen et al., 2009; Christensen et al., 2007b), and increasing levels of the saturated phosphatidylcholine, 1,2-distearoyl-*sn*-glycero-3-phosphocholine (DSPC) was incorporated into the DDA-TDB formulation at a locked DDA-TDB molar ratio (Table 8.1).

Table 8.1: Incorporation of DSPC into DDA-TDB formulations at 25, 50 and 75 mol%. Values of weight or μ moles in the various liposome formulations where DDA-TDB was locked at a 5:1 wt ratio/8:1 molar ratio and increasingly replaced with DSPC in a 50 μ L dose.

Formulation (mol%)	Weight μ g per dose		
	DDA	TDB	DSPC
DDA-TDB	250	50	0
+ 25% DSPC	188	36	88
+ 50% DSPC	125	25	175
+ 75% DSPC	63	14	264

This variation in lipid composition was studied *in-vivo*, relating physical adjuvant properties to adjuvant activity using a tuberculosis antigen vaccine candidate, a combination of the early secreted antigens of Ag85B–ESAT-6 with the latently expressed Rv2660c antigen (H56), known and proved for its protective immunity before and after exposure (Aagaard et al., 2011). PCA was performed to cluster the *in-vivo* derived immunological vaccine responses upon delivery of a subunit protein by the various formulations made, which were linked to the vesicle characteristics, size, zeta potential and DDA concentration by PLS regression analysis.

8.3 Results and Discussion

8.3.1 Summary of *in-vivo* responses

The molar ratio of DDA-TDB remained locked at 8:1, given this ratio was shown the most beneficial in immunological performance (Davidsen et al., 2005). DSPC was incorporated in substitution for DDA-TDB at various molar % ratios, which influenced vesicle characteristics (Table 8.2). Vesicle characteristics prior to protein addition coincided well with previous results, ~500 nm, PDI of 0.3 and ZP of ~-50 mV, (Christensen et al., 2007a; Davidsen et al., 2005; Henriksen-Lacey et al., 2010b). Substitution of DDA-TDB with 25, 50 or 75 mol% DSPC increased vesicle size ($p < 0.05$), yet remained in a sub micrometer size range with reduced ZP with increasing DSPC content (Table 8.2). The addition of the H56 antigen increased the particle size of all formulations ($p < 0.05$) to 850 -1300 nm depending on the formulation, whilst ZP was reduced (Table 8.2). Due to the high content of cationic lipid and anionic antigen, antigen loading was $> 85 \%$ (results not shown), even with the 75 % DSPC formulation ($p>0.05$).

All four of the liposome formulations induced higher ($p<0.05$) IgG immune responses once compared to mice immunised with antigen alone, remaining insignificant within the formulations, $p>0.05$ (Table 8.2). Results suggested that the incorporation of up to 50 % DSPC within the liposome formulation did not compromise the immunogenic effect of the DDA-TDB adjuvant, which has been shown to induce a protective cellular immunity against TB upon co-delivery of a model vaccine antigen (Agger et al., 2008). Results suggests that the IgG and IgG1 responses were independent over a range of DDA and TDB concentrations and independent of resulting liposome characteristics, whilst the decrease DDA content decrease the IgG2b response.

Mice were vaccinated with the liposomal adjuvant and were re-stimulated with the H56 vaccine at increased concentrations from 0-25 $\mu\text{g/mL}$, after which the antigen specific splenocyte proliferation rates were measured. A strong link between cell proliferation and DDA-TDB adjuvant was seen (Table 8.2), with the highest counts obtained for the formulations without DSPC incorporated.

Elevated DSPC content lead to a decrease in IFN- γ , IL-2 and IL-6 levels (Table 8.2). The mice, which received antigen alone showed similar, if not higher, IL-5 levels in comparison to those animals immunized with the liposomal adjuvants, which had a similar and low IL-5 production over the different formulations tested. In contrast, the

incorporation of DSPC in the liposomal adjuvant increased the IL-10 responses (Table 8.2).

The replacement with DSPC was linked to a decrease in ZP, which was related to skewing the immune response towards a Th2 type response, despite the small decreases in ZP noted in these formulations (Table 8.2). The liposomal surface charge has been found linked to the quality of immunity stimulated with Ag85B-EAST-6 antigen (Henriksen-Lacey et al., 2010b), where especially the levels of IFN- γ were linked to a positive surface charge of the liposomal adjuvants, as seen here in the study (Table 8.2). In contrast, a weak cellular immune response was seen with the formulations that included a high content of DSPC, 75 mol%. The subsequent Th2 type immune response was found linked to the increased levels of DSPC, which was overall linked to the resulting ZP of the formulations made (Henriksen-Lacey et al., 2010b).

Table 8.2: DDA-TDB and its substitution with 25-75 mol% DSPC with effect to particle characteristics prior to and post H56 antigen adsorption. Results denote mean \pm SD for three independent experiments. Mean serum H56 specific antibody isotype titres stimulated by DDA-TDB and DSPC substitution (n=5, \pm standard error). Values display the positive reciprocal end point dilution (log10). Spleen cell proliferation stimulated by H56 vaccine antigen and spleen cell cytokine production in response to re-stimulation with H56 antigen. Results represent mean average of five spleens per vaccination group \pm standard error. Experiment performed by M. Jubair Hussain.

Formulation		Antigen H56	DDA/TDB	25% DSPC	50% DSPC	75% DSPC
Vesicle size (nm)			517 ± 29	640 ± 24	856 ± 114	734 ± 67
		+ H56	981 ± 198	1266 ± 151	1036 ± 92	852 ± 52
Polydispersity			0.32 ± 0.01	0.34 ± 0.01	0.32 ± 0.01	0.33 ± 0.02
		+ H56	0.42 ± 0.02	0.46 ± 0.06	0.54 ± 0.14	0.42 ± 0.1
ZP (mV)			45.7 ± 0.7	42.7 ± 1.9	35.4 ± 3.6	33.2 ± 0.5
		+H56	47.4 ± 6.1	41.4 ± 3.7	31.7 ± 6.4	28.7 ± 5.3
Specific titer						
IgG (log 10)	Day 9	1.54±0.26	1.46±0.38	1.88±0.67	1.7±0.47	1.08±0.4
	Day 24	3.52±0.11	4.12±0.06	3.94±0.2	4.08±0.11	3.7±0.19
	Day 37	3.34±0.10	4.54±0.13	4.48±0.11	4.53±0.11	4.24±0.15
	Day 49	3.94±0.05	4.3±0.08	4.3±0.08	4.38±0.06	4.18±0.11
IgG1 (log 10)	Day 9	1.72±0.18	1.44±0.54	1.28±0.38	2.08±0.18	1.26±0.47
	Day 24	3.76±0.10	4.48±0.14	4.66±0.18	4.45±0.12	4.12±0.14
	Day 37	3.94±0.10	4.66±0.10	4.78±0.13	4.83±0.15	4.42±0.13
	Day 49	4.06±0.05	4.72±0.10	4.66±0.05	4.6±0.10	4.48±0.06
IgG2b (log 10)	Day 9	1.22±0.3	1.32±0.5	2.02±0.16	1.67±0.15	0.58±0.32
	Day 24	2.74±0.13	4.66±0.10	4.3±0.22	4.45±0.15	3.04±0.26
	Day 37	3.28±0.34	4.9±0.21	4.9±0.64	4.75±0.30	3.28±0.54
	Day 49	3.52±0.13	4.78±0.08	4.6±0.25	4.82±0.12	3.64±0.22
Re-stimulation H56 antigen (µg/mL)						
Spleen Prolif. (CPM)	0	366.3±60.6	537.7±190.9	294.1±58.9	366.1±95.3	522.9±127.8
	0.05	745.1±208	20394±1759	13770±2956	8482.4±3614	3290.4±1187
	0.5	1335.5±567	32873±2320	22731±3923	16610±5710	6649±2340
	5	2227±837	36524±1914	27097±4421	20325±6005	8216±2660
	25	3530±1550	42750±2985	32285±4894	28861±6541	11540±4081
INF-γ (pg/mL)	0	178.13±17.1	157.38±11.6	100.20±1.8	105.14±2.6	108.74±2.9
	0.5	207.41±30.6	3754.37±250	2015.21±218.9	316.96±47.3	110.26±6.7
	5	220.46±19.2	3938.64±58.4	3237.68±319	674.58±52.1	112.93±5.7
IL-2 (pg/mL)	0	70.82±14.5	66.6±18.7	43.7±17.7	21.9±6.8	29.3±2.2
	0.5	173.7±61.7	2607.7±185	2646.2±303	1383.7±345	39.1±11.3
	5	341.9±93.5	3493.2±307.2	3170.6±230	1753.3±391	38.9±6.7
IL-5 (pg/mL)	0	265.45±13.1	214.56±19.4	81.8±22.9	71.9±13.9	98.7±6.1
	0.5	268.4±44.6	249.3±13.5	85.1±22.3	139.1±12.6	147.3±13.4
	5	282.4±5.8	235.9±14.8	207.3±32.5	224.2±9.3	317.4±30.3
IL-6 (pg/mL)	0	20.1±4.1	20.4±1.9	62.9±3.4	58. ±1.7	60.6±3.9
	0.5	26.4±5.7	325.1±26.2	109.6±16.9	68.2±6.5	52.7±9.3
	5	10.1±4.6	394.4±16.6	172.2±27.6	86.1±8.9	68.3±4.1
IL-10 (pg/mL)	0	51.2±4.4	44.8±1.6	81.8±7.0	69.6±6.2	69.6±8.3
	0.5	65.3±11.6	83.9±4.1	199.2±10.4	102.6±11.9	100.6±7.8
	5	85.8±7.8	73.4±11.3	155.4±12.7	116.2±7.1	140.1±13.5

8.3.2 Multivariate analysis for clustering Th1 and Th2 type immune responses to adjuvant characteristics

8.3.2.1 Principal component analysis and partial least square regression

The aim of this work was to link the multifactorial changes in composition of the lipids to the biological attributes of an adjuvant formulation. Therefore, the data set obtained from above *in-vivo* study was used in a multivariate analysis (MVA) and the liposome characteristics post-addition of the antigen were used (Table 8.2). Initially, two principal components (PC1 and PC2) were fitted, which determined the overall model fit by weights and loadings. The data set was subdivided into two different patterns, initially selecting the liposomes size and DDA concentration as X-variables, leaving 10 Y-variables in the PLS analysis at a total of 12 observations. This data set assessed whether the most influential factor was the size of the vesicles or the DDA concentration for the measured output of the immune response. This model yielded a fraction of the X-variation modelled in PC1 of 62 % (eigenvalue 1.24) and 100 % in PC2 (eigenvalue 0.764). The Y-variation was modelled 46 % and 13 % with the first PC and second PC respectively, with a cumulative goodness of fit of 0.59 and the cumulative goodness of prediction of 0.37.

Secondly, the liposome size, ZP and DDA concentration were selected as X-variables, leaving 9 Y-variables for the total of 12 observations. The reason for this second set of analysis was to verify how the ZP as a variable influenced the immune response of the vaccine *in-vivo*. The model yielded a cumulative goodness of fit of 0.97 and the goodness of prediction of 0.52, by fitting two PC (PC1 with 64% of the fraction in the X-variation modelled (eigenvalue 1.92), 97% respectively in the PC2 (eigenvalue of 0.98); Y-variation modelled in first PC was 44%, 53% in PC2). The TDB concentration once included as a variable resulted in a statistical not valid model, with respective variable found not influencing the immune response. Both model setups comprised satisfactory information using both PCs fitted, and cumulated R^2 and Q^2 values for each Y-variable was analysed (Figure 8.1).

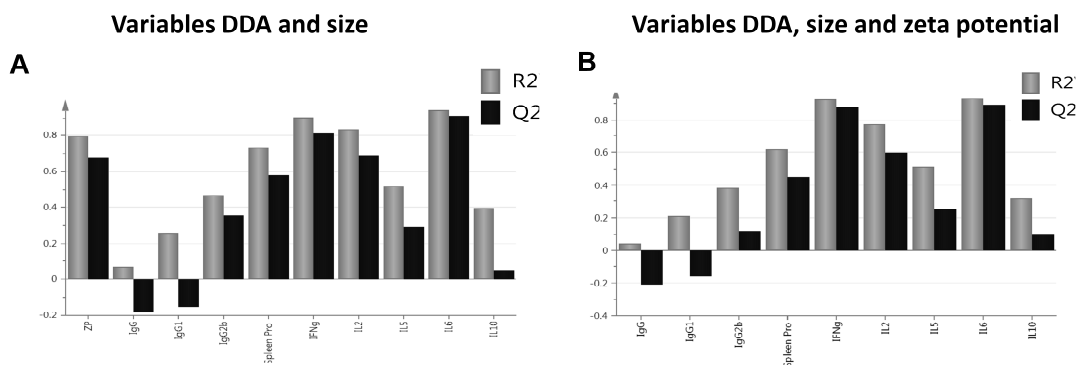


Figure 8.1: X/Y overview plot indicating the cumulated R^2 and Q^2 values for each response for A) DDA and size and B) DDA, size and zeta potential. Well modelled responses show a R^2 and Q^2 value above 0.5 poor model fit was indicated by negative Q^2 (statistical insignificance).

A threshold value for $R^2 > 0.5$ indicated a valid model; values below 0.5 indicated noise. Both designs chosen had insignificant models for the responses IgG and IgG1 (Figure 8.1A and B), as indicated by negative Q^2 . The responses spleen proliferation, INF- γ , IL-2, and IL-6 had a good model fit above 0.5, with respective good prediction power based on a relatively low level of noise in the data set (Figure 8.1A and B). The responses IgG2b, IL-5 and IL-10 had a R^2 at or below 0.5, indicating a higher amount of noise present for these responses, which was further evaluated throughout the model validation. Based on poor model fit, the antibody subtypes IgG and IgG1 were removed from further analysis. The response IgG2b remained, and despite low confidence level, aiming for further confirmation of its validity throughout the MVA analysis.

Modelling of the data revealed no strong or moderate outliers present, as evaluated in the PCA analysis (Figure 8.2). The colour coding in the PCA analysis was used for identification of trends and clusters within the observations made. The colour coding according to ZP (Figure 8.2A) and DDA concentration (Figure 8.2B) and coincided with a colour trend shifting from right to left, suggesting a link between DDA concentration and ZP; opposed to the colour coding according to size (Figure 8.2C), which a colour pattern not coinciding with any of the other responses in the model. Uncorrelated response, here exemplified by IgG (Figure 8.2D) did not show an overlapping colour profile with any of the variables or responses, suggesting no correlation or cluster for this response. The responses INF- γ , IL-2, spleen proliferation and IL-6 (Figure 8.2 E, F, G, H) showed a similar colour pattern, shifting from right to left with the decrease in measurement output; an early indication of a cluster.

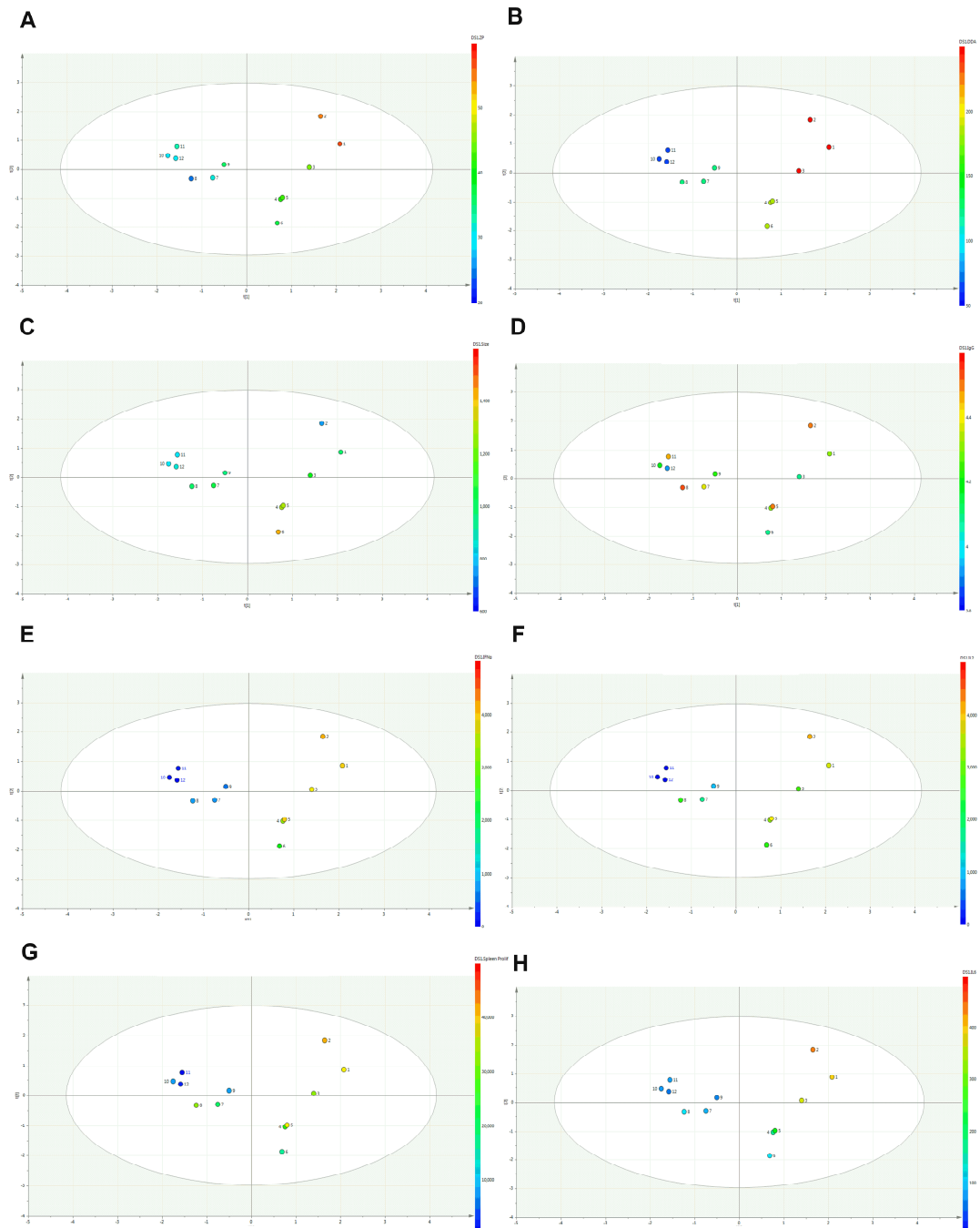


Figure 8.2: PCA cluster analysis with colour coding according to A) ZP, B) DDA concentration, C) vesicle size D) IgG, E) INF- γ , F) IL-2, G) spleen proliferation and H) IL-6.

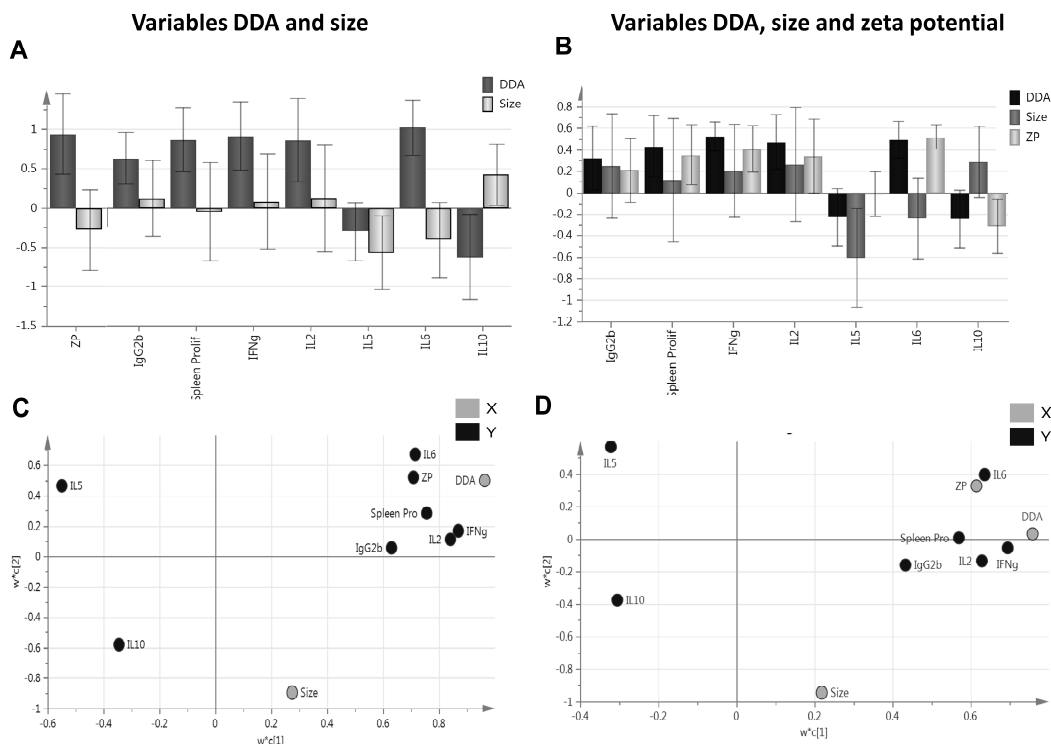


Figure 8.3: PLS analysis results with coefficient overview, displaying the coefficients for all responses to interpret how the X-variables affect the Y-variables for A) DDA and size and B) DDA, size and zeta potential. Loading scatter plot, where the relation between X and Y- variables are displayed for C) DDA and size and D) DDA, size and zeta potential.

The X-Y relation was depicted by specific regression coefficients (Figure 8.3A and B) in the PLS model; streamlining the model overview and coincided with the loading plot. The coefficient plot was used to detect correlated responses due to similar coefficient profiles, whereas uncorrelated responses are revealed due to a different profile in their X-Y relationship. The coefficient plot revealed a strong correlation between the variables DDA (Figure 8.3A) and ZP (Figure 8.3B) to the splenocyte proliferation, indicative of the promotion of splenocyte proliferation upon re-stimulation with the H56 antigen. The variable liposome size did not correlate to any of those responses, as seen by the respective confidence interval crossing zero. The most influential variable for the response spleen proliferation was the variable DDA concentration, due to its high coefficient value approaching 1 with relative small confidence interval. The response splenocyte proliferation was found closely correlating to the variable DDA (Figure 8.4C) and ZP (Figure 8.4D), due to close situation in the loading scatter plot in the upper right hand quadrant. Results indicate that the biggest effect to spleen proliferation rates is the increase in DDA content in a formulation, with the DDA content strongly influencing the ZP of a formulation, the ZP was found correlative as variable and response in both models. The peak of proliferation correlated with the formulation with the highest ZP, here DDA-TDB alone.

The cytokine responses (INF- γ , IL-2, IL-6 and IL-10) were found statistically linked to the variables DDA (Figure 8.3C), and ZP (Figure 8.3D). Both variables showed a positive correlation to cytokine responses INF- γ , IL-2 and IL-6. The opposite situation of the response IL-10 in the loading scatter plot revealed an inverse correlation to the variables DDA concentration and ZP. The coefficient plot showed this inverse relationship due to negative predictions by the DDA concentration as well as the ZP (Figure 8.3A and B). The increase in DDA in a vaccine adjuvant formulation did not influence the size of the liposomes formed significantly, but resulted in a higher surface charge. This link, as seen in Table 8.2, was identified by the PLS analysis, which predicted an increase the specific INF- γ , IL-2 and IL-6 production *in-vivo*. The highest INF- γ production in the *in-vivo* study was detected for the formulation with the strongest cationic ZP, here DDA-TDB (Table 8.2). Literature reported the effect of cationic surface charge to cytokine response *in-vivo*, with enhanced responses of INF- γ as well as IL-6 (Hussain et al., 2014). PLS model predictions were able to detect this relationship in line with reported effect of cationic surface charge (but with constant TDB concentrations across the formulations). Additionally, the model revealed independence of the DDA content on IL-5, and an inverse correlation between the response IL-5 and the liposome size (Figure 8.3C and D), predicting an increase in IL-5 production by smaller vesicles, as seen in the *in-vivo* data given that the highest IL-5 production was measured for the DDA-TDB formulation, which also had the smallest size (Table 8.2). The responses INF- γ , IL-2 and IL-6 showed coincided coefficient profiles for the variables DDA and ZP, which suggested a grouping and relation between those cell mediated responses, as clustered collectively as Th1-specific immune responses. Both loading scatter plots (Figure 8.3C and D) revealed this cluster, showing that the ZP, independent of its use as variable or response, clustering the Th1 specific immune responses INF- γ , IL-2, IL-6 and IgG2b.

Generally, the DDA concentration was overall strongly linked to the ZP of a formulation, as seen once the ZP was selected as a Y-response (Figure 8.3A) as well as a X-variable (Figure 8.3B). The ZP as linked to the DDA concentration, both important variables for initiating a Th1 mediated immune response *in-vivo*. Model generated were found statistically valid for the variables, DDA and ZP (spleen proliferation, IFN- γ , IL-2, IL-6, IL-10, IgG2b). The liposome size was found important only to a limited extent, here in the case of IL-5. The variable influence on projection plot (VIP) (Figure 8.4), revealed all components and Y-variables (Kubinyi, 1993), indicated the importance of the variable DDA content (Figure 8.4A) and ZP (Figure

8.4A, B), both shown as the variables with the highest impact in the PLS models, whereas the size variable was found of only limited importance.

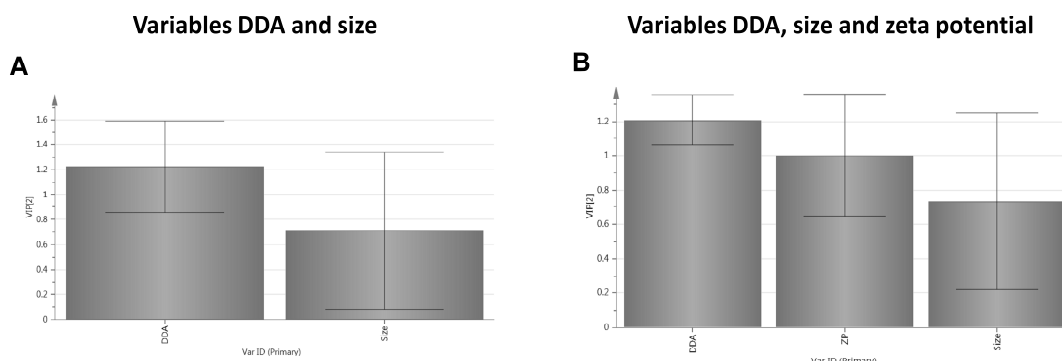


Figure 8.4: VIP plot (variable importance for projection) summarizing the importance of the variables liposome size and zeta potential. The VIP plot is sorted from high to low and indicates the value of the variable DDA and zeta potential as the most important X-variables in the PLS model for A) DDA and size and B) DDA, size and zeta potential.

Results indicate the usefulness of PLS analysis, where a higher dimensional dataset can easily be projected onto a plane, allowing for a simple depiction of several Y-variables, rather than analysing each response at a time in a separate model. Overall it is beneficial to analyse strongly correlated Y-variables together and group them, mainly due to the stabilisation of a model due to variable-correlation (Eriksson, 2006), mainly for dependent responses, which are based on similar measurements. Results confirmed the importance of the DDA concentration in a vaccine formulation as a crucial variable influencing the immunological response to a bigger extend than the size of the vesicles (across the size range considered here).

Results here emphasize on MVA as a novel tool allowing for *in-vitro* to *in-vivo* predictions, cluster analysis for Th1 specific immune responses. In this study, a range of factors were varied, here DDA, TDB and DSPC content which affected vesicle size and ZP. A cluster analysis (PCA) identified trends, outliers and initial links. Developed models clustered and predicted Th1 immune response, which was found dependent on key liposomal adjuvant characteristics, DDA concentration and ZP. DDA-TDB was substituted with DSPC, which reduced the cationic surface charge with limited effect to vesicle size. Some data sets were indicative of a higher level of noise, e.g. for the variables IgG2b, IL-5 and IL-10, which might be associated with the assay accuracy leading to moderate interpretation power. Furthermore, despite this initial analysis, it might be required to expand the analysis on a wider formulation in more complex vaccine adjuvant studies. Obtaining vaccine efficiency data is so far limited to *in-vivo* results, sacrificing animals. The MVA analysis might be a novel and cost effective way, to speed up the drug and process development process, by predictions of an *in-vivo*

immune response based on the characteristics of the adjuvant or delivery system. This might be a powerful tool for vaccine adjuvant characterisation by clustering of *in-vivo* specific immune responses and help to generate future predictions of vaccine efficiency, which may overall accelerate the development process of a vaccine candidate. MVA can be used for summarizing and visualizing data sets, for classification and identification of quantitative relationships between variables (Eriksson, 2006). Its application is flexible and not limited to a number of variables or observations, which determine relationships between several system or process based analytical measurements (Lopes et al., 2004). The effect of one property to another one can be measured and links the dependent and independent variable together in one model by regression analysis. Furthermore, many variables can be analysed simultaneously, achieved by a reduction in the dimensionality of a data set by projection onto a plane of lower dimension interpretations (Kourti et al., 1996). The visualisation and simplification of complex sets of data is highly applicable in any process or product development particularly in pharmaceutical research (Rajalahti and Kvalheim, 2011) as well as in diagnostics tools, often used in industrial processes for product quality control (Kourti et al., 1996).

8.3.2.2 Model validation

In addition to the performed PCA and PLS analysis, the models generated were validated by respective permutations plots for each specific Y-response (Figure 8.5), which is a crucial diagnostic tool in the analysis of a multivariate model. The permutation plots assessed the validity of the PLS model by evaluating the risk of invalidity. Additionally, the permutation plots verified that the model fit is not only valid for the current data set, but can also be applied for new observations and predictions of Y. For the permutation, the X-data was left unchanged while permuting the Y-data and arranging it in a different order. Consequently, a new PLS model is fitted using the permuted data set. R^2 and Q^2 verified the derived models by cross-validation. The Y-data was randomly shuffled, and the permuted values were compared with the real R^2 and Q^2 values of the model. The repetitive permutation generated parallel models according to the number of permutations, mostly between 25 and 100, (here, 40). Based on random data, reference distributions could be made which assessed the validity of the initial PLS model (van der Voet, 1994). The comparison of the goodness of fit and prediction (R^2 and Q^2) of the current model to the ones of the randomly permuted Y-observations was performed at constant X-variables. R^2 and Q^2 of the original model were shown on the far right and the permuted values, 40 for each Y-response, were depicted on the left side of the graphs, with a respective correlation line

between permuted Y-vector to the original X-vector. Model validity was pre-set as the intercept of the Q^2 regression line at or below zero.

The evaluation of the permutation analysis revealed excellent model validity for the ZP as a response (Figure 8.5A), confirming above PLS model. The previously highlighted invalidity of the responses IgG, IgG1, IgG2b, IL-5 and IL10 resulted in poor permutation plots as seen earlier, Figure 8.1 A and B and exemplified here by the permutation plot of IgG, where scattered permutations above the original Q^2 and R^2 were strongly indicative of a poor model validity, Figure 8.5B. Additionally, model validity for the responses spleen proliferation, INF- γ , IL-2 and IL-6 was confirmed (Figure 8.5 C, D, E, F).

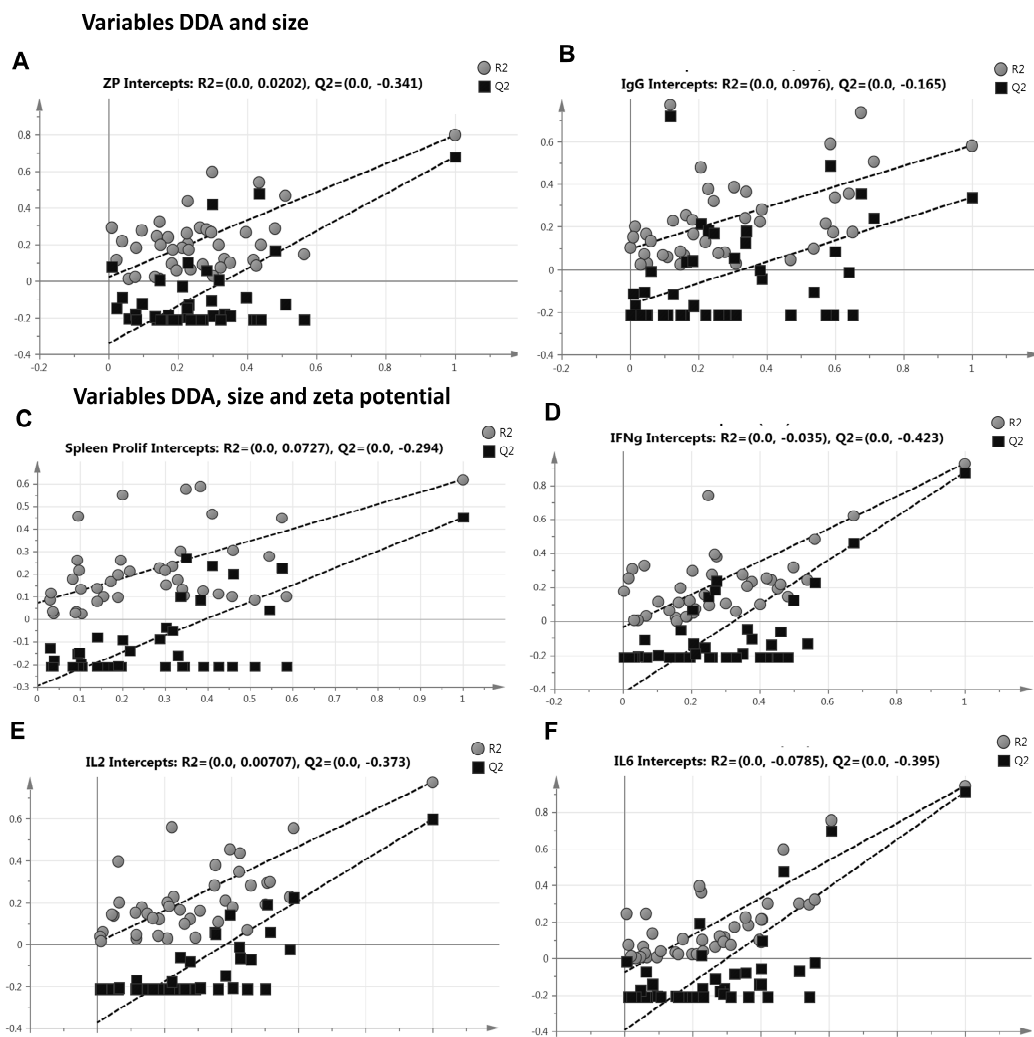


Figure 8.5: Permutations plot for A) zeta potential, B) IgG, C) spleen proliferation, D) IFNg, E) IL-2, F) IL-6. Model validity was assessed for 40 permutations. The correlation between permuted Y-vector to the original X-vector is depicted by the horizontal correlation axis. The criteria for model validity have been selected as the intercept of the Q^2 regression line at or below zero.

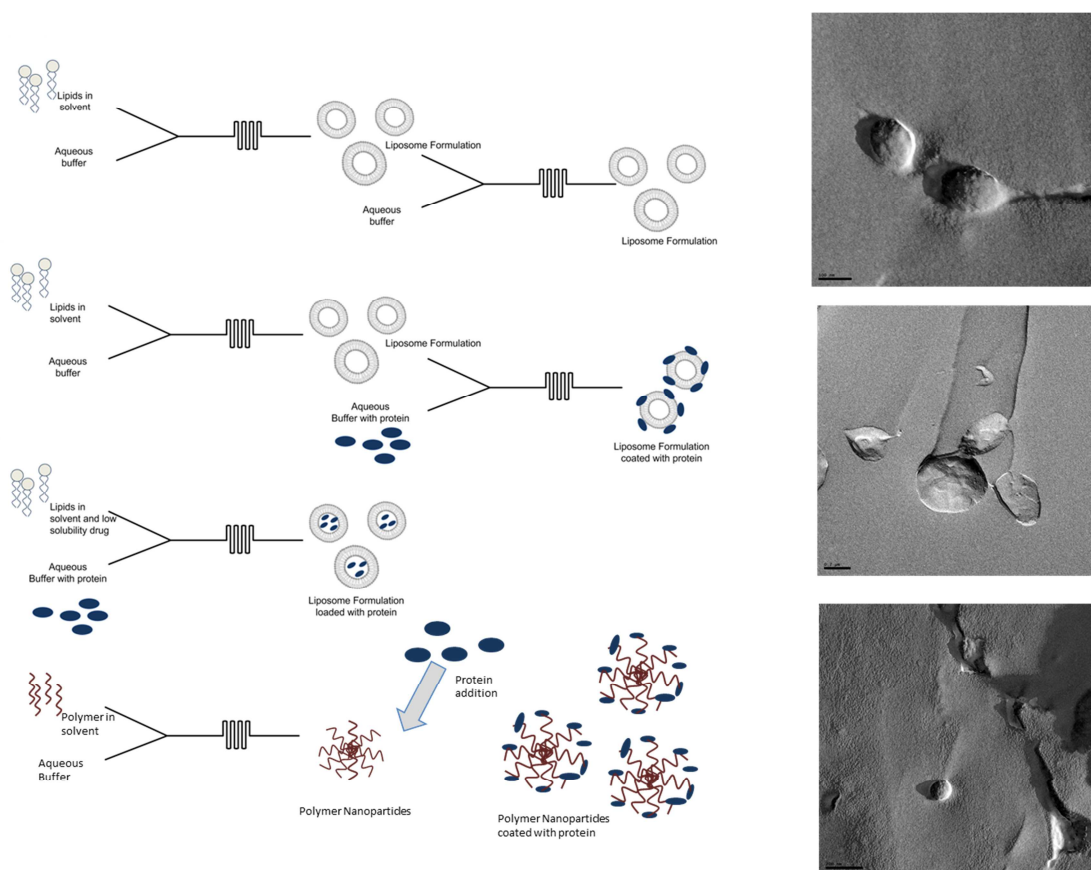
8.4 Conclusion

The accumulation of a large quantity of data is further enhanced by modern and high throughput analytical equipment, leading to the challenge of extraction of valuable data in a reasonable timeframe. The incorporation of computer-based methodologies simplifies the analysis of large data sets, extracting key features within a reasonable timeframe. Tools like DoE and MVA accommodate this need, combining regression models with experimentally obtained data or offline analysis. The aim is to provide extra information and confidence in a given research application based on critical quality parameters (like here the selection of immune responses) of a given system, here liposomes varying in lipid composition, size and ZP. The MVA clustered and predicted key liposome characteristics dependent on specific *in-vivo* immune responses. The validity of derived PLS models was found key for a confidence prediction of *in-vivo* specific immune responses from offline analytical measurements and key characteristics could be correlated to critical quality attributes of a vaccine formulation. The tool presented may accommodate the need for screening many variables at a time, often required in early stage development processes.

Despite potentially curative pharmacotherapies available, tuberculosis (TB) remains the primary cause of preventable deaths worldwide (Sosnik et al., 2010). A host's stimulation of cellular Th1 type immunity is required to inhibit Mycobacterium tuberculosis (MTB) infection. The H56 subunit vaccine, delivered by a liposomal adjuvant consisting of DDA with the glycolipid TDB is capable of stimulating powerful cell-mediated immunity against MTB (Davidsen et al., 2005). Nevertheless, time intensive optimisation required screening over a range of lipid concentration, resulting in different vesicle sizes and surface potential, which quickly accumulates the numbers of formulations tested. The formulation consisting of DDA-TDB with well described adjuvant activity (Christensen et al., 2009; Christensen et al., 2007b) was correlated within this study as the formulation which generated the highest levels of INF- γ , IL-2, IL-6 responses, as required for a strong Th1 type immunity. Therefore, this formulation was further investigated and translated into the on-chip manufacture of adjuvants.

Chapter 9

Protein association with adjuvants and polymer nanoparticles manufactured by microfluidics



Papers relating to this chapter:

Kastner E., Nadella V., Devitt A. and Perrie Y. Microfluidics-directed manufacturing of cationic liposomal adjuvants (in preparation)

9.1 Introduction

Liposomes are well-described delivery systems for vaccines (O'Hagan and De Gregorio, 2009), based on their flexibility, particulate nature and ability to incorporate a range of immunogenic molecules such as proteins, peptides or genetic constructs. A successful vaccine adjuvant should be able to carry and deliver its antigen to the target cells thus raising the desired immune response. Based on Chapter 8 the formulation DDA-TDB was found a potentially effective adjuvant providing a strong Th1 immune response upon delivery of an antigen triggering the formation of a liposome-antigen depot at the site of injection for subcutaneous and intramuscular administration (Henriksen-Lacey et al., 2010a). Previous work investigated the correlation between the adjuvant's *in-vivo* to *in-vitro* activity with formulations containing various amounts of cholesterol using human macrophage-like cells to investigate the interaction of cells and adjuvant formulation (Kaur et al., 2013). However, in addition to liposomes systems nanoparticles prepared with poly(D,L-lactide-co-glycolide) (PLGA) or poly(D,L-lactide) (PLA) have also been shown as effective for *in-vivo* delivery of protein, peptides and DNA antigens (Ataman-Önal et al., 2006), and as controlled release drug delivery systems with proven safety profile (Okada and Toguchi, 1995; Xiao et al., 2012). Here, microfluidics-based nanoprecipitation was exploited for nanoparticle-based adjuvant manufacturing. These nanoparticles were assessed for potential protein loading capabilities based on surface adsorption.

9.2 Aim and Objectives

The aim of this chapter was to investigate the microfluidics-based nanoprecipitation method for manufacturing of vaccine adjuvants. Two formulations were considered:

1. Cationic liposomal vaccine adjuvants: vaccine adjuvants consisting of DDA-TDB (Chapter 8) were prepared by varying the flow rate and ratio in the microfluidics-directed nanoprecipitation method and a model protein was added into the process for assessing qualitatively protein association with adjuvant assembly.
2. Polymer-based nanoparticles: different polymers were used for manufacturing nanoparticles by the microfluidics-based nanoprecipitation method.

Both systems were characterised and compared to system prepared using standard laboratory protocols. The *in-vitro* activity of the microfluidics-manufactured liposomal vesicles was assessed in an assay based on association and migration of APCs.

9.3 Results and Discussion

9.3.1 Manufacturing of lipid-based vaccine adjuvants by microfluidics

The first objective was to manufacture, using microfluidics, DDA-TDB adjuvants with physicochemical attributes matching the key parameters identified in Chapter 8 and manufacturing models in Chapter 3. Initially the impact of the FRR and TFR during the nanoprecipitation-based manufacturing of DDA-TDB liposomes using the 200 μm chip design was considered. Results in Figure 9.1 show that the combined alteration of the TFR and the FRR triggered the assembly of the smallest vesicle size possible at 2.5 mL/min and a FRR of 1:4. The alteration in FRR and TFR correlated well with liposome sizes; smaller vesicles were obtained with enhanced polarity in the assembly process Figure 9.1A, leading to minimum size of about 100 ± 10 nm, coinciding with model predictions at respective TFR and FRR (Chapter 3). Maximum vesicle sizes (350 ± 100 nm) were achieved at a TFR of 1 mL/min combined with a FRR 1:1 further coincided well with model predictions obtained in Chapter 3. ZP remained between 40-50 mV as would be expected given the total cationic lipid content was not varied. The PDI remained between 0.2-0.4 without a notable link to TFR and FRR (Figure 9.1).

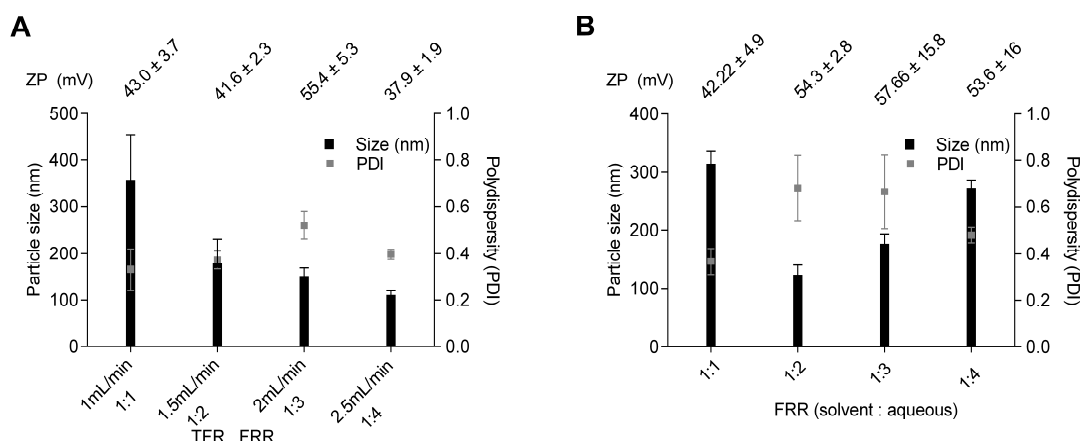


Figure 9.1: The effect of alterations in A) TFR and FRR at a constant solvent flow rate of 0.5 mL/min and B) FRR at constant TFR of 1 mL/min to the physicochemical vesicle characteristics in the 200 μm chip design. Results denote mean \pm SD of 3 separate batches.

Here, only the simultaneous alteration of both factors, TFR and FRR was found influencing the vesicle size significantly, whereas solely enhancing the aqueous content did not result in a reduced vesicle size (Figure 9.1B). This is in contrast to previous chapters, where the FRR was the only important variable influencing the resulting vesicle size (Chapter 4, 5, 6). Here, the heating block maintained the temperature of 60°C as required for the high transition temperature lipids and the solvent flow rate was kept constant at 0.5 mL/min throughout manufacturing of DDA-TDB liposomes. The setup of maintaining a constant solvent flow rate was based on

initial work by Zhigaltsev et al., where all alterations retained a constant solvent flow rate at 0.5 mL/min (Zhigaltsev et al., 2012). This setup allowed for constant introduction of the lipid stream, which, together with increasing the TFR and FRR, was found important for generating the smallest vesicle size possible for high transition temperature lipids formed by microfluidics-directed nanoprecipitation method. Here, the heating block was used for maintaining the lipids above the transition temperature by solely heating the syringe inlet and not the chip compartment itself. Heat transfer limitations by the syringes, together with a rapid cooling within the chip itself might lead to larger vesicles at lower flow rates and ratios, as seen in Figure 9.1A. Only the combined alteration of TFR and FRR might allow for a process where the nanoprecipitation process is faster than the rate of heat transfer and the cooling down of the streams within the chip.

In addition to physicochemical particle characteristics, images by freeze fracturing electron microscopy were obtained and evaluated regarding average liposome size, bilayer configuration and general appearance of the vesicles as manufactured by the nanoprecipitation method. Images showed a unilamellar bilayer confirmation, and verifying the average sizes obtained by DLS, ranging between 100 – 400 nm, depending on the setup used (Figure 9.2 A-D).

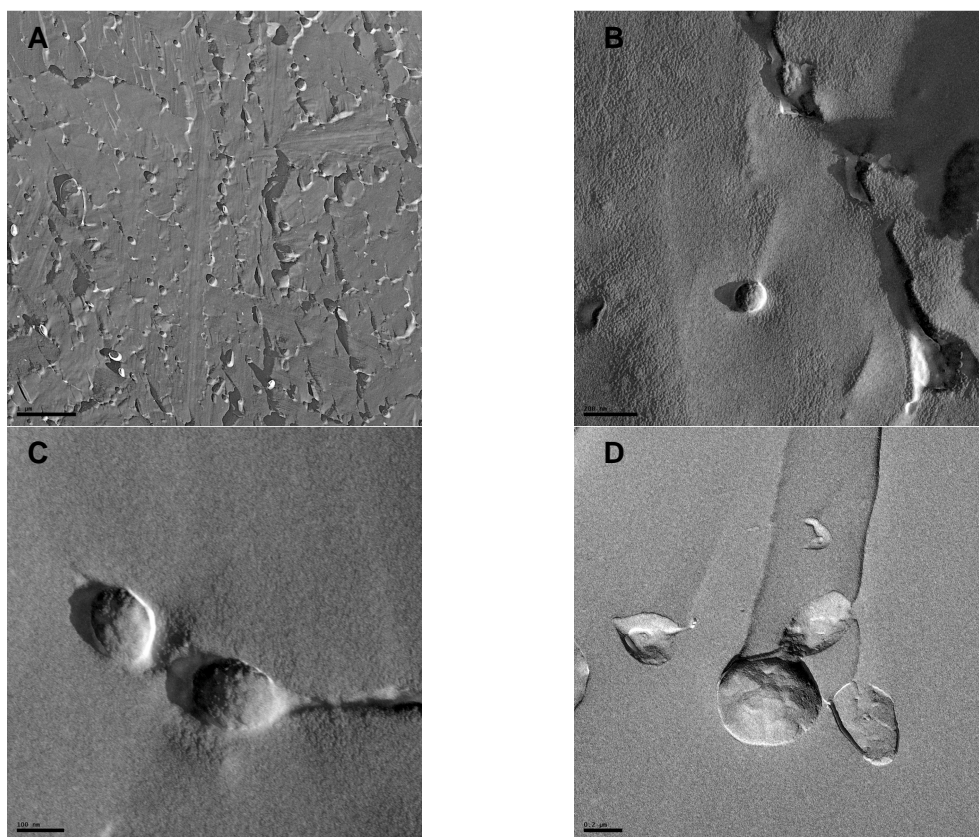


Figure 9.2: Freeze-fractured liposome samples manufactured with the microfluidics-method. Bar represents A) 1 μ m, B) 200 nm, C) 100 nm and D) 200 nm.

The rippled liposome surface visible in Figure 9.2 may be linked to a cluster formation of TDB and DDA, as noted earlier by Meyer and Richter in 2001. Here, the effect was associated with a disorder in the transition of the fatty acid chains in the lipids. Lipids might have varying direction and conformation changes which may alter with the lipid packing. Furthermore, variation in incubation temperature between pre-transition and actual transition temperature might have resulted in ripples (Hope et al., 1989; Meyer and Richter, 2001).

Following the work on manufacturing DDA-TDB liposomes, the applicability of the method to incorporate an antigen was investigated. The simplicity of the method for continuous manufacturing was explored, by incorporating the antigen in the manufacturing process, as schematically depicted in Figure 9.3. Whilst three options can be considered, the options in Figure 9.3A and B avoid exposure of the protein to elevated temperatures. Incorporating protein into the vesicle assembly process itself (Figure 9.3C) would be feasible for low transition temperature lipids only, to avoid protein denaturation and therefore was not considered in these studies.

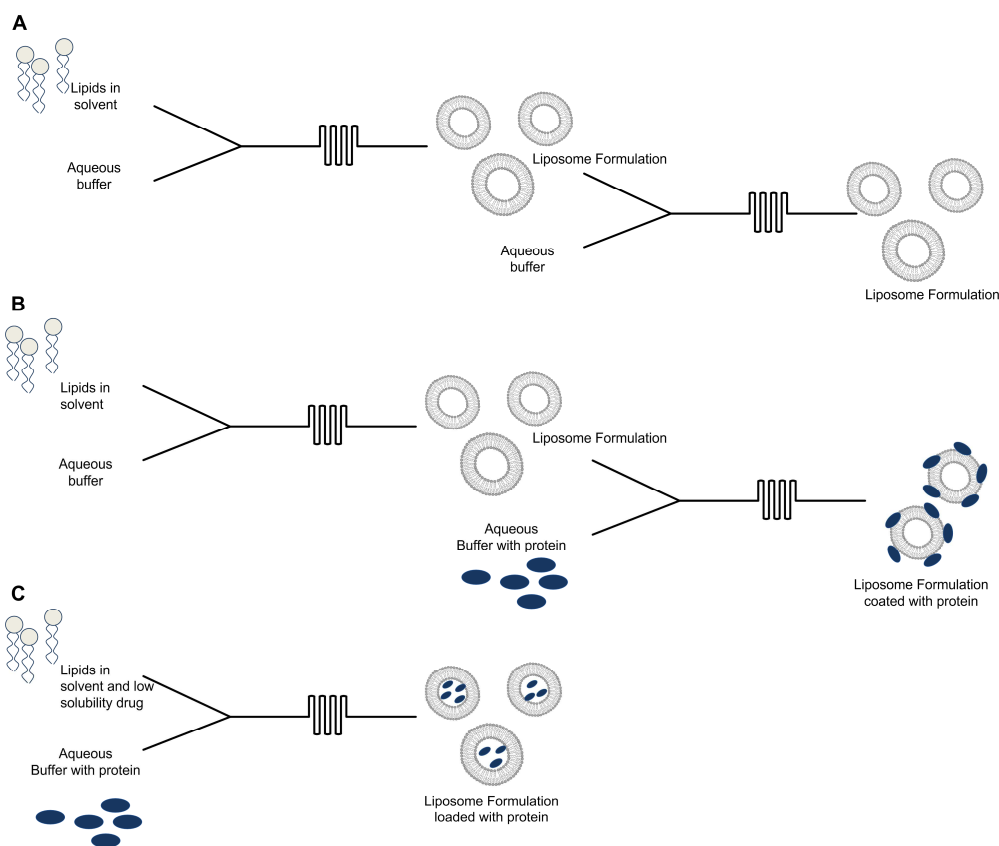


Figure 9.3: Schematic depiction over the setups for antigen incorporation for A) consecutive liposome mixing, B) consecutive mixing of liposomes and antigen and C) direct mixing of lipids and antigen.

First, vesicles were run through the microchip to assess the physicochemical vesicle characteristics and stability (Figure 9.3A). Here, vesicles were manufactured by the nanoprecipitation method and led through the mixing chamber at varying TFR and FRR, assessing the effect of fluid flow, mixing with buffer and shear stresses on the vesicle characteristics. Both an increase in TFR at constant FRR (Figure 9.4 A) as well as increase in FRR at constant TFR did not influence vesicle characteristics (Figure 9.4B). At flow rates of 3 mL/min, a significant ($p < 0.05$) decrease in liposome size was observed, whereas ZP and PDI remained independent ($p > 0.05$) of TFR and FRR (Figure 9.4A, B).

Additionally, a model protein (ovalbumin) was included in the process of forming antigen-loaded vaccine adjuvant particles. Model protein was integrated in the vesicle manufacturing process subsequent to vesicle manufacturing (Figure 9.3B). An increase in vesicle size upon protein addition was noted, the vesicle sizes increase from initially 200 nm to 600 nm, indicative of vesicle aggregation (Figure 9.4C). In addition to the increase in size, the PDI increased upon addition of the protein to 0.8, indicative of a heterogeneous particle population upon protein addition. The significant drop in ZP from initial 55 mV to 15 mV was a qualitative indication of surface adsorbed protein. The process of protein addition was performed at varying TFR, remaining below 3 mL/min as previously determined, and a mixing at 0.5 to 2 mL/min had no effect to vesicle characteristics ($p > 0.05$, Figure 9.4C).

In comparison to the protein addition post vesicle manufacturing without the use of the micromixer, larger vesicles were obtained ($p < 0.05$) compared to the average sizes achieved by mixing the protein within the micromixer. However, similar PDIs indicate no physico-chemical advantage of the resulting formulation. The decrease in zeta potential was in line with results as obtained from protein addition within the micromixer (Figure 9.4C). Therefore, the main advantage of the in-process addition of protein could be considered the potential of implementing continuous manufacturing in a microfluidic system.

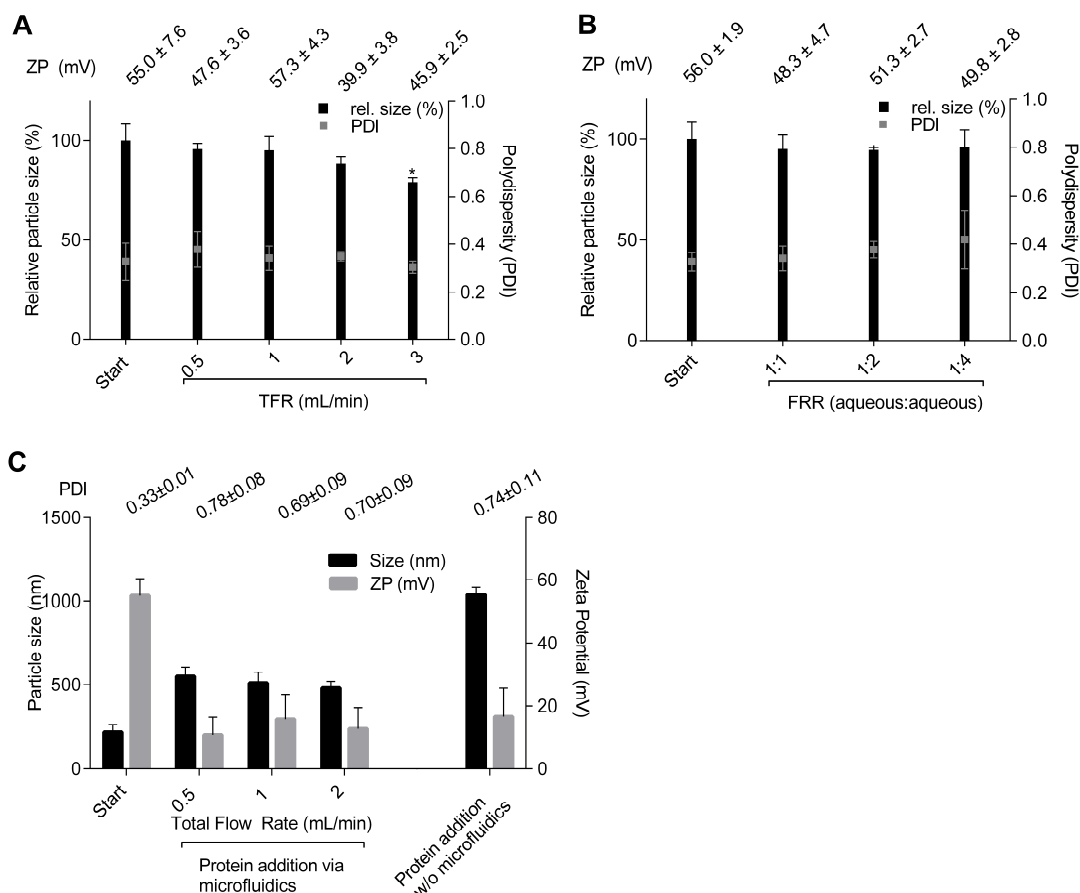


Figure 9.4: The effect of increasing **A)** total flow rate and **B)** flow rate ratio (TRIS buffer only) to liposome vesicle characteristics. **C)** The effect of increase in flow rate to liposome vesicle characteristics at consecutive protein addition in the microfluidic mixing process and addition of the protein to vesicles without microfluidic mixing. Start formulation was manufactured at 2 mL/min, 1:3. Where shown, significance between data is against the start formulation characteristics (* $p < 0.05$). Results denote mean \pm SD of 3 separate batches.

Overall, rerunning vesicles through the mixing chamber was found independent of vesicle characteristics once run at a TFR below 3 mL/min. The significant decrease in liposome size at high TFR could be linked to a rearrangement into smaller vesicles due to shear stresses occurring within the chamber. The efficient protein delivery through cationic liposomes is based on electrostatic attractive force dominating and often leading to a surface-adsorption reaching close to 100% (Kaur et al., 2013). The addition of protein adsorbs to the surface of the cationic liposomes and as expected resulted in a decrease in zeta potential and an increase in measured vesicle size and PDI based on cross-linking and/or aggregation of liposomes. Previous work comprised DDA-TDB liposomes, which were loaded with protein by addition to the formed vesicles, where a drop in zeta potential by ca. 20 mV was linked to a 100% adsorption of protein onto the liposomes surface at a final concentration of 10 $\mu\text{g/mL}$ (Henriksen-Lacey et al., 2011a). The exposure of DDA-TDB liposomes to protein at a

concentration of 10 µg/mL maintained the vesicle size, with 96% antigen association, which has been reported for small (Henriksen-Lacey et al., 2011a) and large (Henriksen-Lacey et al., 2010b) liposomal systems upon antigen loading of 10 µg/mL. Here, a loading of 100 µg/mL was used to trigger an effect to particle characteristics, assessing the capability of the microfluidics method to load the protein to the adjuvant formulation in comparison to a loading without the micromixer method. These results show that the protein loading process was independent of the TFR, suggesting an ideal high flow rate to accommodate the need of a high-throughput loading process.

9.3.2 *In-vitro* activity of adjuvants manufactured via microfluidics

Antigens or other immunostimulatory compounds may be located in the interior, the bilayer, or the particle surface of liposomes, which act as delivery systems of these components, ultimately delivering cargo to antigen presenting cells (APCs). Such immunostimulatory compounds might be specific to natural ligands from specific pathogens (Hafner et al., 2013). For a vaccine adjuvant to be effective it needs to promote involvement of APC and may mediate this through the attraction and activation of APC. In this study, the *in-vitro* behaviour of APCs was evaluated in the presence of liposomes manufactured via the microfluidics method and the standard lipid film hydration method.

Here, DDA-TDB vesicles were manufactured by the lipid film hydration method as previously reported (Henriksen-Lacey et al., 2011a) and via microfluidics (Chapter 3). A comparison of resulting particle characteristics is shown in Table 9.1. As expected, the size of the resulting vesicles was the main difference between the two manufacturing methods, whereas both methods resulted in a cationic ZP round 40-50 mV. Solvent residues in the microfluidics method were removed via dialysis to a remaining solvent concentration <1% v/v (data not shown), whereas in the lipid film hydration method, flushing with N₂ removed residual solvent.

Table 9.1: Vesicle characteristics of DDA-TDB adjuvants manufactured.

Method of manufacturing	Size (nm)	Zeta potential (mV)
Lipid film hydration	600 ± 90	48 ± 8
Microfluidics (TFR 2 mL/min, FRR 1:3)	150 ± 25	41 ± 7

To consider if the microfluidics manufactured liposomes were as effective as the standard DDA-TDB formulation previously demonstrated to be a strong adjuvant (Christensen et al., 2009), both systems were compared using a series of *in-vitro*

assays. First, the migration of APCs (macrophages or immature dendritic cells (iDC)) to the liposomes was assessed via a migration assay. Both, macrophages and DCs are phagocytes, which engulf and digest the liposomes and would later present the antigen from the same to the T-cells in the lymph nodes, which will generate the respective immune response against the antigen. Despite liposomes in this study not carrying an actual antigen, the migration of the cells towards the liposomes is an indication of their *in-vitro* activity. Data showed an enhanced migration for DCs (Figure 9.5A) and macrophages (Figure 9.5B) for DDA-TDB vesicles compared to the control, which was found higher for the microfluidics-directed vesicles ($p < 0.05$, time point 12 hours). Given the low migration for cells without any liposome addition (control), the migration is associated to the formulation (DDA-TDB), with respective *in-vitro* attraction of APCs. Furthermore, the microfluidics-directed formulation was not compromised by the method of manufacturing, with a strong *in-vitro* cell migration triggered as seen for the optimised DDA-TDB formulation manufactured via a lipid film hydration process.

Previous work has demonstrated the ability of this *in vitro* study to test the potency of liposomal vaccine adjuvants; Kaur et al. (2013) showed that increased cholesterol content within the formulation decreased the liposomal uptake by phagocytes from 75% of the cells associated with the liposomes without any cholesterol to 40% of the cells associated with the liposomes with cholesterol incorporated. This reduction in liposomal uptake correlated with a reduced *in-vivo* efficiency based on a reduced Th1 immune response (Kaur et al., 2013). Given the previously investigated impact on lipid composition to the *in-vitro* cell association, Figure 9.5 suggests that the cell migration was independent of the method of manufacture and that these cationic liposomal adjuvants can be prepared by microfluidics thus allowing their translation into high-throughput manufacture.

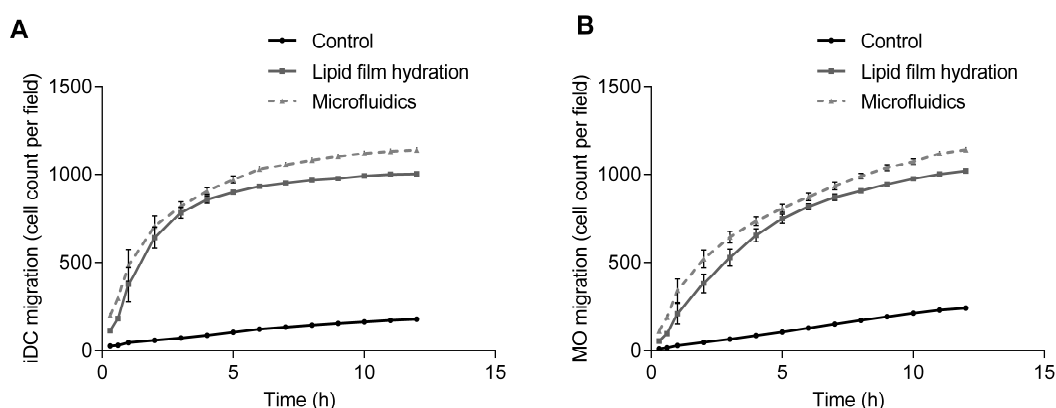


Figure 9.5: Time dependent migration assay for A) immature dendritic cells (iDC) and B) macrophages (MO) over 12h.

To further compare these two liposomal adjuvants, their uptake by phagocytes was measured using fluorescently labelled liposomes. The association of the fluorescently-labelled liposomes with the APCs (iDCs and macrophages) was quantified by a flow cytometric association assay and expressed as mean fluorescence intensity (MFI, mean amount of fluorescence per cell) and %positive cells (%+ve, % of macrophages or DC that are positive for liposomes). Figure 9.6 shows the time dependent uptake of fluorescently labelled DDA-TDB liposomes manufactured via lipid film hydration and microfluidics after application to derived macrophages and DCs.

The liposomes-associated DCs were found with a MFI of 45, remaining overall insignificant ($p>0.05$) if comparing the MFI after 120 min incubation time for the liposomes manufactured via both manufacturing methods (Figure 9.6A). Furthermore, around 75 – 80 % of the DCs were found associated with the fluorescently labelled liposomes (Figure 9.6B), which was found in line with previous studies (Kaur et al., 2013). The liposomes-associated macrophages were found with a MFI of 76-87, remaining overall insignificant ($p>0.05$) if compared after 120 min incubation time for both manufacturing methods (Figure 9.6C). Furthermore, around 94-96 % of the macrophages were found associated with the fluorescently labelled liposomes (Figure 9.6D), significantly higher than the association measured with the DCs. Macrophages are considered as professional phagocytes, with a higher efficient phagocytosis than DCs (Savina and Amigorena, 2007). Despite the lower uptake of fluorescently labelled liposomes by DCs as seen in this study, DCs are efficient in antigen presentation to T-cells, aiding in antibody production (Apostolopoulos et al., 2013). Data suggests that the macrophages and DC association with liposomes was independent of the method of manufacturing and both cell types, were found associated with the fluorescently labelled liposomes.

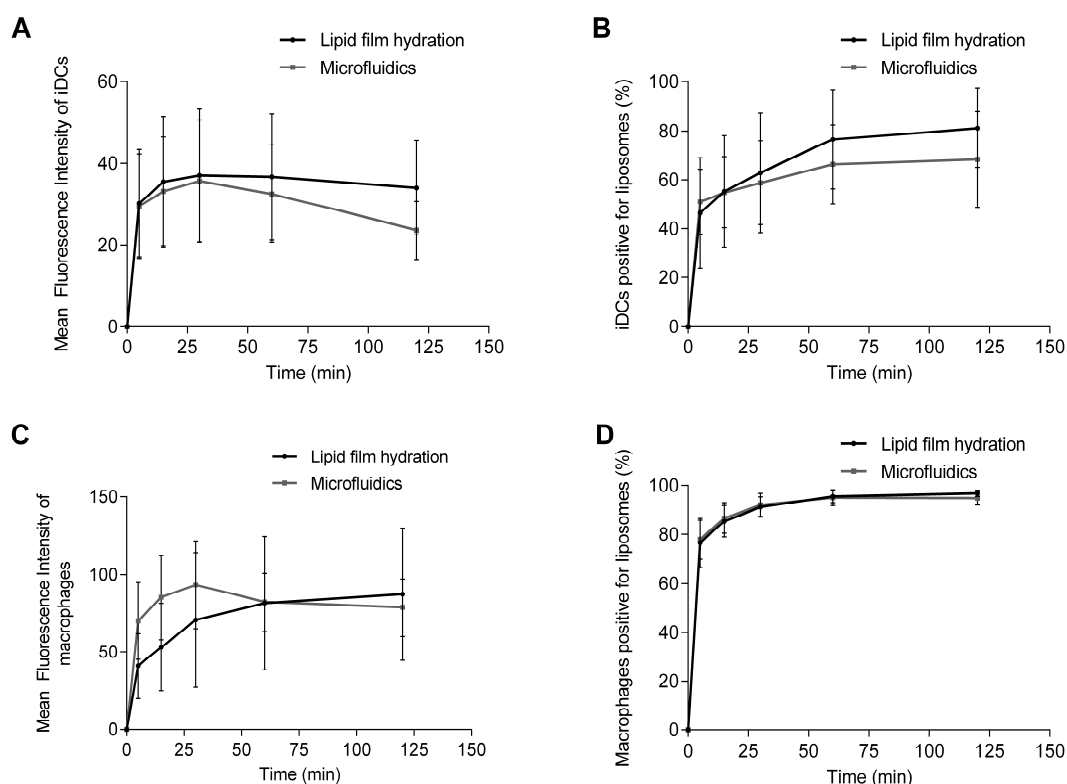


Figure 9.6: Association assay for dendritic cells (DC) expressed as A) MFI, B) %+ve cells over 2h and for macrophages expressed as C) MFI, D) %+ve cells over 2h.

Data here compared the *in-vitro* efficiency of vesicles manufactured with the novel microfluidics method to the vesicles manufactured with the well-established lipid film hydration method using migration and association assays. Overall, liposomes manufactured via both methods were shown to trigger substantially higher APC migration, indicative of the biological activity of DDA-TDB vesicles as seen previously (Kaur et al., 2013). Given the constant liposome to cell ratio, the smaller microfluidics-directed vesicle population comprised a higher number of vesicles. This resulting difference in liposome number to cell ratio was anticipated linked to the higher migration of the microfluidics-manufactured vesicles for both macrophages and DCs. Furthermore, the association of the fluorescently labelled liposomes with the APCs was found independent of the manufacturing method and vesicle size (thereby correlating with the MVA studies in Chapter 8).

Overall, using this *in-vitro* method the microfluidics directed manufacturing of the DDA-TDB adjuvants was shown to be as effective as the previously small scale batch method for liposome production.

9.3.3 Manufacturing of polymer-based nanoparticles

In addition to liposomes, polymeric nanoparticles have been considered as vaccine adjuvants. Therefore, preliminary work to consider if nanoparticles could be formulated using microfluidics was undertaken. Considerations here evolved from previous work, where the ratios were varied between 1:1 and 1:5 (solvent:aqueous phase) at a fixed flow rate of 4 mL/min. The FRR was found to significantly ($p < 0.05$) effect the size of the polymer nanoparticles (Figure 9.7). The lowest ratio of 1:1 showed the largest particle size, around 2 μm with a relatively large standard deviation, remaining statistically significant ($p < 0.05$) to every other ratio used. The optimal region for smallest particle sizes was achieved at a FRR between 1:2 and 1:4, with the smallest sizes of 120 ± 10 nm. A further increase in FRR to 1:5 further increased the size (ca. 300 nm). The ratios between 1:2 to 1:3 had the lowest standard deviation of size, with low average PDI value and highly negative ZP (Figure 9.7A). Overall, polydispersities of 0.2 to 0.3 were in line with previously reported polydispersities of polymer based NP (Ataman-Önal et al., 2006). ZP (Figure 9.7A) was shown to be relatively unaffected by the choice of flow ratio, with strong negative surface potentials recorded overall. Furthermore, solvent removal by dialysis made no impact on vesicle characteristics (Figure 9.7B).

The common trend within the systems evaluated was the ratio between the solvent and the aqueous stream, which was found important in controlling the size of the nanoparticles, whilst remaining the zeta potential. The enhanced aqueous volume present at higher flow ratios resulted in the formation of smaller nanoparticles based on reduced closure time for the vesicles (Zook and Vreeland, 2010), as seen in previous chapters with lipid molecules. Lipid and polymer based systems showed the same trend as the enhancement of the aqueous content FRR was found to increase the heterogeneity within the systems evaluated, as seen in earlier chapters (Chapter 4, 5, 6). This increase in PDI may be a result of increased dilution at higher FRR, which reduces the rate of diffusional mixing within the micromixer.

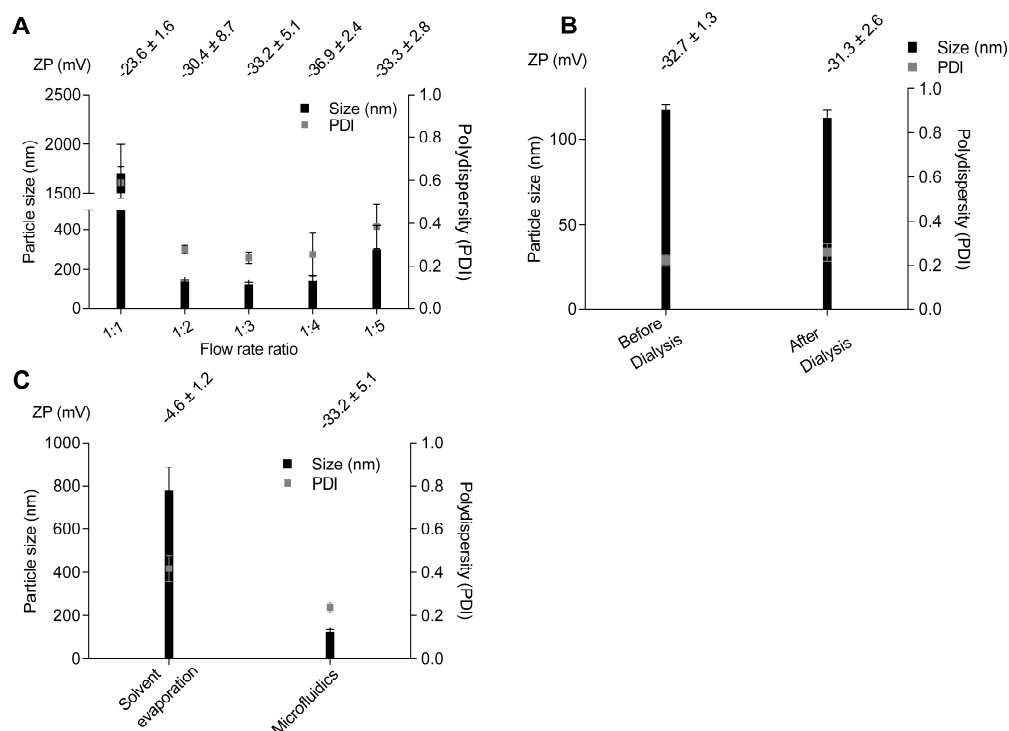


Figure 9.7: A) Effect of alteration in flow rate ratio to particle characteristics. The total flow rate has been maintained constant at 4 mL/min. B) Effect of dialysis for solvent removal to particle characteristics. C) Effect of method of polymer nanoparticle manufacturing to particle characteristics. Nanoparticles were prepared by solvent evaporation (Rescignano et al., 2013) and microfluidics (TFR 4 mL/min, FRR 1:4). The setting in the microfluidics have been maintained at FRR 1:4, TFR 4 mL/min. Results denote mean \pm SD of 3 separate batches. Solvent = Acetonitrile, 200 μ m chip design.

The solvent evaporation method (Rescignano et al., 2013) resulted in particles around 800 nm, significantly larger ($p < 0.05$) than the smallest size achieved by microfluidics (100 nm), which also showed a lower PDI (Figure 9.7C). The fundamental differences between nanoprecipitation and the solvent evaporation method, along with the tight control of fluid flow properties in the nanoprecipitation method were anticipated to result in the enhanced particle characteristics. Furthermore, particles manufactured with the microfluidics-based method had a significantly higher negative surface potential than the ones manufactured by the solvent evaporation method (Figure 9.1C), which was anticipated as beneficial for the later performed surface adsorption of a positively charged protein by electrostatic interaction.

The applicability of the nanoprecipitation method was evaluated by applying the optimised settings for PLA particle formation to the manufacturing of PLGA particles, which showed a slightly larger average size (ca. 130 nm) compared with the PLA nanoparticles (ca. 120 nm), remaining statistically insignificant, with similar PDI values, $p > 0.05$ (Figure 9.8A). A significant difference in the ZP of the two types of nanoparticle was noted; with the PLGA nanoparticles having a significantly larger ZP average

(Figure 9.8A), based on structural differences between the PLGA and PLA polymers. PLGA nanoparticles were shown to remain their critical physicochemical characteristics over a storage duration of 7 days (4°C) (Figure 9.8B). Most importantly, results highlight on the ease of method transfer between different polymers, which can be anticipated to save a considerable amount of time and money in future development and optimisation processes.

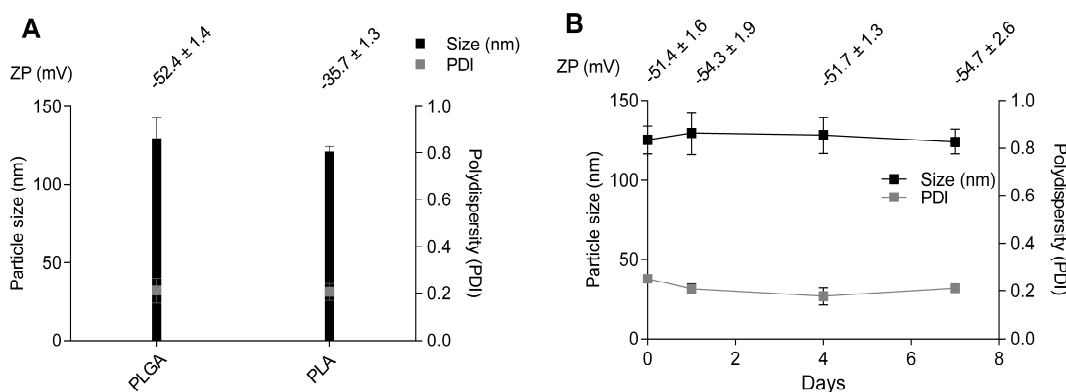


Figure 9.8: A) Effect of polymer choice to particle characteristics. The setting in the microfluidics have been maintained at FRR 1:4, TFR 4 mL/min. B) Stability of PLGA nanoparticles manufactured by microfluidics over a storage period of 7 days at 4°C. Results denote mean \pm SD of 3 separate batches in each method.

Based on above method development, the polymer particles formed were assessed for surface adsorption of two model proteins (lysozyme, IEP 9.3 and ovalbumin, IEP 4.5), based on electrostatic interaction. The addition of 0.05 mg/mL of lysozyme significantly ($p < 0.0001$) increased the size of the nanoparticles, demonstrating that this concentration would not be suitable for loading, as aggregation dominates and the resulting size countered the nanoprecipitation-based manufacturing (Figure 9.9A). The addition of lysozyme affected the PDI of the nanoparticles formed (Figure 9.9C), with significantly increased with the increase in protein concentration. Qualitative protein loading was assessed by relative change in ZP, where the highest concentration of lysozyme caused the biggest effect to the particles surface potential, indicative of surface adsorbed protein (Figure 9.9B). The addition of OVA had no significant impact on the particle size, independent of its concentration.

Based on the lower isoelectric point of OVA, it acted as a control, with expected low protein association to the negatively charged nanoparticles as reflected by its independence to resulting PDI. Furthermore, the increase in ZP was noted upon protein addition, suggesting that a small amount of electrostatic bonding does occur between the nanoparticles and OVA, although significantly lower than that

demonstrated by the change in size and PDI related to the concentration of lysozyme addition. Previous work on assessing antigen association with DDA-TDB vesicles showed high protein loading (>90%) using a tuberculosis subunit protein (Ag85B-ESAT6) at a concentration of 10 $\mu\text{g/mL}$. Loading with lysozyme (10 $\mu\text{g/mL}$) showed only limited adsorption of ca. 30% onto the surface of DDA-TDB vesicles and the injection resulted in rapid draining of the antigen from the injection site, with only about 7% of the antigen recovered after one day at the injection site (Henriksen-Lacey et al., 2010b). Generally, the adsorption of the antigen on the surface of vesicles was linked to a depot effect at the site of injection (Henriksen-Lacey et al., 2010b).

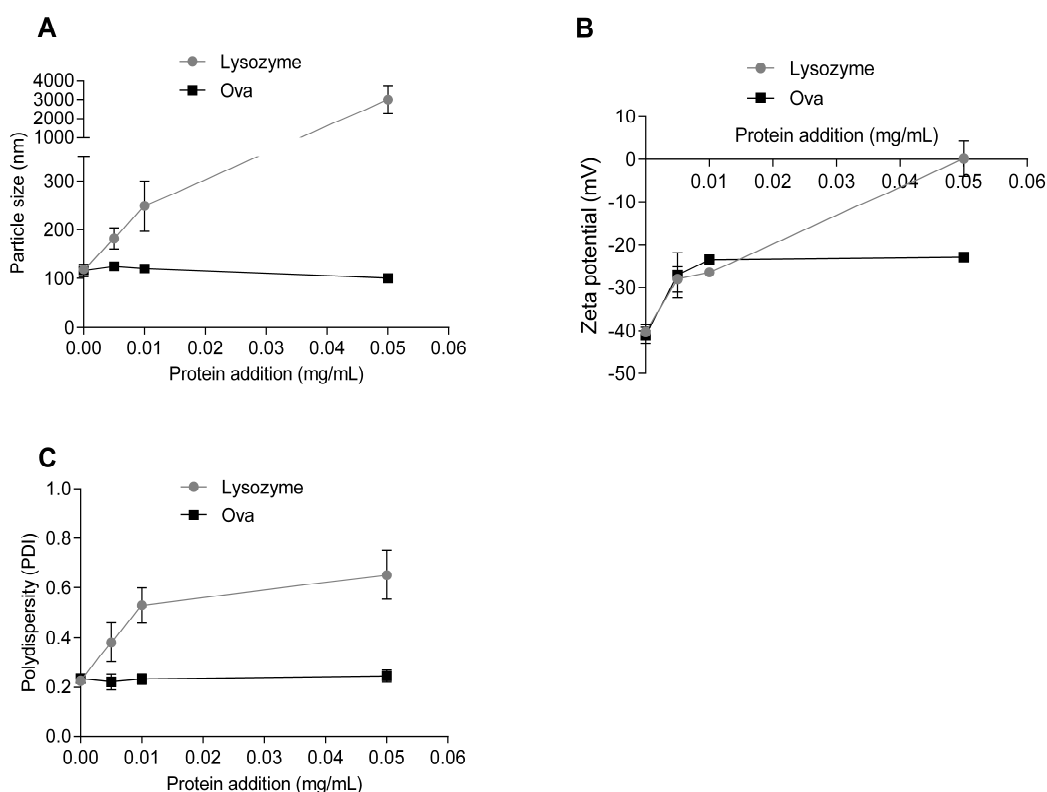


Figure 9.9: Effect of protein loading to A) size, B) zeta potential and C) polydispersity. The setting in the microfluidics have been maintained at FRR 1:4, TFR 4 mL/min, protein has been added post particle manufacturing and particle characteristics were assessed after 45 min incubation time at room temperature. Results denote mean \pm SD of 3 separate batches.

Whilst the loading studies here were qualitative, based on a relative change in particle characteristics and ZP it supports the initial screening of nanoparticles over a range of protein concentrations and demonstrates the effect on physicochemical characteristics by protein adsorption. A known issue during polymer nanoparticle manufacturing is the instability and protein degradation linked to the harsh conditions during traditional manufacturing methods as sonication, exposure to harsh solvents (class 3) (e.g. chloroform), high shear stress conditions and high temperatures (Tamber et al., 2005).

On the contrary, shear stresses in the SHM are low with reported applicability for shear sensitive products like siRNA (Belliveau et al., 2012). Furthermore, solvents used are less harsh (class 2), acetonitrile compared to chloroform in the solvent evaporation method, overall advantageous for using a SHM for nanoparticle manufacturing and protein association. Antigen adsorption onto PLA microparticles was described (Almeida et al., 1993) and surface adsorption was enhanced by modification and inclusion of either cationic or anionic surfactants (Kazzaz et al., 2000). Upon delivery of DNA, immune responses were enhanced in mouse and macaque models (O'Hagan et al., 2001a). The manufacturing of charged polymer particles was promising for vaccine antigen delivery, yet challenged by necessary incorporation of stabilisers like PVA and SDS required during the solvent evaporation method, which are necessary for colloid stabilisation (Ataman-Önal et al., 2006). The addition of those stabilisers will require extensive toxicological and safety studies (Ataman-Önal et al., 2006), whereas the microfluidics-based nanoprecipitation allowed for the manufacturing of stable nanoparticles, without the necessity of including stabilisers into the process and the formulation.

The competitive system on a microfluidic basis is the flow focusing method. However this requires mixing ratios up to 60 (Jahn et al., 2007; Jahn et al., 2004), which are unfavourable regarding material dilutions in comparison to ratios applied in the SHM method, which were found ideal between 1:3 to 1:4. Furthermore, the SHM method allows for a higher throughput, here with flow rates up to 2.5 mL/min. The flow focusing method in contrast required flow rates ranging between 15 to 90 $\mu\text{L}/\text{min}$ for the buffer stream and 1 to 6 $\mu\text{L}/\text{min}$ for the solvent stream, even the maximum resulting TFR of 96 $\mu\text{L}/\text{min}$ still being magnitudes lower than the throughput achieved in the SHM method. Furthermore, the option of parallelisation of the mixer chips, as highlighted in Chapter 6, allows for a clinical based application.

The method of nanoprecipitation for polymer nanoparticle manufacturing has been well described, and generally comprises the precipitation process of a material (here polymers) dissolved in a water miscible solvent (here acetonitrile) after mixing with an aqueous phase (here buffer) resulting in the formation of nanoscale particles. The solvent evaporation method in contrast relies on the use of only partially water miscible solvent (e.g. chloroform, dichlormethane). Interest in these methods was evidenced by patent numbers peaking between the 1950s-1960s (Schubert et al., 2011). The application of the nanoprecipitation method for polymeric nanoparticle manufacturing of colloids was firstly patented by Fessi et al. (Fessi et al., 1992; Fessi et al., 1989) and is

since commonly applied for polymeric systems. Amphiphilic copolymers have since been used and described for delivery of a range of hydrophobic drugs like doxorubicin, clomazepam, as well as for encapsulation of antigens and proteins (Chiellini et al., 2001; Jeong et al., 1998; Oh et al., 1999; Yang et al., 2009). The traditional methods of nanoprecipitation included either a dialysis membrane or the dropping technique under stirring (injection method) (Schubert et al., 2011). However, it has early been noted that the control of the mixing profiles during the nanoprecipitation method is necessary for regulation of the physicochemical particle properties to a sufficient accuracy. Resulting nanoparticles are influenced by the rate of mixing and addition of the solvent into the aqueous phase, together with operator variability those variables were found difficult to control (Basto et al., 2008; Sitnikova et al., 2005; Wang et al., 2005). Furthermore, advances in material science require the implementation of a robust and high-throughput manufacturing method, able to accommodate the need of screening over a range of molecules and concentrations (Schubert et al., 2011), where microfluidic tools were shown to accommodate this need. Hydrodynamic flow focusing device for PLGA-PEG copolymers (Karnik et al., 2008) discovered that the flow rates, polymer composition and concentration were significant factors to influence the size, polydispersity, drug loading and release of the resulting nanoparticles. Flow rates reported range from 0.5 and 10 $\mu\text{L}/\text{min}$ for the acetonitrile and aqueous phase respectively (Karnik 2008). The difference to the here-presented microfluidics method lies in the mixer design, incorporated dilution factor, resulting particle concentration and throughput. Flow focusing devices were found optimised at a FRR (ratio solvent to aqueous phase) of 1:20, at TFR of 0.6 mL/h (Keohane et al., 2014). The here presented method based on a SHM device was found optimised at a FRR between 1:2 to 1:4, at TFR ranging up 4 mL/min, a significant higher throughput compared to the reported flow focusing method. Furthermore, due to lower FRR, the resulting particle concentration is higher, whereas the flow focusing method resulted in an approximately 20 fold dilution of the nanoparticles formed.

9.4 Conclusion

The here presented method based on nanoprecipitation of lipid and polymer molecules was found an effective, reproducible and high-throughput manufacturing technique. The flexibility of the method allows for consecutive processing of vesicles, coated with an antigen allowing for the manufacturing of surface adsorbed vaccine adjuvants. The flexibility of the method allows for tailoring the ratios and concentrations to the desired amount of antigen to be associated with the vesicles. The method of generating loaded nanoparticles based on a SHM design was firstly described by Belliveau et al., where

shear sensitive siRNA was successfully encapsulated into lipid nanoparticles (Belliveau et al., 2012; Zhigaltsev et al., 2012). Here, the size of the resulting particles was controlled by alteration in the PEG content, with siRNA encapsulation efficiencies of 95% (Belliveau et al., 2012).

The flexibility of this nanoprecipitation method is anticipated to accommodate the need for an easy screening method, allowing a range of different surfactants being introduced in the manufacturing process to achieve particles with a desired surface potential and physicochemical properties. Furthermore, the method can be considered less harsh than conventional solvent evaporation or lipid film hydration method, making the nanoprecipitation method a viable method to be considered for manufacturing antigen-associated polymer and lipid based particles. The presented SHM design can be considered as a high-throughput microfluidics method, achieving a significant higher throughput compared to reported microfluidic nanoprecipitation methods, comprising the two main needs for a successful nanoprecipitation method, namely reproducibility and high-throughout. Additionally, based on the scale-up platform developed (Chapter 6), this method would allow for a successful transition into larger clinical based application.

Chapter 10

Overall Discussion and Conclusion

10.1 Development of microfluidics-directed nanoparticle manufacturing

Within the initial studies, the microfluidics-directed vesicle manufacturing method was investigated and compared to the sonication and the high shear mixing (HSM) method for manufacturing of SUV. The effect of solvent to aqueous ratio was found directly linked to the polarity increase throughout the chamber, which was found as the driving mechanism behind the precipitation reaction (Dong et al., 2012). A high volume of aqueous buffer enhances the mixing rate of the lipid phase, given that the fluid velocities in both streams differ dramatically, overall decreasing the diffusion layer thickness of the solvent stream. With decreased diffusion distances and less solvent available for lipid solubilisation, closure time for vesicles decreases, leading to smaller vesicles at a higher aqueous flow (Zook and Vreeland, 2010). At higher solvent volume, hydrophobic components are stabilised for a prolonged time, leading to overall larger vesicles.

The microfluidics method was found less disruptive than the sonication method with reported higher reproducibility than the ethanol dilution method (Batzri and Korn, 1973). Even though the sonication method generated smaller vesicles, respective method might introduce contaminants due to direct contact with the probe tip (Wagner and Vorauer-Uhl, 2011). This makes a translation of the method less applicable for a large scale industrial setting, and adds time associated with vesicle manufacturing. The HSM method was not able to reduce the vesicle size to the same extend as the sonication or microfluidics method, with minimal vesicle sizes of 160 nm achieved. Other than the reported hydrodynamic flow focusing method for vesicle manufacturing in a microfluidic-based precipitation process (Hood et al., 2014b; Jahn et al., 2010; Jahn et al., 2007; Jahn et al., 2004), the here presented SHM chaotic advection method resulted in a 30 times higher throughput, with flow rates ranging up to 2.5 mL/min. Furthermore, particle concentrations due to chosen FRR were significantly higher in the SHM method, given that FRR ranged from 5 (Balbino et al., 2013b) up to 30 (Jahn et al., 2007), leading to a significant lower particle concentration post manufacturing in the flow focusing method.

For high transition temperature lipids, the factor FRR and TFR were found to significantly affect the vesicle size, whereas for low transition temperature lipids, the factor FRR was found most important in affecting the vesicle size. Over the range of amphiphilic molecules investigated, the same trend was visible, with a reduced particle size with the increase in aqueous content FRR. For all compounds tested other than the high transition temperature lipids, the TFR was the prominent factor influencing the

method throughput with minimal or negligible effect to the vesicle characteristics. As such, the method of microfluidics-directed nanoprecipitation was found not only restricted to phospholipids, but furthermore applicable for a range of amphiphilic compounds, with lipids differing in charge and chain length, as well as polymeric-based nanoparticles.

10.2 The role of quantification and recovery studies

Within this thesis, a range of drug and protein delivery systems were manufactured by various methods, which brings along the need for a rapid and accurate quantification methods for the loading as well as the amphiphilic compounds. Here, quantification based on an RP-HPLC was performed, with quantification based on an UV detection or an ELSD. Separation and quantification based on column chromatography is the most applied method, linked to its selectivity, sensitivity and reproducibility compared to assay based quantification methods (Umrethia et al., 2010). These quantification protocols confirmed that the lipid ratios were maintained throughout microfluidics-directed vesicle manufacturing. Furthermore, recovery studies were important to assess that no lipid is lost due to adsorption onto the PDMS matrix, which is known for its adsorption properties of biologic materials, including proteins, mainly due to its porosity and hydrophobicity (Monahan et al., 2002; Toepke and Beebe, 2006). Studies have shown that recoveries were high, with a loss of lipids occurring at high aqueous content FRR (1:5).

10.3 Biological activity of vesicles manufactured by microfluidics-directed nanoprecipitation

Initially, the biological activity of vesicles formed in the microfluidics-directed nanoprecipitation method was investigated with cationic liposomal systems that were used as transfection agents. Cationic liposomes were prepared using lipids, 1,2-dioleoyl-*sn*-glycero-3-phosphoethanolamine (DOPE) and 1,2-dioleoyl-3-trimethylammonium-propane (DOTAP), commonly used in transfection protocols for in vitro mediated gene transfer (Ciani et al., 2007; McNeil et al., 2010). The microfluidics-based liposome manufacturing method was explored by variation of the process parameters TFR and FRR. Results highlighted on the ability to produce liposomes of defined sizes, which gave reproducible transfection results in standard transfection protocols. The factor TFR was found mainly affecting the method throughput, whilst the FRR was found impacting the size and PDI of the resulting vesicles, which overall showed good transfection outcome in a standard transfection protocol.

Similar transfection protocol was verified for the microfluidics-directed manufacturing of DQAsomes, vesicles consisting of cationic bola-amphiphiles with delocalised charge centres (Weissig and Torchilin, 2001). Similarly, the factor FRR was found significantly affecting the vesicle size, with minimal sizes of 250 nm achieved, where the TFR was the prominent factor only influencing the method throughput. Overall, the microfluidics method was found to generate vesicles of better physico-chemical characteristics compared to the ones achieved by lipid film hydration and sonication. Despite chemical instability, the vesicles showed biological activity by achieving a transfection with two different plasmids, highlighting on the feasibility of organelle directed gene delivery.

Cationic liposomal adjuvants were also effectively prepared by microfluidics and shown to be as immunogenic as previously investigated lipid-hydration systems, thereby demonstrating that these systems can be effectively translated from a small-scale laboratory production methods to a high-throughput manufacturing system.

10.4 Drug loading with nanoprecipitation

Having established the importance of the solvent to aqueous ratio for controlling the vesicle size, the method was furthermore explored for simultaneous encapsulation of a low solubility model drug (propofol). The use of liposomes as solubilising agents for low solubility drugs is well explored (Ali et al., 2010; Ali et al., 2013; Mohammed et al., 2004); and linked to a significant amount of new chemical entities in discovery, currently more than 40%, with limited aqueous solubility and subsequently related bioavailability issues (Savjani et al., 2012; Williams et al., 2012). Within this work, the low solubility drug was included in the solvent stream within the microfluidics method.

The microfluidics method was able to manufacture significantly smaller vesicles compared to a top-down sonication method, to a minimum of 50 nm. Furthermore, the concentration of the drug in the solvent stream significantly affected the physicochemical particle characteristics, where a concentration of 1 mg/mL was linked to ideal particle characteristics. The loading of the low solubility drug in the vesicle bilayer was significantly higher as achieved with the sonication method, which was found independent of the FRR tested, ranging from 1:1, 1:3 and 1:5 and remained at approximately 50 mol%. The encapsulation achieved with the sonication method was ~20 mol%, coinciding with literature values (Ali et al., 2013). Overall the efficient mixing process, based on chaotic advection and diffusion in the channel, was anticipated as the key mechanism behind drug encapsulation. The process of encapsulation was

favoured and occurred simultaneously with the synthesis of the vesicles themselves, a major advantage in microfluidics-directed manufacturing and loading. The release of the drug was dictated by the formulation rather than the method of manufacture. Where PC liposomal bilayer-loaded propofol followed a zero-order release kinetics (Ali et al., 2013), the incorporation of cholesterol into the liposomal systems shifted the release rates towards a first-order release model (Ali et al., 2010). The loading of a hydrophilic drug with the nanoprecipitation method showed almost 100% loading efficiency, and formulation remained stable stored at 4°C over the course of eight weeks (Zhigaltsev et al., 2012). A modified solvent-injection method for the production of solid lipid nanoparticles included the encapsulation of a lipophilic drug, which after lyophilisation reached 100% (Wang et al., 2010). Loading of a lipophilic drug into PLA nanoparticles was achieved in a simple nanoprecipitation, method, where the solvent phase was added to the aqueous phase under stirring. The size of resulting PLA nanoparticles was found affected by the PLA amount and the ratio of solvent to aqueous phase, with higher encapsulation values achieved reaching almost 100%. Volumes however were 60 mL per batch, and significantly higher than the here presented chaotic advection method (Chorny et al., 2002).

10.5 The role of continuous manufacturing

In this work, loading was achieved by chaotic advection micromixing with a continuous purification system integrated on a microfluidics based filtration device. This highlights the use of microfluidic tools for convert a multi-step large scale process into a continuous flow microfluidic-scale process, significantly reducing the required processing time. As such, on-chip liposome loading and purification technique was achieved by remote loading, where a chemical medication of the drug after diffusion into the liposomes prevented membrane re-permeation (Hood et al., 2014a). The formation of vesicles was achieved by hydrodynamic flow focusing, and an integrated counter-flow membrane dialysis was used for a pH shift and buffer exchange. The continuous on-chip manufacturing process required less than 3 minutes to produce drug loaded liposomes, with enhanced drug encapsulation properties compared to conventional bulk scale processes (Hood et al., 2014a). Flow ratio of solvent to aqueous stream was 20, at total flow rates of 112 $\mu\text{L}/\text{min}$ (Hood et al., 2014a). Dev et al. developed a continuous flow microfluidic system for the preparation of polymer coated nanoparticles in a scalable microfluidic system (Dev et al., 2011). The nucleation process was controlled by a rotating tube promoting high surface to volume ratios of the organic and aqueous streams, where the rotating speed was found highly

influencing the resulting particle size (Dev et al., 2011). Other than exploring continuous microfluidic tools in drug delivery technologies, a continuous version of microfluidic devices set in sequence was developed for automated nucleic acid purification. Therefore cell isolation, cell lysis, and chromatographic purification of nucleic acids was performed in sequential operation on a single chip, which was found to allow for sample processing in parallelised chips (Hong et al., 2004). With the reduced number of unit operations, development in hot melt extrusion (HME) processes demonstrated the interest in continuous manufacturing technologies (Andrews et al., 2009). Such HME processes have been used as an alternative method for tablet coating, in a process described as rapid and continuous (Andrews et al., 2008). Furthermore, fluidised hot melt granulation processes have been reported for a continuous granulation process where excipients and active pharmaceutical ingredients were mixed and agglomerated into uniform particle blends (Andrews et al., 2007).

Work presented explored the nanoprecipitation technology, which has previously been translated into continuous flow processes in large scale. Other than work shown in this thesis, large scale static mixers have been used for the manufacturing of solid lipid nanoparticles. Flow rates ranged up to 100 mL/min. The nanoprecipitation method was described for its potential for scale-up, with minimal batch-to-batch variations based on the implementation of a continuous flow system (Dong et al., 2012).

10.6 The importance of scale up and scalability

The lack of scale-up technologies for drug-loaded nanoparticle manufacturing is one factor constraining market introduction (Galindo-Rodríguez et al., 2005). The phase of process scale-up is crucial, not only because it allows for realisation of a larger scale process but furthermore limitations negligible in smaller scale might become prominent factors in a larger scale process.

Within work in this thesis, scale-up has been achieved by the increase in channel diameter and mixer parallelisation. Where the increase in channel diameter allowed for a seamless process transfer, particle characteristics and loading efficiencies were influenced in the continuous flow system. The reduced loading and changed particle characteristics may be associated with changes in pressure in the system, affecting the hydrodynamic conditions in the scale-up platform as seen with other work on scalability assessment of the nanoprecipitation method (Galindo-Rodríguez et al., 2005). The lack

of information regarding scale up technologies has been described to hinder the transfer of polymeric nanoparticle manufacturing (Galindo-Rodríguez et al., 2005). A scale-up version of the nanoprecipitation process has been described for manufacturing a 20-fold bigger volume of polymeric nanoparticles (Galindo-Rodríguez et al., 2005). Here, independent peristaltic pumps supplied the aqueous and solvent phase, which were mixed in a 'Tee mixer', where the nanoparticles formed immediately after both stream diffuse into each other in the mixer. The system was run at a solvent to aqueous ratio of 1:2 at a total flow rate of ca. 190 mL/min, which resulted in a difference in particle size of 35 nm from lab scale to pilot-scale process. This difference was attributed to changes in the hydrodynamic conditions, where enhanced turbulences in the pilot-scale process may have led to enhanced diffusion characteristics and reduced particle size, which resulted in a reduced loading efficiency (Galindo-Rodríguez et al., 2005).

10.7 The role of process control and modelling

Within this thesis a range of modelling tools were used to describe the process and aid the identification of the design space. This was achieved by design of experiments (DoE) and multivariate analysis (MVA) (Eriksson, 2006, 2008). Initially, three manufacturing methods, sonication, HSM and microfluidics were investigated in relation to the ability for controlling the size of the vesicles in a DoE approach. The DDA-TDB liposome formulation was used in the optimisation process as it is a well-established cationic adjuvant formulation (Christensen et al., 2007b). For the sonication method, the sonication amplitude was found as the most important factor controlling vesicle size, whereas for the HSM process, the rotational speed was found as the most important variable in the process. In the microfluidics method, both factors TFR and FRR had a impact on the resulting liposome size, with the ratio between solvent and aqueous stream having the most significant impact, emphasised by the quadratic term FRR^2 .

Furthermore, effect of the factors TFR and FRR on liposome size, polydispersity and transfection efficiency (luciferase activity) was investigated in a response surface model. Model evaluation identified statistical significant models and regression models mathematically determined the liposome size, PDI and transfection efficiency as a function of the TFR and FRR in the microfluidics-based nanoprecipitation process for cationic DOPE-DOTAP lipids. Where the TFR was found less impacting the responses, the factor FRR was found significantly affecting the size, PDI and transfection activities.

Maximum luciferase activities around 250% were predicted for a FRR of 1:3, efficiencies were predicted above 180% for FRR between 1:2 and 1:4, independent of the TFR used. Model predictions were validated by direct comparison between predicted and experimentally obtained values. The setup was further investigated in a MVA approach. Here, the PCA and PLS models were used for cluster analysis and outlier detection, regression analysis and predictive modelling (Eriksson, 2006). During the cluster analysis, a link between FRR, PDI and size was identified, a similar trend seen in above DoE study, where a decrease in liposome size was predicted for an increase in FRR along with the increase in PDI. The PLS analysis confirmed the direct correlation between FRR and PDI, as well as a direct correlation between the liposome size and the transfection efficiency. The strong link between particle characteristics (size, PDI) and FRR was revealed in both scores and loading plots, and confirmed above DoE evaluations. Such model analysis verified a mathematical proof that a better transfection results may be expected for vesicles with a larger size at a constant lipid/DNA ratio (Esposito et al., 2006; Felgner et al., 1987; Kawaura et al., 1998; McNeil et al., 2010).

In contrast to OFAT experiments, predictive tools reassure a process or method in pharmaceutical development. The process understanding is deepened, and methods assist in development work and possible scale-up (Singh et al., 2005) whilst enhancing the reproducibility of a process and generating a design space, aligning with recent trends in biopharmaceutical and pharmaceutical development (Lawrence, 2008). Such MVA tools may accelerate the development process of a vaccine candidate due to characterisation by clustering of *in-vivo* specific immune responses, which generates future predictions of vaccine efficiency. A MVA study correlated and analysed *in-vivo* adjuvant activity based on a liposomal adjuvants containing the cationic lipid DDA and TDB, with well described adjuvant activity (Christensen et al., 2009; Christensen et al., 2007b). Increasing levels of the saturated phosphatidylcholine, 1,2-distearoyl-*sn*-glycero-3-phosphocholine (DSPC) were incorporated into the DDA-TDB formulation, at a locked DDA-TDB molar ratio of 8:1. The resulting physical adjuvant properties were linked to adjuvant activity using a tuberculosis antigen vaccine candidate (H56) in a MVA model. Analysis revealed a clustered collectively as Th1-specific immune responses, as the responses INF- γ , IL-2 and IL-6 showed coincided coefficient profiles for the variables DDA and ZP. Analysis confirmed by statistical insignificance for the antibody subtypes, insignificant for the evaluation of vaccine efficacy.

10.8 Overall Conclusion

To summarize, in relation to the aims and objectives highlighted in Chapter 1, studies within this thesis have shown that:

1. Microfluidics-directed nanoprecipitation was used to formulate stable nanoparticles comprised of either lipids (high and low transition temperature), cationic amphiphiles with delocalized charge centres or polymers.
2. The ratio of solvent of aqueous stream was the primary dominant factor for controlling the vesicle size.
3. The total flow rate was the factor primarily dominating the throughput by the method for low transition temperature lipids.
4. Vesicles manufactured with the microfluidics method had good transfection rates in standard transfection protocols.
5. DoE and MVA studies linked the factor FRR to the resulting vesicle size and PDI, where the size of the particles was correlated to the transfection efficiency of lipoplexes.
6. The incorporation of a low solubility model drug in the solvent stream lead to simultaneous encapsulation of the drug within the lipid bilayer.
7. Increasing the channel diameter and parallelising the chips in a planar way lead to an overall 40-fold increase in throughput in a scale-up and scale-out format.
8. A tangential flow filtration system based on microfluidics was developed, which allowed for continuous manufacturing and purification of liposomal products.
9. MVA allowed clustering Th1 immune responses whilst relating physicochemical adjuvant characteristics to in-vivo derived immune responses upon delivery of a tuberculosis antigen.

11 Reference List

- Aagaard, C., Hoang, T., Dietrich, J., Cardona, P.-J., Izzo, A., Dolganov, G., Schoolnik, G.K., Cassidy, J.P., Billeskov, R., Andersen, P., 2011. A multistage tuberculosis vaccine that confers efficient protection before and after exposure. *Nature medicine* 17, 189-194.
- Agger, E.M., Rosenkrands, I., Hansen, J., Brahimi, K., Vandahl, B.S., Aagaard, C., Werninghaus, K., Kirschning, C., Lang, R., Christensen, D., 2008. Cationic liposomes formulated with synthetic mycobacterial cordfactor (CAF01): a versatile adjuvant for vaccines with different immunological requirements. *PloS one* 3, e3116.
- Al-Dosari, M.S., Gao, X., 2009. Nonviral gene delivery: principle, limitations, and recent progress. *The AAPS journal* 11, 671-681.
- Ali, M.H., Kirby, D.J., Mohammed, A.R., Perrie, Y., 2010. Solubilisation of drugs within liposomal bilayers: alternatives to cholesterol as a membrane stabilising agent. *Journal of pharmacy and pharmacology* 62, 1646-1655.
- Ali, M.H., Moghaddam, B., Kirby, D.J., Mohammed, A.R., Perrie, Y., 2013. The role of lipid geometry in designing liposomes for the solubilisation of poorly water soluble drugs. *International journal of pharmaceutics* 453, 225-232.
- Aljaberi, A., Spelios, M., Kearns, M., Selvi, B., Savva, M., 2007. Physicochemical properties affecting lipofection potency of a new series of 1, 2-dialkoylamidopropane-based cationic lipids. *Colloids and Surfaces B: Biointerfaces* 57, 108-117.
- Allen, T.M., 1994. Long-circulating (sterically stabilized) liposomes for targeted drug delivery. *Trends in pharmacological sciences* 15, 215-220.
- Allen, T.M., 1998. Liposomal drug formulations. *Drugs* 56, 747-756.
- Allison, A.C., Gregoriadis, G., 1974. Liposomes as immunological adjuvants. *Nature* 252, 252-252.
- Almeida, A., Alpar, H., Brown, M., 1993. Immune Response to Nasal Delivery of Antigenically Intact Tetanus Toxoid Associated with Poly (l - lactic acid) Microspheres in Rats, Rabbits and Guinea - pigs. *Journal of Pharmacy and Pharmacology* 45, 198-203.
- Almeida, P.F., Vaz, W.L., Thompson, T., 2005. Lipid diffusion, free area, and molecular dynamics simulations. *Biophysical journal* 88, 4434.
- Almgren, M., Edwards, K., Karlsson, G., 2000. Cryo transmission electron microscopy of liposomes and related structures. *Colloids and Surfaces A: Physicochemical and Engineering Aspects* 174, 3-21.
- Altomare, C., Trapani, G., Latrofa, A., Serra, M., Sanna, E., Biggio, G., Liso, G., 2003. Highly water-soluble derivatives of the anesthetic agent propofol: in vitro and in vivo evaluation of cyclic amino acid esters. *European journal of pharmaceutical sciences* 20, 17-26.
- Andersen, P., Doherty, T.M., 2005. TB subunit vaccines—putting the pieces together. *Microbes and infection* 7, 911-921.
- Andrews, G., Jones, D., Abu Diak, O., Margetson, D., McAllister, M., 2009. Hot-melt extrusion: an emerging drug delivery technology. *Pharmaceutical Technology Europe* 21, 24-27.
- Andrews, G.P., Jones, D.S., Diak, O.A., McCoy, C.P., Watts, A.B., McGinity, J.W., 2008. The manufacture and characterisation of hot-melt extruded enteric tablets. *European journal of pharmaceutics and Biopharmaceutics* 69, 264-273.

Andrews, G.P., Jones, D.S., Walker, G.M., Bell, S., Vann, M.A., 2007. Particle design using fluidized hot melt granulation. *Pharmaceutical Technology Europe*.

Apostolopoulos, V., Thalhammer, T., Tzakos, A.G., Stojanovska, L., 2013. Targeting antigens to dendritic cell receptors for vaccine development. *Journal of drug delivery* 2013.

Ataman-Önal, Y., Munier, S., Ganée, A., Terrat, C., Durand, P.-Y., Battail, N., Martinon, F., Le Grand, R., Charles, M.-H., Delair, T., 2006. Surfactant-free anionic PLA nanoparticles coated with HIV-1 p24 protein induced enhanced cellular and humoral immune responses in various animal models. *Journal of controlled release* 112, 175-185.

Babbs, M., Collier, H., Austin, W., Potter, M., Taylor, E., 1956. SALTS OF DECAMETHYLENE - BIS - 4 - AMINOQUINALDINIUM ("DEQUADIN")*, A NEW ANTIMICROBIAL AGENT. *Journal of Pharmacy and Pharmacology* 8, 110-119.

Baker, M.T., Gregerson, M.S., Martin, S.M., Buettner, G.R., 2003. Free radical and drug oxidation products in an intensive care unit sedative: Propofol with sulfite*. *Critical care medicine* 31, 787-792.

Baker, M.T., Naguib, M., 2005. Propofol The Challenges of Formulation. *The Journal of the American Society of Anesthesiologists* 103, 860-876-860-876.

Balbino, T.A., Aoki, N.T., Gasperini, A.A., Oliveira, C.L., Azzoni, A.R., Cavalcanti, L.P., de la Torre, L.G., 2013a. Continuous flow production of cationic liposomes at high lipid concentration in microfluidic devices for gene delivery applications. *Chemical Engineering Journal* 226, 423-433.

Balbino, T.A., Azzoni, A.R., de La Torre, L.G., 2013b. Microfluidic devices for continuous production of pDNA/cationic liposome complexes for gene delivery and vaccine therapy. *Colloids and Surfaces B: Biointerfaces* 111, 203-210.

Bally, F., Garg, D.K., Serra, C.A., Hoarau, Y., Anton, N., Brochon, C., Parida, D., Vandamme, T., Hadziioannou, G., 2012. Improved size-tunable preparation of polymeric nanoparticles by microfluidic nanoprecipitation. *Polymer* 53, 5045-5051.

Bally, M.B., Cullis, P.R., Hope, M.J., 1991. Extrusion technique for producing unilamellar vesicles. Google Patents.

Bangham, A., 1961. A correlation between surface charge and coagulant action of phospholipids.

Bangham, A., Standish, M., Watkins, J., 1965. Diffusion of univalent ions across the lamellae of swollen phospholipids. *Journal of molecular biology* 13, 238-IN227.

Barnadas-Rodríguez, R., Sabés, M., 2001. Factors involved in the production of liposomes with a high-pressure homogenizer. *International journal of pharmaceutics* 213, 175-186.

Barrell, B., Bankier, A., Drouin, J., 1979. A different genetic code in human mitochondria.

Basto, P., Cannizzaro, C., Farokhzad, O.C., Gu, F.X., Karnik, R., Khademhosseini, A., Langer, R.S., 2008. Microfluidic synthesis of organic nanoparticles. Google Patents WO 2007150030 A3.

Batzri, S., Korn, E.D., 1973. Single bilayer liposomes prepared without sonication. *Biochimica et Biophysica Acta (BBA)-Biomembranes* 298, 1015-1019.

Bedi, D., Musacchio, T., Fagbohun, O.A., Gillespie, J.W., Deinnocentes, P., Bird, R.C., Bookbinder, L., Torchilin, V.P., Petrenko, V.A., 2011. Delivery of siRNA into breast

cancer cells via phage fusion protein-targeted liposomes. *Nanomedicine: Nanotechnology, Biology and Medicine* 7, 315-323.

Bell, N.C., Minelli, C., Tompkins, J., Stevens, M.M., Shard, A.G., 2012. Emerging techniques for submicrometer particle sizing applied to stober silica. *Langmuir* 28, 10860-10872.

Belliveau, N.M., Huft, J., Lin, P.J., Chen, S., Leung, A.K., Leaver, T.J., Wild, A.W., Lee, J.B., Taylor, R.J., Tam, Y.K., 2012. Microfluidic synthesis of highly potent limit-size lipid nanoparticles for in vivo delivery of siRNA. *Molecular Therapy—Nucleic Acids* 1, e37.

Bergstrand, N., Arfvidsson, M.C., Kim, J.-M., Thompson, D.H., Edwards, K., 2003. Interactions between pH-sensitive liposomes and model membranes. *Biophysical chemistry* 104, 361-379.

Berlin, K.R.S., Ammini, C.V., Rowe, T.C., 1998. Dequalinium induces a selective depletion of mitochondrial DNA from HeLa human cervical carcinoma cells. *Experimental cell research* 245, 137-145.

Berne, B.J., Pecora, R., 2000. *Dynamic light scattering: with applications to chemistry, biology, and physics*. Courier Corporation.

Bibi, S., Kaur, R., Henriksen-Lacey, M., McNeil, S.E., Wilkhu, J., Lattmann, E., Christensen, D., Mohammed, A.R., Perrie, Y., 2011. Microscopy imaging of liposomes: From coverslips to environmental SEM. *International journal of pharmaceutics* 417, 138-150.

Biebuyck, J.F., Smith, I., White, P.F., Nathanson, M., Gouldson, R., 1994. Propofol: an update on its clinical use. *Anesthesiology* 81, 1005-1043.

Black, M., Trent, A., Tirrell, M., Olive, C., 2010. Advances in the design and delivery of peptide subunit vaccines with a focus on Toll-like receptor agonists. *Expert review of vaccines* 9, 157-173.

Bolton, G., LaCasse, D., Kuriyel, R., 2006. Combined models of membrane fouling: development and application to microfiltration and ultrafiltration of biological fluids. *Journal of Membrane Science* 277, 75-84.

Bootz, A., Vogel, V., Schubert, D., Kreuter, J., 2004. Comparison of scanning electron microscopy, dynamic light scattering and analytical ultracentrifugation for the sizing of poly (butyl cyanoacrylate) nanoparticles. *European Journal of Pharmaceutics and Biopharmaceutics* 57, 369-375.

Bramwell, V.W., Perrie, Y., 2005. Particulate delivery systems for vaccines. *Critical Reviews™ in Therapeutic Drug Carrier Systems* 22.

Brewer, J.M., Pollock, K.G.J., Tetley, L., Russell, D.G., 2004. Vesicle size influences the trafficking, processing, and presentation of antigens in lipid vesicles. *The Journal of Immunology* 173, 6143-6150.

Brewer, J.M., Tetley, L., Richmond, J., Liew, F.Y., Alexander, J., 1998a. Lipid vesicle size determines the Th1 or Th2 response to entrapped antigen. *The Journal of Immunology* 161, 4000-4007.

Brewer, J.M., Tetley, L., Richmond, J., Liew, F.Y., Alexander, J., 1998b. Lipid vesicle size determines the Th1 or Th2 response to entrapped antigen. *The Journal of Immunology* 161, 4000-4007.

Brouwers, J.F., Gadella, B.M., van Golde, L.M., Tielens, A.G., 1998. Quantitative analysis of phosphatidylcholine molecular species using HPLC and light scattering detection. *Journal of lipid research* 39, 344-353.

Cai, W., Deng, W., Yang, H., Chen, X., Jin, F., 2012. A propofol microemulsion with low free propofol in the aqueous phase: Formulation, physicochemical characterization, stability and pharmacokinetics. *International journal of pharmaceutics* 436, 536-544.

Capretto, L., Cheng, W., Hill, M., Zhang, X., 2011. Micromixing within microfluidic devices, *Microfluidics*. Springer, pp. 27-68.

Caracciolo, G., Pozzi, D., Caminiti, R., Marchini, C., Montani, M., Amici, A., Amenitsch, H., 2007. Transfection efficiency boost by designer multicomponent lipoplexes. *Biochimica et Biophysica Acta (BBA)-Biomembranes* 1768, 2280-2292.

Carr, B., Hole, P., Malloy, A., Nelson, P., Smith, J., 2009. Applications of nanoparticle tracking analysis in nanoparticle research--A mini-review. *European Journal of Parenteral Sciences and Pharmaceutical Sciences* 14, 45.

Carr, B., Wright, M., 2008. Nanoparticle tracking analysis. *Innovations in Pharmaceutical Technology* 26, 38-40.

Carstens, M.G., Camps, M.G., Henriksen-Lacey, M., Franken, K., Ottenhoff, T.H., Perrie, Y., Bouwstra, J.A., Ossendorp, F., Jiskoot, W., 2011. Effect of vesicle size on tissue localization and immunogenicity of liposomal DNA vaccines. *Vaccine* 29, 4761-4770.

Chang, H.-I., Yeh, M.-K., 2012. Clinical development of liposome-based drugs: formulation, characterization, and therapeutic efficacy. *International journal of nanomedicine* 7, 49.

Chapman, T., 2005. Protein purification: pure but not simple. *Nature* 434, 795-798.

Cheryan, M., 1998. Ultrafiltration and microfiltration handbook. CRC press.

Chiellini, E., Chiellini, E.E., Chiellini, F., Solaro, R., 2001. Targeted administration of proteic drugs. I. Preparation of polymeric nanoparticles. *Journal of bioactive and compatible polymers* 16, 441-465.

Chorny, M., Fishbein, I., Danenberg, H.D., Golomb, G., 2002. Lipophilic drug loaded nanospheres prepared by nanoprecipitation: effect of formulation variables on size, drug recovery and release kinetics. *Journal of Controlled Release* 83, 389-400.

Christensen, D., Agger, E.M., Andreasen, L.V., Kirby, D., Andersen, P., Perrie, Y., 2009. Liposome-based cationic adjuvant formulations (CAF): past, present, and future. *Journal of liposome research* 19, 2-11.

Christensen, D., Foged, C., Rosenkrands, I., Lundberg, C.V., Andersen, P., Agger, E.M., Nielsen, H.M., 2010. CAF01 liposomes as a mucosal vaccine adjuvant: In vitro and in vivo investigations. *International journal of pharmaceutics* 390, 19-24.

Christensen, D., Foged, C., Rosenkrands, I., Nielsen, H.M., Andersen, P., Agger, E.M., 2007a. Trehalose preserves DDA/TDB liposomes and their adjuvant effect during freeze-drying. *Biochimica et Biophysica Acta (BBA)-Biomembranes* 1768, 2120-2129.

Christensen, D., Korsholm, K.S., Rosenkrands, I., Lindenstrøm, T., Andersen, P., Agger, E.M., 2007b. Cationic liposomes as vaccine adjuvants. *Expert Review of Vaccines* 6, 785-796.

Christman, J.E., Miller, D.S., Coward, P., Smith, L.H., Teng, N.N., 1990. Study of the selective cytotoxic properties of cationic, lipophilic mitochondrial-specific compounds in gynecologic malignancies. *Gynecologic oncology* 39, 72-79.

Chu, B., Liu, T., 2000. Characterization of nanoparticles by scattering techniques. *Journal of Nanoparticle Research* 2, 29-41.

Ciani, L., Casini, A., Gabbiani, C., Ristori, S., Messori, L., Martini, G., 2007. DOTAP/DOPE and DC-Chol/DOPE lipoplexes for gene delivery studied by circular dichroism and other biophysical techniques. *Biophysical chemistry* 127, 213-220.

Congiu, A., Pozzi, D., Esposito, C., Castellano, C., Mossa, G., 2004. Correlation between structure and transfection efficiency: a study of DC-Chol- DOPE/DNA complexes. *Colloids and Surfaces B: Biointerfaces* 36, 43-48.

Cullis, P.R., Hope, M.J., Bally, M.B., 1991. Extrusion technique for producing unilamellar vesicles. Google Patents.

Das, T., Chakraborty, S., 2009. Biomicrofluidics: Recent trends and future challenges. *Sadhana* 34, 573-590.

Davidson, J., Rosenkrands, I., Christensen, D., Vangala, A., Kirby, D., Perrie, Y., Agger, E.M., Andersen, P., 2005. Characterization of cationic liposomes based on dimethyldioctadecylammonium and synthetic cord factor from *M. tuberculosis* (trehalose 6, 6'-dibehenate)-A novel adjuvant inducing both strong CMI and antibody responses. *Biochimica et Biophysica Acta (BBA)-Biomembranes* 1718, 22-31.

De Rosa, M., Gambacorta, A., Gliozzi, A., 1986. Structure, biosynthesis, and physicochemical properties of archaebacterial lipids. *Microbiological reviews* 50, 70.

Deamer, D., Bangham, A., 1976. Large volume liposomes by an ether vaporization method. *Biochimica et Biophysica Acta (BBA)-Biomembranes* 443, 629-634.

Deamer, D.W., 1978. PREPARATION AND PROPERTIES OF ETHER - INJECTION LIPOSOMES*. *Annals of the New York Academy of Sciences* 308, 250-258.

Demello, A.J., 2006. Control and detection of chemical reactions in microfluidic systems. *Nature* 442, 394-402.

Dev, S., Iyer, K.S., Raston, C.L., 2011. Nanosized drug formulations under microfluidic continuous flow. *Lab on a Chip* 11, 3214-3217.

Dittrich, P.S., Manz, A., 2006. Lab-on-a-chip: microfluidics in drug discovery. *Nature Reviews Drug Discovery* 5, 210-218.

Dong, Y., Ng, W.K., Shen, S., Kim, S., Tan, R.B., 2012. Solid lipid nanoparticles: Continuous and potential large-scale nanoprecipitation production in static mixers. *Colloids and Surfaces B: Biointerfaces* 94, 68-72.

Driscoll, D.F., Nehne, J., Peterss, H., Franke, R., Bistran, B.R., Niemann, W., 2002. The influence of medium-chain triglycerides on the stability of all-in-one formulations. *International journal of pharmaceutics* 240, 1-10.

Ducat, E., Brion, M., Lecomte, F., Evrard, B., Piel, G., 2010. The experimental design as practical approach to develop and optimize a formulation of peptide-loaded liposomes. *AAPS PharmSciTech* 11, 966-975.

Egelhaaf, S., Wehrli, E., Adrian, M., Schurtenberger, P., 1996. Determination of the size distribution of lecithin liposomes: a comparative study using freeze fracture, cryoelectron microscopy and dynamic light scattering. *Journal of Microscopy* 184, 214-228.

Ellens, H., Bentz, J., Szoka, F.C., 1984. pH-induced destabilization of phosphatidylethanolamine-containing liposomes: role of bilayer contact. *Biochemistry* 23, 1532-1538.

Erbacher, C., Bessoth, F.G., Busch, M., Verpoorte, E., Manz, A., 1999. Towards integrated continuous-flow chemical reactors. *Microchimica Acta* 131, 19-24.

Eriksson, L., 2006. Multi-and megavariable data analysis. MKS Umetrics AB.

Eriksson, L., 2008. Design of experiments: principles and applications. MKS Umetrics AB.

Esposito, C., Generosi, J., Mossa, G., Masotti, A., Castellano, A.C., 2006. The analysis of serum effects on structure, size and toxicity of DDAB–DOPE and DC-Chol–DOPE lipoplexes contributes to explain their different transfection efficiency. *Colloids and Surfaces B: Biointerfaces* 53, 187-192.

Fang, Y.-P., Wu, P.-C., Huang, Y.-B., Tzeng, C.-C., Chen, Y.-L., Hung, Y.-H., Tsai, M.-J., Tsai, Y.-H., 2012. Modification of polyethylene glycol onto solid lipid nanoparticles encapsulating a novel chemotherapeutic agent (PK-L4) to enhance solubility for injection delivery. *International journal of nanomedicine* 7, 4995.

Felgner, P.L., Gadek, T.R., Holm, M., Roman, R., Chan, H.W., Wenz, M., Northrop, J.P., Ringold, G.M., Danielsen, M., 1987. Lipofection: a highly efficient, lipid-mediated DNA-transfection procedure. *Proceedings of the National Academy of Sciences* 84, 7413-7417.

Fessi, C., Devissaguet, J.P., Puisieux, F., Thies, C., 1992. Process for the preparation of dispersible colloidal systems of a substance in the form of nanoparticles. Google Patents US 5118528 A.

Fessi, H., Puisieux, F., Devissaguet, J.P., Ammoury, N., Benita, S., 1989. Nanocapsule formation by interfacial polymer deposition following solvent displacement. *International journal of pharmaceutics* 55, R1-R4.

Forge, A., Knowles, P., Marsh, D., 1978. Morphology of egg phosphatidylcholine-cholesterol single-bilayer vesicles, studied by freeze-etch electron microscopy. *The Journal of membrane biology* 41, 249-263.

Forge, A., Zajic, G., Davies, S., Weiner, N., Schacht, J., 1989. Gentamicin alters membrane structure as shown by freeze-fracture of liposomes. *Hearing research* 37, 129-139.

Fortunati, E., Bout, A., Antonia Zanta, M., Valerio, D., Scarpa, M., 1996. In vitro and in vivo gene transfer to pulmonary cells mediated by cationic liposomes. *Biochimica et Biophysica Acta (BBA)-Gene Structure and Expression* 1306, 55-62.

Frederiksen, L., Anton, K., Hoogevest, P.v., Keller, H.R., Leuenberger, H., 1997. Preparation of liposomes encapsulating water - soluble compounds using supercritical carbon dioxide. *Journal of pharmaceutical sciences* 86, 921-928.

Fu, Q., Sun, W., 2001. Mie theory for light scattering by a spherical particle in an absorbing medium. *Applied Optics* 40, 1354-1361.

Fuerth, D., Bazylak, A., 2013. Up-scaled microfluidic fuel cells with porous flow-through electrodes. *Journal of Fluids Engineering* 135, 021102.

Fumoto, S., Kawakami, S., Ito, Y., Shigeta, K., Yamashita, F., Hashida, M., 2004. Enhanced hepatocyte-selective in vivo gene expression by stabilized galactosylated liposome/plasmid DNA complex using sodium chloride for complex formation. *Molecular Therapy* 10, 719-729.

Gabrielsson, J., Lindberg, N.O., Lundstedt, T., 2002. Multivariate methods in pharmaceutical applications. *Journal of chemometrics* 16, 141-160.

Galindo-Rodríguez, S.A., Puel, F., Briançon, S., Allémann, E., Doelker, E., Fessi, H., 2005. Comparative scale-up of three methods for producing ibuprofen-loaded nanoparticles. *European journal of pharmaceutical sciences* 25, 357-367.

Gall, D., 1966. The adjuvant activity of aliphatic nitrogenous bases. *Immunology* 11, 369.

Gardiner, C., Dragovic, R., 2014. Nanoparticle Tracking Analysis. *Extracellular Vesicles in Health and Disease*, 261.

Gjetting, T., Andresen, T.L., Christensen, C.L., Cramer, F., Poulsen, T.T., Poulsen, H.S., 2011. A simple protocol for preparation of a liposomal vesicle with encapsulated plasmid DNA that mediate high accumulation and reporter gene activity in tumor tissue. *Results in Pharma Sciences* 1, 49-56.

Gobby, D., Angeli, P., Gavrilidis, A., 2001. Mixing characteristics of T-type microfluidic mixers. *Journal of Micromechanics and microengineering* 11, 126.

Govender, T., Stolnik, S., Garnett, M.C., Illum, L., Davis, S.S., 1999. PLGA nanoparticles prepared by nanoprecipitation: drug loading and release studies of a water soluble drug. *Journal of Controlled Release* 57, 171-185.

Gregoriadis, G., 2007. *Liposome Technology-II-Entrapment of Drugs and Other Materials Into Liposomes*. ed. I. Healthcare.

Gregoriadis, G., Bacon, A., Caparros-Wanderley, W., McCormack, B., 2002. A role for liposomes in genetic vaccination. *Vaccine* 20, B1-B9.

Gregoriadis, G., Davis, D., Davies, A., 1987. Liposomes as immunological adjuvants: antigen incorporation studies. *Vaccine* 5, 145-151.

Grinberg, S., Kolot, V., Linder, C., Shaubi, E., Kas'yanov, V., Deckelbaum, R., Heldman, E., 2008. Synthesis of novel cationic bolaamphiphiles from vernonia oil and their aggregated structures. *Chemistry and physics of lipids* 153, 85-97.

Guan, H.H., Budzynski, W., Koganty, R.R., Krantz, M.J., Reddish, M.A., Rogers, J.A., Longenecker, B.M., Samuel, J., 1998. Liposomal Formulations of Synthetic MUC1 Peptides: Effects of Encapsulation versus Surface Display of Peptides on Immune Responses. *Bioconjugate Chemistry* 9, 451-458.

Gulik, A., Luzzati, V., DeRosa, M., Gambacorta, A., 1988. Tetraether lipid components from a thermoacidophilic archaebacterium: chemical structure and physical polymorphism. *Journal of molecular biology* 201, 429-435.

Hafner, A.M., Corthésy, B., Merkle, H.P., 2013. Particulate formulations for the delivery of poly(I:C) as vaccine adjuvant. *Advanced Drug Delivery Reviews* 65, 1386-1399.

Hauschild, S., Lipprandt, U., Rumpelcker, A., Borchert, U., Rank, A., Schubert, R., Förster, S., 2005. Direct preparation and loading of lipid and polymer vesicles using inkjets. *Small* 1, 1177-1180.

Henriksen-Lacey, M., Bramwell, V.W., Christensen, D., Agger, E.-M., Andersen, P., Perrie, Y., 2010a. Liposomes based on dimethyldioctadecylammonium promote a depot effect and enhance immunogenicity of soluble antigen. *Journal of controlled release* 142, 180-186.

Henriksen-Lacey, M., Christensen, D., Bramwell, V.W., Lindenstrøm, T., Agger, E.M., Andersen, P., Perrie, Y., 2010b. Liposomal cationic charge and antigen adsorption are important properties for the efficient deposition of antigen at the injection site and ability of the vaccine to induce a CMI response. *Journal of controlled release* 145, 102-108.

Henriksen-Lacey, M., Devitt, A., Perrie, Y., 2011a. The vesicle size of DDA: TDB liposomal adjuvants plays a role in the cell-mediated immune response but has no significant effect on antibody production. *Journal of controlled release* 154, 131-137.

Henriksen-Lacey, M., Korsholm, K.S., Andersen, P., Perrie, Y., Christensen, D., 2011b. Liposomal vaccine delivery systems. *Expert opinion on drug delivery* 8, 505-519.

Holten-Andersen, L., Doherty, T., Korsholm, K., Andersen, P., 2004. Combination of the cationic surfactant dimethyl dioctadecyl ammonium bromide and synthetic

mycobacterial cord factor as an efficient adjuvant for tuberculosis subunit vaccines. *Infection and immunity* 72, 1608-1617.

Holtze, C., 2013. Large-scale droplet production in microfluidic devices—an industrial perspective. *Journal of Physics D: Applied Physics* 46, 114008.

Hong, J.W., Studer, V., Hang, G., Anderson, W.F., Quake, S.R., 2004. A nanoliter-scale nucleic acid processor with parallel architecture. *Nature biotechnology* 22, 435-439.

Hood, R., Vreeland, W., DeVoe, D., 2014a. Microfluidic remote loading for rapid single-step liposomal drug preparation. *Lab on a Chip* 14, 3359-3367.

Hood, R.R., DeVoe, D.L., Atencia, J., Vreeland, W.N., Omiatsek, D.M., 2014b. A facile route to the synthesis of monodisperse nanoscale liposomes using 3D microfluidic hydrodynamic focusing in a concentric capillary array. *Lab on a Chip* 14, 2403-2409.

Hope, M.J., Wong, K.F., Cullis, P.R., 1989. Freeze - fracture of lipids and model membrane systems. *Journal of electron microscopy technique* 13, 277-287.

Hussain, M.J., Wilkinson, A., Bramwell, V.W., Christensen, D., Perrie, Y., 2014. Th1 immune responses can be modulated by varying dimethyldioctadecylammonium and distearoyl - sn - glycerol - 3 - phosphocholine content in liposomal adjuvants. *Journal of Pharmacy and Pharmacology* 66, 358-366.

ICH, 2005. Guideline Harmonized Tripartite, Validation of analytical procedures: text and methodology. Q2 (R1) 1.

Ishikawa, E., Ishikawa, T., Morita, Y.S., Toyonaga, K., Yamada, H., Takeuchi, O., Kinoshita, T., Akira, S., Yoshikai, Y., Yamasaki, S., 2009. Direct recognition of the mycobacterial glycolipid, trehalose dimycolate, by C-type lectin Mincle. *The Journal of experimental medicine* 206, 2879-2888.

ISO, I., 2008. 22412: 2008. Particle Size Analysis—Dynamic Light Scattering (DLS). International Organization for Standardization, Geneva, Switzerland.

Ito, T., Sun, L., Bevan, M.A., Crooks, R.M., 2004. Comparison of nanoparticle size and electrophoretic mobility measurements using a carbon-nanotube-based coulter counter, dynamic light scattering, transmission electron microscopy, and phase analysis light scattering. *Langmuir* 20, 6940-6945.

Jaafar-Maalej, C., Diab, R., Andrieu, V., Elaissari, A., Fessi, H., 2010. Ethanol injection method for hydrophilic and lipophilic drug-loaded liposome preparation. *Journal of liposome research* 20, 228-243.

Jackson, J.E., 2005. A user's guide to principal components. John Wiley & Sons.

Jahn, A., Reiner, J.E., Vreeland, W.N., DeVoe, D.L., Locascio, L.E., Gaitan, M., 2008. Preparation of nanoparticles by continuous-flow microfluidics. *Journal of Nanoparticle Research* 10, 925-934.

Jahn, A., Stavis, S.M., Hong, J.S., Vreeland, W.N., DeVoe, D.L., Gaitan, M., 2010. Microfluidic mixing and the formation of nanoscale lipid vesicles. *Acs Nano* 4, 2077-2087.

Jahn, A., Vreeland, W.N., DeVoe, D.L., Locascio, L.E., Gaitan, M., 2007. Microfluidic directed formation of liposomes of controlled size. *Langmuir* 23, 6289-6293.

Jahn, A., Vreeland, W.N., Gaitan, M., Locascio, L.E., 2004. Controlled vesicle self-assembly in microfluidic channels with hydrodynamic focusing. *Journal of the American Chemical Society* 126, 2674-2675.

Jain, N., Goldschmidt, V., Oncul, S., Arntz, Y., Duportail, G., Mély, Y., Klymchenko, A.S., 2012. Lactose-ornithine bolaamphiphiles for efficient gene delivery in vitro. *International journal of pharmaceutics* 423, 392-400.

Jensen, K.F., 2001. Microreaction engineering—is small better? *Chemical Engineering Science* 56, 293-303.

Jeon, J.S., Chung, S., Kamm, R.D., Charest, J.L., 2011. Hot embossing for fabrication of a microfluidic 3D cell culture platform. *Biomedical microdevices* 13, 325-333.

Jeong, Y.-I., Cheon, J.-B., Kim, S.-H., Nah, J.-W., Lee, Y.-M., Sung, Y.-K., Akaike, T., Cho, C.-S., 1998. Clonazepam release from core-shell type nanoparticles in vitro. *Journal of Controlled Release* 51, 169-178.

Johnson, L.V., Walsh, M.L., Bockus, B.J., Chen, L.B., 1981. Monitoring of relative mitochondrial membrane potential in living cells by fluorescence microscopy. *The Journal of Cell Biology* 88, 526-535.

Jones, D.S., 1995. The effects of sub-inhibitory concentrations of cationic, non-antibiotic, antimicrobial agents on the morphogenesis of *Candida albicans* in vitro. *Pharmaceutical research* 12, 2057-2059.

Kamath, A.T., Mastelic, B., Christensen, D., Rochat, A.-F., Agger, E.M., Pinschewer, D.D., Andersen, P., Lambert, P.-H., Siegrist, C.-A., 2012. Synchronization of Dendritic Cell Activation and Antigen Exposure Is Required for the Induction of Th1/Th17 Responses. *The Journal of Immunology* 188, 4828-4837.

Karmali, P.P., Chaudhuri, A., 2007. Cationic liposomes as non - viral carriers of gene medicines: Resolved issues, open questions, and future promises. *Medicinal research reviews* 27, 696-722.

Karn, P.R., Cho, W., Hwang, S.-J., 2013. Liposomal drug products and recent advances in the synthesis of supercritical fluid-mediated liposomes. *Nanomedicine* 8, 1529-1548.

Karnik, R., Gu, F., Basto, P., Cannizzaro, C., Dean, L., Kyei-Manu, W., Langer, R., Farokhzad, O.C., 2008. Microfluidic platform for controlled synthesis of polymeric nanoparticles. *Nano letters* 8, 2906-2912.

Kastner, E., Perrie, Y., 2015. Particle size analysis for micro- and nanoparticles. submitted.

Kastner, E., Schmidt, S.T., Wilkinson, A., Christensen, D., Perrie, Y., 2015. The Application of Liposomes as Vaccine Adjuvants, Subunit Vaccine Delivery. Springer, pp. 77-94.

Kataria, S., Sandhu, P., Bilandi, A., Akanksha, M., Kapoor, B., 2011. STEALTH LIPOSOMES: A REVIEW. *International Journal of Research in Ayurveda & Pharmacy* 2.

Kaur, R., Bramwell, V.W., Kirby, D.J., Perrie, Y., 2012a. Manipulation of the surface pegylation in combination with reduced vesicle size of cationic liposomal adjuvants modifies their clearance kinetics from the injection site, and the rate and type of T cell response. *Journal of controlled release* 164, 331-337.

Kaur, R., Bramwell, V.W., Kirby, D.J., Perrie, Y., 2012b. Pegylation of DDA: TDB liposomal adjuvants reduces the vaccine depot effect and alters the Th1/Th2 immune responses. *Journal of controlled release* 158, 72-77.

Kaur, R., Henriksen-Lacey, M., Wilkhu, J., Devitt, A., Christensen, D., Perrie, Y., 2013. Effect of Incorporating Cholesterol into DDA: TDB Liposomal Adjuvants on Bilayer Properties, Biodistribution, and Immune Responses. *Molecular pharmaceuticals* 11, 197-207.

Kawaura, C., Noguchi, A., Furuno, T., Nakanishi, M., 1998. Atomic force microscopy for studying gene transfection mediated by cationic liposomes with a cationic cholesterol derivative. *FEBS letters* 421, 69-72.

Kazzaz, J., Neidleman, J., Singh, M., Ott, G., O'Hagan, D., 2000. Novel anionic microparticles are a potent adjuvant for the induction of cytotoxic T lymphocytes against recombinant p55 gag from HIV-1. *Journal of controlled release* 67, 347-356.

Keohane, K., Brennan, D., Galvin, P., Griffin, B.T., 2014. Silicon microfluidic flow focusing devices for the production of size-controlled PLGA based drug loaded microparticles. *International journal of pharmaceutics* 467, 60-69.

Kirby, B.J., 2010. *Micro-and nanoscale fluid mechanics: transport in microfluidic devices*. Cambridge University Press.

Kirby, C., Clarke, J., Gregoriadis, G., 1980. Effect of the cholesterol content of small unilamellar liposomes on their stability *in vivo* and *in vitro*. *Biochem. J* 186, 591-598.

Kockmann, N., Gottsponer, M., Roberge, D.M., 2011. Scale-up concept of single-channel microreactors from process development to industrial production. *Chemical Engineering Journal* 167, 718-726.

Kourti, T., Lee, J., Macgregor, J.F., 1996. Experiences with industrial applications of projection methods for multivariate statistical process control. *Computers & chemical engineering* 20, S745-S750.

Kubinyi, H., 1993. *3D Qsar in Drug Design: Volume 1: Theory Methods and Applications*. Springer.

Lasic, D.D., 1998. Novel applications of liposomes. *Trends in Biotechnology* 16, 307-321.

Lawrence, X.Y., 2008. Pharmaceutical quality by design: product and process development, understanding, and control. *Pharmaceutical Research* 25, 781-791.

Lee, C.-Y., Chang, C.-L., Wang, Y.-N., Fu, L.-M., 2011. Microfluidic mixing: a review. *International journal of molecular sciences* 12, 3263-3287.

Lee, J.N., Park, C., Whitesides, G.M., 2003. Solvent compatibility of poly (dimethylsiloxane)-based microfluidic devices. *Analytical chemistry* 75, 6544-6554.

Leung, A.K., Hafez, I.M., Baoukina, S., Belliveau, N.M., Zhigaltsev, I.V., Afshinmanesh, E., Tieleman, D.P., Hansen, C.L., Hope, M.J., Cullis, P.R., 2012. Lipid nanoparticles containing siRNA synthesized by microfluidic mixing exhibit an electron-dense nanostructured core. *The Journal of Physical Chemistry C* 116, 18440-18450.

Li, N., Schwartz, M., Ionescu-Zanetti, C., 2009. PDMS compound adsorption in context. *Journal of biomolecular screening*.

Liu, D., Mori, A., Huang, L., 1992. Role of liposome size and RES blockade in controlling biodistribution and tumor uptake of GM₁-containing liposomes. *Biochimica et Biophysica Acta (BBA)-Biomembranes* 1104, 95-101.

Liu, F., Huang, L., 2002. Development of non-viral vectors for systemic gene delivery. *Journal of controlled release* 78, 259-266.

Lonez, C., Vandenbranden, M., Ruyschaert, J.-M., 2008. Cationic liposomal lipids: from gene carriers to cell signaling. *Progress in lipid research* 47, 340-347.

Lopes, J.A., Costa, P.F., Alves, T.P., Menezes, J.C., 2004. Chemometrics in bioprocess engineering: process analytical technology (PAT) applications. *Chemometrics and Intelligent Laboratory Systems* 74, 269-275.

Lui, V.W.-Y., Huang, L., 2003. Nonviral approaches for cancer gene therapy. *DRUGS AND THE PHARMACEUTICAL SCIENCES* 131, 279-320.

- Lukyanov, A.N., Torchilin, V.P., 2004. Micelles from lipid derivatives of water-soluble polymers as delivery systems for poorly soluble drugs. *Advanced drug delivery reviews* 56, 1273-1289.
- Luzzati, V., Gambacorta, A., DeRosa, M., Gulik, A., 1987. Polar lipids of thermophilic prokaryotic organisms: chemical and physical structure. *Annual review of biophysics and biophysical chemistry* 16, 25-47.
- MacDonald, R.C., MacDonald, R.I., Menco, B.P.M., Takeshita, K., Subbarao, N.K., Hu, L.-r., 1991. Small-volume extrusion apparatus for preparation of large, unilamellar vesicles. *Biochimica et Biophysica Acta (BBA)-Biomembranes* 1061, 297-303.
- Maeda, H., 1992. The tumor blood vessel as an ideal target for macromolecular anticancer agents. *Journal of controlled release* 19, 315-324.
- Majeti, B.K., Singh, R.S., Yadav, S.K., Bathula, S.R., Ramakrishna, S., Diwan, P.V., Madhavendra, S.S., Chaudhuri, A., 2004. Enhanced intravenous transgene expression in mouse lung using cyclic-head cationic lipids. *Chemistry & biology* 11, 427-437.
- Malone, R.W., Felgner, P.L., Verma, I.M., 1989. Cationic liposome-mediated RNA transfection. *Proceedings of the National Academy of Sciences of the United States of America* 86, 6077.
- Mandenius, C.F., Brundin, A., 2008. Bioprocess optimization using design - of - experiments methodology. *Biotechnology progress* 24, 1191-1203.
- Mann, J.F.S., Shakir, E., Carter, K.C., Mullen, A.B., Alexander, J., Ferro, V.A., 2009. Lipid vesicle size of an oral influenza vaccine delivery vehicle influences the Th1/Th2 bias in the immune response and protection against infection. *Vaccine* 27, 3643-3649.
- Manolova, V., Flace, A., Bauer, M., Schwarz, K., Saudan, P., Bachmann, M.F., 2008. Nanoparticles target distinct dendritic cell populations according to their size. *European journal of immunology* 38, 1404-1413.
- Martel, J.M., Smith, K.C., Dlamini, M., Pletcher, K., Yang, J., Karabacak, M., Haber, D.A., Kapur, R., Toner, M., 2015. Continuous Flow Microfluidic Bioparticle Concentrator. *Scientific reports* 5.
- Maruyama, K., Yuda, T., Okamoto, A., Kojima, S., Suganaka, A., Iwatsuru, M., 1992. Prolonged circulation time in vivo of large unilamellar liposomes composed of distearoyl phosphatidylcholine and cholesterol containing amphipathic poly (ethylene glycol). *Biochimica et Biophysica Acta (BBA)-Lipids and Lipid Metabolism* 1128, 44-49.
- May, S., Harries, D., Ben-Shaul, A., 2000. The phase behavior of cationic lipid-DNA complexes. *Biophysical Journal* 78, 1681-1697.
- Mbanjwa, M.B., Chen, H., Fourie, L., Ngwenya, S., Land, K., 2014. Fabrication of a multiplexed microfluidic system for scaled up production of cross-linked biocatalytic microspheres, Third Conference on Sensors, MEMS and Electro-Optic Systems. International Society for Optics and Photonics, pp. 92570M-92570M-92577.
- McNeil, S., Vangala, A., W Bramwell, V., J Hanson, P., Perrie, Y., 2010. Lipoplexes formulation and optimisation: in vitro transfection studies reveal no correlation with in vivo vaccination studies. *Current drug delivery* 7, 175-187.
- McNeil, S.E., Perrie, Y., 2006. Gene delivery using cationic liposomes.
- Mengeaud, V., Josserand, J., Girault, H.H., 2002. Mixing processes in a zigzag microchannel: finite element simulations and optical study. *Analytical Chemistry* 74, 4279-4286.
- Meure, L.A., Foster, N.R., Dehghani, F., 2008. Conventional and dense gas techniques for the production of liposomes: a review. *AAPS PharmSciTech* 9, 798-809.

Meyer, H., Richter, W., 2001. Freeze-fracture studies on lipids and membranes. *Micron* 32, 615-644.

Milicic, A., Kaur, R., Reyes-Sandoval, A., Tang, C.-K., Honeycutt, J., Perrie, Y., Hill, A.V., 2012. Small cationic DDA: TDB liposomes as protein vaccine adjuvants obviate the need for TLR agonists in inducing cellular and humoral responses. *PloS one* 7, e34255.

Moghaddam, B., McNeil, S.E., Zheng, Q., Mohammed, A.R., Perrie, Y., 2011. Exploring the Correlation Between Lipid Packaging in Lipoplexes and Their Transfection Efficacy. *Pharmaceutics* 3, 848-864.

Mohammed, A., Weston, N., Coombes, A., Fitzgerald, M., Perrie, Y., 2004. Liposome formulation of poorly water soluble drugs: optimisation of drug loading and ESEM analysis of stability. *International Journal of Pharmaceutics* 285, 23-34.

Mohammed, A.R., Bramwell, V.W., Kirby, D.J., McNeil, S.E., Perrie, Y., 2010. Increased potential of a cationic liposome-based delivery system: enhancing stability and sustained immunological activity in pre-clinical development. *European journal of pharmaceutics and biopharmaceutics* 76, 404-412.

Monahan, J., Gewirth, A.A., Nuzzo, R.G., 2002. Indirect fluorescence detection of simple sugars via high - pH electrophoresis in poly (dimethylsiloxane) microfluidic chips. *Electrophoresis* 23, 2347-2354.

Montgomery, D.C., Montgomery, D.C., Montgomery, D.C., 1997. Design and analysis of experiments. Wiley New York.

Moore, J.D., Caufield, W.V., Shaw, W.A., 2007. Quantitation and standardization of lipid internal standards for mass spectroscopy. *Methods in enzymology* 432, 351-367.

Mora-Huertas, C., Fessi, H., Elaissari, A., 2011. Influence of process and formulation parameters on the formation of submicron particles by solvent displacement and emulsification–diffusion methods: Critical comparison. *Advances in colloid and interface science* 163, 90-122.

Muller, R.H., Keck, C.M., 2004. Challenges and solutions for the delivery of biotech drugs—a review of drug nanocrystal technology and lipid nanoparticles. *Journal of biotechnology* 113, 151-170.

Nandi, I., Bateson, M., Bari, M., Joshi, H.N., 2003. Synergistic effect of PEG-400 and cyclodextrin to enhance solubility of progesterone. *AAPS PharmSciTech* 4, 1-5.

Nguyen, N.-T., Wu, Z., 2005. Micromixers—a review. *Journal of Micromechanics and Microengineering* 15, R1.

Nisisako, T., Torii, T., 2008. Microfluidic large-scale integration on a chip for mass production of monodisperse droplets and particles. *Lab on a Chip* 8, 287-293.

Nordly, P., Korsholm, K.S., Pedersen, E.A., Khilji, T.S., Franzyk, H., Jorgensen, L., Nielsen, H.M., Agger, E.M., Foged, C., 2011. Incorporation of a synthetic mycobacterial monomycoloyl glycerol analogue stabilizes dimethyldioctadecylammonium liposomes and potentiates their adjuvant effect in vivo. *European Journal of Pharmaceutics and Biopharmaceutics* 77, 89-98.

O'Hagan, D., Singh, M., Ugozzoli, M., Wild, C., Barnett, S., Chen, M., Schaefer, M., Doe, B., Otten, G.R., Ulmer, J.B., 2001a. Induction of potent immune responses by cationic microparticles with adsorbed human immunodeficiency virus DNA vaccines. *Journal of virology* 75, 9037-9043.

O'Hagan, D.T., MacKichan, M.L., Singh, M., 2001b. Recent developments in adjuvants for vaccines against infectious diseases. *Biomolecular engineering* 18, 69-85.

O'Sullivan, B., Al-Bahrani, H., Lawrence, J., Campos, M., Cázares, A., Baganz, F., Wohlgemuth, R., Hailes, H.C., Szita, N., 2012. Modular microfluidic reactor and inline filtration system for the biocatalytic synthesis of chiral metabolites. *Journal of Molecular Catalysis B: Enzymatic* 77, 1-8.

O'Hagan, D.T., De Gregorio, E., 2009. The path to a successful vaccine adjuvant—'the long and winding road'. *Drug discovery today* 14, 541-551.

Oh, I., Lee, K., Kwon, H.-Y., Lee, Y.-B., Shin, S.-C., Cho, C.-S., Kim, C.-K., 1999. Release of adriamycin from poly (γ -benzyl-L-glutamate)/poly (ethylene oxide) nanoparticles. *International journal of pharmaceutics* 181, 107-115.

Ohvo-Rekilä, H., Ramstedt, B., Leppimäki, P., Slotte, J.P., 2002. Cholesterol interactions with phospholipids in membranes. *Progress in lipid research* 41, 66-97.

Okada, H., Toguchi, H., 1995. Biodegradable microspheres in drug delivery. *Critical Reviews™ in Therapeutic Drug Carrier Systems* 12.

Olsen, A.W., van Pinxteren, L.A., Okkels, L.M., Rasmussen, P.B., Andersen, P., 2001. Protection of mice with a tuberculosis subunit vaccine based on a fusion protein of antigen 85b and esat-6. *Infection and immunity* 69, 2773-2778.

Owen Iv, R., Lewin, A.P., Peel, A., Wang, J., Guy, J., Hauswirth, W.W., Stacpoole, P.W., Flotte, T.R., 2000. Recombinant adeno-associated virus vector-based gene transfer for defects in oxidative metabolism. *Human gene therapy* 11, 2067-2078.

Park, J.W., Park, E.-S., Chi, S.-C., Kil, H.Y., Lee, K.-H., 2003. The effect of lidocaine on the globule size distribution of propofol emulsions. *Anesthesia & Analgesia* 97, 769-771.

Pasqualoto, K.F., Teófilo, R.F., Guterres, M., Pereira, F.S., Ferreira, M., 2007. A study of physicochemical and biopharmaceutical properties of Amoxicillin tablets using full factorial design and PCA biplot. *Analytica chimica acta* 595, 216-220.

Pattnaik, P., Ray, T., 2009. Improving liposome integrity and easing bottlenecks to production. *Pharmaceutical Technology Europe* 22.

Pecora, R., 2000. Dynamic light scattering measurement of nanometer particles in liquids. *Journal of nanoparticle research* 2, 123-131.

Perrie, Y., Gregoriadis, G., 2000. Liposome-entrapped plasmid DNA: characterisation studies. *Biochimica et Biophysica Acta (BBA)-General Subjects* 1475, 125-132.

Perrie, Y., Kastner, E., Kaur, R., Wilkinson, A., Ingham, A.J., 2013. A case-study investigating the physicochemical characteristics that dictate the function of a liposomal adjuvant. *Human Vaccines & Immunotherapeutics* 9, 1374-1381.

Perrie, Y., McNeil, S., Vangala, A., 2003. Liposome-mediated DNA immunisation via the subcutaneous route. *Journal of drug targeting* 11, 555-563.

Perrie, Y., Mohammed, A.R., Kirby, D.J., McNeil, S.E., Bramwell, V.W., 2008. Vaccine adjuvant systems: enhancing the efficacy of sub-unit protein antigens. *International journal of pharmaceutics* 364, 272-280.

Perrie, Y., Obrenovic, M., McCarthy, D., Gregoriadis, G., 2002. Liposome (Lipodine™)-mediated DNA vaccination by the oral route. *Journal of liposome research* 12, 185-197.

Pradhan, P., Guan, J., Lu, D., Wang, P.G., Lee, L.J., Lee, R.J., 2008. A facile microfluidic method for production of liposomes. *Anticancer research* 28, 943-947.

Quevedo, E., Steinbacher, J., McQuade, D.T., 2005. Interfacial polymerization within a simplified microfluidic device: capturing capsules. *Journal of the American Chemical Society* 127, 10498-10499.

Rajalahti, T., Kvalheim, O.M., 2011. Multivariate data analysis in pharmaceutics: a tutorial review. *International journal of pharmaceutics* 417, 280-290.

Rathore, A.S., Bhushan, N., Hadpe, S., 2011. Chemometrics applications in biotech processes: a review. *Biotechnology progress* 27, 307-315.

RemziáBecer, C., 2009. Synthetic polymeric nanoparticles by nanoprecipitation. *Journal of Materials Chemistry* 19, 3838-3840.

Rescignano, N., Tarpani, L., Tiribuzi, R., Montesano, S., Martino, S., Latterini, L., Kenny, J.M., Armentano, I., 2013. Protein encapsulation in biodegradable polymeric nanoparticles: morphology, fluorescence behaviour and stem cell uptake. *Macromolecular bioscience* 13, 1204-1212.

Riaz, M., 1996. Liposomes preparation methods. *Pak J Pharm Sci* 9, 65-77.

Rosenkrands, I., Agger, E.M., Olsen, A.W., Korsholm, K.S., Andersen, C.S., Jensen, K.T., Andersen, P., 2005. Cationic Liposomes Containing Mycobacterial Lipids: a New Powerful Th1 Adjuvant System. *Infect. Immun.* 73, 5817-5826.

Rotenberg, S.A., Smiley, S., Ueffing, M., Krauss, R.S., Chen, L.B., Weinstein, I.B., 1990. Inhibition of rodent protein kinase C by the anticarcinoma agent dequalinium. *Cancer research* 50, 677-685.

Ruysschaert, T., Marque, A., Duteyrat, J.-L., Lesieur, S., Winterhalter, M., Fournier, D., 2005. Liposome retention in size exclusion chromatography. *BMC biotechnology* 5, 11.

Savina, A., Amigorena, S., 2007. Phagocytosis and antigen presentation in dendritic cells. *Immunological reviews* 219, 143-156.

Savjani, K.T., Gajjar, A.K., Savjani, J.K., 2012. Drug solubility: importance and enhancement techniques. *ISRN pharmaceutics* 2012.

Scheffler, I.E., 1999. Evolutionary origin of mitochondria, in: Scheffler, I.E. (Ed.), *Mitochondria*. Wiley-Liss, New York, pp. 7-14.

Schneider-Berlin, K.R., Bonilla, T.D., Rowe, T.C., 2005. Induction of petite mutants in yeast *Saccharomyces cerevisiae* by the anticancer drug dequalinium. *Mutation Research/Fundamental and Molecular Mechanisms of Mutagenesis* 572, 84-97.

Schneider, T., Sachse, A., Röbling, G., Brandl, M., 1994. Large-scale production of liposomes of defined size by a new continuous high pressure extrusion device. *Drug development and industrial pharmacy* 20, 2787-2807.

Schubert, S., Delaney Jr, J.T., Schubert, U.S., 2011. Nanoprecipitation and nanoformulation of polymers: from history to powerful possibilities beyond poly (lactic acid). *Soft Matter* 7, 1581-1588.

Seedher, N., Bhatia, S., 2003. Solubility enhancement of Cox-2 inhibitors using various solvent systems. *Aaps Pharmscitech* 4, 36-44.

Shabir, G.A., 2003. Validation of high-performance liquid chromatography methods for pharmaceutical analysis: Understanding the differences and similarities between validation requirements of the US Food and Drug Administration, the US Pharmacopeia and the International Conference on Harmonization. *Journal of chromatography A* 987, 57-66.

Shabir, G.A., 2005. Step-by-step analytical methods validation and protocol in the quality system compliance industry. *Journal of validation technology* 10, 314-325.

Sim, J.Y., Lee, S.H., Park, D.Y., Jung, J.A., Ki, K.H., Lee, D.H., Noh, G.J., 2009. Pain on injection with microemulsion propofol. *British journal of clinical pharmacology* 67, 316-325.

Singh, B., Kapil, R., Nandi, M., Ahuja, N., 2011. Developing oral drug delivery systems using formulation by design: vital precepts, retrospect and prospects. *Expert opinion on drug delivery* 8, 1341-1360.

Singh, B., Kumar, R., Ahuja, N., 2005. Optimizing drug delivery systems using systematic" design of experiments." Part I: fundamental aspects. *Critical Reviews™ in Therapeutic Drug Carrier Systems* 22.

Sitnikova, N.L., Sprik, R., Wegdam, G., Eiser, E., 2005. Spontaneously formed trans-anethol/water/alcohol emulsions: mechanism of formation and stability. *Langmuir* 21, 7083-7089.

Smith Korsholm, K., Agger, E.M., Foged, C., Christensen, D., Dietrich, J., Andersen, C.S., Geisler, C., Andersen, P., 2007. The adjuvant mechanism of cationic dimethyldioctadecylammonium liposomes. *Immunology* 121, 216-226.

Song, Y., Holmes, J., Kumar, C.S., 2008. Microfluidic synthesis of nanomaterials. *Small* 4, 698-711.

Sosnik, A., Carcaboso, Á.M., Glisoni, R.J., Moretton, M.A., Chiappetta, D.A., 2010. New old challenges in tuberculosis: potentially effective nanotechnologies in drug delivery. *Advanced drug delivery reviews* 62, 547-559.

Squires, T.M., Quake, S.R., 2005. Microfluidics: Fluid physics at the nanoliter scale. *Reviews of modern physics* 77, 977.

Stainmesse, S., Orecchioni, A.-M., Nakache, E., Puisieux, F., Fessi, H., 1995. Formation and stabilization of a biodegradable polymeric colloidal suspension of nanoparticles. *Colloid and Polymer Science* 273, 505-511.

Steichen, J.D., Weiss, M.J., Elmaleh, D.R., Martuza, R.L., 1991. Enhanced in vitro uptake and retention of 3H-tetraphenylphosphonium by nervous system tumor cells. *Journal of neurosurgery* 74, 116-122.

Stensrud, G., Sande, S.A., Kristensen, S., Smistad, G., 2000. Formulation and characterisation of primaquine loaded liposomes prepared by a pH gradient using experimental design. *International journal of pharmaceutics* 198, 213-228.

Stroock, A.D., Dertinger, S.K., Ajdari, A., Mezić, I., Stone, H.A., Whitesides, G.M., 2002. Chaotic mixer for microchannels. *Science* 295, 647-651.

Summerhayes, I.C., Lampidis, T.J., Bernal, S.D., Nadakavukaren, J.J., Nadakavukaren, K.K., Shepherd, E.L., Chen, L.B., 1982. Unusual retention of rhodamine 123 by mitochondria in muscle and carcinoma cells. *Proceedings of the National Academy of Sciences* 79, 5292-5296.

Sunamoto, J., IWAMOTO, K., KONDO, H., SHINKAI, S., 1980. Liposomal membranes VI. Polysaccharide-induced aggregation of multilamellar liposomes of egg lecithin. *Journal of biochemistry* 88, 1219-1226.

Szoka Jr, F., Papahadjopoulos, D., 1980. Comparative properties and methods of preparation of lipid vesicles (liposomes). *Annual review of biophysics and bioengineering* 9, 467-508.

Tamber, H., Johansen, P., Merkle, H.P., Gander, B., 2005. Formulation aspects of biodegradable polymeric microspheres for antigen delivery. *Advanced drug delivery reviews* 57, 357-376.

Tanudji, M., Hevi, S., Chuck, S.L., 2002. Improperly folded green fluorescent protein is secreted via a non-classical pathway. *Journal of cell science* 115, 3849-3857.

Taylor, R.W., Turnbull, D.M., 2005. Mitochondrial DNA mutations in human disease. *Nature Reviews Genetics* 6, 389-402.

Taylor, T.M., Weiss, J., Davidson, P.M., Bruce, B.D., 2005. Liposomal nanocapsules in food science and agriculture. *Critical Reviews in Food Science and Nutrition* 45, 587-605.

Tischer, M., Pradel, G., Ohlsen, K., Holzgrabe, U., 2012. Quaternary ammonium salts and their antimicrobial potential: targets or nonspecific interactions? *ChemMedChem* 7, 22-31.

Toepke, M.W., Beebe, D.J., 2006. PDMS absorption of small molecules and consequences in microfluidic applications. *Lab Chip* 6, 1484-1486.

Torchilin, V.P., Weissig, V., 2003. *Liposomes: a practical approach*. Oxford University Press.

Umrethia, M., Kett, V.L., Andrews, G.P., Malcolm, R.K., Woolfson, A.D., 2010. Selection of an analytical method for evaluating bovine serum albumin concentrations in pharmaceutical polymeric formulations. *Journal of pharmaceutical and biomedical analysis* 51, 1175-1179.

Uyechi-O'Brien, L.S., Szoka, F., 2003. Mechanisms for cationic lipids in gene transfer. *DRUGS AND THE PHARMACEUTICAL SCIENCES* 131, 79-108.

Valencia, P.M., Basto, P.A., Zhang, L., Rhee, M., Langer, R., Farokhzad, O.C., Karnik, R., 2010. Single-Step Assembly of Homogenous Lipid- Polymeric and Lipid- Quantum Dot Nanoparticles Enabled by Microfluidic Rapid Mixing. *ACS nano* 4, 1671-1679.

van der Voet, H., 1994. Comparing the predictive accuracy of models using a simple randomization test. *Chemometrics and Intelligent Laboratory Systems* 25, 313-323.

Van Reis, R., Zydney, A., 2001. Membrane separations in biotechnology. *Current Opinion in Biotechnology* 12, 208-211.

van Reis, R., Zydney, A., 2007. Bioprocess membrane technology. *Journal of Membrane Science* 297, 16-50.

van Swaay, D., 2013. Microfluidic methods for forming liposomes. *Lab on a Chip* 13, 752-767.

Vandervoort, J., Ludwig, A., 2002. Biocompatible stabilizers in the preparation of PLGA nanoparticles: a factorial design study. *International journal of pharmaceutics* 238, 77-92.

Vasconcelos, T., Sarmiento, B., Costa, P., 2007. Solid dispersions as strategy to improve oral bioavailability of poor water soluble drugs. *Drug discovery today* 12, 1068-1075.

Vercesi, A.E., Bernardes, C., Hoffmann, M., Gadelha, F., Docampo, R., 1991. Digitonin permeabilization does not affect mitochondrial function and allows the determination of the mitochondrial membrane potential of *Trypanosoma cruzi* in situ. *Journal of Biological Chemistry* 266, 14431-14434.

Vladislavljević, G.T., Khalid, N., Neves, M.A., Kuroiwa, T., Nakajima, M., Uemura, K., Ichikawa, S., Kobayashi, I., 2013. Industrial lab-on-a-chip: design, applications and scale-up for drug discovery and delivery. *Advanced drug delivery reviews* 65, 1626-1663.

Wagner, A., Vorauer-Uhl, K., 2010. Liposome technology for industrial purposes. *Journal of drug delivery* 2011.

Wagner, A., Vorauer-Uhl, K., 2011. Liposome technology for industrial purposes. *J Drug Deliv* 2011, 591325.

Wagner, A., Vorauer-Uhl, K., Katinger, H., 2002a. Liposomes produced in a pilot scale: production, purification and efficiency aspects. *European journal of pharmaceutics and biopharmaceutics* 54, 213-219.

Wagner, A., Vorauer-Uhl, K., Kreismayr, G., Katinger, H., 2002b. The crossflow injection technique: an improvement of the ethanol injection method. *Journal of liposome research* 12, 259-270.

- Walsh, G., 2010. Biopharmaceutical benchmarks 2010. *Nature biotechnology* 28, 917-924.
- Wang, F., Han, M.-Y., Mya, K.Y., Wang, Y., Lai, Y.-H., 2005. Aggregation-driven growth of size-tunable organic nanoparticles using electronically altered conjugated polymers. *Journal of the American Chemical Society* 127, 10350-10355.
- Wang, T., Wang, N., Zhang, Y., Shen, W., Gao, X., Li, T., 2010. Solvent injection-lyophilization of tert-butyl alcohol/water cosolvent systems for the preparation of drug-loaded solid lipid nanoparticles. *Colloids and Surfaces B: Biointerfaces* 79, 254-261.
- Wasungu, L., Hoekstra, D., 2006. Cationic lipids, lipoplexes and intracellular delivery of genes. *Journal of Controlled Release* 116, 255-264.
- Watson, D.S., Endsley, A.N., Huang, L., 2012. Design considerations for liposomal vaccines: Influence of formulation parameters on antibody and cell-mediated immune responses to liposome associated antigens. *Vaccine* 30, 2256-2272.
- Weibel, D.B., Whitesides, G.M., 2006. Applications of microfluidics in chemical biology. *Current opinion in chemical biology* 10, 584-591.
- Weigl, B.H., Bardell, R.L., Cabrera, C.R., 2003. Lab-on-a-chip for drug development. *Advanced drug delivery reviews* 55, 349-377.
- Weigl, B.H.B., Ron L; Cabrera, Catherine R., 2003. Lab-on-a-chip for drug development. *Advanced Drug Delivery Reviews* 55, 349-377.
- Weiss, M.J., Wong, J.R., Ha, C.S., Bleday, R., Salem, R.R., Steele, G.D., Chen, L.B., 1987. Dequalinium, a topical antimicrobial agent, displays anticarcinoma activity based on selective mitochondrial accumulation. *Proceedings of the National Academy of Sciences* 84, 5444-5448.
- Weissenbacher, E.R., Donders, G., Unzeitig, V., Martinez De Tejada Weber, B., Gerber, S., Halaška, M., Špaček, J., 2012. A comparison of dequalinium chloride vaginal tablets (Fluomizin®) and clindamycin vaginal cream in the treatment of bacterial vaginosis: a single-blind, randomized clinical trial of efficacy and safety. *Gynecologic and obstetric investigation* 73, 8-15.
- Weissig, V., 2015. DQAsomes as the Prototype of Mitochondria-Targeted Pharmaceutical Nanocarriers: Preparation, Characterization, and Use. *Mitochondrial Medicine: Volume II, Manipulating Mitochondrial Function*, 1-11.
- Weissig, V., Hughes, J.A., Lasch, J., Rowe, T.C., 2000. Materials and methods for intracellular delivery of biologically active molecules. *Google Patents* WO 1999013096
- Weissig, V., Lasch, J., Erdos, G., Meyer, H.W., Rowe, T.C., Hughes, J., 1998. DQAsomes: a novel potential drug and gene delivery system made from dequalinium™. *Pharmaceutical research* 15, 334-337.
- Weissig, V., Torchilin, V., 2000. Mitochondriotropic Cationic Vesicles A Strategy Towards Mitochondrial Gene Therapy. *Current pharmaceutical biotechnology* 1, 325-346.
- Weissig, V., Torchilin, V.P., 2001. Cationic bolosomes with delocalized charge centers as mitochondria-specific DNA delivery systems. *Advanced drug delivery reviews* 49, 127-149.
- Werninghaus, K., Babiak, A., Groß, O., Hölscher, C., Dietrich, H., Agger, E.M., Mages, J., Mocsai, A., Schoenen, H., Finger, K., 2009. Adjuvanticity of a synthetic cord factor analogue for subunit *Mycobacterium tuberculosis* vaccination requires FcRγ-Syk-

Card9-dependent innate immune activation. *The Journal of experimental medicine* 206, 89-97.

Whitesides, G.M., 2006. The origins and the future of microfluidics. *Nature* 442, 368-373.

Williams, R.O., Watts, A.B., Miller, D.A., 2012. *Formulating poorly water soluble drugs*. Springer.

Wold, S., Albano, C., Dunn III, W., Edlund, U., Esbensen, K., Geladi, P., Hellberg, S., Johansson, E., Lindberg, W., Sjöström, M., 1984. *Multivariate data analysis in chemistry, Chemometrics*. Springer, pp. 17-95.

Wold, S., Sjöström, M., Eriksson, L., 2001a. PLS-regression: a basic tool of chemometrics. *Chemometrics and intelligent laboratory systems* 58, 109-130.

Wold, S., Trygg, J., Berglund, A., Antti, H., 2001b. Some recent developments in PLS modeling. *Chemometrics and intelligent laboratory systems* 58, 131-150.

Wu, Z., Nguyen, N.-T., 2005. Rapid mixing using two-phase hydraulic focusing in microchannels. *Biomedical microdevices* 7, 13-20.

Xiao, L., Wang, B., Yang, G., Gauthier, M., 2012. *Poly (lactic acid)-based biomaterials: synthesis, modification and applications*. INTECH Open Access Publisher.

Xu, X., Khan, M.A., Burgess, D.J., 2011. A quality by design (QbD) case study on liposomes containing hydrophilic API: I. Formulation, processing design and risk assessment. *International journal of pharmaceutics* 419, 52-59.

Xu, X., Khan, M.A., Burgess, D.J., 2012. A quality by design (QbD) case study on liposomes containing hydrophilic API: II. Screening of critical variables, and establishment of design space at laboratory scale. *International journal of pharmaceutics* 423, 543-553.

Yang, Y., Hua, C., Dong, C.-M., 2009. Synthesis, self-assembly, and in vitro doxorubicin release behavior of dendron-like/linear/dendron-like poly (ϵ -caprolactone)-b-poly (ethylene glycol)-b-poly (ϵ -caprolactone) triblock copolymers. *Biomacromolecules* 10, 2310-2318.

Yoshioka, H., 1991. Surface modification of haemoglobin-containing liposomes with polyethylene glycol prevents liposome aggregation in blood plasma. *Biomaterials* 12, 861-864.

Zhigaltsev, I.V., Belliveau, N., Hafez, I., Leung, A.K., Huft, J., Hansen, C., Cullis, P.R., 2012. Bottom-up design and synthesis of limit size lipid nanoparticle systems with aqueous and triglyceride cores using millisecond microfluidic mixing. *Langmuir* 28, 3633-3640.

Zook, J.M., Vreeland, W.N., 2010. Effects of temperature, acyl chain length, and flow-rate ratio on liposome formation and size in a microfluidic hydrodynamic focusing device. *Soft Matter* 6, 1352-1360.

Zupančič, S.p., Kocbek, P., Zariwala, M.G., Renshaw, D., Gul, M.O., Elsaid, Z., Taylor, K.M., Somavarapu, S., 2014. Design and development of novel mitochondrial targeted nanocarriers, DQAsomes for curcumin inhalation. *Molecular pharmaceutics* 11, 2334-2345.